Cellular and molecular characterization of Ostreopsis cf. ovata cell cycle

David Velasquez Carvajal

Sorbonne Université

Ecole Doctorale Complexité du vivant - ED515

Laboratoire de biologie du développement de Villefranche sur mer (LBDV) – UMR 7009

Equipe : Mitosis and spindle checkpoints

Cellular and molecular characterization of *Ostreopsis* cf. *ovata* cell cycle

Par David Velasquez Carvajal

Thèse de doctorat en biologie cellulaire et moléculaire

Dirigée par Elisabeth Christians and Stefania Castagnetti

Présentée et soutenue publiquement le 21 May 2021 à Villefranche sur mer

Devant un jury composé de :

Dr. Elisa Berdalet, rapporteur

Pr. Ross Waller, rapporteur

Pr. Angela Falciatore, examinatrice

Pr. Elisabeth Chrisitians, directrice de thèse

Dr. Stefania Castagnetti, encadrante (invité)

Esta tesis está dedicada especialmente a los desplazados por la violencia en Colombia y en el mundo; a “los nadie”.

This thesis is dedicated specially to those displaced by violence, in Colombia and in the world, to “the nobodies”.

No eres mi amigo, no eres mi hermano ni mi familia, ni siquiera un conocido. Eres un nadie. Vas caminando sin poder comprar un tiquete, quizás sentado en una esquina del vagón del tren o en la silla de atrás del bus, incomodas con tu presencia al turista y al local; te vas a dormir tarde de manera prohibida en las bancas escuchando el mar, como si dormir te fuera prohibido, y te levantas temprano para que no te vean. Tratas de pasar lo más desapercibido posible. Para el común de la gente lo logras, no quieres molestarlos con tu presencia, no quieres sacarlos de su burbuja, sólo quieres estar tranquilo. Quieres ser alguien aunque sabes que conviene ser nadie.

Siempre eres a quien la policía detiene, al que piden papeles, quien recibe multas. Vas a trabajar, si es que encuentras trabajo, con la esperanza de vivir mejor, y en eso quieres ser igual que ellos. Pero tú eres nadie. No te puedes enfermar, no te puedes accidentar, no llames la atención porque vendrán problemas. Es mejor seguir siendo nadie.

> “Sueñan las pulgas con comprarse un perro y sueñan los nadies con salir de pobres, que algún mágico día llueva de pronto la buena suerte, que llueva a cántaros la buena suerte; pero la buena suerte no llueve ayer, ni hoy, ni mañana, ni nunca, ni en lloviznita cae del cielo la buena suerte, por mucho que los nadies la llamen y aunque les pique la mano izquierda, o se levanten con el pie derecho, o empiecen el año cambiando de escoba.
>
> Los nadies: los hijos de nadie, los dueños de nada.
>
> Los nadies: los ningunos, los ninguneados, corriendo la liebre, muriendo la vida, jodidos, rejodidos:
>
> Que no son, aunque sean.
>
> Que no hablan idiomas, sino dialectos.
>
> Que no profesan religiones, sino supersticiones.
>
> Que no hacen arte, sino artesanía.
>
> Que no practican cultura, sino folklore.
>
> Que no son seres humanos, sino recursos humanos.
>
> Que no tienen cara, sino brazos.
>
> Que no tienen nombre, sino número.
>
> Que no figuran en la historia universal, sino en la crónica roja de la prensa local.
>
> Los nadies, que cuestan menos que la bala que los mata”.

Eduardo Galeano

Acknowledgments

I would like to thank everyone who either helped me directly with my PhD, or who shared a word, a bit of time or even the complicit silence of a speechless conversation.

Thanks to those that had a word of encouragement when I needed it, even more if you did not know that I needed it.

Thanks to those that stopped doing their things for something stupid that I might have asked.

Thanks to those who held their breath while I was competing, good vibes were around; a natural mystic blowing in the air… Moments that gave color to life.

Thanks to you for accepting a coffee.

Thanks to you because you are reading this.

Thanks to the jury and the members of my thesis committee, for the time that was dedicated to reading my manuscript which gives importance to this effort, your feedback is essential for me.

Jocelyne, Thierry and Didier, ce fut un grand plaisir d'être nourri par vos repas, merci pour votre bonne humeur; Christelle and Frédéric; Martine, Sameh, mes amis Faisal et Mohamed, Guy, Jennifer -thanks for your words ;)- ; Sébastien; Rémi, Bennoit, Michael, Céline; Alex – thanks for sharing with me your thoughts about life and about what is life. Clare!, Evelyn, Cat!, Carine, Yas!, Tsuyo; Stefano -gracias parcero; A. Alie and to everyone from LBDV and from the LOV who shared a moment with me; life is beyond science.

To Marianne; to Geraldine and Marion “las monitas”; Martica -you’re awesome; Manon, Rita, Maciej, Sophie, Julia “Bromas”, Anne, Alex J and all the students.

My favorite place in France and the people who gave life to such incredible place, the Ponton: Lolo!, David, Didier, Sandra, Ben. Merci d’être avec moi a côté de la mer.

To all who were involved in my project: Philippe Dru (tu n'étais pas seulement d'une grande aide, mais aussi d’une grande disponibilité), Richard, B. Lacroix, Sophie Marro, Alan, Anaïs, Lucas Gutierres, Rodolph.

Elisabeth, thanks for accepting me in first instance and for your feedback!

Jannet and Gerard, ‘the doors’ of my home will be open for you.

Lydia, you helped me more than you can imagine! Je te serai éternellement reconnaissante.

All the B@#$%ches: Cora & mon bb Oxi; Meb -my bro, Isa and your family!!, I hope life will give us more chances to laugh together. Lucas L. -you can't imagine how grateful I'm with you; Kevin and Anne-So, you were always there!; Alberto, amico! the blondie italian Mussel f@#%r and your uke-le-le gave me peace; Fede "el compa"; Anna & Andrea -los parceritos-; all the "Italian mafia of science"; All my friends.

Stefania, you and 'your nice way to be mean' have tought me rigor, patience, kindness, and that there is always something more to give, that science is important but life goes on, and that learning is a curve, even if some of us take more time (although I think that it is more like a roller coaster, at least in my case). It is always nice to meet people who give positive things to the world, even if sometimes people like me push your patience to the limit. Also, thanks for allowing me to meet Mate and Ale, great people they are, I wish all the best to you and your family.

I would not have been able to finish this thesis without Sci-Hub. The only privilege of knowledge should be reserved to those who want to search for it.

A mis amigos en Colombia y en otras partes del mundo, quienes siempre me apoyaron y me alentaron aun cuando no lo pedí.

Mi familia, mi hermano -compañero de viajes y a mi sobri. A mis padres; a mi papá quien me enseñó a tener la frente en alto y a luchar a pesar de las utopías, y a ti Chila que entregaste tu vida al sacrificio para que de la mejor manera posible, pudiéramos mi hermano y yo enfrentar al mundo. Ese es su legado.

Todavía, El mar y tú.

Table of contents

Table of Figures

Acronyms

A
APC/C - anaphase promoting complex (protein complex)
ATP: Adenosine triphosphate

B
Bub1 - Budding uninhibited by benzimidazoles 1
Bub3- Budding uninhibited by benzimidazoles 3
BubR1- Budding uninhibited by benzimidazoles Related 1.

C
CAK - CDK-activating kinases
CCAN - Constitutive Centromere Associated Network (protein complex)
Cdc20- Cell division cycle protein 20
Cdh1- Cdc20 homolog 1
CDK - Cyclin-Dependent Kinases
CKI – CDK- inhibitors.
CPC - chromosomal passenger components

D
DNA – Deoxyribonucleic acid
DMSO – Dymetilsulphoxide
L
LECA – Last Eukaryotic Common Ancestor

H
HAB – Harmful Algae Bloom

I
IFT - Intraflagellar Transport (protein complex)

K
KMN – Knl1–Mis12–Ndc80 (protein complex)
KNL1- Kinetochore null protein, also called CASC5, blinkin, AF15q14, Spc7 or Spc105

M
Mad1: Mitotic arrest deficient 1
Mad2: Mitotic arrest deficient 2
Mad3 - Mitotic arrest deficient 3
MCCV - Mediterranean Culture Collection of Villefranche-sur-Mer
MEN - Mitotic Exit Network
Mps1 - Monopolar spindle 1, TTK or Mph1
MTOC - Microtubules Organizing Centers

N
Ndc80 - Nuclear division cycle 80, also called Hec1

P
PBS - Phosphate Buffered Saline
PCD Programed Cell Death
PIM - Plateforme d'Imagerie Microscopique
PFA – Paraformaldehyde
Plk1 - Polo like kinase 1, also called Polo, Cdc5 or Plo1
PP1 - phosphoprotein phosphatase 1, also PPP1
PP2A - phosphoprotein phosphatase 2A, also PPP2A

R
RNA – Ribonucleic acid
RZZ - Rod-ZW10-Zwilch
RT-qPCR - reverse transcription quantitative PCR

S
SAC - Spindle Assemble Checkpoint
Smc- Structural Maintenance of Chromosomes (protein complex)
SPBs - spindle poles bodies

Z
ZW10 - Zeste White 10
ZWINT - ZW10 interacting kinetochore protein

Long resumé

Il y a 102 ans, Edouard Chatton soumit à l'Université de Paris, sa thèse intitulée "Peridiniens Parasites. Morphologie, Reproduction, Ethologie". Il y décrivait les caractéristiques nucléaires du dinoflagellé *Odinium Chatton*. C'est sur la base de ses résultats que les dinoflagellés avaient été classées dans un groupe intermédiaire situé entre les procaryotes et les eucaryotes: les mésocaryotes .

Aujourd'hui, il est reconnu que les dinoflagellés sont des eucaryotes qui présentent un cycle cellulaire canonique avec des phases G1, S, G2 et M. Néanmoins, leurs noyaux particuliers et leur mitose atypique appelée dinomitose les gardent à part des autres eucaryotes tandis que se pose la question de l'origine évolutive et moléculaire de ces structures et processus.

D'un point de vue écologique, la prolifération des dinoflagellés peut présenter des phases tellement intenses que les toxines qu'elles produisent sont source de problèmes environnementaux : ces phases sont appelées efflorescences toxiques ou "Harmful Algae Blooms" (HABs) ou plus simplement "Blooms". Les HABs sont des phénomènes saisonniers caractérisés par différentes phases définies par la concentration cellulaire. Dans des conditions environnementales optimales, les cellules végétatives originaires d'un inoculum formés de cystes subissent plusieurs cycles de division qui, avec la migration cellulaire, sont la cause principale de l'augmentation de biomasse observée pendant les blooms (phase proliférative).

Ostreopsis cf. *ovata* est un dinoflagellé cosmopolite toxique qui produit des blooms saisonniers dont la fréquence et la distribution ont augmenté à travers le globe pendant ces vingt dernières années (Rhodes, 2011). Plusieurs études écologiques ont abordé les paramètres physiques impliqués dans la dynamique de prolifération d'*Ostreopsis* comme la température, la lumière, les nutriments, la turbulence, la salinité et les interactions allélochimiques mais également les relations biologiques. Cependant, la manière dont cet organisme se divise et comment sont contrôlés ses cycles cellulaires restent largement inconnus.

Le but de mon travail de thèse a été de caractériser au niveau cellulaire et moléculaire le cycle cellulaire mitotique qui est à la base de la prolifération de *O.* cf. *ovata* durant la croissance végétative.

Pour mes analyses, j'ai utilisé deux sources de cellules: des cellules "sauvages" collectées pendant les blooms estivaux dans la baie de Villefranche sur Mer et des cellules cultivées *in vitro*. J'ai utilisé une culture monoclonale, MCV054, qui a été obtenue à partir

d'un bloom ayant eu lieu sur le même site en 2014. J'ai d'abord analysé le taux de croissance in vivo pendant trois blooms consécutifs (2018-2020) et dans la culture. J'ai montré que la souche MCV054 reprenait une dynamique similaire de croissance que le bloom ce qui suggère que les études concernant la prolifération pouvaient être effectuées sur cette souche.

La morphologie des cellules collectées pendant les différentes phases du bloom permet d'identifier les différentes phases du cycle végétatif de *O. cf. ovata* incluant les cellules en division. En utilisant cette classification, j'ai montré que pendant le bloom *O. cf. ovata* se divisent exclusivement la nuit. La division cellulaire a été observée durant toutes les phases du bloom à des pourcentages variables, la phase prolifération étant caractérisée par 20-30% de cellules en division

En raison de leurs très grands génomes, les approches génomiques et transcriptomiques qui sont de nos jours largement utilisées, n'ont été que très peu exploitées pour étudier la biologie des dinoflagellés. Pour caractériser le cycle cellulaire de *O. cf. ovata* au niveau moléculaire, j'ai décidé d'adopter une approche fondée sur l'exploration du génome entier et j'ai cherché des gènes homologues aux gènes régulateurs des cycles cellulaires "classiques". J'ai généré un transcriptome de référence à partir de culture cellulaire et des jeux de données méta-transcriptomiques pour différentes étapes du bloom de 2019. J'ai utilisé le transcriptome de référence pour identifier chez *O.* cf. *ovata* les homologues des protéines connues pour être impliquées dans le cycle mitotique d'organismes modèles traditionnels: la levure *Saccharomyces cerevisiae*, l'algue verte *Chlamydomonas reinhardtii* et le parasite apicomplexe *Plasmodium falciparum*. J'ai choisi une approche conservative et très utilisée, « reciprocal best hits », où deux gènes de deux génomes différents sont considérés homologues si leurs protéines sont les best hit l'une de l'autre dans le génome opposé. En utilisant cette approche, j'ai identifié des composants majeurs qui régulent le cycle cellulaire comme les cyclines et les CDKs, des protéines qui régulent l'entrée en mitose, des composants du *checkpoint* mitotique, des composants des kinetochores et des composants de la sortie de mitose de la levure. Des composants du corps basal et de la cytokinèse ont également été identifiés lors de cette analyse.

Afin de déterminer si ces gènes sont régulés au niveau transcriptionnel pendant le cycle cellulaire de *O. cf. ovata*, j'ai réalisé une analyse d'expression différentielle (Kallisto pour quantifier l'abondance des transcrits et Sleuth in R-studio pour l'analyse exploratoire et l'analyse d'expression différentielle) en utilisant les jeux de données de méta-transcriptomique correspondant à des échantillons enrichis en cellules en interphase (milieu de la journée), cellules en pré-division (soir) et cellules en division (nuit) que j'ai généré lors

du bloom 2019. Plus de 5000 transcrits exprimés différentiellement ont été identifiés en comparant les échantillons enrichis en cellules en interphase (jour) et les échantillons enrichis soit en cellules en pré-division (soir) soit en cellules en division (nuit). Parmi ces transcrits, j'ai retrouvé notamment la cycline B, des composants des kinétochores et des protéines du SAC. En revanche, seulement 241 transcrits exprimés différentiellement ont été trouvés entre les cellules en pré-division (soir) et les cellules en division (nuit). Aucun de ces transcrits n'est associé à la division cellulaire ce qui suggère qu'une fois que les cellules sont engagées dans la mitose (stade pré-division), les régulations majeures se font au niveau post-transcriptionnel.

En parallèle, j'ai caractérisé les modifications de l'organisation du cytosquelette associées avec le cycle cellulaire mitotique d'*O. cf. ovata* en analysant des marquages immunofluorescents par microscopie confocale. Pendant l'interphase, un faisceau ventral de microtubules avance depuis la région du corps basal du côté ventral de la cellule vers le noyau. Le faisceau ventral s'allonge vers le noyau et le déplace au centre de la cellule en pré-division. Une fois que le noyau est au milieu de la cellule, «acentriolar spindle poles (kinetosomes) » organise le fuseau mitotique sans aster. Le fuseau mitotique est orienté perpendiculairement à l'axe long de la cellule et reste en contact avec la région ventrale grâce aux structures de microtubules appelées desmose qui sont originaires du faisceau ventral. Les chromosomes sont répartis par le fuseau de microtubules qui traverse le noyau alors qu'une plaque cytokinetique composée de microtubules commence à se former dans la région dorsale, à l'opposé des corps basaux. La plaque cytokinetique croît et divise la cellule le long de l'axe longitudinal. La division cellulaire génère deux cellules filles avec un noyau en position latérale. Le noyau sera de nouveau déplacé en région dorsale par le faisceau ventral ce qui marquera le début d'un nouveau cycle. Pendant la totalité du cycle, les microtubules corticales et le flagelle restent présents.

La détection par anticorps spécifiques de formes de l'alpha-tubuline modifiées post-traductionnellement, soit tyrosinée soit acétylée ont permis de déterminer différentes sous-populations de microtubules. La tubuline acétylée marque préférentiellement le faisceau ventral, les desmoses et les pôles du fuseau alors que la tubuline tyrosinée marque le fuseau mitotique central. Ces différences montrent que la dinomitose est un processus dynamique durant lequel différentes sous-populations de microtubules effectuent des fonctions spécifiques: la tubuline tyrosinée marquent des structures transitoires utilisées pour séparer les chromosomes alors que la tubuline acétylée est retrouvée dans des microtubules plus durables utilisées pour déplacer le noyau.

Le rôle des microtubules lors de la division cellulaire a été étudié partir de deux types de perturbations soit une exposition à la colchicine, une drogue qui dépolymérise les microtubules soit une exposition à une agitation du milieu. Des résultats préliminaires suggèrent que les microtubules ne sont pas requises pour le processus de division des cellules d'*O. cf. ovata* mais qu'elles sont nécessaires pour l'orientation correcte du plan de division.

J'ai intégré l'ensemble de ces résultats dans un schéma global récapitulant les étapes du cycle cellulaire d'*O. cf. ovata* dans lequel l'activité des cyclines et des CDKs dicte la transition entre l'interphase et la mitose. J'ai émis l'hypothèse que les cellules avec un noyau situé au centre, que j'appelle "cellules en pré-division", sont engagés dans la mitose car le fuseau mitotique se forme alors que le noyau est situé au milieu de la cellule, et des hauts niveaux de transcrits pour les cyclines mitotiques, les protéines du kinétochore et les composants du SAC sont déjà présents ou détectables dans les cellules en pré-division.

Long summary

Dinoflagellates are protists with unique features among eukaryotes. The particular nucleus with chromosomes that remain condensed through the cell cycle and their unique kind of mitosis, called dinomitosis, set them apart from canonical eukaryotes and rise questions of how their cell cycle is controlled. Moreover, dinoflagellates are interesting from an ecological perspective, as they are the cause of massive and sometimes toxic proliferation events, called Harmful Algae Blooms (HABs). HABs are seasonal phenomena, which result mainly from an increase in cell division and aggregation through cell migration (Burkholder, et al., 2006).

Ostreopsis cf. *ovata* is a cosmopolitan toxic dinoflagellate that produces seasonal blooms. Many ecological studies have addressed the parameters involved in the dynamic of *Ostreopsis* proliferation (Cohu, et al., 2011). However, it is currently unknown how this organism divides or how its cell cycle is controlled. The aim of this thesis was to provide a cellular and molecular characterization of the mitotic cell cycle, which underlies cell proliferation during vegetative growth, for the dinoflagellate *O.* cf. *ovata.*

Morphological classification of cells collected at different phases of the bloom, allowed to identify different phases of the *O.* cf. *ovata* vegetative cycle, including cells undergoing division. Using this classification, I showed that during blooming, *O.* cf. *ovata* divides exclusively at night.

Using immuno-fluorescence and confocal microscopy, I then characterized the changes in cytoskeletal organization associated with the *O.* cf. *ovata* cell cycle. During interphase, a ventral microtubule bundle protrudes from the ventral area, where the basal bodies are located, towards the nucleus and moves it to the center of the cell. Cells with a central nucleus are considered as pre-dividing. Once the nucleus is in the cell center, the mitotic spindle is organized perpendicularly to the long axis of the cell and segregates chromosomes to opposite cell ends. A cytokinetic plate made of microtubules starts to form in the dorsal area, opposite the basal bodies, already in anaphase. The cytokinetic plate grows unidirectionally towards the ventral side, dividing the cell along the longitudinal axis.

To characterize *O.* cf. *ovata* cell cycle at the molecular level, I searched for *O.* cf. *ovata* homologues of conserved cell cycle regulators identified in model organisms, using a *de novo* transcriptome that I generated from cultured cells. This analysis revealed the presence of major components of the cell cycle such as cyclins and CDKs, proteins that are known to regulate mitotic entry, mitotic checkpoint components, kinetochore components and

components of the budding yeast mitotic exit network. Cytokinetic and basal body components were also identified in the analysis.

A differential expression analysis using meta-trascriptomic datasets corresponding to bloom samples enriched in interphase cells, pre-dividing cells and dividing, which I generated during the 2019 bloom, showed that more than 5000 transcripts were differentially expressed when comparing samples enriched in interphase cells and samples enriched in either pre-dividing or dividing cells. Among these transcripts, cyclin B, kinetochore and SAC components were up-regulated during the period of division. Instead, only 241 differentially expressed transcripts were present between pre-dividing or dividing cells. None of these transcripts was related with cell division, suggesting that once the cell is committed to mitosis (pre-dividing stage), the major regulations occur at the post-transcriptional level.

By integrating the results obtained from the transcriptomic analysis with the cytological characterization I propose a first model of *O.* cf. *ovata* cell cycle, in which cyclins and CDK activities dictate the transition from interphase to mitosis.

Chapter 1

General introduction

"If the doors of perception were cleansed everything would appear to man as it is, infinite." William Blake

1.1 Ecological importance of dinoflagellates

Dinoflagellates are unicellular eukaryotes that appeared ~400 MYA and have adapted to most marine and fresh water ecosystems, from tropical to polar waters (Bachvaroff et al., 2014). They are dominant primary producers in tropical and subtropical oceans; they are also abundant in late spring/summer plankton of temperate and subarctic seas and in ice communities from the Antarctic to northern temperate lakes (J. M. Burkholder et al., 2006).

Many dinoflagellates are photosynthetic and although they represent only 1% of the total photosynthetic biomass, together with diatoms, they are responsible for more than 45% of the planet annual net photosynthetic primary production and fix half of the carbon in the oceans, and thus roughly a quarter of the total amount fixed worldwide (Field, 1998).

Dinoflagellates are diverse in shapes, growth habits and nutritional modes, occurring both in the plankton and in the benthos and as photosynthetic, heterotrophic, symbiotic, parasitic and mixotrophic (combination of photosynthesis and food ingestion to harvest energy and nutrients). There are predator dinoflagellates such as *Pfiesteria* or *Protoperidinium*; other dinoflagellates live as free organisms and some species can undergo explosive proliferative events forming massive aggregates that spread in the sea; other species, such as those belonging to the *Symbiodinium* genus are symbiotic with corals (*Anthozoans*) (Dagenais-Bellefeuille and Morse, 2013) and supply reef corals with the nutrients necessary for their survival in tropical nutrient-poor waters (Davy et al., 2012). Dinoflagellates can also be found in epiphytic associations with macroalgae and in benthic sediments (Vila et al., 2001a), often as cysts. This plethora of different lifestyles has enabled dinoflagellates to adapt to a wide variety of ecological niches and probably underlays their ecological success (Dagenais-Bellefeuille & Morse, 2013). Despite being poor competitors within their ecosystems and despite their low division rate compared to other protists (chlorophytes, haptophytes and diatoms), dinoflagellates are known to cause huge tides that can reach hundreds of kilometers and impact heavily on the marine ecosystem (Driscoll et al., 2016), a phenomenon known as Harmful Algae Blooms.

1.2 Harmful Algae Blooms, HABs

Harmful Algae Blooms (HABs), herein referred to as blooms, are generally defined as massive concentrations of marine protists with deleterious effects on the environment.

The existence of HABs has been observed for centuries. The water discoloration in the lower Nile that appears as the first of the ten plagues in the Old Testament, in which the Nile River turns bloody, fouling drinking water and killing fish (English Standard Version Bible, 2001, Ex 1-12), was likely produced by algal bloom (Granéli and Turner, 2006). In a more recent but still ancient report, Darwin described discolored seawater from South America, which can be attributed to algal bloom:

> *'Some of the water placed in a glass was of a pale reddish tint and, examined under a microscope, was seen to swarm with minute animalculae darting about and often exploding. Their shape is oval and contracted in the middle by a ring of vibrating curved ciliae" (The Voyage Of The Beagle By Charles Darwin, 1839).*

Despite the occurrence of HABs throughout history, their frequency, geographic range and intensity have greatly increased in recent years (Berdalet et al., 2016; Gustaaf M. Hallegraeff, 2010; Zingone & Oksfeldt Enevoldsen, 2000). This increase has been attributed to climate change and eutrophication (Sellner et al., 2003; H. W. Paerl & Huisman, 2008; Griffith & Gobler, 2020; Visser et al., 2016), anthropogenic influences (Hans W. Paerl et al., 2011; Davidson et al., 2014) as well as to sampling intensification and methodological improvements (Donald M. Anderson et al., 2012).

Currently, it is accepted that HABs are seasonal phenomena (Watson et al., 2015) occurring in all aquatic environments (e.g. freshwater, brackish and marine) and at all latitudes (Berdalet et al., 2016; G. M. Hallegraeff, 1993; Prince et al., 2008). HABs can result from rapid proliferation of cells or from the maintenance of a high cell concentration via behavioral adaptations (swimming, sinking), successful resource competition, life-history transitions or allelochemical interactions (A. Cembella & John, 2006).

About ¾ of HABs are produced by dinoflagellates, whereas the other ¼ is caused by cyanobacterias and diatoms (Watson et al., 2015), with cyanobacteria being more common in freshwater.

HABs can be generated by toxic species which produce potent toxins which directly impact on organismal survival and can cause human intoxication, and by non-toxic species which alter the equilibrium of the ecosystem affecting its homeostasis (Donald M. Anderson et al., 2012). High biomass of nontoxic blooms in coastal marine waters, for example, can

cause anoxia/hypoxia with consequent mass death of finfish and shellfish. One of the most famous examples was a bloom produced by a dinoflagellate of the genus *Ceratium*, in 1976, which caused massive death of fish and shellfish over a 13,000 km^2 area in the New York Bight (Guy, 2014). The high concentration of cells present during blooms can also interfere with light penetration and influence subsurface communities, such as submerged aquatic vegetation, and co-occurring organisms (Donald M. Anderson et al., 2012; Watson et al., 2015). The effects of HABs although generally transient and sporadic, can be observed across multiple trophic levels, from primary producers to humans (J. H. Landsberg, 2002; Pavaux et al., 2020).

Physical, biological, and chemical factors influence and determine the development of algal blooms. For dinoflagellate species, blooms are often associated with periods of calm weather and good sea conditions. Nutrient enrichment, mainly phosphorus, nitrogen, and carbon, and high light intensity also promote HAB development. Temperature, one of the most studied factors associated with HABs, influences both cellular proliferation and the production of toxins in toxic HABs.

1.2.1 Toxicity of HABs

Dinoflagellates can produce diverse natural toxins that can affect the marine environment and cause human health problems and death. Human consumption of these toxins and their derivatives can cause a wide range of symptoms. Five major seafood poisoning syndromes caused by toxins have been identified from dinoflagellates including paralytic shellfish poisoning, diarrhetic shellfish poisoning, ciguatera shellfish poisoning, amnesic shellfish poisoning and neurotoxic shellfish poisoning, although other yet uncharacterized harmful effects are thought to be related to dinoflagellate produced toxins (A. Cembella & John, 2006; Zaccaroni & Scaravelli, 2008). Based on the syndromes they cause and their chemical composition, dinoflagellate toxins have been divided into 7 major groups: saxitoxins/gonyautoxins, brevetoxins, ciguatoxins, maitotoxins, azaspiracids, yessotoxin and playtoxins (A. D. Cembella, 2003).

Among those, playtoxin (PLTX) is considered as one of the most potent non-bacterial toxin of biological origin (Rex Munday, 2011). PLTX and its derivatives (PLTX like, PLTX-L), are complex polyketides with long unsaturated aliphatic carbon backbones that contain cyclic ethers, hydroxyl, amino and amide functional groups in their structure (Richard E. Moore & Bartolini, 1981; Verma et al., 2019). These toxins are known to block the sodium/potassium (Na+/K+)-ATPase channel, a trans-membrane protein that generates

electrochemical gradient essential for physiological processes in many cells and that has an essential role in stabilizing the resting membrane potential of the cell, in regulating cell volume and in transduction of cell signals for cellular homeostasis (Habermann, 1989; Hirsh & Wu, 1997). PLTX and PLTX-L inhibit the active transport of Na+ and K+ ions across the cell membrane, transforming the pump into a non-specific permanently open channel. As a consequence of the membrane depolarization, a large amount of calcium ions enters the cytosol, inducing cell apoptosis (Habermann, 1989).

Dinoflagellate toxins have become a global concern due to their poisonous effect on animals and humans. The toxic effect of these compounds can be either direct in the organisms which first ingest or come in contact with them, or a consequence of vectorial intoxication whereby toxins are accumulated and transported to higher trophic levels through the food chain, leading to mortality at different trophic levels (Hoagland & Scatasta, 2006; Pavaux et al., 2020). Human intoxication is generally due to direct contact with the toxin through water or aerosol exposure during recreational activities (swimming, diving, fishing) or through the consumption of contaminated seafood. Given the high toxicity of dinoflagellate toxins, their concentration in seafood for human consumption is now regulated and as an example, for PLTX, the European Food Safety Authority Panel on contaminants in the food chain has recommended an upper limit of 30 mg/kg in shellfish meat (R Munday, 2006).

Besides the toxic effect on marine organisms and humans, HABs have also a detrimental impact on the local economy of contaminated coastal areas. Occurrence of HABs near recreational beaches, often results in temporary closures striking the tourism industry, whereas fisheries and aquaculture are impacted by fish mortality and fish and shellfish contaminations (Hoagland & Scatasta, 2006)

1.2.2 HAB phases

Toxic and non-toxic HABs develop with similar dynamics and based on cell concentration it is possible to recognize 5 phases during dinoflagellate blooms (Figure 1).

The early stage of the bloom, here indicated as **initiation** phase, is characterized by low cell concentration prior to the explosive increase, which defines the bloom. The initiation requires an inoculum of cells to seed the bloom. The inoculum can be from several sources and may involve different life stages depending on the organism involved (Garcés et al., 1998; Granéli & Turner, 2006).

The growth phase or proliferative phase is characterized by population growth, with a rapid increase in cell concentration. This increase can be due to cell division, predominantly

by vegetative mitotic divisions, or to clustering of cells in a certain area (E. Granéli & Turner, 2006), although the relative contribution of these processes to the increase in cell population has not been dissected.

The proliferative phase culminates with **the stationary phase, or peak of the bloom**, when the cell number remains constant and the net growth rate is therefore null. Then, cell concentration starts to decrease during the **senescence** of the bloom. Different factors that negatively impact on the organism proliferation are associated with this phase. Among them, the most studied are turbulence, which can result in bloom dispersion and has been hypothesized to also arrest cell division (Bertelet 1992; Llaveira, 2009); changes in temperature and nutrient availability, which affect directly cell division and can induce cell death and cyst formation; and proliferation of competitors and/or predators (Granéli & Turner, 2006). A combination of reduction in cell proliferation, increase in cell death, grazing, predation and competition with other organisms results in a negative net growth rate and a consequent decrease in cell concentration that leads to **the end** of the bloom, when the bloom forming organism disappears and transits to a resting form, known as cyst, until the following bloom (Granéli & Turner, 2006).

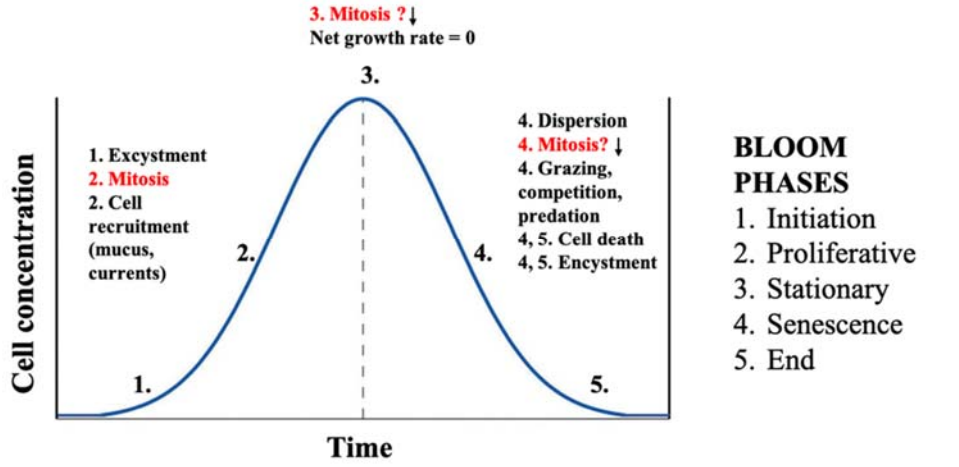

Figure 1. Dynamic of dinoflagellate blooms.
The graph shows changes in cell concentration over time with the respective associated bloom phases: 1– Initiation; 2- Proliferative; 3- Stationary; 4- Senescence; 5- End. Factors contributing to changes in bloom dynamics are reported next to each phase. Mitosis is marked in red as its contribution to each phase has not been yet properly analyzed.

1.3 Dinoflagellate life cycle

The seasonality of dinoflagellate blooms and their limited presence during other periods of the year, raises the question of where and how these organisms survive in between

blooms. The answer is to be found in their complex heteromorphic life cycle (Kremp, 2013), which includes morphologically and functionally different forms and which, with its versatility in reproduction and survival strategies, allows adaptation to different and changing environmental conditions.

The multi-stage life cycle of dinoflagellates generally includes a haploid vegetative form, sexual gametes, diploid zygotes and cysts (Ellegaard et al., 2013). Vegetative cells are swimming cells and they are found primarily in the water column (pelagic or planktonic). These vegetative cells, which are haploid for the large majority of species, divide by mitosis (asexual division). Mitosis is the predominant kind of cell proliferation observed during HAB development, when environmental conditions are optimal (Granéli & Turner, 2006). Under conditions not yet fully understood (nutrient shortage, adverse environmental conditions, light variations and so on), dinoflagellate cells can switch to sexual reproduction, which through genetic recombination underlies phenotypical variation and species adaptation. During sexual reproduction, fusion of haploid gametes (mating, syngamy) gives rise to a diploid planozygote. Gamete mating happens usually under adverse environmental conditions, but it has been also observed during blooms, albeit at low frequency (Bravo & Figueroa, 2014; Kremp, 2013).

The planozygotes can undergo two different paths: it can directly divide by meiosis and restore the vegetative stage (Figure 2) or, more frequently, it transitions to a quiescent non-motile stage with low metabolic rate, known as cyst. Cysts, which are found in the sediment niche, can be distinguished in thin-walled pellicle cyst, thick-walled resting cyst and a less well characterized form known as the dividing cyst found in few dinoflagellate species (Bravo & Figueroa, 2014).

Cysts formation is known as encystment. The germination of cysts is known as excystment and produces new vegetative cells. The planozygotes can follow two different routes to cyst formation: a short-term encystment and a long-term encystment, depending on environmental conditions. In the long-term encystment, the planozygote forms a resting cyst named hypnozygote (sexual cysts or resting cyst), which can remain dormant for several months to years (Bravo & Figueroa, 2014; J. M. Burkholder et al., 2006). This form of cyst is associated with survival during long periods, as it is observed during cold seasons for dinoflagellates that proliferate during the summer. Resting cysts can survive in the sediment for prolonged periods and can provide the inoculum at the beginning of a bloom once favorable environmental conditions are reached. Following excystment, hypnozygote emerges in an intermediate state, the planomeiocyte, which then undergoes meiosis and gives rise to

vegetative haploid cells (Figure 2). Excystment is tightly controlled by internal and external factors that ensure that germination occurs exclusively under optimal environmental conditions, preventing unwanted germination and subsequent loss of viable cells due to spells of unseasonable weather (Brosnahan et al., 2020; Nuzzo, 1999).

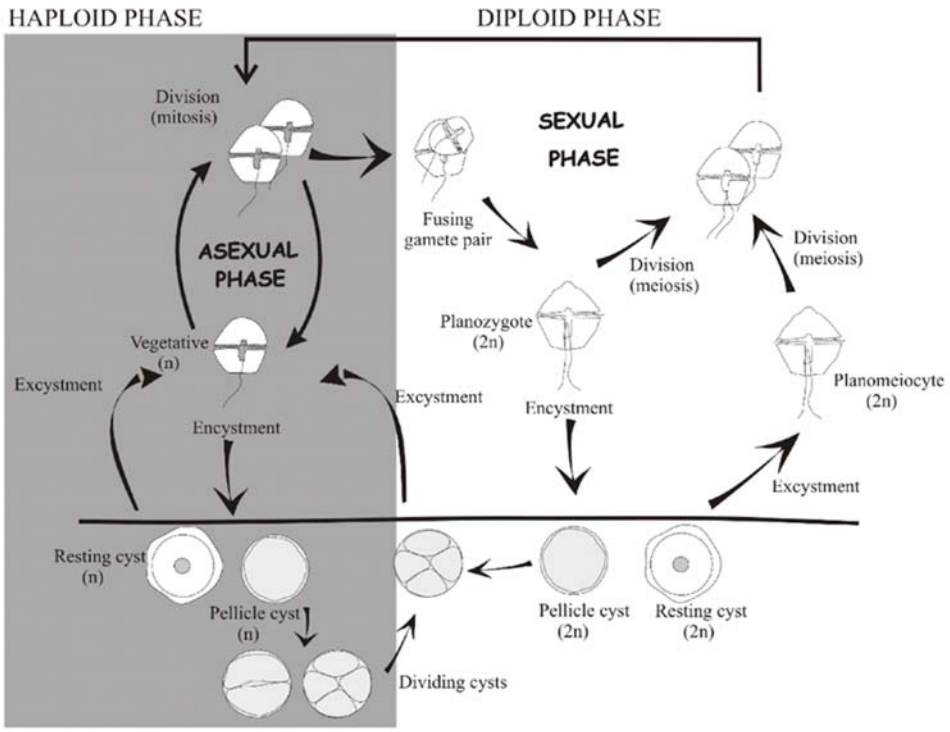

Figure 2. The life cycle of dinoflagellates, including all possible described transitions. Figure from: Bravo & Figueroa, 2014.

In short term encystment, instead, the planozygote gives rise to thin-walled pellicle cysts also known as 'ecdysal' or 'temporary' cysts, which undergo short dormancy periods. Short-term encystment has been associated with survival stages under transitory adverse conditions, such as in response to stress induced by exposure to toxins, allelopathic compounds and other substances released in the environment, or to changes in physical parameters of the environment (i.e., small turbulence). Indeed, pellicle cysts can be found during transient storms that produce turbulence and then revert to vegetative cells when favorable conditions are restored (Bravo et al., 2010; Bravo & Figueroa, 2014).

As for many other organisms, the dinoflagellate life cycle also includes a phase of senescence, corresponding to the decline of a population by programed cell death (PCD) with important consequences for ocean dynamics. Indeed, PCD has been recently introduced as a mechanism contributing to bloom termination, both under natural conditions and in the

presence of toxic chemicals, such as the algicides used for bloom management. Hallmarks of PCD are chromatin and organelles autocatalytic degradation, alteration in membrane permeability, cytoplasmic shrinking and cell lysis. Although the first example of PCD in dinoflagellates was reported more than two decades ago (Vardi et al., 1999), our understanding of the mechanisms and of the signals that trigger PCD in dinoflagellates remains limited. The best characterized cause of dinoflagellate cell death is environmental stress, such as exposure to oxidative stress, which induces the production of reactive oxygen species and subsequent activation of metacaspases, cysteine proteases with homology with caspases. Interestingly inhibition of caspase activity in *Peridinium gatunense*, blocked cell death and instead caused a transition towards cyst formation (Vardi et al., 1999), suggesting a selection mechanism whereby stressed cells undergo PCD and only non-stressed cells are preserved to form cysts and persist in the environment to initiate new blooms.

1.4 Cellular features of Dinoflagellates

Dinoflagellate is a compound word that comes from the Greek word dinos (δῖνος) meaning whirling, and the Latin 'flagellum', indicating the distinctive whirling motion of these organisms while swimming forward. This swimming pattern is due to the movement of two flagella located respectively in a transverse groove, called the cingulum, and in a longitudinal groove, called the sulcus. The cingulum also divides the cell into an upper half, called epitheca or epicone, and a lower half know as hypotheca or hypocone (Figure 3); whereas the sulcus divides the organism into left and right halves (Spector, 1984; Uzbekov, 2018).

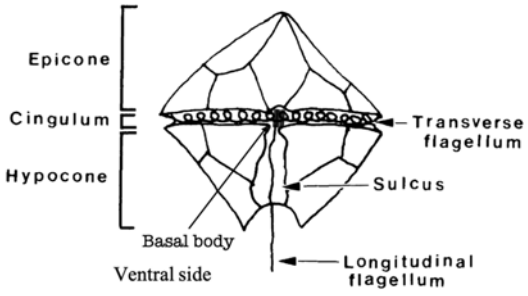

Figure 3. Flagella of dinoflagellates.
Diagram of a frontal view of a dinoflagellate (likely peridinium) with its two flagella and the insertion places. The upper epicone and the lower hypocone are divided by the cingulum where the transverse flagellum resides. The longitudinal flagellum is in the sulcus, inserted in the basal body. In dinokonts, the side where the flagella is inserted is the ventral side. Diagram adapted from Spector, 1984

Dinoflagellates are characterized by a number of distinctive cellular features which unite them in a single monophyletic lineage. Along with ciliates and apicomplexans, dinoflagellates belong to the clade of alveolates, which are characterized by the presence of

flattened vesicles, known as alveoli, located beneath the plasma membrane (Wake, 2016). This cell covering comprising the outer membrane and the alveoli is known as amphiesma. The alveoli can be empty or contain cellulosic material used to build an armor, known as theca (Pozdnyakov & Skarlato, 2012).

Most dinoflagellate species share also a characteristic nucleus, the dinokaryon, whose chromosomes remain condensed throughout the cell cycle in a liquid crystal structure without typical eukaryotic nucleosomes (Borhmann et al, 1993; Fukuda & Suzaki, 2015). Mitotic division in these organisms occurs in the absence of nuclear membrane breakdown (closed mitosis) but with a cytoplasmic microtubule spindle which transverses the nucleus through channels (Spector & Triemer, 1981). The lack of well established dinoflagellate laboratory model organisms, combined with the difficulty in keeping dinoflagellates in culture, has greatly limited studies to dissect this unusual kind of mitosis, leaving several open questions on the underlying cellular and molecular mechanism, which will be further discussed in chapter 3.

Additional unique cellular features of dinoflagellates are their characteristic plastids that possess an unusual genomic architecture and are involved in cell pigmentation (Waller & Kořený, 2017); their mitochondria that encode fewer genes than those of any other eukaryotes (Nash et al., 2007); their different types of extrusomes (organelles that secrete material to the exterior) whose function is generally associated with protection, toxin discharge and secretion (Sheng et al., 2007). Trichocysts, mucocysts, and/or nematocysts are the most common. Some dinoflagellates have also an elongated structure, the peduncle, which is used to puncture preys and extract cell contents (Kiφrboe & Titelman, 1998).

In the following sections I will describe in more details some of these dinoflagellate organelles and structures.

1.4.1 Dinoflagellate nucleus

The nucleus of core dinoflagellates, the dinokaryon, is their most distinctive organelle due to its unique features that distinguish it from other eukaryotes (Fukuda & Suzaki, 2015). Dinoflagellates have usually a high DNA content, with genomes that can be several times the size of the human genome (3 pg/cell in *Symbiodinium* to almost 200pg/ cell in *Alexandrium tamarense* and *Prorocentrum micans*) (Gornik et al., 2019; Lin, 2006). The DNA is organized in chromosomes, which vary in numbers from 4 to over 200, depending on the species, (Spector, 1984). The DNA contains a high proportion of modified nucleotides, such as 5-hydroxymethyluracil in place of thymine (Herzog et al., 1982), whose biological function

remains unknown. Finally, dinoflagellate DNA is not packed in repetitive nucleosome units, like most other eukaryotes (Talbert & Henikoff., 2012; Gornik et al., 2019). This observation led to the general understanding that dinoflagellates do not possess histones (Rizzo, 2003). However, transcriptomic analysis of different species has revealed the presence of genes encoding the four core nucleosomal histones (H2A, H2B, H3 and H4), as well as several families of prokaryotic histone-like proteins in dinoflagellate (Bayer et al., 2012a; Kohli et al., 2015; Riaz et al., 2018; Riaz & Sui, 2018). Differently from other eukaryotes, dinoflagellate histones are present at very low level. DNA is instead associated with basic nuclear proteins, namely: histone-like proteins (HLPs) and a family of DNA-binding proteins of putative viral origin, called dinoflagellate/viral nucleoproteins (DVNPs), that are present at the chromosome periphery in transcriptionally active loops (Soyer et al., 1990). The DNA to protein ratio in dinoflagellate chromosomes is very low, roughly 1:10, compared to 1:1 in all other eukaryotic cells (Riaz et al., 2018). The mostly naked DNA instead is associated with large amounts of ions, mainly Mg^{2+} and Ca^{2+} cations and various transition metal ions, which stabilize the chromosome structure by neutralizing the DNA charge and allowing maximal compaction of the naked DNA filaments (Levi-Setti et al., 2008).

The nucleus of dinoflagellates has a conventional double nuclear envelope with nuclear pores, about 100 nm in diameter (Spector, 1984), to allow communication with the cytoplasm and to control trafficking of molecules between the two compartments.

1.4.2 Flagella and the microtubule cytoskeleton

Dinoflagellates have a highly organized and complex microtubule cytoskeleton that consists of four main types of microtubular structures (N. Okamoto & Keeling, 2014; Perret et al., 1993; Uzbekov, 2018): cortical microtubules, cingular microtubules, flagellar microtubules associated with the basal body and spindle microtubules.

The cortical microtubules are composed of longitudinal microtubules that ran under the membrane of the cell. In the vast majority of dinoflagellates with a symmetrical dinokont morphology, that is when the flagella arise from the ventral area, the microtubules present in the episome have similar size and radiate from the ventral area towards the cingulum in a regular pattern, like umbrella ribs (Sekida et al., 2012; Spector, 1984). In the hyposome, microtubules run from the posterior transversal band of the cingulum towards the posterior end of the sulcus, mirroring those present in the episome. These cortical microtubules lie beneath the theca, and are thought to regulate the organization and shape of thecal plates in armored dinoflagellates (Perret et al., 1993).

Typically, dinoflagellate cells have two flagella: a longitudinal one that emerges from a pore at the cingular-sulcal interface and a transverse one that emerges from a second pore near the base of the longitudinal flagellum. Coordinated movement of the two flagella allows the cell to swim in three-dimensions.

The transverse flagellum is ribbon-shaped and lies in an equatorial groove called girdle or cingulum which is lined with tightly packed microtubules organized parallel to each other (Escalera et al., 2014; Perret et al., 1993).

The transverse flagellum beats with a helical wave propagation mode that allows cell rotation and provides most of the cell forward propelling force. The longitudinal flagellum instead lies in the longitudinal sulcus and is generally much longer than the transversal one. As a result of its planar sine waves, the cell moves in a linear fashion (Uzbekov, 2018). The combined action of these two flagella allows forward movement, orientation in the three dimensions and phototaxis orientation. At the biochemical level two mechanisms underlie flagellar movements. The flagellar sine wave propagation results from ATP-dependent microtubules sliding over one another. The second mechanism is based on the contraction of non-actin based nanofilaments. This movement is ATP-independent but requires Ca2+ (M. Cachon et al., 1991).

The dinoflagellate flagellar apparatus is composed of two basal bodies, which lay at different angles from each other depending on the species, 3 to 4 flagellar rootlets and various fibrous structures. A bundle of about 20 microtubules, known as the microtubule strand or basket, is also associated with the flagellar apparatus, although it is usually not considered as an integral part of the flagellar apparatus. This structure is often associated with electron dense vesicles (N. Okamoto & Keeling, 2014)

The basal bodies represent the flagellar motors, define the orientation of the two flagella and attach the flagella to the cell body. Basal bodies are complex structures formed by nine triplets of microtubules that, arranged with a ninefold symmetry into cylinders that are inserted in a cartwheel structure, exactly as centrioles present in centrosomes (Figure 4) (Preble et al., 2001). The cartwheel is a structure located at the interior of centrioles, consisting of a central hub and nine radially arranged spokes, located at the proximal end of the centriole. It appears at the initial stage of the centriole assembly process as the first ninefold symmetrical structure (Hirono, 2014). In the transition zone (Figure 4) the microtubule triplets are converted to the doublet microtubules of the axoneme. Electron microscopy studies have shown that centrioles and basal body have the same basic composition (Bloodgood, 2009). However the basal body is generally anchored below the

plasma membrane where it organizes cilia or flagella, whereas centrioles that are always found in pairs, are part of the centrosome located near the nucleus which organizes the mitotic spindle (Lara-Gonzalez et al., 2012) to segregate chromosomes during mitosis.

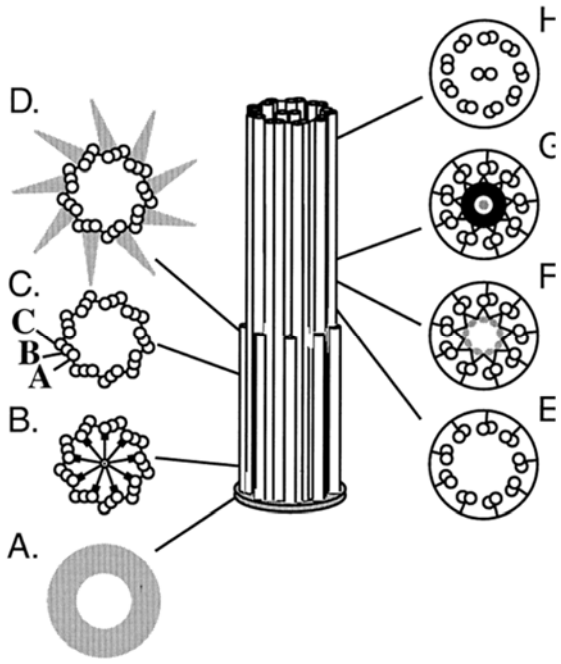

Figure 4. Diagram of basal body.
The basal body contains microtubule triplets arranged cylindrically. The tubules are designated A, B, and C, with the innermost tubule being the A-tubule. Cross-sections through the basal body from proximal to distal show: A) An amorphous, electron-dense ring. (B–D) Cross sections through the structures of a basal body shared with centrioles. (B) The proximal end contains a cartwheel structure in the center of the basal body with a central hub and spokes. Each spoke is connected to an A tubule. (C) The middle portion of the basal body lacks recognizable structures or appendages. (D) At the distal end of the triplet microtubules are transitional fibers that extend radially from each triplet. (E–H) Cross sections through the transition zone, which is unique to the basal body and contains doublet microtubules. (E) The doublets are attached to the plasma membrane. (F) A nine-pointed star with attachment to the A tubule is observed in the interior. Small electron-dense spots are observed around an inner circumference. (G) The nine-pointed star is still present, but a dense ring with a central hub is observed. (H) The flagellar axoneme is observed with a central pair, but no dynein arms. Figure from Preble, et. al (2000).

The flagellar rootlets are made of microtubules and thin filaments. The microtubules are organized in complex ribbons. The thin filaments can be composed by either centrin (striated filaments) or assemblin (non-striated filaments) (N. Okamoto & Keeling, 2014). Centrin (previously known as caltractin) is a calmodulin-like Ca^{2+}-binding protein that was shown to be involved in flagellum contraction (Salisbury et al., 1988).

1.4.3 Theca and Alveoli

The amphiesma is the cell covering of dinoflagellates and is composed of an outermost plasma-membrane and underlying single-membrane-bound vesicles, called alveoli (Figure 5). Based on the content of the alveoli, dinoflagellates can be distinguished into two groups: naked (athecate) and armored (thecate). In thecates, the alveoli (thecal vesicle)

contain thecal plates made of cellulose which provide rigidity to the cell covering, whereas in athecates, the alveoli are empty (Kwok & Wong, 2003). Recently it was shown that thecate have a monophyletic origin and have evolved from an athecate ancestor (Janouškovec et al., 2017).

In thecates, the arrangement of thecal plates forms patterns known as tabulation, which are used as a distinguishing feature for species classification. The theca confers to the cell different external shapes characteristic of each species, although morphological variability may also depend on the physiological state of the organism (Richlen et al., 2008; Zingone et al., 1998).

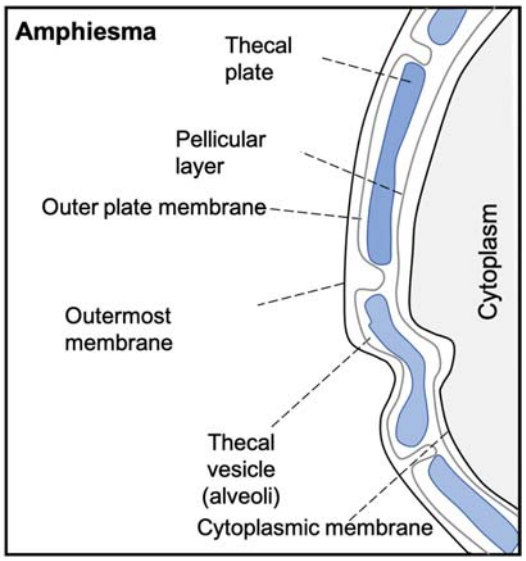

Figure 5. Schematic representation of the amphiesma of a thecate dinoflagellate.
The amphiesma consists of an outermost membrane, the outer plate membrane, which is a continuous membrane surrounding the alveoli or thecal vesicles, the thecal plates (in blue), a pellicular layer and the cytoplasmic membrane. The alveoli contain cellulose that is mainly deposited in the thecal plates. Figure published in Kwok & Wong, 2003.

The amphiesma is a dynamic structure that undergoes several rearrangements during the dinoflagellate life cycle. During vegetative growth, following cell division, each daughter cell inherits half of the parental theca in a process known as desmoschisis. Although the mechanism underlying the generation of the new theca is not fully understood, studies in *Crypthecodinium cohnii* (*C. cohnii*) and *Glenodinium foliaceum* have shown that synthesis of cellulose, the major component of the thecal plates, and its incorporation into thecal plates is upregulated in G2/M and continues during G1 phase, following cytokinesis as the two daughter cells emerge from the mother theca. In these species, production of cellulose dropped at the end of S-phase in preparation for mitosis and cell division (Bricheux et al., 1992; Kwok & Wong, 2003).

In many dinoflagellate species, the amphiesma, including the outer membrane and the amphiesmal vesicles, can be entirely shed in a process known as ecdysis. During this process

fusion of inner amphiesmal vesicles produces the new plasma membrane (Berdieva et al., 2019). Ecdysis is not associated with cell division and can be induced by different environmental stresses. Ecdysis seems to be an initial step in the formation of both temporary and resting cysts and often precedes the formation of a pellicle (Bravo & Figueroa, 2014).

1.4.4 Plastids

Plastids are organelles that are thought to have originated from red algae via secondary endosymbiosis (Falkowski, 2004; Keeling, 2004). In dinoflagellates however this ancestral plastid was replaced several times by repeated endosymbiotic events. At least five different kinds of plastids have been identified in dinoflagellates, each with its own evolutionary history, making these organisms the group with more plastid endosymbiotic events among eukaryotes (Hackett et al., 2004)

Plastids are an interesting feature of dinoflagellates; they produce pigments used in photosynthesis and that give to cells the golden-brown color characteristic of many dinoflagellates (Zapata et al., 2012). Plastids are also essential for symbiotic associations with other organisms such as corals and loss of plastid-bearing symbionts leads to coral bleaching (Waller & Kořený, 2017). Dinoflagellate plastids are also involved in the generation of dimethyl sulfide emissions, gases that play an important role in cloud formation and drive important climatic processes, including those over terrestrial habitats (Charlson et al., 1987).

Most photosynthetic dinoflagellates contain chlorophylls a and c (in chloroplasts), the carotenoid beta-carotene and a group of xanthophylls unique to dinoflagellates: the well-studied peridinin, and the less described dinoxanthin and diadinoxanthin. Peridinin plastids are cellular organelles composed of three stacks of thylakoids and containing chlorophyl a and c along with the characteristic peridinin, from which the plastid gets its name (Schnepf & ElbräChter, 1999). Having been found exclusively in dinoflagellates, peridinin plastids are considered as the archetypical plastid and an ancestral feature of dinoflagellates (Patron et al., 2005; Eberhard Schnepf & ElbräChter, 1999).

1.5 Phylogenetic classification of dinoflagellate

The current eukaryotic tree of life aims to integrate earlier morphological and biochemical information with the results of more recent phylogenomic analysis (Burki et al., 2020). The last eukaryotic classification recognizes seven supergroups, one of which referred to with the acronym TSAR includes three major groups: Stramenopila, Alveolate and Rhizaria and a minor group of single celled non-flagellated organisms, Telonemia (Figure 6).

The TSAR supergroup is estimated to include as many as 50% of all eukaryotic species (Strassert et al., 2019).

Within TSAR, alveolates represent one of the most biologically diverse group of eukaryotic microorganisms, comprising a total of ~17000 named species in the Open Tree Taxonomy (Hinchliff et al., 2015). It is a monophyletic supergroup which includes ciliates, apicomplexans, dinoflagellates and other minor groups (i.e., *Perkinsids, Colpodellids*, and *Chromera*). Dinoflagellates include exclusively aquatic unicellular organisms, apicomplexans are mostly non-flagellated intracellular parasites, like the malaria-causing *Plasmodium,* (Coombs, 1998), and ciliates are the most diverse group, characterized by a distinctive cytoskeleton with several cilia and associated root system (Katz, 2001).

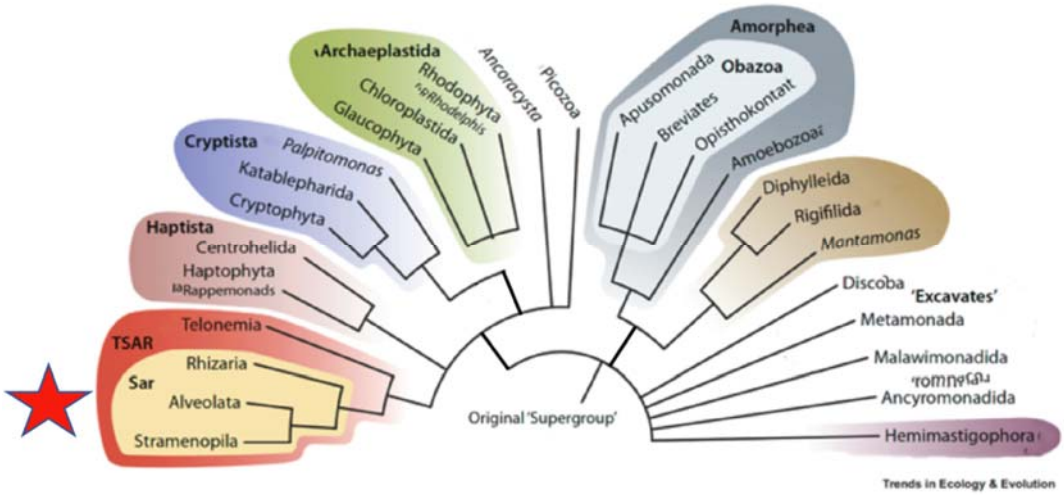

Figure 6. Phylogenetic position of alveolates in the eukaryotic tree.
Colored groupings correspond to main recognized supergroups. The monophyletic TSAR (Telonemia, Stramenopila, Alveolata and Rhizaria) group is colored in red and marked by a red star. The tree shows the phylogenetic relations within the monophyletic TSAR supergroup. Telonemia is a small group at the base of the known SAR. Stramenopila and Alveolata are sister groups and Rhizaria is an outer group to both of them. The Figure was adapted from (Burki et al., 2020).

Within TSAR, dinoflagellates are more closely related to apicomplexans than to ciliates. Dinoflagellates and apixomplexans, have plastids, and most share a bundle or cone of microtubules at the top of the cell (Gould et al., 2008). Molecular phylogenetic analyses of several different protein genes have confirmed their closest relation than with ciliates (Fast et al., 2002; Leander & Keeling, 2004).

The monophyletic group of dinoflagellates is estimated to contain approximately 4500 species assigned to more than 550 genera (Saldarriaga & Taylor, 2017). The dinoflagellate lineage (Figure 6) consists of an outlying ‘primitive’ genus – *Oxyrrhis* and two major clades:

Syndiniales and core dinoflagellates. Because of significant differences in important dinoflagellate features such as flagellation (no typical dinoflagellate transverse flagellum), nuclear organization (e.g., an intranuclear mitotic spindle) and position in molecular phylogenetic analyses, *Oxyrrhis* is classified as pre-dinoflagellate or 'protalveolate' (Cavalier-Smith & Chao, 2004; Lowe et al., 2011).

Syndiniales, *Syndinea* or *Syndiniophyceae* are naked (no theca) parasitic dinoflagellates with two dissimilar flagella typical of dinoflagellates. *Syndiniales* are multinucleated in their trophic form and do not have a dinokaryon; their low number of chromosomes are condensed only during mitosis (Fukuda & Suzaki, 2015; Soyer & Haapala, 1974).

The core dinoflagellates instead are characterized by the presence of a dinokaryon. In place of the canonical nucleosomes present in other eukaryotes, the dinokaryotic chromosomes contain 'dinoflagellate/viral nucleoproteins' (DVNPs) and HLPs, highly basic proteins that bind DNA with similar affinity to histones. These proteins are thought to be responsible for chromosome condensation through the core dinoflagellate cell cycle (Fukuda & Suzaki, 2015).

The evolutionary relationship between different core dinoflagellate species was initially evaluated based on morphological and cytological characters, such as number and pattern of thecal plates, flagellar organization or nuclear features. Based on the presence or absence of the theca, the core dinoflagellates were distinguished into thecate and athecate. In early classifications, these two groups were not clearly separated and naked species were found at different positions within the tree, suggesting that the thecal plates had arisen multiple times during dinoflagellate evolution. However, recent molecular phylogenetic analysis of large datasets corresponding to all major core dinoflagellates showed that athecate are a paraphyletic group to thecate. Based on this study, thecates are monophyletic and evolved from a common athecate dinoflagellate ancestor through the acquisition of genes involved in cellulose biosynthesis (Janouškovec et al., 2017).

Based on tabulation patterns, thecates have been traditionally divided into 4 orders: Dinophysiales, Gonyaulacales, Peridiniales, and Prorocentrales. Janouškovec et al., (2017), used dataset of dinoflagellate transcriptomes to validate the tabulation patterns and inferred a strongly supported phylogeny to map major morphological and molecular transitions in dinoflagellates. Accordingly, 5 main thecate lineages were identified (Figure 6): Gonyaulacoid, Dinophysoid, Prorocentroid, Symbiodiniaceae and Peridinioid. All these orders, with the exception of *Symbiodiniaceae,* belong to the class Dinophyceae.

Prorocentroid or Prorocentrales are characterized by two flagella inserted apically, rather than ventrally as in all other groups (Murray et al., 2009).

Dynophisis includes species characterized by a polarized cell morphology where the hypocone occupies the major part of the cell while the hypocone represents around 1/10 of the cell. Their theca is divided in half by a sagittal fission suture (Gómez et al., 2011).

Symbiodiniaceae includes the most prevalent group of endosymbiotic dinoflagellates and one of the most studied group of dinoflagellates, *Symbiodinium*. Several published genomes are available for this group.

Finally, most thecate dinoflagellates (both living and fossil) belong to the groups of Gonyaulacales and Peridiniales. These two different orders are not closely related but share tabulations involving five to six latitudinal series of thecal plates (Janouškovec et al., 2017).

The Peridiniales, abundant in the plankton, have endosymbiotic plastids derived from diatoms, characterized by the presence of signature diatom pigments such as fucoxanthin as well as chlorophyll c2 (Tamura et al., 2005).

The Gonyaulacales possess similar plastids than *Peridiniales*, but can be distinguished because of their armored asymmetrical plate pattern with an arrangement that lacks the typical canal plate of the Peridiniales (Not et al., 2012). *Ostreopsis* cf. *ovata*, a species responsible for seasonal blooms along the Mediterranean coast and the organism studied in this manuscript, belongs to the Gonyaulacales (Figure 7).

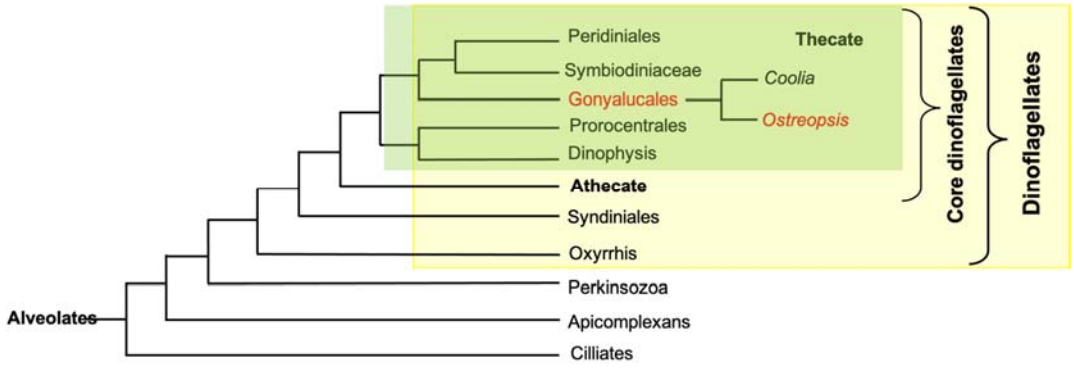

Figure 7. Phylogenetic tree of dinoflagellates showing main thecate orders and the position of Ostreopsis cf. ovata. Alveolates include ciliates, positioned at the base of the tree, apicomplexans and dinoflagellates, which are more closely related to each other than ciliates. Dinoflagellates are shown in a yellow rectangle. Oxyrrhis was included as deep branch of dinoflagellates and Syndiniales as a sister group to the core dinoflagellates. Core dinoflagellates branch in two groups: athecate and thecate (green rectangle). Only orders that belong to thecate dinoflagellates are indicated. Dinophysis is placed at the base of all thecates (Gonyaulacales) with low support. The position of Prorocentrales is also uncertain. The branching order of the core thecate lineages is well established: the Gonyaulacales branch early, and the Symbiodiniaceae are always late-branching within the thecates and consistently recover close to the Peridiniales. The family Symbiodiniaceae includes the clades Symbiodinium, Polarella, and their modern relatives to distinguish them from the exclusively fossil Suessiaceae

(Suessia and related forms) which is not included in the tree (Janoškovec et. al., 2016). Figure adapted from Janoškovec et al., 2016.

1.6 *Ostreopsis* cf. *ovata* blooms

The genus *Ostreopsis* has been identified mainly in tropical and sub-tropical waters of South and Central America, Asia, North Africa and Europe (reviewed in Parsons et al., 2012). Based on morphological features as tabulation patterns and cell size (Gómez, 2015), 9 different species of *Ostreopsis* have been identified: *O. ovat*a , *O. lenticularis* (Fukuyo, 1981), *O. heptagona* (Norris et al., 1985), *O. labens* (Faust & Morton, 1995), *O. mascarenensis* (Quod, 1994), *O. belizeanus, O. caribbeanus* and *O. marinus* (Faust, 1999) and more recently, *O. fattorussoi* (Accoroni et al., 2016; Chomérat et al., 2019).

Among those, *O.* cf. *ovata* is considered the most abundant and widely distributed benthic dinoflagellate in the Mediterranean Sea (Ninčević Gladan et al., 2019). *O.* cf. *ovata* was first observed along the coast of Villefranche-sur- Mer (France) in 1972 (in: Blanfune et al., 2012) and, then in 1994, along the Tyrrhenian shore in Italy (Tognetto et al., 1995). However, it was not until the end of the 1990s that massive blooms were reported in a number of coastal sites along the Mediterranean coast, in France, Italy, Monaco, Lebanon, Algeria, the Catalan sea, Tunisia, Balearic Islands, Egypt (reviewed in Ninčević Gladan et al., 2019). Since then, reports of *O.* cf. *ovata* blooms have been recurring every summer with increasing geographical distribution (Rhodes, 2011).

O. cf. *ovata* is a benthic dinoflagellate, epiphytic on red and brown seaweeds and on rocks, sand, mussel shells and benthic invertebrates (Ballantine et al., 1988). It produces a brownish mucilaginous film in which the cells are suspended in the water column near the surface (Figure 8). Cells and associated toxins released by cell lysis from *O.* cf. *ovata* can be trapped in the mucus or aerosolized in sea spray (Amzil et al., 2012).

O. cf. *ovata* produces PLTX in low quantity and PLTX-L as ostreocin, mascarenotoxin and their main toxin, ovatoxin (OVTX) in amounts that impact the marine environment at different trophic levels with subsequent repercussions on the structure of the ecosystems (Figure 8). Humans can also be affected either by direct contact or through vectorial intoxication through the consumption of contaminated seafood (Pavaux et al., 2020).

The impact of *O.* cf. *ovata* blooms on humans and animals has been described since the first decade of 2000 (reviewed in Pistocchi et al., 2011). Mortality of benthic organisms and human health problems broke out in summer 2005 with an extensive phenomenon along the Ligurian coast, where hundreds of people exposed to marine aerosol during recreational

activities required medical care due to symptoms that mainly affected the respiratory apparatus. This event coincided with intense proliferation of *O.* cf. *ovata* that reached concentrations up to 10^6 cell/ml near the coast of Genoa (Mangialajo et al., 2008).

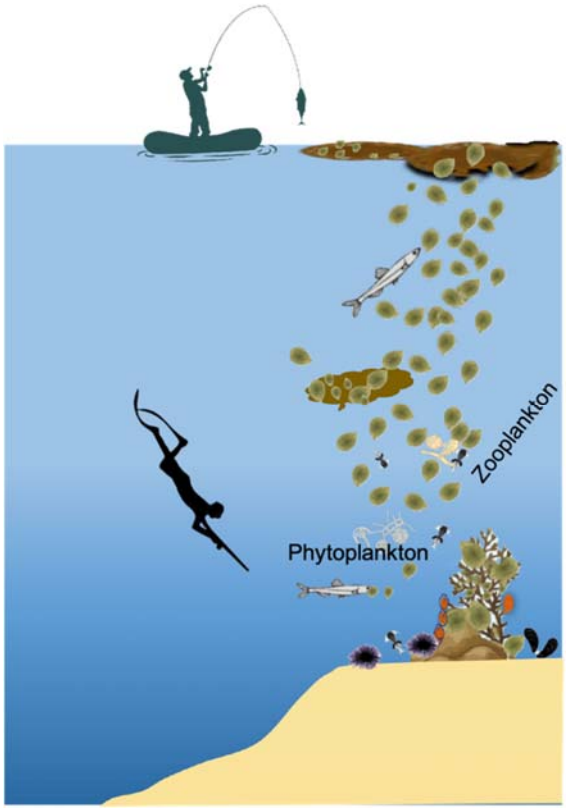

Figure 8. Relationship between the toxic dinoflagellate *Ostreopsis* spp. and other organisms co-occurring in the same environment.
O. cf. *ovata* cells release mucilaginous material (brown cloud in the water column and the surface) where primary producers and toxins can be trapped. Bioaccumulation of *O.* cf. *ovata* cells and toxins in organisms at different trophic levels makes those organisms vectors for toxin transfer to higher trophic levels, including animals like fish, mussels, sea urchins and humans. Human activities (e.g. fishing, spearfishing, diving, snorkeling, freediving) are another source of toxin exposure. Figure modified and adapter from (Pavaux, 2019).

The first sanitary report involving *O.* cf. *ovata* in France dates back to August 2006, when four divers were affected after diving close to Marseille. In general, human symptoms shown by patients exposed to *O.* cf. *ovata* blooms include high fever associated with serious respiratory distress such as watery rhinorrhea, dry or mildly productive cough and bronchoconstriction. Conjunctivitis and skin irritation have also been observed. Some cases require extended hospitalization, but generally symptoms are not durable and are resolved without hospitalization (Tichadou et al., 2010). The economic cost of *O.* cf. *ovata* blooms in France has been estimated at several hundred thousand to several million euros from lost tourism (Lemée et al., 2012).

Despite the enormous impact of *O.* cf *ovata* blooms on the environment and on public health and the dramatic increase in the number of toxic events in the last two decades, the processes underlying bloom initiation, maintenance and termination remain poorly understood. Several field studies have analyzed the environmental conditions that contribute

to *O. cf. ovata* bloom development, but how these stimuli affect cell proliferation and are translated into the explosive increase in cell concentration observed during blooming is not been addressed. This is particularly difficult due to the limited information available on the modes of proliferation and cell division of *O.* cf. *ovata* and of dinoflagellates in general.

1.7 General features of *Ostreopsis* cf. *ovata*

O. cf. *ovata* cells range in size between 20 and 80 μm. Morphologically, the cells have a teardrop shape with a pointy ventral side and rounded dorsal side (Figure 9A). The cell body is flattened along the anterior-posterior axis. An elongated nucleus, visible by fluorescent staining, is located it the dorsal area during interphase, within the epicone (Figure 9B). Similarly to other eukaryotes, the smooth endoplasmic reticulum is continuous with the outer membrane of the nuclear envelope. The cytoplasm contains several rounded translucent bodies containing lipids, which hide all other cellular structures when observed under light microscopy (Figure 9A and 9C), as well as several mitochondria with tubular cristae and plastids, which give the organism its brownish color (Figure 9C) (Honsell et al., 2013). Chloroplasts, which are bigger than other plastids, are generally present near the periphery of the cell.

In the ventral side of the cell, there is an array of vesicles filled with fibrous mucilaginous material composed of acidic polysaccharides, known as mucocyst. These vesicles secrete the mucilage or mucus through a large canal that opens in the ventral part of the cell. The mucus has a role of adhesion allowing *O.* cf. *ovata* cells to colonize benthic substrates (Ternon et al., 2020) and underlies the formation of aggregates containing many cells which float in the water column during *O.* cf. *ovata* bloom and confer an unpleasant aspect to seawater (Figure 9E).

The longitudinal flagellum is inserted in the sulcus in the ventral area, where the basal bodies are probably located. The transversal flagellum lies in the cingulum, a narrow and straight groove that surrounds the cell. Strands of parallel microtubules run transversally in the groove of the cingulum. The cingulum converges in the posterior end of the sulcus, in the ventral area (Figure 9F). The sulcal groove runs obliquely from the left side of the ventral area into the hypotheca. Based on their position relatively to the sulcus and the cingulum, the thecal plates are defined as sulcal plates and cingular plates (Figure 9G).

Aside from the parallel microtubule of the cingulum, cortical microtubules *O.* cf. *ovata* were described in interphase *O.* cf. *ovata* cells (Escalera et al., 2014). To date, there is no available information about the changes in microtubule organization associated with cell

division or with other stages of the life cycle of *O.* cf. *ovata*. Other cytoskeletal elements have also not yet been described for this organism and are generally not well known in dinoflagellates.

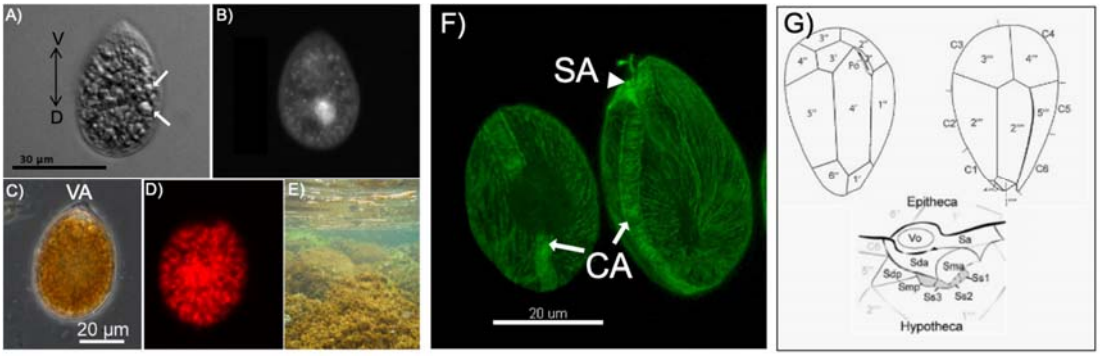

Figure 9. Cellular features of *Ostreopsis cf. ovata*.
A) Bright field picture of O. cf. ovata. Arrows point to lipid bodies. All cells with the exception of G are oriented with the ventral side at the top and dorsal side at the bottom. B) Picture of cell stained with Hoechst to label DNA shows the nucleus in basal position. Multiple dots likely correspond to DNA from organelles as plastids and mitochondria. C) Bright field picture showing the typical brown color. D) Unstained cell, viewed by epifluorescence microscopy under blue excitation shows red autofluorescence. E) Typical O. cf. ovata bloom in the Mediterranean Sea. The macroalgal communities are covered by brownish O. cf. ovata biofilm and mucilaginous aggregates are visible floating at the surface. Image adapted from Mangialajo et al., 2017. F) Confocal image of cells with microtubules labeled with anti-ß tubulin antibody, showing the Sulcal Area (SA, arrowhead) and the Cingular Area (CA, arrows). Note that the Cingulum is defined by a strand of parallel microtubules. The cingulum and the sulcus converge at the ventral side. G) Schematic representation of thecal plates at the cingular area and at the sulcal area. The drawing in the upper left illustrates the plate pattern of the cingulum epitheca. The cingular hypotheca is shown in the upper right drawing. The bottom scheme shows the distribution of the sulcal plates. Plate1 that partially covers the sulcus is not completely illustrated; note that plates Ss1, Ss2 and Ss3, represented with dashed lines, are curved. Markedly curved plates are grey shaded. Sa, sulcalanterior plate; Sda, right anterior sulcal plate; Sdp, right posterior sulcal plate; Sma, anterior median sulcalplate; Smp, posterior median sulcal plate; Ss1-3, left sulcal plates; Vo, ventral opening; Vt, ventral tube. Schemes from Escalera et al. (2014).

Thesis objectives

Notwithstanding the enormous contribution of dinoflagellates as primary producers in all aquatic environments worldwide and their ability to give rise to massive proliferation underlying seasonal HABs, the biology of these organisms remains largely elusive. However, scientific interest in dinoflagellates has greatly risen in the last two decades due to the increased frequency and geographical distribution of HABs (Rhodes et al., 2011; Berdalet et al., 2016; Berdalet et al., 2017).

HABs are affected by many environmental variables and depend on community interactions and available resources. Those factors and their influence on dinoflagellate proliferation have been greatly studied. However, very little molecular and functional data about the mechanisms underlying cell division is currently available.

The objective of this work was to provide a cellular and molecular characterization of the mitotic cell cycle, which underlies cell proliferation during vegetative growth, for the cosmopolitan dinoflagellate *O.* cf. *ovata*. To reach this objective, I developed the following specific aims

1) To obtain a comparative description between wild bloom proliferation and *in vitro* proliferation of monoclonal cell strain MCV-054 (Chapter 2)
2) To describe the different phases of the vegetative cycle of *O.* cf. *ovata* and in particular the M phases with a focus on the microtubular apparatus (Chapter 3)
3) To build a *de novo* transcriptome and phase specific meta-transcriptome of *O.* cf. *ovata* vegetative cycle.

The second chapter of this manuscript shows that the strain MCV-054 has a similar growth rathe than *O. cf. ovata* during the proliferative phases over three consecutive blooms (2018-2020) in the Bay of Villefranche (PACA, France) and that cells divide exclusively at nights during the bloom.

During vegetative growth, typical of bloom development, *O.* cf. *ovata* divides by mitosis. I took advantage of the similarities between the culture and blooming cells and I used optimized immunofluorescence protocols and confocal microscopy to show that *O.* cf. *ovata* uses a dynamic microtubular apparatus to reposition its nucleus to the center of the cell, to segregate chromosomes in mitosis and to divide the cell during cytokinesis (chapter 3).

Finally using transcriptomic data, which I obtained form cultured *O.* cf. *ovata*, I identified a set of cell cycle regulatory proteins which are conserved between *O. cf. ovata* and three reference species: the yeast *Saccharamyces cerevisiae (S. cerevisiae)*, the green algae *Chlamydomonas reinhardtii (C. reinhardtii)* and one species of apicomplexa, the dinoflagellate sister group, *Plasmodium falciparum (P. falciparum)*. This analysis, which is reported in chapter 4, allowed to identify part of the molecular toolbox used for *O.* cf. *ovata* mitotic cell cycle. To determine whether transcriptional control underlies cell cycle progression in *O.* cf. *ovata* I generated metatranscriptomic datasets corresponding to different bloom phases and I used the knowledge generated in chapter 2, to obtain different cell cycle stages. I then analyzed whether any components of the *O.* cf. *ovata* toolbox were differentially expressed. This analysis suggests that there is transcriptional regulation in the transition from interphase to mitosis. Integration of the cytological description and of the molecular analysis provided a first description of mitotic progression in *O.* cf. *ovata*.

Chapter 2

Proliferation of *Ostreopsis* cf. *ovata* in culture and during the bloom

2.1 Introduction

2.1.1 Dinoflagellate cell proliferation

Marine organisms are exposed to different geological cycles, such as tides, lunar month, seasons and the diurnal cycle. These cycles influence and often regulate many biological processes at different time scales.

In dinoflagellates many biochemical and behavioral responses are controlled by the light-dark cycle, with varying periodicity; among others photosynthesis, bioluminescence, vertical migration and cell cycle progression.

If the periodicity of this cyclical variation is about 24 hours, those phenomena are said to be under circadian control (Mazuski & Herzog, 2015). However, if the periodicity is a multiple of 24 hours the cycle is said to be gated or phased by the dark-light cycle (diel-phased) (Wong & Kwok, 2005).

In dinoflagellates that show diel-phased cell cycles, cell division occurs only during a specific window of time, in a species-specific manner. If the periodicity of cell cycle transitions is maintained when cells are transferred from dark-light cycles to continuous light or continuous darkness, the cell cycle is said to be under the control of the circadian clock (Wang et al., 2008a; Wong & Kwok, 2005). This is the case for some dinoflagellates, like *Pyrocystis fusiformis* (Sweeney, 1982) and *Lingulodinium polyedrum* (Dagenais-Bellefeuille et al., 2008) which divide with a 24 hour period. However, most dinoflagellates have doubling times longer than 24 hours, with cell cycle durations varying among species and reaching even 5 to 6 days (Stolte & Garcés, 2006). In these species, cell division is often gated by the circadian cycle, with cell division taking place mostly during the dark phase. In these cells, mitosis and cytokinesis can only occur at night, but only cells that have reached minimal cell size and are at the appropriate phase in their cell cycle will commit to cell division each night (Wong & Kwok, 2005). The remaining cells will remain in interphase until the following window of opportunity in the next dark period. In *Lingulodinium polyedrum*, for example, only 40% of cells undergo mitosis each night, while the rest of the population remains in G_1 until the following night (Dagenais-Bellefeuille et al., 2008).

Although it is clear that dark/light transitions are key elements controlling dinoflagellate cell cycle (Vaulot et al., 1986; L.-H. Wang et al., 2008b; Wong & Kwok, 2005), the mechanism underlying circadian gating and linking the diel cycle with the cell cycle remain largely elusive.

2.1.2 Dinoflagellate growth rate

For unicellular organisms such as dinoflagellates, the generation of daughter cells through cell division, in the absence of negative factors, directly leads to population growth. The growth rate of a population, μ, provides a measure of this change in cell number over a specific period of time and it depends on the interaction between intrinsic organismal characteristics and environmental conditions.

Specific growth rate indicates the increase in cell number over time due exclusively to cell division and it is usually measured in culture, by counting cell numbers at specific time intervals (Grimaud et al., 2017). Studies of specific growth rate in different algal cultures showed that dinoflagellates generally have substantially lower specific growth rates than other phytoplanktonic organisms (Figure 10), such as diatoms (Banse, 1982) and ciliates (Strom & Morello, 1998). Several studies suggested that these lower growth rates can be attributed to the low photosynthetic capacity of most dinoflagellate species. Dinoflagellate specific growth rate have been estimated to range between 0.2 to 2 divisions per day, depending on species and culture conditions. For *O.* cf. *ovata* the specific growth rate calculated for culture cells ranges between 0.2 to 1.0 day^{-1} (Carnicer et al., 2016; Scalco et al., 2012).

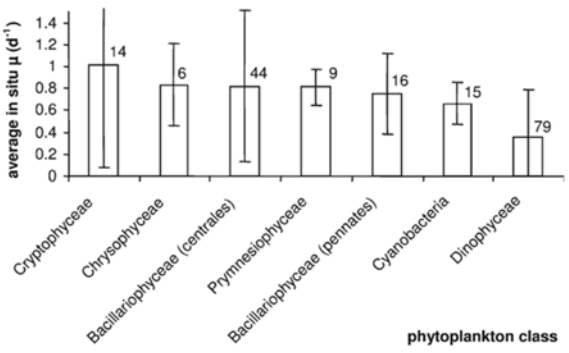

Figure 10. Low growth rate of dinoflagellates. Average in situ per capita growth rates (d^{-1}) with standard deviations for each phytoplankton class in descending order. The number of species considered stated above each column. Figure from Stolte & Garces, 2006.

In the wild, several factors, other than cell proliferation, contribute to changes in cell concentration. Grazing, predation, dispersion, encystment and cell death negatively influence growth of a population, whereas aggregation, cell migration and excystment contribute

positively. By taking into account the combined effect of all these contributing factors, the apparent or net growth rate provides a measure of the real changes in biomass of a species in a complex environment. For *O.* cf. *ovata* the net growth rates reported for several locations over several years range between 0.6 and 1.3 in the Adriatic Sea (Accoroni, Glibert, et al., 2015), while a maximum of 0.56 was reported in the Mediterranean Sea (Larvotto, Monaco) between 2007 and 2019 (Drouet, 2021).

2.1.3 Environmental parameters that regulate *Ostreopsis* cf. *ovata* proliferation

The rate of growth is influenced by several cellular parameters, such as phyletic differences and cell size, as well as by environmental conditions, such as nutrient availability, light irradiation, temperature and turbulence just to mention a few. Turbulence and nutrient limitation tend to inhibit growth, whereas light irradiation usually favors growth, particularly for autotrophic species, although few dinoflagellate species have been shown to grow in the dark if provided with prey to feed on (Hansen, 2011). However, the response of organisms to changes in environmental factors depends on the interaction between these factors creating a combinatorial effect, which makes dissecting individual contributions extremely complex.

Below I will briefly summarize our current understanding of the effects of specific parameters: temperature, hydrodynamics, nutrient availability, salinity, substrate and light, on the growth rate of *O.* cf. *ovata*.

Temperature

Several studies have analyzed the effect of temperature on *O.* cf. *ovata* growth both *in vitro* and *in situ* (Totti et al., 2010; Pistocchi et al., 2011; Tanimoto et al., 2011; Tawon et al., 2013; Tawon et al., 2015; Drouet, 2021). Although differences can be found depending on strains, isolates, environmental condition, sampling year and location, there is general agreement that, as for other dinoflagellates, seawater temperature is the major factor influencing *O.* cf. *ovata* growth (Pistocchi et al., 2011), with optimal growth temperature -*in situ*- ranging between 22ºC and 27ºC (Tanimoto et al., 2013), with species from Thailand and South China Sea tolerating temperature up to 32.5ºC (Tawong et al., 2015). Indeed, in the Mediterranean Sea, the presence of *O.* cf. *ovata* has been recorded from June to November when sea temperature ranges between 19 and 28ºC, with blooms occurring in early summer in the Ligurian Sea and in late summer in the Adriatic and Aegean Sea. Long-term survey of water temperature in the Conero Riviera (northern Adriatic Sea) before, during and after *O.* cf. *ovata* blooms, showed that bloom onset occurs always at temperatures above 25ºC,

whereas the lowest temperature recorded was always associated with the decline of the bloom (Totti et al., 2010).

Recently, Drouet et al. (2021) evaluated the relationship between temperature and bloom phenology (timing, length and maximum cell abundance) during *O.* cf. *ovata* HABs at different locations along the Mediterranean coast. Consistently with earlier analysis the highest growth rates were observed at temperatures between 21ºC and 25ºC, with a maximum of 0.53 day^{-1} occurring at 24ºC.

In vitro, *O.* cf. *ovata* has been reported to grow in a wide range of temperature ranging from 19ºC to 30ºC, with the lowest growth rate reported for a Brazilian strain grown at 24ºC (0.22 div day^{-1}) (Nascimento et al., 2012), and the highest growth rate observed for a Japanese strain grown between 25ºC and 30ºC (1.03 div day^{-1}) (Yamaguchi et al., 2012). Although optimal growth temperatures observed in laboratory tend to be similar to those observed *in situ*, shifts has been observed, potentially due to the effect of environmental parameters affecting *in situ* growth rates (Drouet 2021).

Hydrodynamics

It is generally accepted that *O.* cf. *ovata* proliferates mainly in calm and shallow waters, with stormy events causing a sudden decrease in cell abundance and arrest of cell proliferation, which then starts up again after some days of calm sea conditions (Shears & Ross, 2009; Totti et al., 2010). Comparative studies of cell abundance in sheltered and exposed sites showed higher cell concentration in sheltered location (Accoroni et al., 2011, 2012; Mabrouk et al., 2011; Shears & Ross, 2009; Totti et al., 2010). However, analysis of *O.* cf. *ovata* cell concentration in sheltered and exposed sites at different bloom phases along the Conero Riviera in 2009 and 2010, showed higher concentrations in sheltered sites only during the proliferative phase, suggesting that hydrodynamics affect cell abundance mainly during periods of active cell division.

In vitro, cultured *O.* cf. *ovata* cells grown under constant agitation and in static conditions had comparable growth rates (0.32 d^{-1} and 0.39 d^{-1} in control and turbulence, respectively, (Berdalet et al., 2017). However, the proliferative phase of static grown cultures lasted twice that of cultures grown under continues agitation, supporting a negative effect of turbulence on cell proliferation.

Nutrients, salinity and substrate

O. cf. *ovata* is thought to be a mixotrophic dinoflagellate (Burkholder et al., 2008) that grows in both eutrophic (Accoroni et al., 2011) and oligotrophic (Shears & Ross, 2009) areas. The information available on the impact of nutrient availability of *O*. cf. *ovata* growth is scarce and therefore the role of nutrients in bloom development is still uncertain. Few *in situ* studies showed that for *Osteropsis spp*., cell abundance generally negatively correlates with nitrate, phosphate and silicate concentrations (Parsons & Preskitt, 2007; Cohu & Lemee, 2012). However, several field studies in the Mediterranean Sea showed no correlation between *O*. cf. *ovata* proliferation and concentration of inorganic nutrients (Accoroni et al., 2011). *In vitro* studies instead, showed that exposure to limiting levels of either nitrogen or phosphorus reduces growth rate (Vanucci et al., 2012), with a more marked effect at higher temperatures (Vidyarathna & Granéli, 2013).

The influence of salinity on *O.* cf. *ovata* proliferation has been evaluated during the bloom (Accoroni, Percopo, et al., 2015; Parsons & Preskitt, 2007), providing inconclusive results as the effect of salinity seems to vary according to species and geographical areas.

Although it is thought that *O.* cf. *ovata* proliferates preferentially on epiphytic macroalgae, it is found on both abiotic and biotic substrates, including rocks and pebbles (Totti et al., 2010), soft sediments (Vila et al., 2001b), mollusks and other marine invertebrates (Bianco et al 2007), as well as free living in the water column (Accoroni et al., 2011).

Light

O. cf. *ovata* cells are found generally in shallow waters between 0.5 and 1 meters and their abundance then decreases sharply with depth. This distribution is likely related with light availability as both intensity and spectral quality of light change with depth in the water column. Moreover *O.* cf. *ovata* HABs occur during the summer when the illumination period is more than 12 hours long. Consistently, *in vitro* studies showed that *O*. cf. *ovata* growth decreases with low light intensities (Monti & Cecchin, 2012; Yamaguchi et al., 2014), and stops below 10 µmol photons/m^2/s. Growth is also inhibited at high photon flux density, although there are discrepancies in the literature as of the upper limit of light intensity compatible with cell growth, varying between 100 µmol photons/m^2/s and 263 µmol photons/m^2/s (Yamaguchi et al., 2014), depending on the study.

In summary, in the sea optimal growth conditions for *O*. cf. *ovata* are between 21ºC and 28ºC, in well-lit, shallow and sheltered waters. *In vitro*, where cells are grown under controlled conditions, cells are generally grown at temperature between 21-18ºC depending on the study, with 12 to 14 hours of light exposure in sea water with salinity of 38 g/L supplemented with nutrients (nitrates, phosphates, vitamins and metal traces). In the work presented here, I maintained cells at 22ºC, with a light:dark cycle of 14:10 hours.

2.1.4 *Ostreopsis* cf. *ovata* life cycle

The life cycle of benthic dinoflagellates is poorly understood, despite the clear contribution of different life cycle stages to HAB development. For *O.* cf. *ovata*, there are two studies that describe its sexual and asexual reproduction as well as characteristics of the cyst (Accoroni et al., 2014; Bravo et al., 2012). Based on morphological features and on the characteristic position of the nucleus within the cell, Bravo et al. (2012) identified 5 phases during the vegetative cycle: (i) non-dividing cells, the most common morphotype in the population characterized by the nucleus in dorsal position; (ii) pre-dividing cells, recognized by the central position of the nucleus; (iii) mitotic or karyokinetic cells, recognized by two nuclei within the same cell; (iv) cytokinetic cells, binucleated cells with a partition wall; and (v) post-dividing cells recognized by the presence of the nucleus in lateral position. Quantification of the different morphotypes during the proliferative phase of the 2010 *O*. cf. *ovata* bloom (Mediterranean Sea, Catalan coast) identified a single peak of division during the night.

During the vegetative cycle, cells divide by desmoschisis in the sagittal (dorsal-ventral) plane. During sexual reproduction instead two gametes fuse to form a zygote. For *O*. cf. *ovata* gamete fusion has been observed both in culture and *in situ*. Putative mating gametes can be distinguished from asexual dividing cells, as vegetative division always occurs in the sagittal plane (Figure 11A), while gametes are either joined at the epitheca, with the point of attachment positioned centrally (Figure 11B) or laterally with perpendicular cingula (Accoroni et al., 2014). Moreover, prior to cell division, asexually dividing cells can be recognized by the presence of two nuclei in a single theca (Figure 11C), while pairing gametes have two thecae (one from each gamete), each with its own nucleus (Figure 11D).

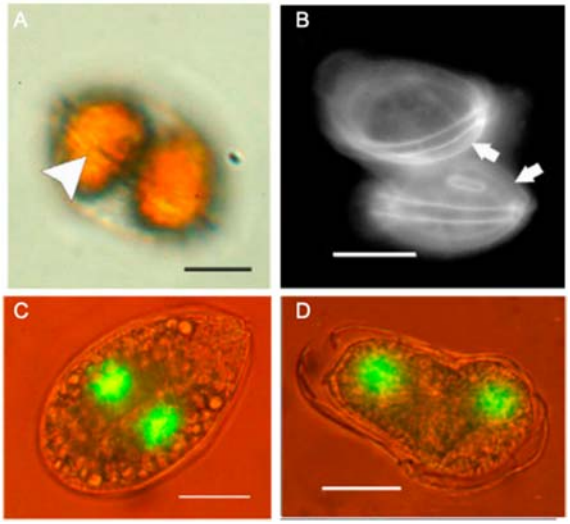

Figure 11. Asexual and sexual stages of *Ostreopsis cf. ovata.*
Main differences between asexual (A, C) and sexual life (B, D) stages of O. cf. ovata. A) Arrowhead points to the cingulum in a cultured dividing cell seen from a dorsal view; B) cultured mating gamete pair attached by epithecas (arrows); C) double-nucleated cells with slight indications of a partition wall, likely in mitosis; D) cultured mating gamete pair. Adapted from Bravo et al., 2012.

As described in Chapter 1, following gamete fusion, the planozygote can either undergo meiosis and re-enter the vegetative cycle or alternatively can differentiate into a resting state known as cyst (Figure 12). Both pellicle cyst and thin-walled cysts had been observed *in vitro* and in natural population. *In vitro*, cyst formation was induced by incubation in nitrogen poor medium. Excystment could be induced by inoculation into rich medium containing nitrogen at 25ºC (Accoroni et al., 2014), but not at 21ºC, suggesting that temperature may be a major factor in the onset of *O.* cf. *ovata* bloom.

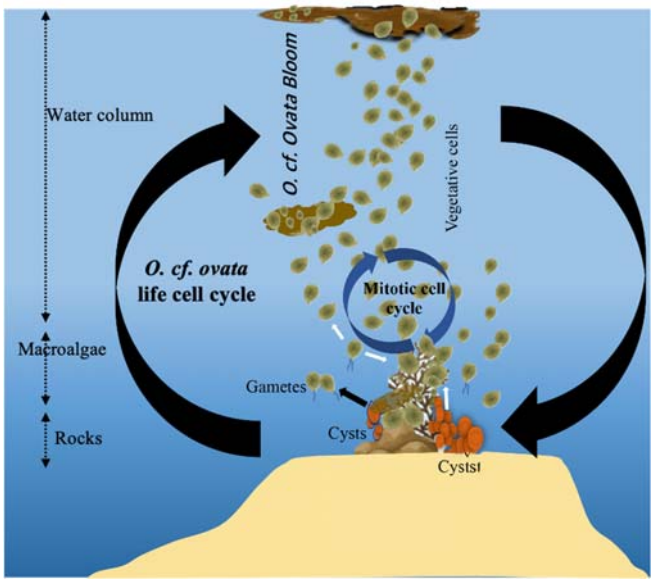

Figure 12. Graphic representation of *Ostreopsis cf. ovata* life cycle and its relation with the bloom.
Pellicle cysts, resting cysts and planozygotes are source of vegetative cells (white arrow). Vegetative cells divide by mitosis (blue circle), mostly in the benthos, increasing cell population; mucus produced by O. cf. ovata during the bloom (brownish clouds) can be found in the benthic niche attached to the macroalga, in the water column and in the surface. Gametes are represented by cells with one flagellum and paired gametes are represented by cells with two flagella. Schematic representation without scale.

In order to study dynamics of *O.* cf. *ovata* proliferation, I measured and compared the growth rates of cells *in vitro* and *in situ* to determine how the growth of *O.* cf. *ovata* compares in cultures and in the wild and whether the proliferation dynamics observed during the bloom could be recapitulated *in vitro*.

For *in vitro* studies, I used a monoclonal culture, MCCV054, obtained from the Mediterranean Culture Collection of Villefranche-sur-Mer (MCCV), EMBRC-France. The strain was originally established by the Lemée team (LOV/UMR7093) from sea samples collected during the *O.* cf. *ovata* bloom in 2014. *In situ* sampling of *O.* cf. *ovata* bloom was carried out for three consecutive years (2018-2020) in collaboration with the team of dr. Lemée. For the analysis reported in Figure 14, I used long-term data for cell abundances obtained by the Lemée team. Otherwise, I performed all the experiments and analysis described in this chapter. Here I show that under the culture conditions used in the lab, strain MCCV054 grows with a similar rate of division to those observed *in situ*.

The description of *O.* cf. *ovata* cell proliferation in the wild described below is part of a manuscript in preparation: "Vertical distributions of *Ostreopsis* cf. *ovata* in NW Mediterranean Sea: impact on monitoring strategy", presented in Annex 1.

2.2 Results

2.2.1 *Ostreopsis* cf. *ovata* proliferation *in vitro*

In order to determine the dynamics of *O.* cf. *ovata* proliferation *in vitro*, I quantified cell concentration in statically grown cultures of strain MCCV054 over a 22 day-long period and I compared its growth rate with that of single cell cultures isolated from proliferative phase flask-grown cultures.

For population growth rate, cell concentration was measured every 2 days in triplicates by counting the number of cells per milliliter. As shown in Figure 13, when cell concentration is plotted over time, three main phases can be recognized: a lag phase which lasts 6 days, a proliferative phase between day 6 – 16 and a stationary phase starting from day 16. An exponential phase could not be identified and based on cell concentration, following the initial dilution, the strain MCCV-054 duplicated only 2-3 times before entering the stationary phase. The average doubling time during the proliferative phase was 48 hours. The growth rate was calculated during the proliferative phase (day 6-16).

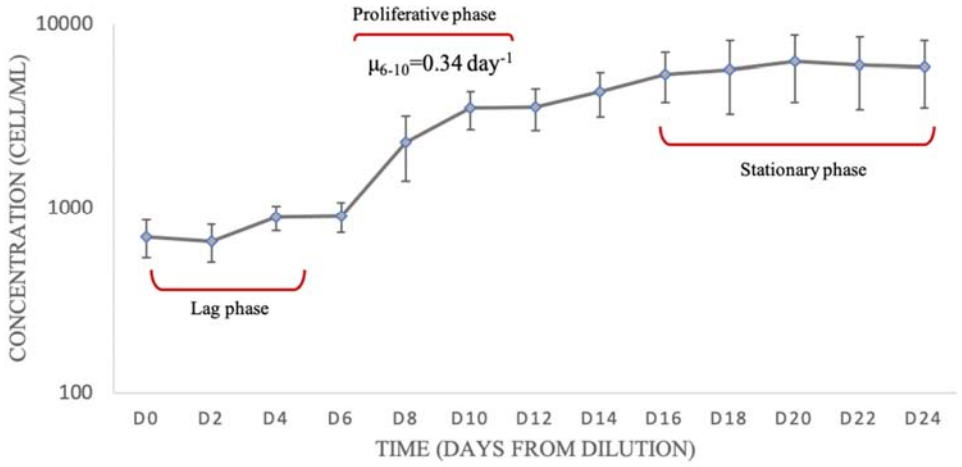

Figure 13. Growth curve of *Ostreopsis cf. ovata*, strain MCCV054,
maintained at 22oC with a light-dark cycle of 14:10 hours. The axes show cell concentration in a logarithmic scale and sampling day. Day 0 (D0) corresponds to the day when 26-days old cultures were diluted into fresh medium. Each data point corresponds to two biological repeats each one performed in triplicates. Standard deviation was calculated for each data point. Growth rate was calculated between day 6-10 for the proliferative phase.

A maximum growth rate, μ of 0.34 day^{-1} was observed between day 6 and day 10, whereas between day 12 and 16 the growth rate was reduced to 0.12 day^{-1}.

Single cell cultures were used to obtain an independent measurement of *O.* cf. *ovata* growth rates. To my knowledge, no such data is currently available for cultured *O.* cf. *ovata.* Single cells were isolated from flask-grown cultures during the proliferative phase, at day 7. Isolated cells were placed in conditioned medium, spent medium harvested from the original culture, to stop cells from entering lag phase. Cells were then observed each day for 4 days. I analyzed a total of 72 isolated cells. The mean growth rate calculated for those cells was 0.23 day^{-1} (mean ± 0.049, standard deviation). The growth rate in flask cultures calculated for the mother culture during the same period (day 7 to 11), was 0.2 day^{-1}. Thus, considering the growth rates measured for the strain MCCV054 grown at 22ºC with a light:dark cycle of 14:10 in L1 media has a doubling time of 2 to 3 days.

2.2.2 *Ostreopsis cf. ovata* proliferation during the bloom in Villefranche-sur-mer.

To determine how the growth of strain MCCV-054 compares with *O.* cf. *ovata* proliferation during the bloom, I then measured growth rate of *O.* cf. *ovata* in the wild. For this analysis I used benthic samples, associated with macroalgae (*Padina pavonica, Dictyota*

spp. and Halopteris scoparia), when analyzing samples I found a very limited number of cells present in the water column after sample processing. Samples were collected during three consecutive blooms, from 2018 to 2020 (Figure 14) in the Bay of Villefranche-sur-mer, Mediterranean Sea at depths included between 0.5 and 1 meter. Blooms always occurred at the end of June/ beginning of July, with a peak around 2-to-3 weeks after the onset of proliferation.

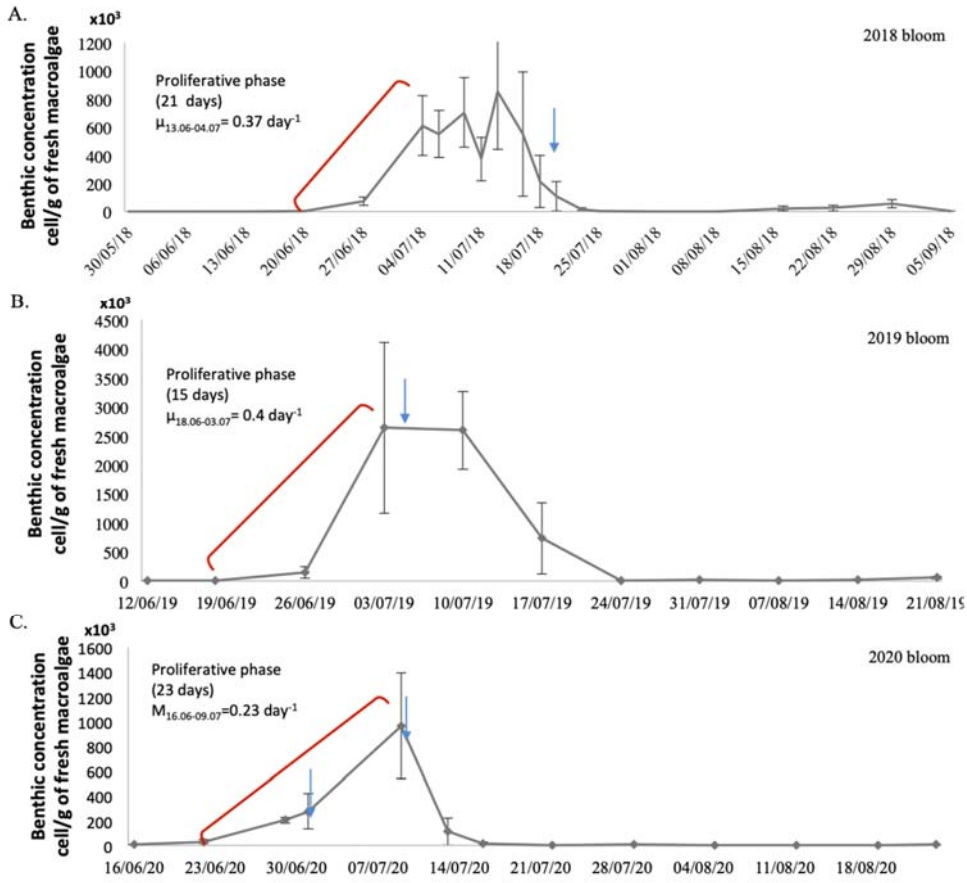

Figure 14. Evolution of cell concentration during *Ostreopsis cf. ovata* blooms at Rochambeau (Villefranche-sur-Mer, France) in 2018 (A), 2019 (B) and 2020 (C). Cell concentration (x- axis x103) in the benthos is reported for each sampling day. The mean of the cell concentrations at three sampling stations close to each other in the area of the bloom is reported for each time point. Standard deviation is reported.
The net growth rate, μ, was calculated for the proliferative phase, indicated by the red bracket.
The blue arrows indicates the dates of the intense over-night sampling performed during 2018 (A), 2019 (B) and 2020 bloom (C).

In 2018, the cell concentration in the benthos reached > 800.000 cell/g of fresh algae at the peak (Figure 14A, 13/07/2018). As shown in Figure 14A, the proliferative phase, defined as the period when the net growth rate remained above 0.1 day^{-1}, lasted 21 days. The net growth rate over the entire proliferative phase was 0.37 day^{-1}. In 2019 the proliferative

phase lasted 14 days, and cell concentrations raised above $2x10^6$ cells/g of fresh algae at the peak of the bloom (Figure 14B, 3-10/07/2018). The net growth rate for the proliferative phase in 2019 was 0.4 day^{-1}. In 2020, the benthic cell concentration increased for 23 consecutive days, reaching maximum abundances of 10^6 cell/g of fresh algae at the peak of the bloom (Figure 14C, 09/07/2020). In 2020 the mean net growth rate was 0.23 day^{-1}. For the 3 years 2018-2020, the doubling time of *O.* cf. *ovata* during the bloom varied between 2 and 3 days.

Comparison of the growth rates measured in culture for the strain MCCV-054 and the net growth rates measured *in situ* (table 1) showed no statistical difference (p-value = 0.4). Thus, strain MCCV-054 recapitulates the rate of proliferation for *O.* cf. *ovata* during the bloom.

Table 1: *Ostreopsis* cf. *ovata* growth rates *in situ* (net growth rate) and *in vitro*

	In situ			**In vitro**	
Origin of the cells	2018 bloom	2019 bloom	2020 bloom	Population (flask)	Single cell culture
Growth rate (day-1)	0.37	0.4	0.23	0.34	0.23

2.2.3 *Ostreopsis* cf. *ovata* divides during the night *in situ*

Having established that during the proliferative phase *O.* cf. *ovata* doubles on average every 2-3 days, I decided to perform a more detailed analysis to determine when cell division occurred in each cycle. In 2018 and 2019, I therefore performed frequent samplings for 3 consecutive days, every 4 hours. The 3-day period was chosen based on the pattern of the bloom, as I aimed at sampling at the end of the proliferative phase when the net growth rate is maximal. In 2018 sampling was performed between the 18th of July at 8:00 am and the 21st of July 8:00 am (Figure 15A). Due to adverse meteorological conditions prior to the day of sampling, however, the behavior of the bloom was altered and the sampling was performed during what later was identified as the senescence of the bloom. In 2019, frequent sampling was performed between 5th of July at 8:00 am and the 8th of July at 8:00 am, at the peak of the bloom as programmed (Figure 15A).

It was previously shown that in interphase cells the nucleus is located in dorsal position, whereas as cells prepare for mitosis the nucleus repositions to the cell center (Bravo et al., 2012). I therefore analyzed nuclear position in each sample, following staining with Hoechst-33342 to label DNA and classified cells in two groups: cells in interphase, with nucleus in dorsal position and cells in division, with nucleus in central position. As expected,

based on previous analysis (Bravo et al., 2012), dorsal nucleated interphase cells were the main phenotype in all samples and were almost exclusive in samples collected between 8:00 am and 20:00 (Figure 15B, C). Cells in division were found only in the night samples, which were collected at 00:00 and 4:00 am.

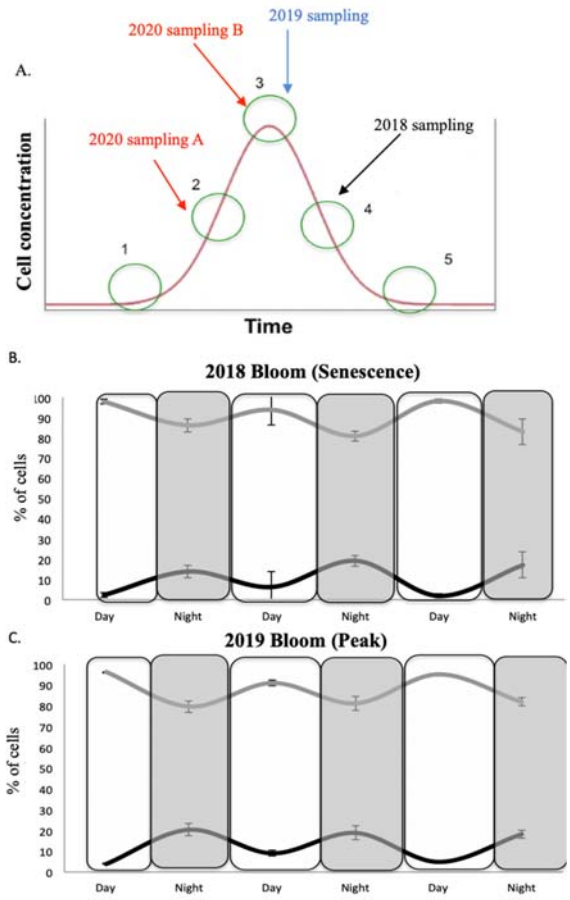

Figure 15. *Ostreopsis* cf. *ovata* divides during the night *in situ*.
A) Schematic representation of time of frequent sampling with respect to bloom phase in 2018-2020. B) Quantification of cells in interphase (gray curve) and cells in division (black curve) during the senescence phase of the bloom in 2018 and C) at the peak of the bloom in 2019. Results are shown as percentages of cells in each group (interphase or dividing) over the total number of cells analyzed in the same sample. Night (grey boxes) corresponds to 00:00 and 4:00 samples, whereas day (white boxes) includes all samples from 8:00 to 0:00. At each time points three samples corresponding to three sampling stations were analyzed and the mean is reported. Raw data is presented in annex 2, supplementary data, tables 1 and 2.

As shown in Figure 15, however, I found that only 20% of cells were in division each night. The percentage of dividing cells was similar in 2018 (Figure 15B) and 2019 (Figure 15C), despite the difference in bloom phase at time of sampling. This observation suggested that the same proportion of cells may undergo cell division throughout the bloom and that factors other than cell proliferation, contribute to the difference in net growth rate at different bloom phases. To test this hypothesis, I decided to compare cell division at different bloom phases within the same year. In 2020 therefore, I collected samples for two consecutive nights during the proliferative phase (June 26th - Figure 14C, left arrow) and at the peak of the bloom (July 06th - Figure 14C, right arrow). As shown in Figure 16A, dividing cells were more abundant during the proliferative phase (30.5 ±2.64%) than at the peak of the bloom (18.86

±5.31%; p value=0.039). Thus, although cell proliferation continues throughout the bloom, even when the net growth rate is negative, a higher growth rate is observed during the proliferative phase. To determine whether the measured growth rate is sufficient to explain *O.* cf. *ovata* proliferation during the bloom, I then, performed a simple simulation of cell growth considering a constant increase in cell population of 30% per day. As shown in Figure 16B, the increase in cell concentration predicted in the simulation overlapped that observed during the proliferative phase of the 2020 bloom. Thus, the increase in cell population observed during the proliferative phase of *O.* cf. *ovata* bloom in 2020 can be explained exclusively by cell division.

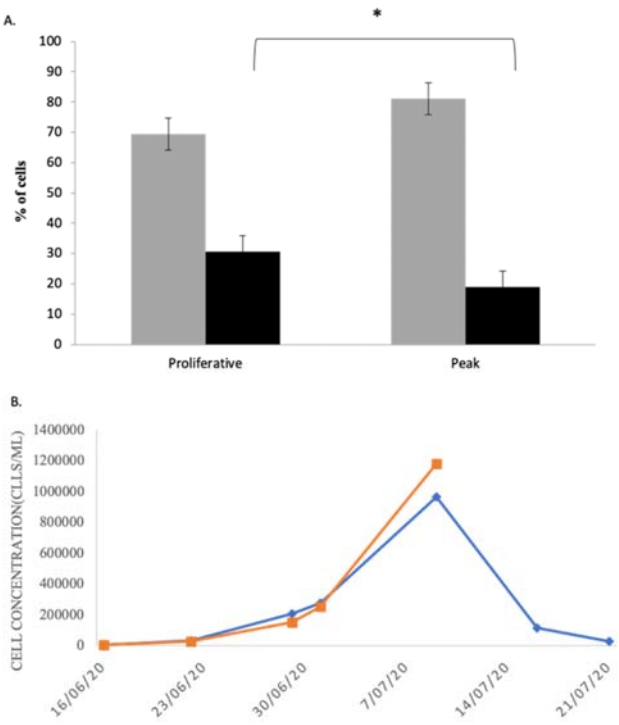

Figure 16. Cell division is reduced at the peak of the bloom compared to the proliferative phase.
A) Quantification of cells in interphase (grey) and in division (black) during the proliferative phase (left) and at the peak (right) of the bloom in 2020. *P<0.05. Raw data is presented in annex 2, supplementary data, tables 3A and 3B.
B) Comparison of changes in cell concentration observed during the bloom in 2020 (blue) and those predicted assuming a constant increase in cell concentration of 30% per day (orange).

Based on morphological features and on nuclear position (Bravo et al., 2012), *O.* cf. *ovata* cells undergoing division can be further subdivided into: pre-dividing cells, recognized by the central location of the nucleus (Figure 17B, G); dividing cells, which include mitotic (or karyokinetic) binucleated cells (Figure 17C, H) and binucleated cells undergoing desmoschisis, herein called cytokinetic cells (Figure 17D, I); and post-dividing cells recognized by the nucleus in lateral position (Figure 17E, J). To determine when cells underwent division during the night, I analyzed in more details cells in bloom samples for all three years (2018-2020) and classified them based on the characteristics described above.

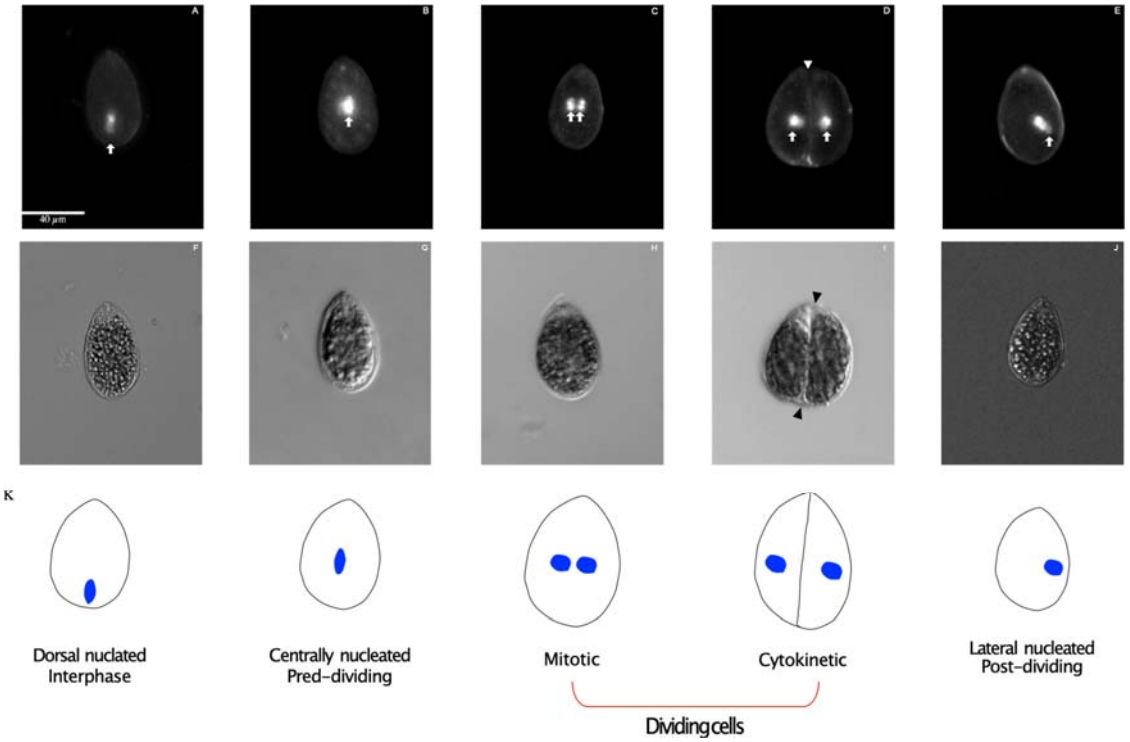

Figure 17. Nuclear position changes during the mitotic cycle in *Ostreopsis* cf. *ovata*.
A-E) Representative pictures of Hoechst 33342 stained vegetative cells and F-J) corresponding brightfield pictures. Arrows mark the position of the nucleus. Arrowhead point to site of cytokinesis, along the longitudinal axis. Cells were sampled during the bloom in 2018. K) Schematic representation of cells at each stage. Scale bar is 40 µm

Figure 18 shows the distribution of cells at different stages of division over three consecutive day-night cycles during the blooms in 2018 (Figure 18A) and 2019 (Figure 18B). In both years pre-dividing cells first appeared at 20:00 and peaked between 20:00 – 0:00. This peak preceded division which was more intense between 0:00 – 4:00 am, although a clear peak was not detected. Post-dividing cells then reached their maximum between 4:00 – 8:00 am. This analysis indicates that cell division occurs between 00:00 and 8:00 am. However, the lack of a clear peak of dividing cells indicates that either cell division occurs throughout the night, or that the sampling was too sparse and I missed the peak of division. To distinguish between these two possibilities in 2020 I sampled only between 18:00 and 6:00, every two hours, both during the proliferative phase (Figure 19A) and at the peak of the bloom (Figure 19B). As shown in Figure 19 no clear peak of division was observed in either phase, suggesting that mitosis and cytokinesis occur between mid-night and dawn. Alternatively, it is still formally possible that in this species cell division (mitosis and cytokinesis) is extremely fast and to detect a peak of division hourly (or even more frequent) sampling would be required.

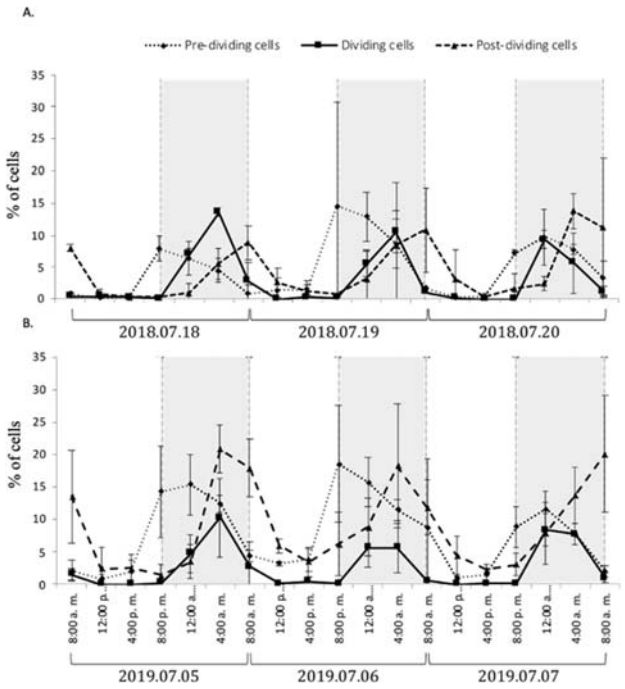

Figure 18. Progression of cell division during day-night cycles in 2018 and 2019 blooms.

A) Quantification of cells at different stages of division, based on nuclear position, during the bloom in 2018 and B) in 2019. Results are shown as percentage of cells in each group: pre-dividing (dotted line), dividing (line) or post-dividing (dashed line) over total number of cells per sample. For each time point, three samples were collected and quantified. Average of the three samples and standard deviation are reported. Grey boxes correspond to night samples, whereas white boxes to daylight samples. Interphase cells, which represent the largest percentage, are not shown in the graph

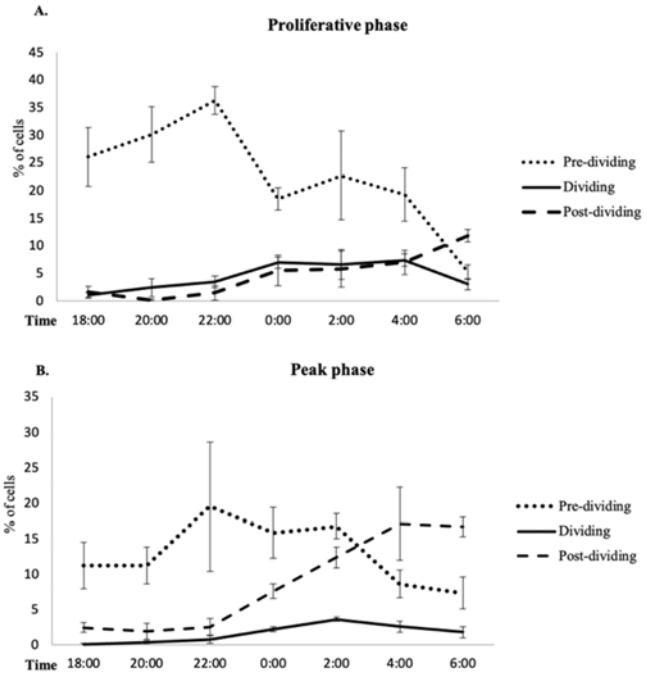

Figure 19. Progression of cell division during day-night cycle in 2020 bloom.

A) Quantification of pre-dividing (dotted line), dividing (line) and pre-dividing (dashed line) cells during a 12 hour period during the proliferative phase and B) at the peak of the bloom for the 2020 bloom. Interphase cells, which are the most abundant, are not indicated in the graph for simplicity. Three benthic samples were collected every 2 hours. Average of the three data sets and standard deviation are plotted for each time point.

2.3 Discussion

The growth rate of *O*. cf. *ovata* has been analyzed extensively and different values have been reported. The diffeneces reported in the literature are mostly explained by differences in environmental parameters that regulate proliferation, such as light, temperature and nutrients availability as well as by phyletic differences (Pistocchi et al., 2011; Tester et al., 2020; Drouet K., 2021).

Here, I showed that the growth rate during the proliferative phase of the strain MCCV054, grown under static conditions at 22ºC with a light/dark cycle of 14/10 hours, was similar to the net growth rate observed *in situ* during the blooms in 2018-2020 in the Bay of Villefranche-sur-Mer.

Given that the net growth rate *in vitro* is a measure of the division rate, the similarities observed between cell cultures and the bloom raise the question of whether mitotic division represents the main contribution to the increase in biomass observed during *O*. cf. *ovata* HABs. Indeed, the simulation reported in Figure 16B, whereby a constant division rate of 30% allowed to recapitulate the proliferative phase observed during the bloom, supports the idea that cell proliferation alone is sufficient to explain the explosive increase in cell population observed during bloom development. Alternative possibilities whereby negative factors such as cell death, grazing, predation and dispersion, and positive factors such as mucus recruitment, migration and currents, contribute to the final net growth rate are also possible and further analysis will be required to distinguish all different contributions.

Another surprising observation was the similarity in the number of dividing cells present at the peak of the bloom (2019) and during the senescence of the bloom (2018), which suggests that changes in net growth rate occur in the presence of constant division rates. This hypothesis was not confirmed by comparison of division rates at different bloom stages within the same bloom (2020). Although at reduced levels compared to the proliferative phase, however, cell division took place both at the peak of the bloom and during senescence when the net growth rate is either null or negative, suggesting the significant influence of negative factors in the shift in bloom dynamics from growth to senescence. It would be interesting to develop bioassays to quantify cell death to compare the relative ratio between cell proliferation and cell death at different phases of the bloom.

Previous analysis by Bravo et al. (2012), reported very low division rates of 2.5% during the proliferative phase of the bloom. Instead, I observed up to 15% of bi-nucleated cells (Figure 18A), and up to 30% of pre-dividing cells (Figure 19A) and 20% of post-

dividing cells (Figure 19B), which were not identified *in situ* by Bravo et (2012). These differences could be accounted for by technical differences, such as the method used for collection, fixation and staining, or alternatively by the cell concentration reached during the bloom.

Despite these differences, however, consistently with the findings of Bravo et al, (2012) and with the generally accepted idea that dinoflagellates divide during the dark period, I observed that *O.* cf. *ovata* division occurs during the night (Figure 18). The presence of a peak of pre-dividing cells in the evening and one of post-dividing cells in the morning, suggests that karyokinesis and cytokinesis should take place between 00:00 and 4:00. However, as previously observed by Bravo et al. (2012), a clear peak of division was not detectable. As it was previously suggested that cytokinesis is a very fast process that takes in less than an hour (Bravo et al 2012), the time resolution of my sampling (every 2 hours) might not have been sufficient to capture this process. Alternatively, cell division may occur asynchronously throughout a long window of darkness without a clear peak. This hypothesis is supported by the result of the intense sampling I carried out in 2020 (Figure 19), which shows a constant low level of division at 00:00, 2:00 and 4:00.

The observation that cell division occurs only at night raises the question of whether *O.* cf. *ovata* cell cycle is circadian. As *O.* cf. *ovata* divides every 2 to 3 days its division is not directed by the circadian rhythm. It is then possible that, as for other dinoflagellates, *O.* cf. *ovata* cell cycle is gated by light rather than directly controlled by the circadian clock.

Interestingly *in vitro* cultures cells of strain MCCV054 divide during the day, although being maintained under the same 14:10 light:dark cycle as during bloom development *in situ*. This different behavior *in situ* and *in vitro* may be related with *O.* cf. *ovata* ability to produce energy using two alternative sources, sunlight and organic nutrients. Although there are no conclusive proves yet, *O.* cf. *ovata* is considered a mixotroph dinoflagellate (Faust & Morton, 1995). In the sea, where organic nutrients may become limiting, the sun provides a constant source of energy, allowing cells near the surface to produce and accumulate energy during the day and use it to divide during the night (Arias et al., 2020).

In vitro, instead, where nutrients are artificially added and cells can feed *ad libitum* without competition, there is no constrain for cells to divide during the dark period. In this scenario, nutrients would be the limiting factor regulating proliferation in vitro, whereas in situ light/dark transitions would indirectly control mitotic division, by providing during the day the energy necessary for cell division during the night.

In line with the idea that nutrients are a major factor controlling cell proliferation *in vitro*, cultures that were diluted during the proliferative phase (Drouet 2021; Guidi et al., 2018; Jauzein et al., 2017; Lassus, 2016) behaved differently from cultures diluted during the stationary phase, as in my study. The latter showed a 6 days period (lag phase) when growth was absent, whereas cultures diluted during the proliferative phase continued dividing without any adaptation period. A possible explanation for this difference could be that only cells that have stopped dividing, such as those in stationary phase, require a recovery time (lag phase) when placed in optimal growth conditions, whereas cycling cells will just continue without a delay.

At the molecular level, this could be explained by the presence in the media of secreted molecules, which regulate proliferation and/or cell cycle progression. To my knowledge, it is unknown whether *O*. cf. *ovata* cells respond to secreted factors. However, some studies have addressed the response of other dinoflagellates, such as *Prorocentrum lima, Prorocentrum triestinum*, *Alexandrium tamarense,* and *Gymnodinium catenatum* to the addition of external growth factors as PDGF, a small mitogenic peptide, and PMA, a phorbol ester analogue of DAG which activates cell division (E. Costas et al., 1993; Eduardo Costas et al., 1993). In all cultures supplemented with those factors, the growth rates were significantly higher than in unsupplemented medium, suggesting that dinoflagellates respond to growth factors like other eukaryotes.

2.4 Materials and methods

2.4.1 Cell cultures

Strains of *O.* cf. *ovata* (MCCV054) obtained from the Mediterranean Culture Collection of Villefranche-sur-Mer (MCCV), EMBRC-France, were cultured in autoclaved and filtered seawater, at a salinity of 38 g/L, adding nutrients at L1 concentration: $NaNO_3$ - 8.8 x 10^{-4}M; $NaH_2PO_4 \cdot H_2O$ - 3.6 x 10^{-5} M; Na_2SiO_3 - 1.06 x 10^{-4}; trace element solution - see below; Vitamins: B_1 - 2.96 x 10^{-7} M; biotin - 2.05 x 10^{-9} M; B_{12} 3.69 X 10^{-10} M. All cultures were incubated at 22 °C under a 14:10 light/dark cycle (250 µmol m-2 s-1).

Metal traces components:

Component	Stock Solution	Quantity	Molar Concentration in Final Medium
$Na_2EDTA \cdot 2H_2O$	---	4.36 g	1.17×10^{-5} M
$FeCl_3 \cdot 6H_2O$	---	3.15 g	1.17×10^{-5} M
$MnCl_2 \cdot 4\ H_2O$	178.10 g L^{-1} dH_2O	1 mL	9.09×10^{-7} M
$ZnSO_4 \cdot 7H_2O$	23.00 g L^{-1} dH_2O	1 mL	8.00×10^{-8} M
$CoCl_2 \cdot 6H_2O$	11.90 g L^{-1} dH_2O	1 mL	5.00×10^{-8} M
$CuSO_4 \cdot 5H_2O$	2.50 g L^{-1} dH_2O	1 mL	1.00×10^{-8} M
$Na_2MoO_4 \cdot 2H_2O$	19.9 g L^{-1} dH_2O	1 mL	8.22×10^{-8} M
H_2SeO_3	1.29 g L^{-1} dH_2O	1 mL	1.00×10^{-8} M
$NiSO_4 \cdot 6H_2O$	2.63 g L^{-1} dH_2O	1 mL	1.00×10^{-8} M
Na_3VO_4	1.84 g L^{-1} dH_2O	1 mL	1.00×10^{-8} M
K_2CrO_4	1.94 g L^{-1} dH_2O	1 mL	1.00×10^{-8} M

2.4.2 *In vitro* growth rate

Cells were inoculated at a starting concentration of 600-700 cells/mL in 75mL of L1 medium. Three 1 ml samples were collected every two days for 24 days and fixed in 1% acid lugol. Fixed cells were mounted in a Sedgewick Rafter Counting Chamber and counted using an inverted microscope Nikon SMZ1000.

Specific growth rate (GR - μ, day^{-1}) was determined using the following formula,

$$\mu = \frac{ln\ N_1 - ln\ N_0}{t_1 - t_0}$$

where N_0 and N_1 are cell density values at time t_0 and t_1.
The doubling time was calculated based on:

$$DT = \frac{\ln(2)}{\mu}$$

For single cell cultures, individual cells were place in 96 multi well cell culture plates (Nunc™) containing 20 µL of conditioned medium (spent medium harvested from the original culture).

2.4.3 Bloom sampling

Bloom samples were collected in Villefranche-sur-mer (Rochambeau beach), on the Mediterranean French coast (Figure 20 - 43°41′34.83″ N and 7°18′31.66″ E), where yearly blooms occur and are monitored by the Lemee group. Three sampling stations approximately a meter apart from each other (square on Figure 20, “A, B, C”) were selected because of the ease of access for sampling, even during the nights, good quality and abundant available

macroalgae. Samples were collected at 50 cm of depth with macroalgae (mainly *Dictyota sp* with a fresh weight between 3-6 g) in a 250 ml bottle, as described by Cohu et al. (2013).

Frequent sampling was performed every 4 hours for 72h in 2018 and 2019: from the 18th of July at 8:00 until the 21st of July 8:00 am in 2018; from the 5th of July at 8:00 am to the 8th of July at 8:00 am in 2019. In 2020 sampling was performed every 2 hours on the 25th of June from 20:00 to 6:00 am of the following day and on the 6th of July from 20:00 to 6:00 am of the following day.

Samples were vigorously shaken to detach the *Ostreopsis* cells from the epiphytic macroalgae before fixation. For bloom monitoring, the samples collected every week in collaboration with the Lemee group were fixed adding acid lugol to the collection bottles (1%v/v) and were kept at 4ºC until counting. Before addition of acidic lugol, aliquots of 10 mL of cells were removed and fixed in 2% paraformaldehyde (PFA, F8775, Sigma-Aldrich) over-night at 4ºC. PFA fixed samples were used for nuclear staining.

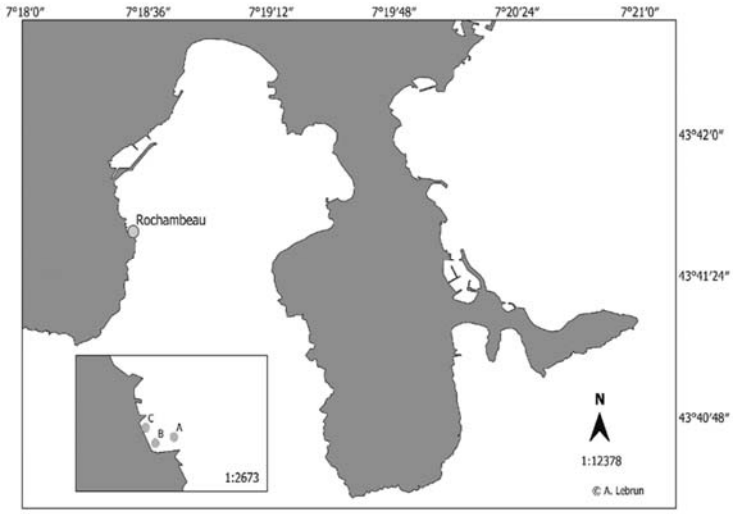

Figure 20. Sampling sites in Villefranche-sur mer in 2018, 2019 and 2020. Source: Pavaux A-S; 2020.

2.4.4 Nuclear staining

PFA fixed cells were washed 3 times with 1x Phosphate Buffered Saline (PBS) and stained adding 1µg/L Hoechst-33342 (Sigma-Aldrich) in 1ml PBS for 20 minutes at room temperature. Cells were then washed twice with PBS, and finally resuspended in 200 µl of PBS. 50 µl of resuspended cells were mixed with 50 µl of citoflour and mounted on slides.

Nuclear position was evaluated using an epifluorescence microscope (Imager-A2, Zeiss) equipped with an Axiocam 506 camera (Zeiss).

2.4.5 Statistical analysis

Data presented as mean are showed with error bars indicating standard deviation (mean±SD).

Normality of data and equality of variances was verified using the Shapiro. One-way ANOVA test was used to compare the three growth rates (culture, single cell culture and bloom).

T-student with normality analysis was used to compare the % of division during proliferation and at the peak of 2020 bloom.

Chapter 3

Microtubular changes during the vegetative cycle of *Ostreopsis* cf. *ovata*

"The gifts of the microscopes to our understanding of cells and organisms are so profound that one has to ask: What are the gifts of the microscopist? Here is my opinion. The gift of the great microscopist is the ability to think with the eyes and see with the brain". Dan Mazia, 1996

3.1 Introduction

Nearly half century ago, Édouard Chatton coined the term 'mesokaryotes' to describe dinoflagellates, suggesting that this group had intermediate nuclear features between prokaryotes and eukaryotes (in: Soyer-Gobillard, 2006). Although dinoflagellates contain a well-defined nucleus like other eukaryotes, their chromosomes have an atypical organization, remain condensed through the cell cycle and, up until 2003, were though to lack histones (O. K. Okamoto & Hastings, 2003). Moreover, the early observation that DNA replication continues throughout interphase suggested the absence of a typical eukaryotic cycle with well-defined stages (Filfilan & Sigee, 1977), whereas the atypical mitosis without a canonical spindle, suggested a microtubule independent mechanism for mitosis, typical of prokaryotic cells (Spector, 1984). The concept of 'mesokaryotes' was discarded once it was shown that dinoflagellates have a common eukaryotic cell cycle, with an unusual mitotic division (Riaz et al., 2018). Mitotic division in dinoflagellates occurs in the presence of an intact nuclear envelope (closed mitosis), but differently from other eukaryotes that undergo closed mitosis, the dinoflagellate spindle is cytoplasmic (extranuclear) and interacts only indirectly with the mitotic chromosomes (Drechsler & McAinsh, 2012). This unique form of mitosis has deserved its own name: dinomitosis. The mechanism of this unique nuclear division remains mostly elusive, as well as most of the players involved in dinomitosis.

Here I analyze the changes in microtubule organization associated with different stages of the *O.* cf. *ovata* vegetative cell cycle. My analysis confirmed that a cortical microtubule array is present throughout the cell cycle. Instead, I describe, for the first time, a microtubule-based structure, which forms from the ventral area in preparation for mitosis to allow repositioning of the nucleus from the dorsal side to the center of the cell, where mitosis takes place. Following mitosis, cytokinesis occurs along the longitudinal axis of the cell where a microtubule rich plate is formed. My results suggest that differently from animals and

yeasts, which divide using an actomyosin ring, in *O.* cf. *ovata* cytokinesis requires a microtubule-rich structure.

3.1.1 Cell cycle and mitosis, a general description

Cell division is central to growth of all organisms and requires proper duplication of the genome and correct segregation of the duplicated chromosomes to daughter cells. These events are coordinated during the cell cycle, an ordered sequence of events during which the cell prepares to divide. The cell cycle can be divided in four main phases: gap phase 1 (G1), S-phase, and gap phase 2 (G2) during which the cell respectively grows, duplicates its genome and prepares to divide, and mitosis when duplicated chromosomes are segregated to opposite cell poles prior to cytokinesis (Cooper, 2000). Work carried out in canonical model organisms has revealed that chromosome segregation is mediated by a bipolar microtubule-based structure, known as the mitotic spindle, which is nucleated and organized by centrosomes, located at spindle poles. Three classes of microtubules are organized by the centrosomes: (i) the astral microtubules that connect the centrosome with the cell cortex; (ii) the interpolar microtubules that connect the two centrosomes with each other; and (iii) the kinetochore microtubules, known as well as k-fibers that connect the spindle poles to chromosomes through a multiprotein complex known as the kinetochore assembled on centromeric DNA. The k-fibers allow segregation of sister chromatids (Meunier & Vernos, 2012).

Mitosis is divided in four main steps: prophase, metaphase, anaphase and telophase. Prophase is characterized by the condensation of chromosomes and the migration of centrosomes to opposite poles. During this phase, the spindle microtubules start to be organized from the centrosomes. In animal cells the transition from prophase to metaphase is marked by the disassembly of the nuclear membrane nuclear envelope breakdown (open mitosis). However, nuclear envelope breakdown is not a conserved step of mitosis and several organisms, such as yeast, apicomplexans parasites and dinoflagellates among others, undergo mitosis in the presence of an intact nuclear envelope (closed mitosis). In metaphase, the kinetochores become attached to microtubule k-fibers. Each kinetochore is connected to microtubules emanating only from one spindle pole and kinetochores of sister chromatids attach to microtubules polymerized from opposite poles. Microtubules then move chromosomes towards the spindle equator where they align on the metaphase plate. Once all chromosomes are aligned on the metaphase plate, sister chromatids are segregated during anaphase (Cooper, 2000) by the elongation of the spindle towards the spindle poles. The last

step of mitosis is telophase, which is marked by the formation of the two daughter nuclei and in animal cells correspond to the reformation of the nuclear membrane around the segregated decondensing chromosomes (nuclear envelope reformation) (Lara-Gonzalez et al., 2012).
Although the basic machinery required for chromosome segregation during mitosis appears to be well conserved among eukaryotes, several variations on the theme have been described with dinomitosis representing one of the most extreme and less understood example.

3.1.2 Dinomitosis

Dinomitosis was first described in 1920 for the genus *Atelodinium* from the order peridinales (Chatton, 1920), where it was observed that chromosomes were segregated within an intact nuclear membrane. Differently from yeasts, diatoms and euglenoids, which undergo closed mitosis with a nuclear spindle, in dinoflagellates spindle microtubules are cytoplasmic and traverse the nucleus through tunnels without ever entering the nucleoplasm. The number of tunnels depends on the species, with early branching lineages having one tunnel and core dinoflagellates presenting multiple parallel tunnels. Differently from what observed in other eukaryotes there is no direct contact between spindle microtubules and chromosomes in dinomitosis (Drechsler & McAinsh, 2012). Instead, the chromosomes, which are attached to the nuclear membrane in the nucleoplasm, contact the spindle microtubules indirectly across the nuclear membrane (Drinnenberg & Akiyoshi, 2017; Gavelis et al., 2019; Ris & Kubai, 1974). A kinetochore-like structure has been observed by electron microscopy in several dinoflagellate species and consists of a dense amorphous disc associated with the inner side of the nuclear envelope (Bhaud et al., 2000).

The spindle of core dinoflagellates, with the exception of *Syndiniales*, is not organized by centrioles at the spindle poles (Bhaud et al., 2000; Drechsler & McAinsh, 2012; Moon et al., 2015). Studies performed in *C. cohnii* showed that the bipolar spindle is organized from two acentriolar Microtubular Organizing Centers (MTOCs) located in the cytoplasm on either side of the nucleus (Jérome Ausseil et al., 2000; E. Perret et al., 1993; Eric Perret et al., 1991) (Figure 21A, left). In these cells, the basal bodies, or kinetosomes, are linked with each centrosome, present at the spindle poles, by a bundle of about ten microtubules, the desmoses, recognized by electron microscopy and by immunofluorescence against β-tubulin as a three-pronged fork emerging from the kinetosome towards the spindle poles (E. Perret et al., 1993) (Figure 21C). As asters are never present in any core dinoflagellate (Kubai & Ris, 1969; E. Perret et al., 1993), it was suggested that the desmoses have a similar function to asters of animal cells, connecting the spindle to the cell cortex.

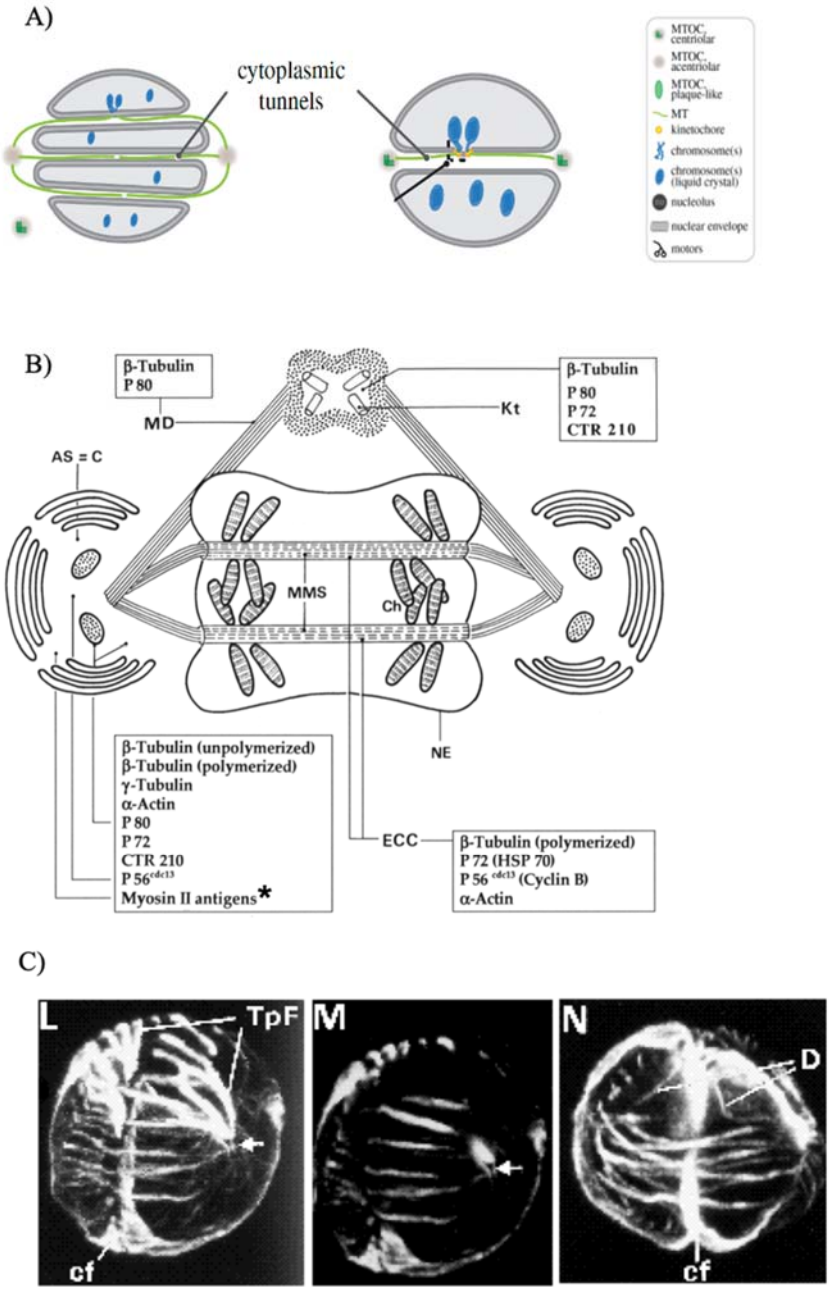

Figure 21. Dinomitosis, a specific dinoflagellate mitosis.

A) Comparison of dinomitosis between core dinoflagellates (left) and Syndiniales (right). Adapted from Drechsler & McAnish, 2012. B) Schematic representation of the dinoflagellate mitotic apparatus in *C. cohnii*. Proteins thought to be associated with the mitotic structures are indicated in the boxes linked with the corresponding structure. AS, Archoplasmic Sphere; C, Centrosome; ECC, Extranuclear Cytoplasmic Channel; MMS, Microtubular Mitotic Spindle; MD, Microtubular Desmose; Kt, Kinetosomes; N, Nucleus; NE, Nuclear Envelope, Ch, Chromosomes. Adapted from Ausseil, et al., 2000. C) Representative images of *C. cohnii* in mitosis, from Perret et. al. (1993). The split three-pronged fork (TpF) is associated with the spindle poles (left, arrows). The incipient cleavage furrow (cf) in the kinetosome region is labelled with anti-ß-tubulin (right). The two desmoses (D) link the poles of the spindle to the kinetosome region, and the microtubular spindle is elongated, with the poles close to the cortex. The cleavage furrow (cf) is fully formed.

In *C. cohnii,* the kinetosome was described as a multilobed, vesiculate body composed of β-tubulin, the homologue of the human centromeric protein Ctr210 and two proteins p80 and p72 (Figure 21B), whereas the centrosomes are thought to contain unpolymerized tubulin, γ-tubulin, α-actin, P80, Ctr210, myosin (recognized by the polyclonal antibody M7648-sigma, that recognizes myosin II, IX and X) and a protein homologues to cyclin B (identified by an anti-yeast $p56^{Cdc13}$ antibody) (Jérome Ausseil et al., 2000; E. Perret et al., 1993; Eric Perret et al., 1991).

In *Amphidinium carterae,* Barlow & Triemer (1988) observed that the extranuclear spindle is composed of microtubules interdigitating in the central spindle and converging at the poles where they are inserted into 2 multilobed vesiculate bodies containing electron opaque amorphous material, called the archoplasmic sphere, which appears to interact with the Golgi apparatus.

The only exception to the acentriolar organization of the spindle is observed in Syndiniales, where a pair of centrioles was reported to be present near the nuclear envelope at both spindle poles (Bhaud et al., 2000; Ris & Kubai, 1974). In these dinoflagellates, the V-shaped chromosomes are permanently attached at their apex to the nuclear membrane through a kinetochore-like disk inserted in the membrane. Microtubules connect the dense layer of each kinetochore to the base of the two centrioles located in an invagination of the nuclear envelope (Figure 21A, right). During mitosis, a bundle of microtubule forms between the duplicated centrioles and then elongates to form the mitotic spindle. The nuclear envelope then wraps around the spindle microtubules forming a single tunnel. So, in these species, centrioles or basal bodies are intimately involved in chromosome segregation (Ris & Kubai, 1974; Drechsler & McAinsh, 2012).

No description of the microtubule organization during mitosis exists for *O.* cf *ovata*.

Mitotic phases in dinoflagellates

The different phases of mitosis are recognized in dinoflagellates. Chromosomes which are easily visible during the whole cell cycle because of their permanent condensation, become tightly condensed in G2, prior to mitosis. In prophase, chromosomes then elongate and split longitudinally acquiring a characteristic V or Y shape attached to the nuclear membrane (Bhaud et al., 2000). During prophase centrosomes in *C. cohnii* can be identified at the nuclear poles (Ausseil et al., 2000) and some channels begin to be visible across the nucleus (Bhaud et al., 2000). For several years it was accepted that dinoflagellates lack typical metaphase plates (Cuadrado et al., 2019; Ris & Kubai, 1974). However, the appearance of flat

nuclei before chromosome segregation has been associated with a metaphase-like alignment of chromosomes (Bhaud et al., 2000). In anaphase, the chromosomes are separated towards opposite poles with little change in the chromosome to pole distance by the elongating spindle bundles, which extend towards the plasma membrane. The spindle microtubules then depolymerize in telophase. The nucleus expands laterally while chromatids move toward opposite sides. The process finishes with the separation of two daughter nuclei. A cleavage furrow containing both tubulin (Figure 21C) and actin has been reported to form in the kinetosome region during anaphase in *C. cohnii* (Perret et. al. 1993).

3.1.3 Spindle assembly checkpoint in dinomitosis

In yeast and animal cells a surveillance system, known as spindle assembly checkpoint or SAC, monitors the interaction between kinetochores and spindle microtubules to allow correct chromosome segregation and mitotic progression (Jia et al., 2013). In those organisms, the presence of unattached kinetochores results in activation of the checkpoint and a delay in mitotic progression until all kinetochores are properly attached to the spindle (Musacchio and Salmon, 2007).

The relationship between the microtubular apparatus and mitotic progression has been tested in dinoflagellates using microtubule depolymerizing drugs (Cho et al., 2011; Yeung et al., 2000; Zhang et al., 2018) and turbulence which it is thought to interfere with proper microtubule organization (chapter 2) (Berdalet, 1992; Llaveira & Berdalet, 2009). In yeast and animal cells microtubule poisons activate the SAC delaying mitotic progression (Chenevert et al., 2020; Endo et al., 2010). The results obtained in dinoflagellates are variable depending on the treatment and the species used, but generally suggest that microtubules have a role in controlling major cell cycle transitions and suggest that the SAC is active in dinoflagellates.

Treatment with the microtubule depolymerizing drug nocodazole, which prevents proper assembly of the mitotic spindle, resulting in an arrest in M-phase in both animals and yeast, arrests *C. cohnii* cells in G2/M following activation of the spindle checkpoint (Yeung et al., 2000). In *C. cohnii* cells, treatement with nocodazole (2 µg/ml) during G1, results in prolongation of the G2/M phase by 5-6 hours (from 2 to 3 h in control cells to 8-9 hours in nocodazole treated cells). DAPI staining of nuclei showed that nocodazole treatment transiently arrested cells between metaphase and anaphase. Moreover, the mitotic cyclin, cyclin B was stabilized for 6-8 hours in nocodazole treated cells and only extracts from G1 cells, but not G2/M cells or from nocodazole treated cells were able to degrade exogenous

human cyclin B1. Thus, the spindle checkpoint appears to be present in dinoflagellates and to control cyclin B degradation, as it occurs in other eukaryotic cells (Qiao et al., 2016).

Differently from nocodazole, treatment with colchicine, another microtubule depolymerizing drug, in *Alexandrium catenella* (Cho et al., 2011) and *Alexandrium tamarense* (Zhang et al., 2018), prolonged G1 but not G2/M. Zhang et al (2018), found that PCNA, a protein required for progression through G1 and G1/S transition in animals, was downregulated after colchicine treatment, suggesting that the protein could play a role in cell cycle arrest at the G1 phase.

In spite of the results obtained with nocodazole, the existence of a functional SAC controlling mitotic progression in dinoflagellates is further supported by bioinformatic analysis that showed the presence of some of the SAC components in the genome of *Symbiodinium* (Hooff et al., 2017) and in the transcritpome of *C. cohnii* (Morse et al., 2016a). Moreover, cultures of dinoflagellate cells have been shown to arrest in G2/M when subjected to agitation (Berdalet et al., 2007; Llaveria & Berdalet, 2009). In *Peridinium cinctum*, shaking during the dark phase, when cells divide, but not during the light phase, decreased the cell growth rate and inhibited nuclear division (Pollingher & Zemel, 1981). Although this work did not directly evaluate whether the alteration in growth rate was due to an arrest in mitosis or to cell damage, as the effect was observed only when cells were in division, this data suggests that agitation interferes with mitotic progression. Consistently, Accoroni et al. (2012) observed that turbulence affected *O.* cf. *ovata* bloom division only during the proliferative phase but not at other phases. *Alexandrium minutum* cells subjected to turbulence also showed an extended G2/M phase, without an arrest in any other cell cycle phase (Llaveria & Berdalet, 2009). *Gymnodinium nelsonii* cells grown in the presence of agitation (100rpm) showed an increase in DNA content and in cell volume without increase in cell number (Berdalet, 1992). Changes in the nuclear morphology were reported for these cells, with an alteration in the orientation of of the axis of nuclear division during mitosis.

Taken together, these observations suggest that dinoflagellate sensitivity to turbulence is linked to mechanical signals that arrest cell cycle progression. As previously postulated by Berdalet (1992) in the "microtubule hypothesis", turbulence may interfere with the correct assembly of the mitotic spindle, resulting in the activation of the SAC and mitotic delay. The microtubule hypothesis was tested directly in athecate (*Akashiwo sanguinea*, *Karenia brevis* and *Oxyrrhis marina*) dinoflagellates subjected to growth in the presence of turbulence (Llaveria & Berdalet, 2009). In these cells spindle microtubules were present both in control and stir conditions. Although the experiment did not work in thecate dinoflagellates probably

because of technical reasons linked to an immunofluorescence protocol that was not optimized for the presence of the theca, the presence of spindle microtubules in the turbulence experiments suggests that the inhibition of cell proliferation by agitation is not related to the disruption of the mitotic spindle apparatus. However, it is still formally possible, as suggested by the authors that a decrease in the microtubule elongation rate causes spindle defects that delay mitotic progression, or alternatively that turbulence causes erroneous attachments of chromosomes to spindle microtubules responsible for their segregation.

3.1.4 Cytokinesis

Following mitosis, cells complete their division undergoing cytokinesis, a process that results in the formation of two physically separated daughter cells each with a full chromosome set and partitioned organelles.

The best studies mechanism of cytokinesis is based on the assembly and constriction of a contractile actomyosin ring, composed of actin, myosin II, and other associated proteins, which forms perpendicularly to the mitotic spindle (Cheffings et al., 2016). This cytokinetic mechanism is common in opisthokonts (Figure 22A-C, red square). It is currently known that members of all other supergroups, with the only exception of *Naegleria spp*., use different mechanisms to divide, since they lack myosin II (Hammarton, 2019). Work carried out in plants (Figure 22D) (Gerien & Wu, 2018), viridiplantae (Figure 22E) (Cross & Umen, 2015) and in some parasites, like the protozoan parasite *Trypanosoma brucei* (Figure 22F) (McKean, 2003), has shown that in these organisms cytokinesis relies mostly on microtubules. In plants cytokinesis is based on the assembly of a phragmoplast a plate made mainly of microtubules which forms centrifugally, from the cell center towards the cell membrane, dividing the cell transversally by targeted membrane deposition. In alveolates (Figure 22G) the cytokinetic mechanisms are more variable although there are common characteristics as the dependency on microtubules and the association with basal bodies (Striepen et al., 2007).

Positioning of the plane of cell division also varies in different cells both in terms of time of determination and of the signals, which define it. In the budding yeast *S. cerevisiae,* the position of cytokinesis is determined in G1, in the fission yeast *S. pombe* it occurs in G2. In animals, the site of cell division is chosen generally during late mitosis (anaphase to telophase), while in plants it is chosen in early mitosis (prometaphase) (Balasubramanian et al., 2004; Gillies & Cabernard, 2011).

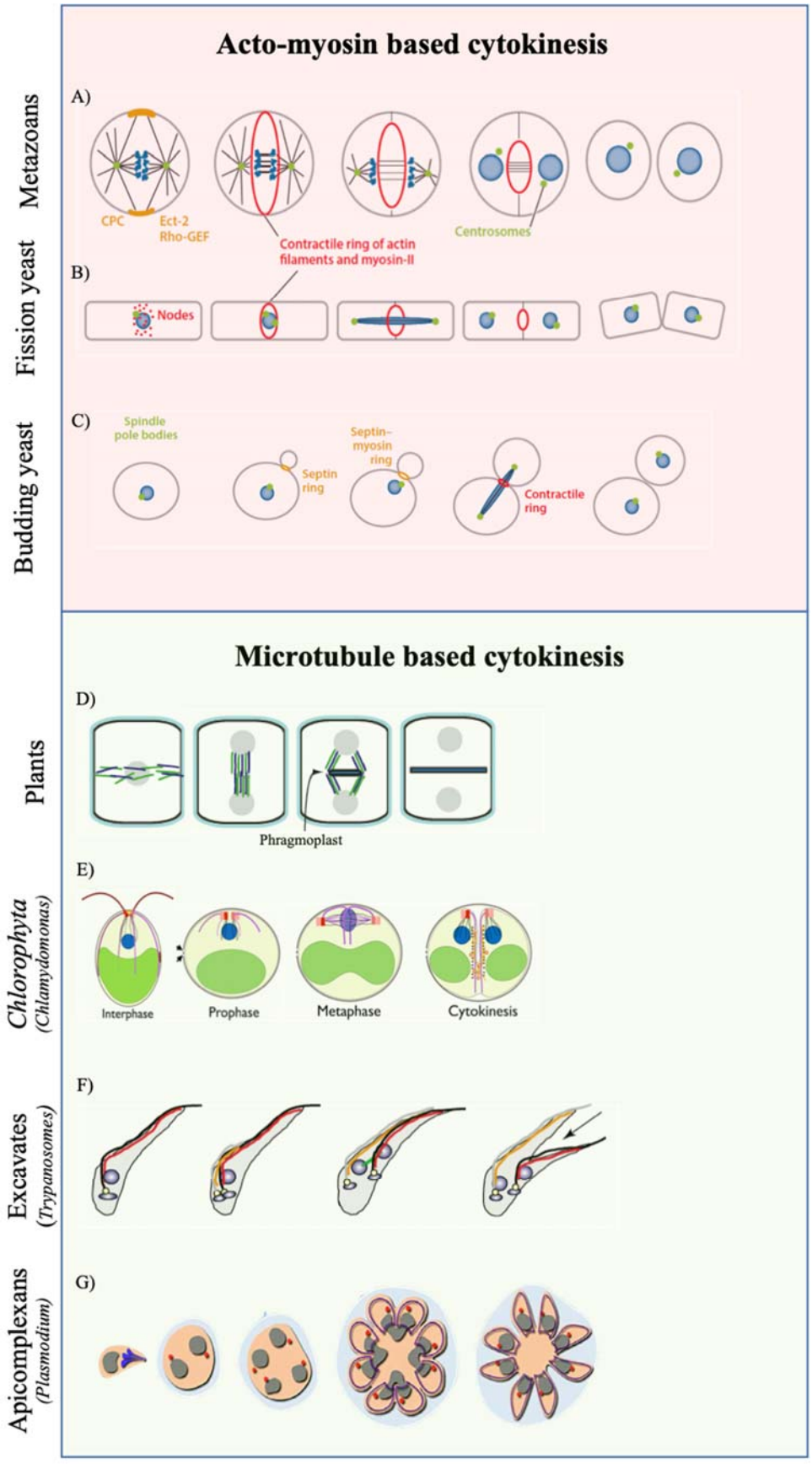
Acto-myosin based cytokinesis
Metazoans
A)
CPC
Ect-2
Rho-GEF
Contractile ring of actin filaments and myosin-II
Centrosomes
Fission yeast
B)
Nodes
Budding yeast
C)
Spindle pole bodies
Septin ring
Septin–myosin ring
Contractile ring
Microtubule based cytokinesis
Plants
D)
Phragmoplast
Chlorophyta (Chlamydomonas)
E)
Interphase
Prophase
Metaphase
Cytokinesis
Excavates (Trypanosomes)
F)
Apicomplexans (Plasmodium)
G)

Figure 22. Cytokinesis is different in eukaryotes.
A) Schematic representation of cytokinesis in animals, B) in fission yeast, and C) in budding yeast. Abbreviations: CPC, chromosomal passenger complex; Rho-GEF, Rho GTPase guanine nucleotide exchange factor. Figure from Pollard and O'Shaughnessy (2019).
D) Schematic representation of cytokinesis in plants. Formation of the preprophase band, containing actin and microtubules, marks the division site. The phragmoplast mediates the formation and expansion of the cell plate. Maturation and expansion of the cell plate completes cell division by fusing with the plasma membrane. Figure from Gerien and Wu (2018).
E) Schematic representation of cell division in *Chlamydomonas*. Cells are shown at different cell cycle phases, from left to right: Interphase: cell with two flagella; Prophase: flagella have been resorbed and the protoplast has rotated 90° within the mother cell wall. Arrows mark the former site of basal bodies and flagella, with respect to the mother cell wall; Metaphase: newly replicated BB pairs are present at spindle poles. Spindle microtubules enter the nucleus through polar fenestrae and attach to chromosomes; Cytokinesis: post-mitotic nuclei and basal bodies have moved towards the center of the cell. The mitotic spindle has been replaced with the phycoplast: the 4 MTRs and cleavage microtubules extend down into the cell along the plane of division, whereas additional phycoplast MTs lie roughly perpendicular to the cleavage microtubules, also along the plane of cleavage. Figure from Cross and Umen (2015).
F) Schematic representation of *Trypanosome* cell division. The black arrow indicates the direction and position of the cleavage furrow. Figure from McKean (2003).
G) Schematic representation of schizogony, one of the multiple divisions in the apicomplexans *Plasmodium.* DNA, grey; IMC, purple; centrosome, red. Note that a centriole as center of the spindle plaque body has not been clearly demonstrated in *Plasmodium.* Figure from Striepen et al. (2007).

According to the long-axis rule in the absence of other constraints, the mitotic spindle, by default, aligns with the long axis of the cell while the division machinery is placed perpendicular to the long axis between the segregating chromosomes, to ensure that each daughter cell receives a full complement of chromosomes (Finegan & Bergstralh, 2019). While the ''long axis rule'' applies to the majority of known cell types, there are exceptions particularly in embryos, in cells within tissues and among unicellular eukaryotic organisms, which align the mitotic spindle along the short axis and as a consequence divide along the long axis (Minc et al., 2011). In the majority of excavate parasites the spindle is oriented along the short cell axis and the cell divides along the long axis, employing mechanisms that heavily rely on flagellar motility and cytoskeletal rearrangements (Hammarton, 2019). Below, I present general characteristics of the main types of cytokinesis described so far.

Cytokinesis in animals

In animals contraction of an actomyosin ring drives the formation of a cleavage furrow that separates the two daughter cells (Figure 22A). Positioning and formation of the cytokinetic site is controlled in space and time and relies on elements of the mitotic spindle apparatus (Pollard & O'Shaughnessy, 2019). Generally, two distinct components of the spindle direct positioning of the cell division site: the astral microtubules emanating from the spindle poles and the central spindle. In *C. elegans* embryos both elements act redundantly in

positioning of the cleavage furrow (Werner et al., 2007). However, depending on the organism and the cell type, the contribution of these two structures may vary and one or the other may be not required or predominant.

The cleavage furrow contains actin and non-muscle myosin II, but also proteins required for the nucleation and dynamics of microfilaments, such as the Arp2/3 complex, CapZ, formins, tropomyosin, cofilin, Rock and the Rho-GTPases. The GTPase RhoA is required for the formation of the contractile ring and the concentration of RhoA around the equator determines the future site of the cleavage furrow independently of actin and myosin. Tight RhoA accumulation at the equatorial cortex depends on the prior localization of the Rho-GEF Ect2 on the central spindle. Dephosphorylated Ect2 localizes to the central spindle in anaphase and recruits RhoA to the equatorial cortex, while astral microtubules inhibit its accumulation at other locations on the cell membrane. RhoA in turn activates formin, which promotes actin polymerization and the formation of the actin ring, and the Rho-dependent kinase (ROCK), which activates myosin for ring contractility and furrow ingression (Kamijo et al., 2006; Mendes Pinto et al., 2013).

Although cytokinesis is driven by actin, microtubules are also required to transport vesicles toward the cleavage furrow. Furrow ingression ends at the midbody and sealing of the membrane, a process called abscission, is then achieved by plus-end–directed vesicle trafficking to the center of the midbody and ESCRT-III–mediated abscission. Abscission, completes cell division, generating two daughter cells (König et al., 2017). Proteins like dynamins and clathrins which are involved in endocytosis, syntaxins, which is required for vesicle fusion, and Fib3 and Rab11 which are necessary for endosome recycling, have all been shown to be required for cytokinesis.

Cytokinesis in fission yeast

Saccharomyces pombe cells are rod-shaped, grow by tip elongation and divide medially by fission, using a contractile actomyosin ring. Differently from animal cells, the positional information for the localization of the site of cell division comes from the nucleus and not from the spindle. During interphase, inhibitory signals emanating from cell ends preclude the accumulation of Cdr2 and Mid1 at cell tips, defining a central region where cell division can take place. Pom1 present at cell tips, however, avoids cell division in the middle region when the cell is small. As the cell grows Pom1 inhibition is relieved from the middle region allowing Cdr2 activation and mitotic entry. When cells enter mitosis Mid1 is released from the nucleus by the activation of Polo kinase and accumulates at the cell cortex nearest

the nucleus in structures called cortical nodes. The position of the cell division site is therefore coupled with nuclear position and artificially displacing the nucleus results in delocalization of the site of cell division (Akamatsu et al., 2014). In fission yeast therefore microtubules play an indirect role in positioning of the cell division site by keeping the nucleus centered in the cell.

The nodes then organize into a discrete ring around the equator, which is visible from early mitosis until the end of anaphase when the ring begins to contract and guides the formation of the new cell wall, called septum (Bathe & Chang, 2010). Bundles of actin are formed during this condensation process and follow the ring. The ring matures with additional proteins as myosin II, capping proteins and actin related proteins (Figure 22B).

Cytokinesis in budding yeast

S. cerevisiae divides asymmetrically, producing a small cell, the bud (Figure 22C) and a larger cell called the mother cell. The bud neck, the site that separates the mother cell for the bud is positioned next to the previous bud site, based on a series of landmarks that locally activate the Ras-like Rsr1 protein, which in turn recruits and activates Cdc24, the GEF of Cdc42. Cdc42-GTP then recruits a complex set of proteins and lipids to allow bud growth, correct mitosis and cytokinesis. The first proteins recruited to this site are Septins, GTP-binding and filament-forming proteins conserved from yeast to humans and absent in plants (Wloka & Bi, 2012). Septins associate with the cell membrane and form a ring around the bud neck, which acts as a landmark for spindle movement, as a barrier for membrane compartimentalization and for the recruitment of actomyosin ring components and formation of the actomyosin ring. Seven classes of proteins are required for the formation of the actomyosin ring: actin, myosin-II heavy and light chains, IQGAP, Rho, formins and tropomyosins (Meitinger & Palani, 2016).

In late anaphase the actomyosin ring contracts and the septum forms centripetally leading to the physical separation of the two daughter cells (Figure 22C).

Cytokinesis in plants

Differently from opisthokonta, plants lack myosin II (Richards & Cavalier-Smith, 2005) and cytokinesis is achieved thorough microtubule driven membrane trafficking to build a cell wall and new plasma membrane between the two daughter cells. In most plant cells the cues for positioning of the cell division site come from the mitotic spindle apparatus, the preprophase band which is a ring-like structure composed of microtubules and F-actin whose

position corresponds to that of the future division site, and the phragmoplast (Figure 22D) (Geelen & Inzé, 2006; Mineyuki, 1999).

In plant cells the formation of the new cell plate occurs centrifugally by expansion of the microtubule based phragmoplast from the center of the cell towards the cortical area. The site where the cell plate fuses with the cell-wall, is dictated by the pre-prophase band, whose site is specified by polarity cues before mitosis, as in yeasts. The position of the division site has been related with the position of the pre-mitotic nucleus (Paoletti & Chang, 2000). In plants, displacement of the interphase nucleus is sufficient to trigger the establishment of the preprophase band and the division site close to the new nuclear position (Murata & Wada, 1991).

Once the cell enters mitosis, the pre-prophase band disassembles, and the phragmoplast forms after chromosome segregation from the remnants of the anaphase spindle. The phragmoplast directs vesicles from the Golgi network towards the midzone (Nishihama & Machida, 2001). Vesicular trafficking and fusion, targeted by microtubule bundles at the edge of phragmoplast, lead to the formation of a cell plate that separates the two daughter cells. Eventually, the membrane of the cell plate fuses with the plasma membrane to form a new cell wall (van Oostende-Triplet et al., 2017).

Cytokinesis in *Chlamydomonas reinhardtii*

Cytokinesis in *Chlamydomonas*, relies on the activity of microtubules associated with the basal bodies (Figure 22E). The microtubule rootlets, which are located at the basal body, have been proposed to function analogously to astral microtubules in animal cells by providing positional cues for cleavage and furrow formation (Cross & Umen, 2015). In *Chlamydomonas*, and in many related green algae, cytokinesis is associated with a special set of microtubules, termed the phycoplast. The phycoplast microtubules begin to form between the nucleus and the microtubule rootlets of the basal body. Proteins that are associated with the basal body, like γ-tubulin, are important for the assembly of this microtubule structures required for the flagella and for the construction of the phycoplast. The phycoplast contains cleavage microtubules emanating from the rootlets and oriented in the direction of the cleavage, which starts at the anterior end of the cell and proceeds downwards (Figure 22E). Treatment of *Chlamydomonas reinhardtii* cells with microtubule inhibitors causes aberrant spindle formation and blocks cytokinesis (Ehler & Dutcher, 1998). In inhibitor-treated cells that had completed mitosis but not cytokinesis the phycoplast microtubules were partially disrupted and disorganized. These results show the microtubule dependency for cytokinesis in

the green algae.

Vesicles can be seen accumulating in the vicinity of the cleavage plane near the phycoplast, and as in plants, their transport and fusion is thought to contribute to cleavage furrow formation (Pickett-Heaps, 1979). Although cytokinesis does not rely directly on actin, F-actin is associated with the furrow region. However, interfering with actin, either by drug treatment or in actin mutants, does not affect furrows formation and cells divide, although less efficiently than un-treated cells (Onishi et al., 2020).

Cytokinesis in excavates

A review of a wide variety of ways to perform cytokinesis independently of an acto-myosin ring is presented by Hammarton (2019). The author describes the difference in cell division strategies from the primitive cytokinesis in *Entamoeba* spp. to very precise and tightly regulated microtubule rearrangements that lead to intricate assembly and segmentation of new daughter cells during apicomplexan budding. For example, in *Trichomonads*, basal body migration signals the start of mitosis, and flagellar-driven propulsion leads to morphological changes that drive crossing of duplicated flagella, resulting in constriction of the cell. In the euglenozoan *Trypanosoma*, a single motile flagellum emerges from a flagellar pocket at the posterior of the cell and is linked laterally to the cell body by a flagellum attachment zone (Langousis & Hill, 2014). After flagellar duplication, a cleavage fold forms from the flagellum attachment zone, by invagination of the plasma membrane and extends towards the posterior pole (Figure 22F). In parasitic protozoans -excavates-, several mechanisms of division have been described that do not rely on an acto-myosin ring, although some of them require actin. In some cases, actin was shown to promote furrow ingression via alterations of cortical tension, or to be required for vesicular trafficking and for furrowing/abscission (Hardin et al., 2017).

Cytokinesis in alveolates

Ciliates divide by transverse binary fission. A furrow forms at the midpoint of the cell. From there, a divergent contractile ring, which contains actin but not myosin II, grows constricting the cell along the anterior-posterior axis. Contributing forces exerted by ciliary beating complete cytokinesis (Hammarton, 2019).

In apicomplexan parasites, cell division is a complex process achieved in different modes according not only to the species but also to the stage of the parasite. Often, cell division occurs by budding and is directed by the microtubule apparatus associated with basal

bodies (Francia & Striepen, 2014). Depending on the species and their host, apicomplexan parasites can undergo multiple rounds of karyokinesis without cytokinesis, before a final (usually synchronous) budding cycle that produces multiple daughters. This is the case for example of *Plasmodium* spp., the causing agent of malaria. Within the mosquito, *Plasmodium* cells undergo three subsequent rounds of DNA replication and nuclear division (S/M), producing eight basal bodies, each with its own flagellar axoneme. At this stage, vesicles containing membranolytic proteins are secreted and a single event of cytokinesis occurs through budding, known as exflagellation, whereby eight cells known as microgametes are formed (Figure 22G). The microgametes swim out of the residual gametocyte body, each carrying a copy of the genome and its associated basal body (Rudlaff et al., 2020). Some proteins have been identified as essential for exflagellation. A calcium dependent protein kinase 4 (Cdpk4) together with its substrate Soc3, an axoneme-associated protein, appears to be the effector for driving axonemal motility and cytokinesis (H. Fang et al., 2017).

In general, protozoan parasites including excavates and alveolates, share two characteristics related to cytokinesis which are different from opisthokonta. Firstly, none of them is known to use a contractile actomyosin ring, with most species lacking myosin II. However, even in *Entamoeba*, where a myosin II gene was identified, there is no evidence for contractile actomyosin ring formation. Secondly, the majority of these organisms divide along the long cell axis, employing mechanisms that heavily rely on flagellar motility and microtubular rearrangements (Hammarton, 2019).

Cytokinesis in dinoflagellates

Cytokinesis in dinoflagellates has been poorly studied. Generally, separation of the cells is thought to occur with the formation of a cleavage furrow (Schnepf, 1988; Eberhard Schnepf et al., 1990; Tippit & Pickett-Heaps, 1976), but whether the process is driven by actin, like in yeast and animal cells, or by microtubules, as in plant cells and many protists, is controversial. Electron microscopy studies performed with dividing cells of *Ceratium tripos* (Wetherbee, 1975) showed a distinct layer of microtubules beneath the cleavage furrow, which was implicated in determining both the direction of division and development of cell shape. Association of the cleavage furrow with enrichment of microtubule below the plasma membrane along the place of division was reported also for the Gonyaulax *L. polyedra* (in: Schnepf, 1988) and for *Amphidinium cartae* (Oakley & Dodge, 1976a).

In *C. cohnii* and in *Prorocentrum micans* (Soyer-Gobillard et al., 1996), actin has been observed in the nucleus and enriched in the cleavage furrow during cell division. In *C. cohnii*

a tubulin and actin-rich cleavage furrow was described which forms, in early anaphase, from the kinetosome region (Perret et al., 1993). Despite the enrichment of microtubules in the invaginations of the plasma membrane observed at the site of cytokinesis (Figure 23), the authors suggested that cytokinesis was similar to animal cells because of the presence of actin. This hypothesis was further supported by the identification of myosin in the nucleus of *C. cohnii* throughout the entire cell cycle, although the antibody used for this analysis actually recognized myosin IX and X and not the cytokinesis-specific myosin II, as reported (Ausseil et al., 1999).

The involvement of actin was supported by studies carried out in the thecate species *Prorocentrum micans* and *Scripsiella acuminata*. In these cells treatment with low doses of the actin depolymerizing drug, cytochalasin D, caused alterations in the thecal plates resulting in aberrant morphologies and problems in cytokinesis. Following cytochalasin D treatment the cleavage furrow begun to ingress, but division was never completed. Based on this study the authors suggested that cell division in dinoflagellates consists of two phases: a first one that corresponds to the initiation of cytokinesis, when the cleavage furrow forms independently of actin microfilaments, and a second phase which results in completion of cytokinesis which requires actin, like in animal cells. The lack of microfilaments observed in the cleavage furrow of many dinoflagellates was accounted for as a fixation problem (E. Schnepf, 1988).

Cytokinesis and the actin cytoskeleton have not been described in *O.* cf. *ovata*.

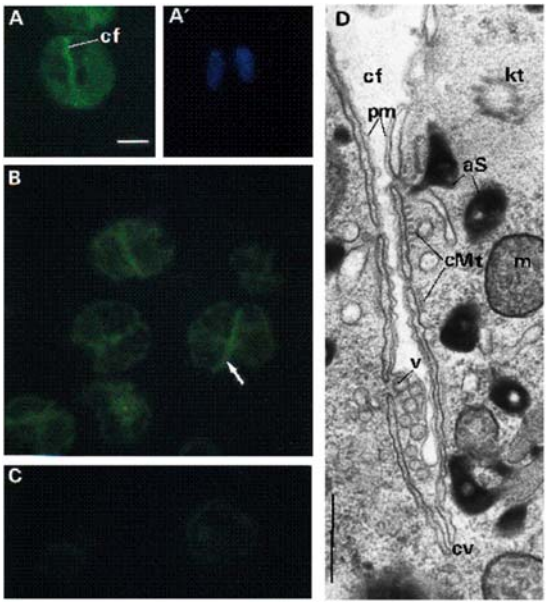

Figure 23. Organization of the cleavage furrow in *Crypthecodinium cohnii*.

A-B) Representative pictures of *C. cohnii* cells in telophase immunolabelled with anti-actin antibody and A') co-stained with Dapi to label DNA. Arrows point to cleavage furrow (cf). C) Control specimen incubated in GAM fluorochrome without anti-actin antibody shows no staining. Scale bar 0.5 mm (A-C). D) Electron microscopy image of semi-thin section (2 μm thickness) of a telophase cell following helium cryofixation and cryosubstitution. The cleavage furrow (cf) forms in the vicinity of kinetosome (kt). Groups of cortical microtubules (cMt) lie under the numerous flat cortical vesicles (cv), which are located beneath the plasma membrane (pm). Amorphous substance (aS) and mitochondria (m) are also present in the same cortical region. v, vesicle. ×56,000; Bar, 0.5 μm. Figure from Perret et al., 1993.

3.2 Results

3.2.1 Microtubules in *Ostreopsis* cf. *ovata*

The only description of the *O.* cf. *ovata* microtubule cytoskeleton available in the literature, reports the presence of a cortical microtubule array present under the cell surface and a complex internal microtubule structure that runs from the site of flagellar insertion towards the center of the cell (Escalera et al., 2014).

To obtain a more comprehensive description of the changes in microtubule organization associated with progression through the mitotic cell cycle and with cell division I optimized the immunofluorescence protocol used by Escalera et al., (2014) to label interphase microtubules. As I had previously observed that, in culture, cell division occurs at low level throughout the morning during the proliferative phase (chapter 2), fixation of culture cells was carried out between day 6 and day 10 following culture dilution, to obtain the greatest number of cells in division in each sample. Based on the analysis described in chapter 2, sea samples for immuno-staining, instead, were collected during the night between 00:00 and 4:00, when the highest percentage of dividing cells was observed. As turbulence is known to affect microtubule stability and to induce microtubule depolymerization in dinoflagellates, cells were collected without centrifugation and fixed immediately in large volumes of 80% cold methanol containing 0.5 mM EGTA to chelate Ca^{2+} and stabilize microtubules. 10% DMSO was also added to the fixation buffer to permeabilize the membrane and facilitate antibody penetration.

For the initial analysis I used an antibody against β-tubulin from sea urchin *Lytechinus pictus* (clone D66), as the epitope used to produce the *L. pictus* antibody was conserved in the *O.* cf. *ovata* protein (Figure 24). All samples were co-stained with Hoechst 33342 to identify different cell cycle stages based on nuclear position (Bravo et al., 2012).

β-Tubulin protein sequence of *O.* cf. *ovata*
>TRINITY_DN5283_c0_g1_i9.
MRELVHIQGGQCGNQIGAKFWEVISDEHGIDPTGTYHGDSDLQLERINVYYNEATGG
RYVPRAVLMDLEPGTMDSVRAGPFGQLFRPDNFVFGQTGAGNNWAKGHYTEGAEL
IDSVLDVVRKEAEGCDCLQGFQMCHSLGGGTGSGMGTLLISKVREEYPDRIMETFSVI
PSPKVSDTVVEPYNAVLSFHQLVENADECFLLDNEALYDICFRTLKLTTPTYGDLNHL
VSAAMSGVTTCLRFPGQLNCDLRKIAVNLVPFPRLHFFMTGFAPLTSRGSQQYRALT
VPELTQQMFDAKNMMCAADPRHGRYLTAAALFRGRMSTKEVDEQMLNVQNKNSS
YFVEWIPNNIKASVCDIPPKGLKMAVAFAGNSTAIQEMFKRVAEYFTAMFRRKAFLH
WYTGEGMDEMEFTEAESNMNDLVSEYQQYQDATAEEEGEFDEEEGEYDMQA*

Figure 24. *Ostreopsis* cf. *ovata* ß-tubulin.
The protein sequence of *O.* cf. *ovata* β-tubulin obtained from the reference transcriptome (described in chapter 4) shows the presence of the epitope recognized by the antibody D66 against *L. pictus* ß-tubulin (highlighted in yellow - aminoacids 427-432, DATAEE).

Figure 25 shows a typical interphase cell, the most abundant stage present in both culture and natural samples. As previously described by Escalera et al. (2012), I observed that a cortical array of microtubules is present under the cell surface. On the anterior side (episome), recognized by the presence of the apical pore (Figure 25A, left cell 'AP'), cortical microtubules run obliquely from the apical pore to the side of the cell. Two parallel bands of microtubules delimit the cingulum (Figure 25A, double arrowhead) from the ventral to the dorsal side. The groove of the cingulum contains tightly packed parallel microtubules that run transversally, perpendicular to the lateral bands. On the posterior side (hyposome, Figure 25A right cell), cortical microtubules ran parallel to each other traversing the cell for its entire length in the dorso-ventral direction. Two thick bundles of microtubules can also be observed. Both bundles originate from microtubular roots present in the ventral sulcal area ('VA', arrow Figure 25A), and I will, therefore, refer to them in this work as 'ventral bundles'. The two ventral bundles run towards opposite side of the cell, the episome and the hyposome (Figure 25- C).

Finally, ß-tubulin D66 antibody labels both the longitudinal flagellum ('LF', Figure 25B) and the transverse flagellum in the cingulum ('TF', Figure 25C).

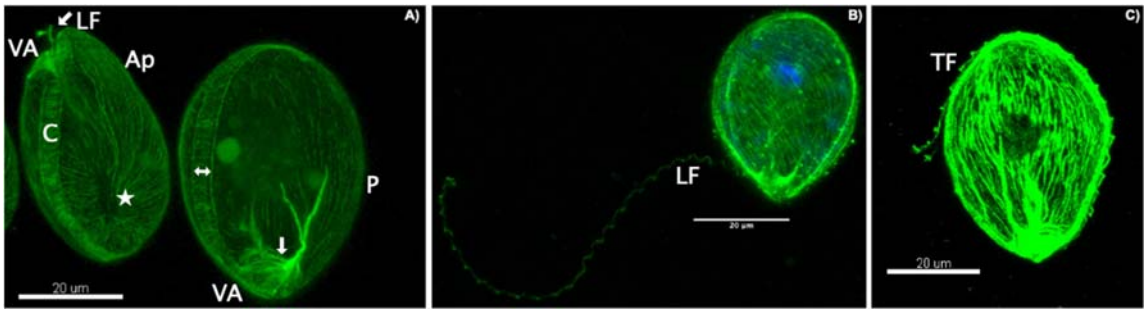

Figure 25. Microtubule staining of cultured *Ostreopsis* cf. *ovata* cells.
A-C) Representative confocal images of the most common cells found in the strain MCV054 immunostained with the D66 ß-tubulin antibody. Microtubules are visualized in green. Cortical microtubules are always present. Some microtubular structures are identified: the Longitudinal Flagellum (LF), the Transverse Flagellum (TF), the Cingulum (C) which contain parallel microtubule bands (double arrow); bundles of microtubules at the ventral area (VA, arrow); the apical pore (star) from where oblique cortical microtubules emanate and that identifies the apical side of the cell (Ap in A, left cell). A) Anterior (left) and posterior (right) view of cells, recognized by the Apical pore at the anterior side and the parallel cortical microtubules at the posterior (P) side. B) Cell with its longitudinal flagellum. C) Transversal flagellum recognized because it surrounds the cingulum all around the cell. Scale bar 20 µm.

In order to confirm the specificity of the staining, I treated culture cells with two microtubule depolymerizing drugs, colchicine and nocodazole, prior to fixation. Control cells

(Figure 26A – C) showed the presence of cortical microtubules and the ventral bundles. In cells treated with 2 mM colchicine for 1 hour no structures were labeled with the ß-tubulin D66 antibody (Figure 26H), whereas treatment with the solvent, $_{d}H_2O$, did not affect the ß-tubulin staining (Figure 26E). On the contrary, treatment with 20 µM nocodazole did not depolymerize microtubules, suggesting that this drug either does not depolymerize microtubules in *O.* cf *ovata* or is not efficiently internalized by the cells (Figure 26K).

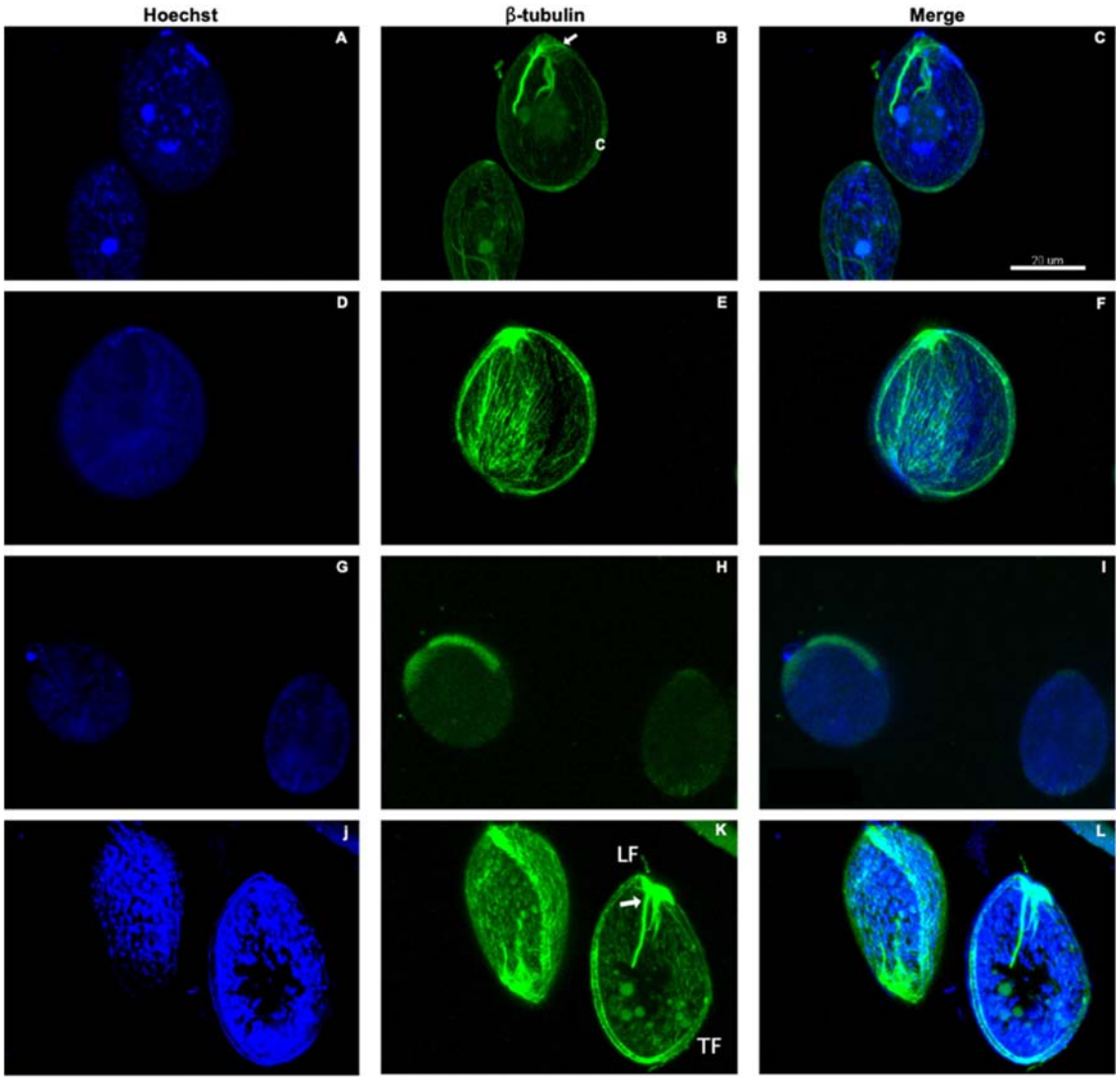

Figure 26. Effect of colchicine and nocodozale on microtubule organization in cultured *Ostreopsis* cf. *ovata* cells-strain MCV054.
Representative image of O. cf. ovata cells labeled with Hoechst 33342 (DNA, blue, left) and ß-tubulin D66 antibody (green, middle). A-C) Control untreated cells. D-F) Cells were treated with distilled water (solvent of colchicine), or G-I) with 2mM colchicine for one hour, or J-L) with 20 µM nocodozale for one hour. Note that Hoechst 33342 also labels mitochondria and chloroplasts. Scale bar is 20µm.

3.2.2 Microtubule changes in *Ostreopsis* cf. *ovata* vegetative cycle

As described in chapter 2, different stages in *O.* cf. *ovata* mitotic cycle can be recognized based on nuclear position. I therefore co-stained cells for ß-tubulin and the DNA dye Hoechst 33342 to be able to recognize different cell cycle stages and describe the microtubule cytoskeleton at different phases of the mitotic cycle.

As previously described for other dinoflagellates (Kato et al., 2000; Perret et al., 1993), I observed that the cortical microtubule array is present throughout the cell cycle, including mitosis, as it can be observed in Figures 27B (interphase), 27L (pre-dividing), 28C (mitosis), Figure 29I (cytokinesis), and Figure 29K (post-dividing cells). Similarly, the flagella can be observed throughout the cell cycle and are not lost during mitosis, as described instead for other species (Bhaud et al., 1991; Uzbekov, 2018). Flagella were observed both in mitotic cells (Figure 28H and K) and in cytokinetic cells (Figure 29H).
Specific structures, however, were identifiable at each stage and are described in details below.

Interphase

Interphase cells are characterized by the position of the nucleus in the dorsal area (Figure 27A, D, G, Hoechst). In these cells the ventral bundles are anchored to a microtubule rich structure in the ventral area, where the basal bodies are probably located,. The bundles can be of different lengths but often reach the middle of the cell. The bundle that grows towards the hyposome is often branched (Figure 27E, H, K) and multiple thin ramifications can be observed towards the cell center (Figure 27H and I.1) in some cells. These ramifications vary in length (Figure 27E, H and K) and can extend to reach the dorsal side of the nucleus (Figure 27I.1). In pre-dividing cells, then, once the nucleus has repositioned to the cell center, microtubules branching from the ventral bundle envelope the nucleus on opposite sides (Figure 27K and 27L.1), forming a structure that resembles an inverted “Y”. This microtubule structure that connects the nucleus to the ventral area, where the basal bodies are located, resembles the microtubule ‘three-pronged fork’ which was described in *C. cohnii* (Perret et al., 1993) to connect the mitotic spindle with the basal bodies.

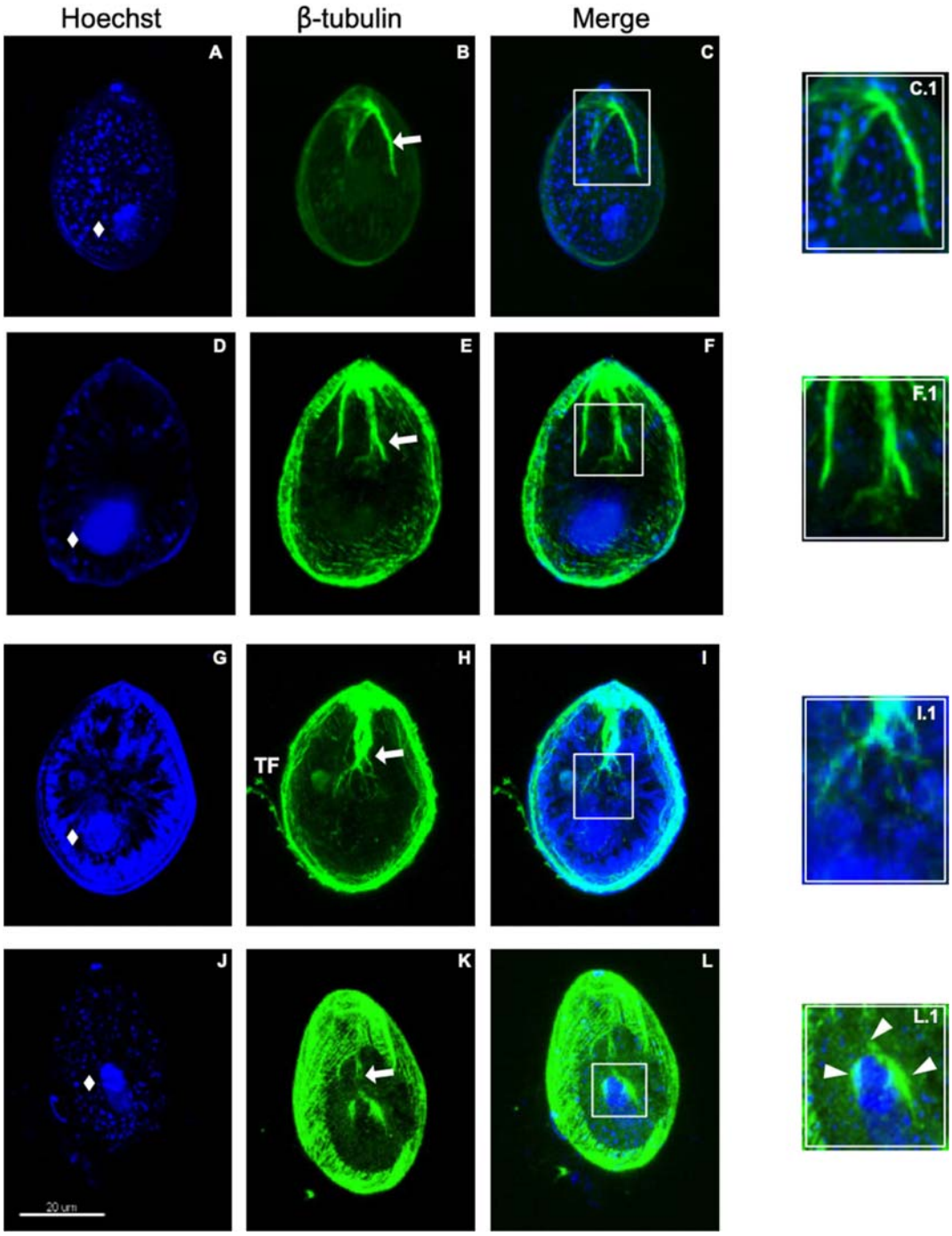

Figure 27. Microtubule organization in interphase and pre-dividing cells.

Representative confocal images of cells ordered based on length of ventral bundle and microtubule branching toward the nucleus. Cells are labelled with Hoechst 33342 (blue, left) to stain DNA and with anti-ß tubulin D66 antibody (green, middle). Diamonds indicate position of nuclei. Arrows point to ventral bundle. White squares indicate the end of the ventral bundles, and are enlarged 2.5 times on the right. Scale bar is 20µm.

Mitosis

In mitotic cells, recognized by the position of a single nucleus in the middle of the cell, microtubules organize in 6 to 7 parallel bundles that align along the short axis of the cell to form the mitotic spindle (Figures 28B, E, H, K), suggesting the presence of 6 to 7 nuclear channels. Spindle microtubules converge at both poles (indicated in white square in 28C, F, I, and L), likely at the kinetosomes. However, as I have not tested whether any markers of kinetosomes localize at these sites, I will herein call them kinetosome-like structures.

The spindle appears anchored to the ventral side of the cell through the ventral bundle, which contacts the spindle at the kinetosome-like structures (arrowhead Figures 28B, E, H, K, N). These thin microtubule connections are reminiscent of the desmoses, thin microtubular fibers connecting the basal bodies and the kinetosomes described in *C. cohnii* (Ausseil et al., 2000; E. Perret et al., 1993; Perret et al., 1991).

Early mitotic cells can be recognized by the presence of metaphase-like plates in the central region of the spindle where chromosomes are aligned along the longitudinal axis of the cell (double arrow, Figure 28A). As cells progress through mitosis and chromosomes are clearly segregated, the mitotic spindle elongates along the short cell axis. In cells where chromosomes are well separated, microtubules begin to be enriched at both the ventral and the dorsal poles of the cell (Figure 28K, N).

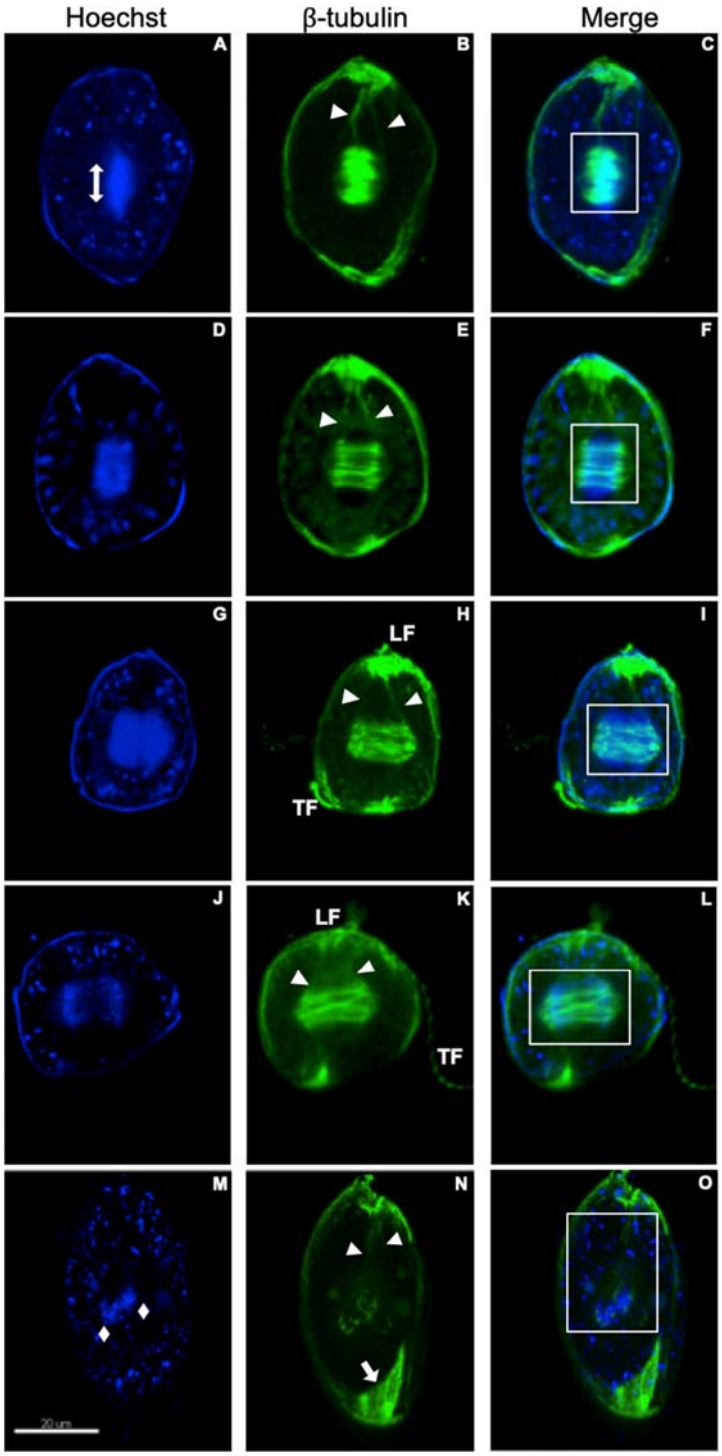

Figure 28. Microtubule organization during mitosis.

A-O) Representative confocal images of cells in mitosis organized based on extent of chromosome segregation. Cells are labeled with Hoechst 33342 (blue, left) to stain DNA and with anti-ß tubulin D66 antibody (green, middle). White squares indicate the spindle area. Note that the ventral bundle (arrowheads) is always connected with the ventral area on one side and with the mitotic spindle on the other side. Double arrow in A indicates metaphase plate. Arrowheads point the desmoses. Diamonds in M point to separated DNA masses. Arrow in M points to the site where the cytokinetic plate begins to form. TF=transversal flagellum and LF= longitudinal flagellum. Scale bar is 20µm

Cytokinesis

As cells progress through mitosis microtubules accumulate in the dorsal area (arrow, Figure 28N). A microtubule plate seems to grow from the dorsal to the ventral area along the longitudinal axis of the cell, eventually forming a microtubule plate, which I will call the cytokinetic plate, that transverses the cell at the site of cytokinesis, along the dorsal-ventral axis (double arrows in Figures 29B, E, H). As the cytokinetic plate grows from the dorsal side towards the cell center, the microtubule rich area present in the ventral area, where the basal bodies are located, expands laterally and sometimes divides into two independent structures (arrowhead, Figure 29B). In these cells, short spindle microtubules are still associated with chromosomes (arrows Figure 29C, F, I, L) and anchor them to the ventral side of the cell through the ventral bundle (Figure 29B, E, H, K).

Once the cytokinetic plate reaches the ventral side, it thickens and separates to give rise to the new sides of the daughter cells (Figure 29H). At this stage the nucleus, which was relocated to a lateral position by the growing spindle, is anchored to the ventral area by the ventral bundle (arrows Figure 29F, I). Following cell division therefore the newborn cell, or post-dividing cell, can be recognized by a nucleus in lateral position still associated with the ventral bundle (Figure 29L).

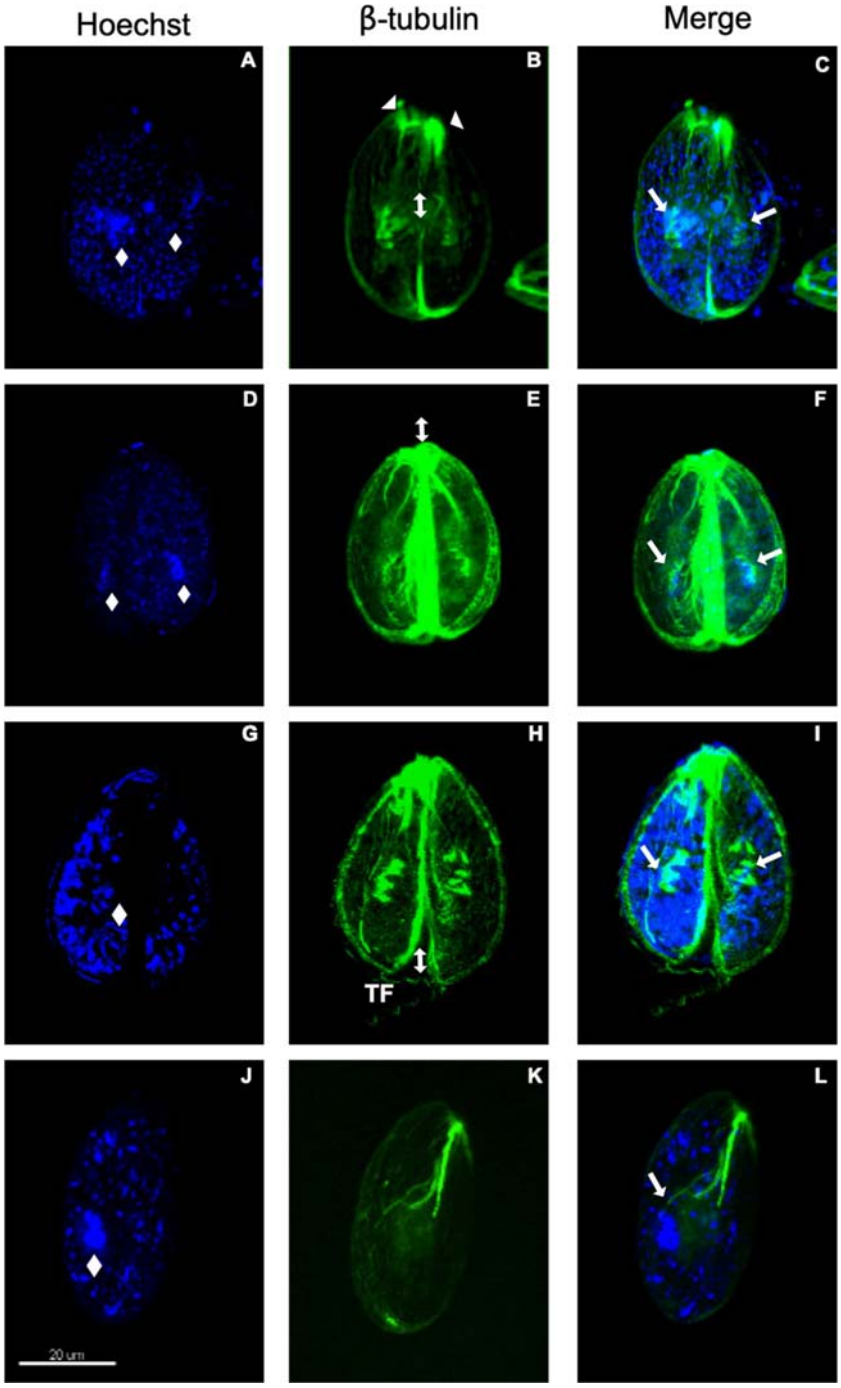

Figure 29. Microtubule organization in telophase, cytokinesis and post-dividing cells.
A-C) Representative confocal images of cells labeled with Hoechst 33342 (DNA, blue, left) and anti ß-tubulin D66 antibody (green, middle) in telophase, D-I) cytokinesis and J-L) postdividing cells. Pictures are organized in order based on extent of chromosome segregation and of cytokinetic plate formation. Diamonds indicate position of nuclei. The cytokinetic plate is indicated by double-headed arrows in B, E, H. Arrowheads in B point to duplicated ventral area with an enrichment of microtubules. Arrow in L points to bundle still connected with nucleus in postdividing cell. Scale bar is 20µm.

3.2.3 An actomyosin ring does not form during cytokinesis in *Ostreopsis* cf. *ovata*

Differently from yeast, animal cells and possibly some dinoflagellates species, my analysis showed that a microtubule plate is present at the site of cytokinesis in *O. cf. ovata*, suggesting that cytokinesis is driven my microtubules and not by actin in this organism. To begin to test this hypothesis I first examined actin localization and organization during cytokinesis. I labelled the actin cytoskeleton using phalloidin-iFluor 488. Both, interphase (Figure 30A) and dividing cells (Figures 30B- D) showed a cortical grid pattern, similar to that described in another dinoflagellate, *S. kawagutii* (Villanueva et al., 2014). Nuclear accumulation of actin was observed in some cells (arrows 30A, B, D) as previously observed in *C. cohnii* (Perret et al., 1993); *L. polyedra* (Schnepf, 1988) and in *Lingolodilium polyedra* (Stires & Latz, 2018). Cells undergoing cytokinesis showed a more intense staining in the ventral side, near the area where the cytokinetic plate finishes its formation (arrowhead Figure 30C). However, no enrichment of actin along the dorsal-ventral axis was observed in dividing cells. To validate the actin staining, I treated cells with the actin depolymerizing drug latrunculin-B, (10 µM). Five minutes after treatment, cells stopped swimming and changed their typical oval shape to a rounded shape (Figure 30E, J). Cells were then fixed in PFA and stained with phalloidin-iFluor 488. The actin grid pattern previously described was lost after latrunculin-B treatment (Figure 30E). These observations confirm that the grid like network observed with phalloidin-iFluor 488 is actin based and suggest the absence of an actin ring at the site of cytokinesis.

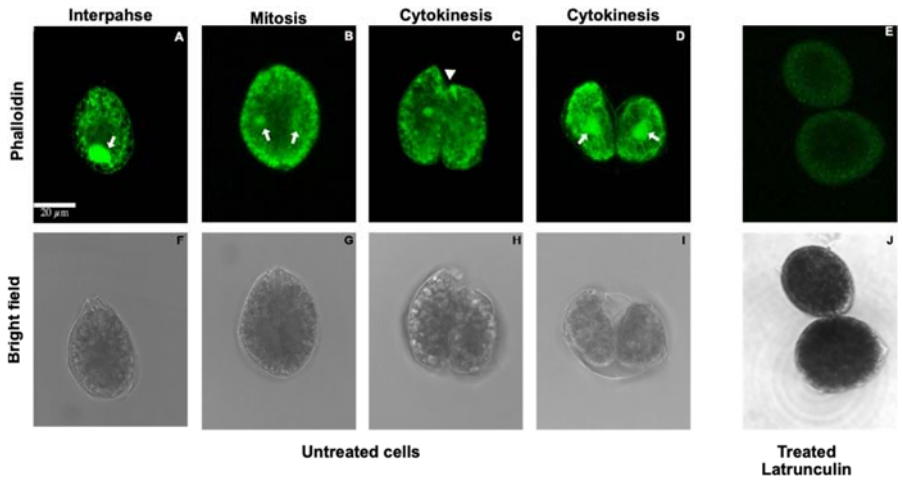

Figure 30. Microfilament cytoskeleton in *Ostreopsis* cf. *ovata*.
A-E) Representative confocal images of culture cells fixed in PFA and stained with CytoPainter Phalloidin-iFluor 488. F-I) Bright field images of same cells as in A-E. E and J show cells treated with Latranculin-B for 5 minutes before fixation. Arrows point to nuclei. Arrowhead points to area of actin enrichment in the ventral side of the cell. Scale bar is 20µm.

3.2.4 Electron microscopy analysis

To complement the analysis carried out by immunofluorescence, I obtained funding from Assemble Plus (Project: "Cell division in the dinoflagellate *Ostreopsis cf. ovata*") to collaborate with dr. Benvenuto and dr. Montresor at Stazione Zoologica Anton Dohrn in Naples to perform a characterization of the microtubule cytoskeleton during mitosis by transmission electron microscopy (TEM). Unfortunately, (due to Covid-19) only one sample was processed and microtubules were not preserved in the preparation. Pictures of interphase and pre-dividing cells were obtained and are shown in Figure 31. Eleven chromosomes-like structures can be seen near the dorsal tip of the nucleus (arrows 31A, B; and enlargement in A.1, B.1).

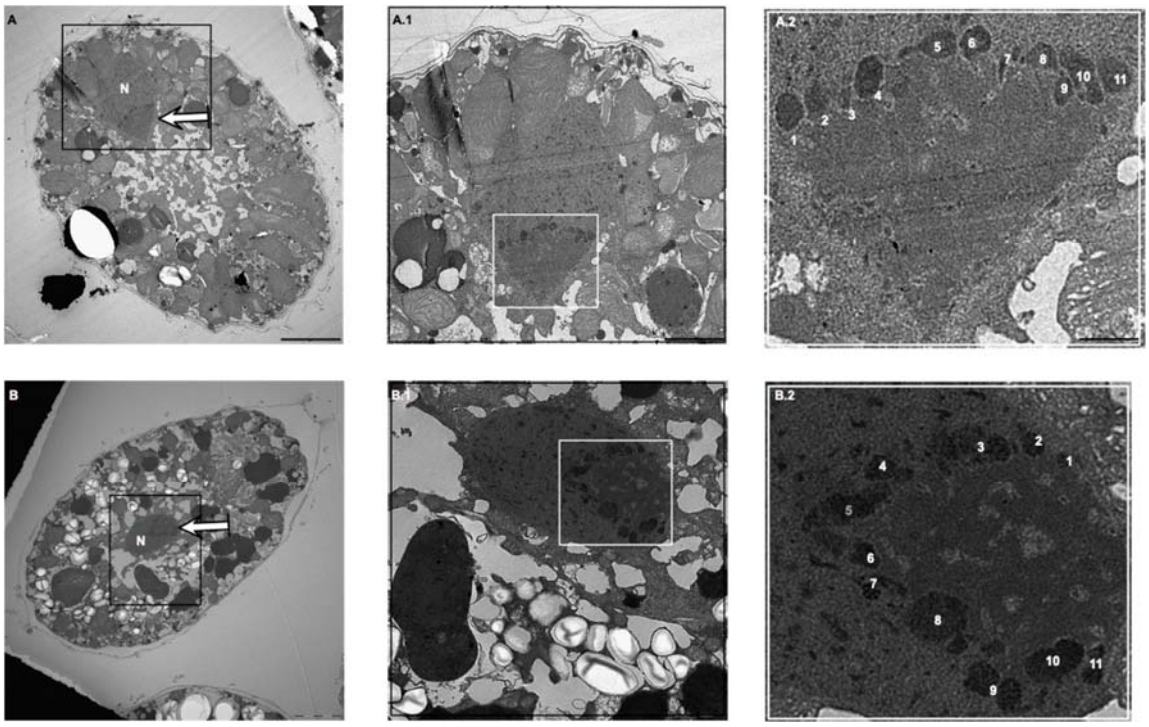

Figure 31. Chromosomes visualized by TEM.
Pictures of interphase (A) and pre-dividing (B) cells were obtained after processing one sample of 2020 bloom collected at 4:00 am. Black square indicate nuclear areas enlarged in the middle panel. White squares in A.1 and B.1 indicate chromosomal elements enlarged in the right panels (A.2 and B.2). Scale bar A, B - 5 µm; A.1, B.1 - 2µm; A.2, B.2 – 1 µm.

3.2.5 Post-translational modification of microtubules during the mitotic cell cycle in *Ostreopsis* cf. *ovata*

All microtubules are formed by α/ß tubulin heterodimers whose properties can be modulated by post-translational modifications of specific subpopulations. Many modifications have been identified with different functions, often not yet characterized. To date, post-translational modifications of microtubules have never been studied in dinoflagellates. I therefore decided to characterize two modifications, tyrosination and acetylation, whose functions have been extensively studied in yeast and animals.

Acetylation of α-tubulin on lysine 40 is common and is found on stable microtubules in most cell types (Eshun-Wilson et al., 2019). Generally, it prevents microtubule breakage, facilitates protofilament sliding and increases microtubule flexibility (Janke & Magiera, 2020). Microtubule acetylation is catalyzed by α-tubulin acetyltransferase-1 (ATA-1) (Shida et al., 2010) whose gene is expressed in the *O*. cf. *ovata* transcritpome (described in chapter 4). Tyrosination of α -tubulin, instead, occurs on soluble heterodimers and is catalyzed by the tubulin–tyrosine ligase (TTL) (Szyk et al., 2011), which is also expressed in the *O*. cf. *ovata* transcriptome (chapter 4). Tyrosinated tubulin had been reported to label core spindle microtubules but not astral microtubules in fibroblast (Peris et al., 2006).

To analyze the distribution of acetylated microtubules I used a monoclonal antibody, T6793-sigma, which recognizes acetylated lys40 of α-tubulin. For tyrosinated α-tubulin, I used the YL1/2 rat monoclonal antibody, which specifically recognizes the C-terminal EEF and EEY sequences of yeast α-tubulin (Janke, 2013). Both epitopes, the lys40 and the EEF sequence are conserved in *O*. cf. *ovata* α-tubulin (Figure 32).

>TRINITY_DN2223_c0_g1_i8.p. *α*- tubulin sequence. *O.* cf. *ovata* reference transctiprome..
MRECICIHIGQAGIQIGNACWELFCLEHGIQPDGQMPSDKTIGGGDDAFNTFFSETGAGK
HVPRCVFVDLEPTVVDEVRTGTYRQLFHPEQLISGKEDAANNFARGHYTIGKEIVDLVL
DRIRKLADNCTGLQGFMVFNACGGGTGSGLGCLMLERLSVDYGKKSKLSFTVWACPQ
VATAVVEPYNTVLCVHSLLEHTDVTIMMDNEALYDICRRNLDIERPTYTNLNRLLGQIIS
SLTASLRFDGALNVDITEFQTNLVPYPRIHFMLSSYAPVISAEKAYHEQLSVAEITMSVFE
PASMYVKCDPRHGKYMACCMMYRGDVVPKDVNAAVATIKTKRTIQFVDWCPTGFKC
GINYQPPTVVPGGDLAKVMRACCMISNSTAIAEVFSRIDHKFDLMYSKRAFVHWYVGE
GMEEGEFSEAREDLAALEKDYEEVGIETAEGEGEEFGYGDEF*

Figure 32. Sequence of *Ostreopsis* cf. *ovata* α-tubulin indicating sites of post-transcriptional modifications. The epitope recognized by the antibody YL1/2 against tyrosinated tubulin (aminoacids EEF) is highlighted in yellow and the epitope recognized by the antibody T6793 against acetylated tubulin (aminoacid K) is highlighted in red.

Both antibodies labeled subpopulations of the microtubule structures observed with the ß–tubulin antibody. In interphase cells (Figure 33), tyrosinated tubulin is concentrated mainly at the ventral area, at the site of flagellar insertion, and labels the microtubule ventral bundles (arrowhead, Figures 33B, J, N). Acetylated tubulin showed a similar pattern, in the ventral area (arrowhead Figures 33C, G, K, O). Co-staining of tyrosinated and acetylated tubulin showed that tyrosinated microtubules were also present in the distal part of the ventral bundle in contact with the nucleus (arrows, Figure 33H, L, P), while acetylated microtubules were enriched in the thin ramifications that grow towards the nucleus (arrows Figure 33C, D; O, P). The staining of the desmoses with acetylated tubulin antibody becomes more intense in mitotic cells (Figures 33P; 34C, G), whereas tyrosinated tubulin is rarely detected in those structures (Figure 33N; 33 B). Interestingly in several cells spindle microtubules are present only in the ventral side of the nucleus, suggesting that channels begin to form on the ventral side and then progress towards the dorsal side of the nucleus (Figure 33L, P).

Both antibodies label the spindle microtubules (arrowhead in Figures 34B, F, J, N; arrows in 34C, G, K, O). Once chromosomes are aligned on the metaphase-like plate (Figure 34A), tyrosinated tubulin appears to be excluded from the regions of the spindle near the poles (arrows 34D). As cells progress through mitosis, determined by separation of chromosomes, the difference between the two populations of microtubules becomes more evident, with tyrosinated tubulin marking the center of the mitotic spindle (Figures 34B, F, J and N), and acetylated tubulin labelling the poles of the spindle (arrows in Figures 34D, H, L).

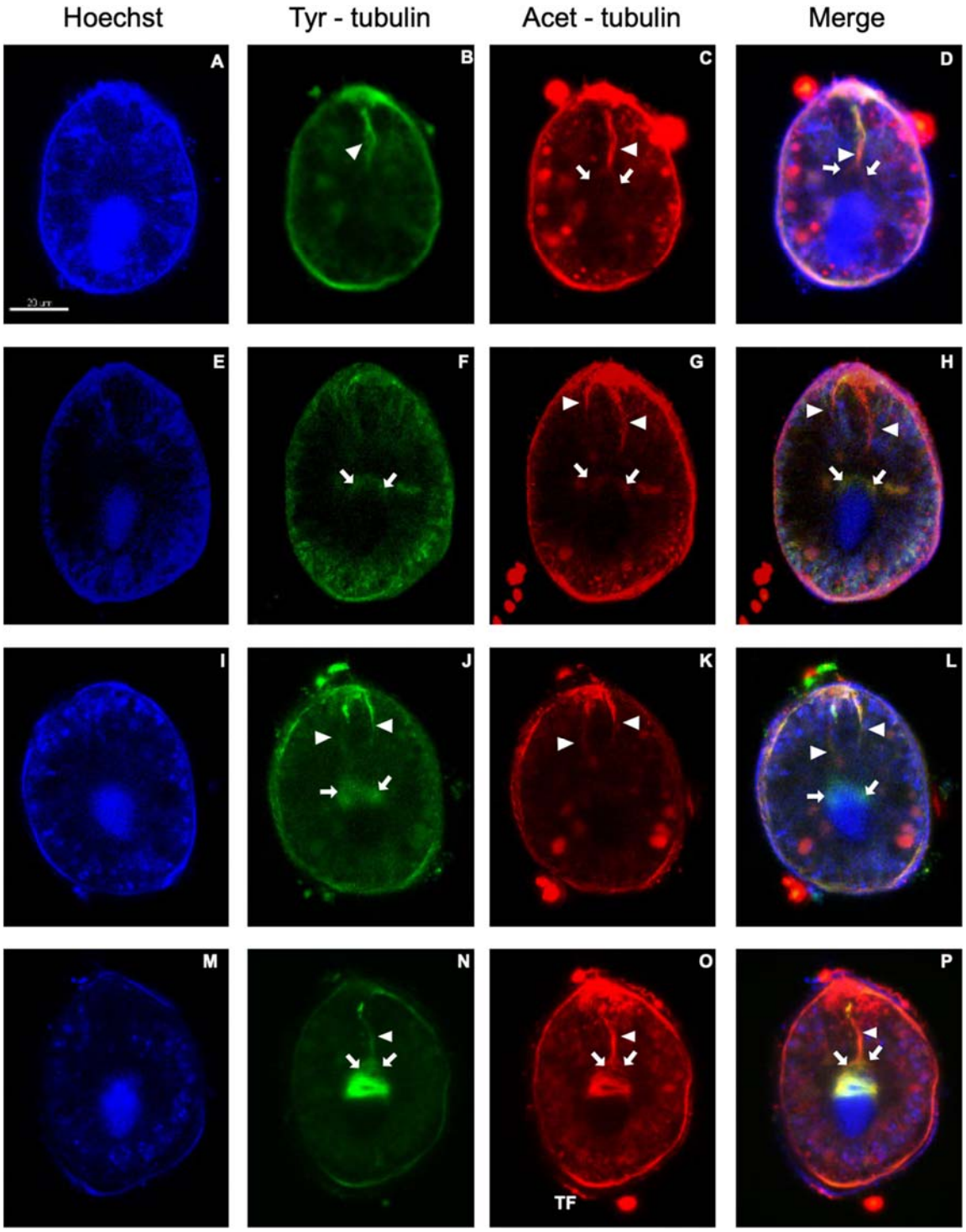

Figure 33. Microtubule post-translational modifications in interphase.
Representative confocal images of *O.* cf. *ovata* cells labeled with Hoechst 33342 (DNA, blue, left) and anti tyrosinated tubulin antibody (tyr-tubulin, green) and anti acetylated tubulin antibody (acet-tubulin, red). A-D) Interphase cells, E-P) pre-dividing cells. Arrowheads point to ventral bundle; arrows point to distal part of the ventral bundles including ramifications.

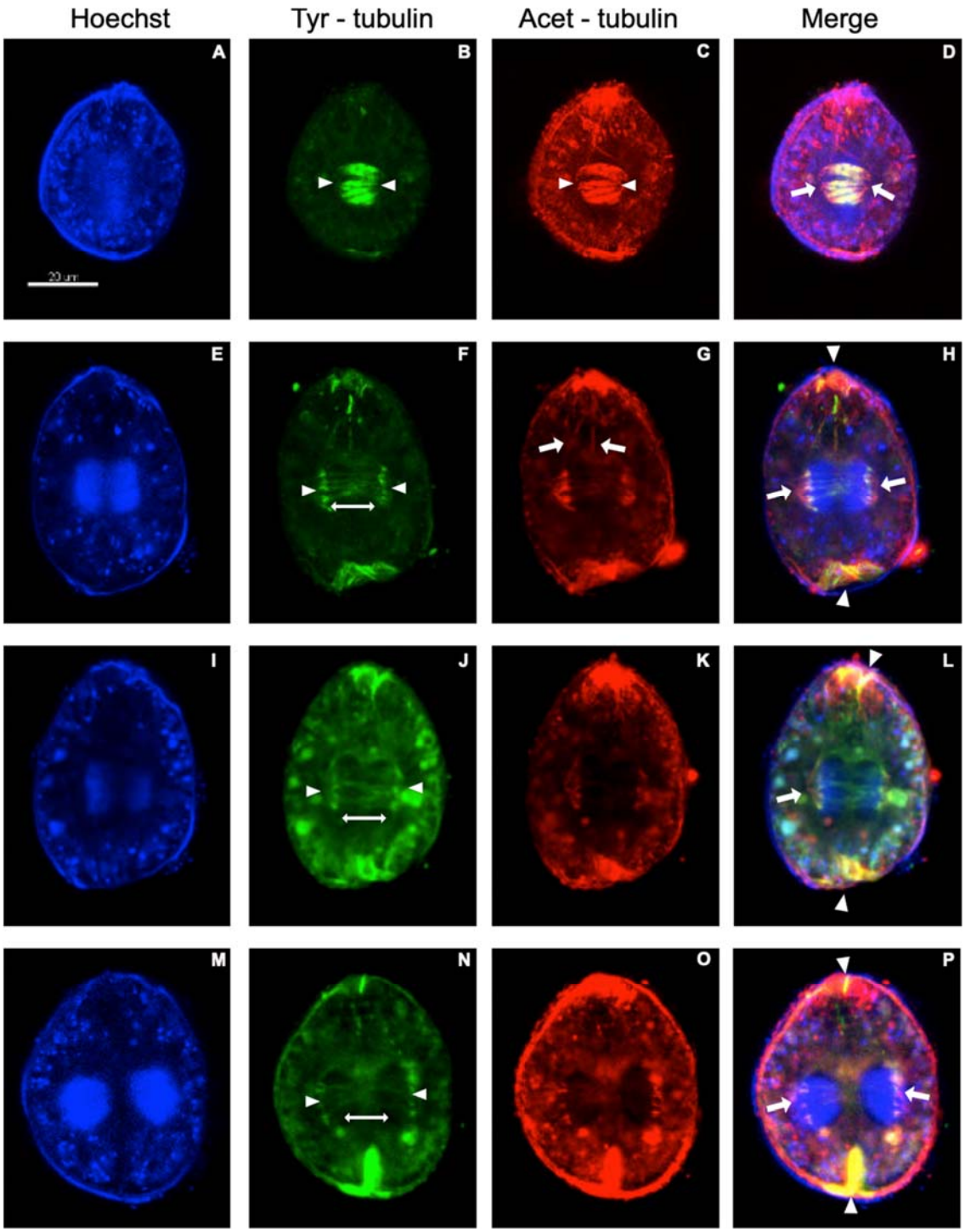

Figure 34. Microtubule post-translational modifications in mitosis.
Representative confocal images of *O.* cf. *ovata* cells labeled with Hoechst 33342 (DNA, blue, left) and anti tyrosinated tubulin antibody (tyr-tubulin, green) and anti acetylated tubulin antibody (acet-tubulin, red). Arrowheads point to mitotic spindle. Tyrosinated tubulin stained the center of the mitotic spindle (double arrow, B, F, J and N), whereas acetylated tubulin stained desmoses (arrows C, G) and microtubules near the spindle poles (arrows in D, H, L and P). Both antibodies labeled the site where the cytokinetic plate starts to form (P). Both antibodies stained at opposite poles of the cell: the ventral area and the dorsal area (arrowhead, H, L, P) where the cytokinetic plate started to form (P).

As the spindle extends both tyrosinated and acetylated tubulin accumulate at opposite sides of the longitudinal axis of the cell: in the ventral area and in the dorsal side, where the cytokinetic plate forms (arrowheads in Figures 34H, L, P). Both antibodies then label the cytokinetic plate, throughout cytokinesis (arrowhead Figures 35D, H, L).

In post-dividing cells the ventral bundle that is still associated with the top of the nucleus (arrow, Figure 35P), is co-stained by both antibodies.

Consistently with what was observed for other organisms (Marute, et al., 1986; Piperno et al., 1987; Janke & Magiera, 2020), the transversal flagellum contains acetylated tubulin (33G, O) but not tyrosinated tubulin (33F, N).

In summary, acetylated tubulin labels preferentially the ventral bundle and the spindle tips associated with kinetosome-like structure. On the contrary, tyrosinated tubulin is present in the central spindle region throughout mitosis until its depolymerization when the cytokinetic plate reaches the middle of the cell.

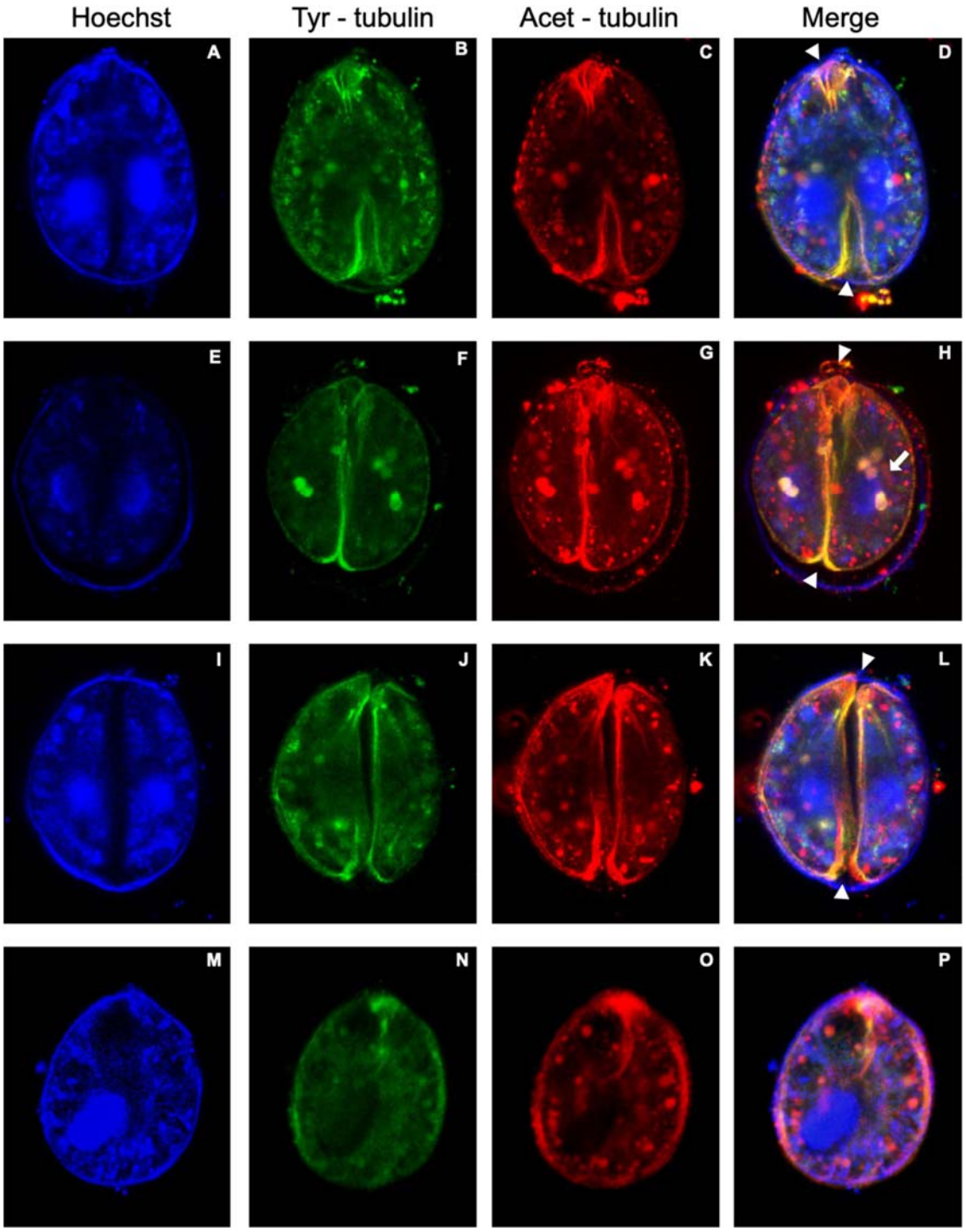

Figure 35. Microtubule post-translational modifications in cytokinesis and post-dividing cells.
Representative confocal images of *O.* cf. *ovata* cells labelled with Hoechst 33342 (DNA, blue, left), anti tyrosinated tubulin antibody (tyr-tubulin, green) and anti acetylated tubulin antibody (acet-tubulin, red). Both antibodies stained similarly the cytokinetic plate (arrowhead D, H, L). Arrow in H points to kinetosomes enriched in acetylated tubulin. Scale bar is 20µm.

3.2.6 γ-tubulin and MTOCs in *Ostreopsis* cf. *ovata*

Having characterized the major changes in microtubule organization I was interested in identifying the position of the microtubule organizing centers (MTOCs), sites where microtubules are nucleated and that underlay the organization of the microtubule arrays. These sites, which include centrosomes in animals and spindle pole bodies in yeasts, contain microtubule nucleating complexes, such as γ-tubulin, and microtubule stabilizing complexes. γ-tubulin is one of the best characterized proteins from centrosomes and spindle poles bodies (SPBs), and is responsible for the nucleation of microtubules during mitotic spindle formation in animals and fungi. In *C. cohnii*, γ-tubulin localizes at centrosomes present at the spindle poles (Ausseil et al., 2000).

Given the conservation of γ-tubulin across several organisms, I decided to analyze γ-tubulin distribution during the mitotic cycle of *O.* cf. *ovata*. For this analysis, I used an antibody against human γ-tubulin (T6557), whose sequence showed 34% identity with the *O.* cf. *ovata* γ-tubulin retrieved from the reference transcriptome (Figure 36A).

Figure 36B shows a dorsal view of a cell with the transversal flagellum labelled by γ-tubulin. Unlike β-tubulin, γ-tubulin did not label the cingulum but only the transversal flagellum, which is visible at both sides of the cell.

γ-tubulin also marks the ventral (where basal bodies are reported) and dorsal tips of the cell in interphase and pre-dividing cells (arrows Figure 36F and I). In late mitotic cells, when the chromosomes are fully separated, γ-tubulin remains visible in the ventral area which, as already observed with ß-tubulin, in some cells divides into two distinct zones (Figure 36L). At the dorsal side the γ-tubulin rich region extends in the direction of the long axis, in the same direction of the cytokinetic plate (Figures 36L and 36B) and by the end of division γ-tubulin was found along the entire cytokinetic plate. Surprisingly, γ-tubulin was never observed at spindle poles. Given the unexpected pattern of localization of γ-tubulin that I observed in *O.* cf *ovata*, this preliminary analysis needs to be complemented with other known markers of MTOCs to validate this study and describe with confidence *O.* cf *ovata* MTOCs. Given the limited sequence identity between *O.* cf *ovata* and human γ-tubulin, generation of a specific *O.* cf *ovata* γ-tubulin antibody is also envisageable.

A

```
sp|P23258|TBG1_HUMAN          MPREIITLQLGQCGNQIGFEFWKQLCAEHGISPEGIVEEFATEGTDRKDVFFYQADDEHY   60
TRINITY_DN5283_c0_g1_i9.p1    -MRELVHIQGGQCGNQIGAKFWEVISDEHGIDPTGTYHGDSDLQLERINVYYNEATGGRY   59
                                **:: :* ******** :**: :. ****.* *  .  :    :* :*:: :* . :*

sp|P23258|TBG1_HUMAN          IPRAVLLDLEPRVIHSILNSPYAKLYNPENIYLSEHGGGAGNNWASG-FSQGEKIHEDIF   119
TRINITY_DN5283_c0_g1_i9.p1    VPRAVLMDLEPGTMDSVRAGPFGQLFRPDNFVFGQT--GAGNNWAKGHYTEGAELIDSVL   117
                              :*****:**** .:.*:  .*:.:*:.*:*: :.:   *******.* :::* :: :.::

sp|P23258|TBG1_HUMAN          DIIDREADGSDSLEGFVLCHSIAGGTGSGLGSYLLERLNDRYPKKLVQTYSVFPNQDEMS   179
TRINITY_DN5283_c0_g1_i9.p1    DVVRKEAEGCDCLQGFQMCHSLGGGTGSGMGTLLISKVREEYPDRIMETFSVIPSP-KVS   176
                              *:: :**:*.*.*:** :***:.******:*: *:.::.:.**.::::*:**:*.  ::*

sp|P23258|TBG1_HUMAN          DVVVQPYNSLLTLKRLTQNADCVVVLDNTALNRIATDRLHIQNPSFSQINQLVSTIMSAS   239
TRINITY_DN5283_c0_g1_i9.p1    DTVVEPYNAVLSFHQLVENADECFLLDNEALYDICFRTLKLTTPTYGDLNHLVSAAMSGV   236
                              *.**:***::*:::::*.:***  .:*** **  *.   *:: .*::.::*:***: **.

sp|P23258|TBG1_HUMAN          TTTLRYPGYMNNDLIGLIASLIPTPRLHFLMTGYTPLTTDQSVASVRKTTVLDVMRRLLQ   299
TRINITY_DN5283_c0_g1_i9.p1    TTCLRFPGQLNCDLRKIAVNLVPFPRLHFFMTGFAPLTSRGSQQ-YRALTVPELTQQMFD   295
                              ** **:** :* **  : ..*:* *****:***::***:  *    *  ** :: :::::

sp|P23258|TBG1_HUMAN          PKNVMVSTGRDRQTNHCYIAILNIIQGEVDPTQVHKSLQRIRERKLANFIPWGPASIQVA   359
TRINITY_DN5283_c0_g1_i9.p1    AKNMMCAADP---RHGRYLTAAALFRGRMSTKEVDEQMLNVQNKNSSYFVEWIPNNIKAS   352
                               **:* ::.     :  *::   :::*.:. .:*.:.: .::::: : *: * * .*:.:

sp|P23258|TBG1_HUMAN          LSRKSPYLPSAHRVSGLMMANHTSISSLFERTCRQYDKLRKREAFLEQFRKEDMFKDNFD   419
TRINITY_DN5283_c0_g1_i9.p1    VCDIPP---KGLKMAVAFAGNSTAIQEMFKRVAEYFTAMFRRKAFLHWYTGEGMDEMEFT   409
                              :.   *   .. :::  : .* *:*..:*:*... :  : :*:***. :  *.* : :*

sp|P23258|TBG1_HUMAN          EMDTSREIVQQLIDEYHAATRPDYISWGTQEQ------- 451
TRINITY_DN5283_c0_g1_i9.p1    EAESNMNDLVSEYQQYQDATAEEEGEFDEEEGEYDMQA* 447
                              * ::. : : .  ::*: **  :  .:. :*
```

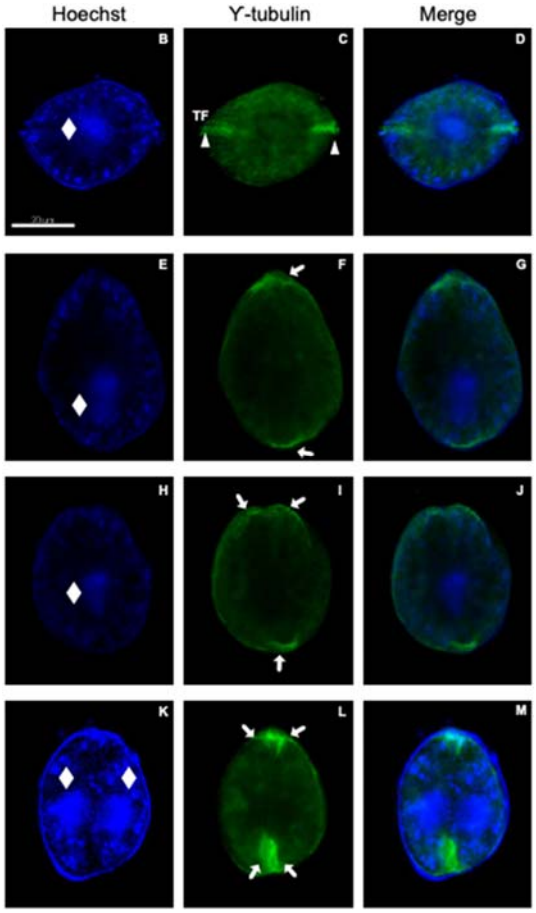

Figure 36. *Ostreopsis* cf. *ovata* γ-tubulin localizes to dorsal and ventral sides of the cytokinesis plate.

A) Clustal alignment of human and *O.* cf. *ovata* γ-tubulin sequences. B-D) Representative confocal images of interphase cells from a dorsal view, (E-G) from a frontal view, H-J) a pre-dividing cell and K-M) a mitotic cell labelled with Hoechst 33342 (blue, DNA) and with anti-γ-tubulin T6557 antibody (green, middle). Diamonds indicate nuclei. γ-tubulin labels the transversal flagellum (TF, arrowheads in C), the ventral and the dorsal area (arrows in F, I, L)

3.2.7 Preliminary analysis of the role of microtubules during the mitotic cycle in *Ostreopsis* cf. *ovata*

Having shown that mitotic division in *O.* cf. *ovata* occurs in the center of the cell and that during its re-localization from the interphase dorsal position to the cell center, the nucleus associates with the ventral microtubule bundle, I then asked whether nuclear repositioning depends on microtubules and whether it is a pre-requisite for proper cell division.

To address these questions, I decided to analyze nuclear position and cell division in the absence of microtubules. I used two methods to interfere with microtubule organization: treatment with the microtubule depolymerizing drug colchicine, which as I previously described, fully depolymerizes microtubules in *O.* cf. *ovata*; and constant agitation which has been associated with altered microtubule dynamics (Berdalet, 1992) and affects *O.* cf. *ovata* proliferation (Berdalet et al., 2017).

As culture cells divide only at very low level, I performed the treatments on natural samples collected during the bloom. Based on the characterization of cell division carried out during the 2020 bloom and reported in Chapter 2, I collected cells at 00:00 during the proliferative phase (bloom 2020) when the peak of cell division was expected. As shown in the scheme in Figure 37, following collection, cells were immediately transferred to flasks containing either sea water (control) or sea water + 2mM colchicine (colchicine) and then maintained at 28ºC in static incubators in the dark. One flask was placed on an orbital rotator with constant agitation at 70 rpm in the dark at 28ºC (same temperature of the sea).

Aliquotes for all treatments were fixed every two hours (2:00, 4:00 and 6:00 am). At each time point (00:00, 2:00, 4:00 and 6:00 am), a sea sample was also collected and fixed to follow the actual progression of cell division under unperturbed conditions (herein called external control) to control for the effect of the experimental manipulation. Following DNA labelling with Hoechst 33342, cell morphology and nuclear position was analyzed for all samples.

With the aim to determine if colchicine or agitation inhibits *O.* cf. *ovata* cell division, I quantified the percentage of cells undergoing mitosis and cytokinesis for each group. Tables 2-4 show that neither of these treatments inhibited mitosis or cytokinesis.

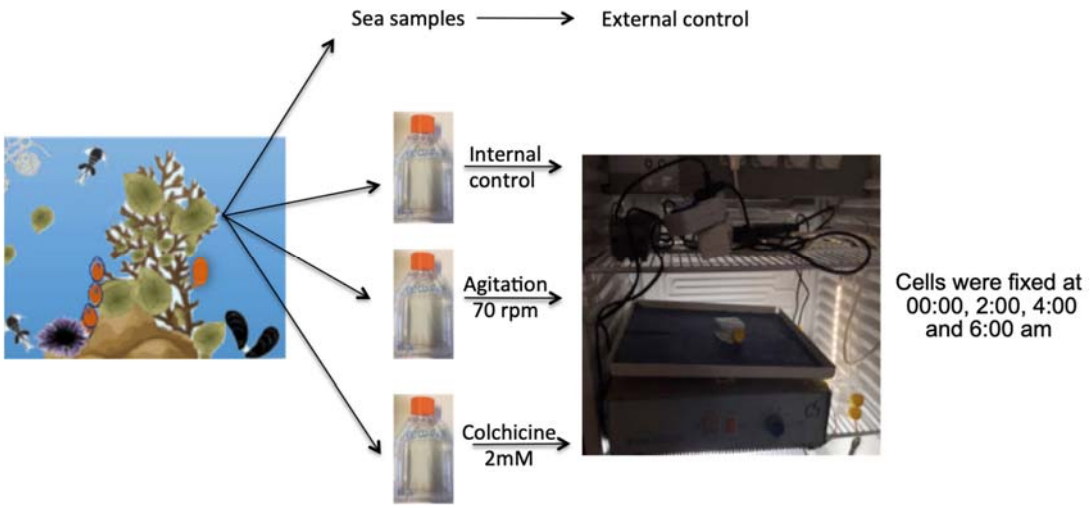

Figure 37. Diagram of experimental procedure to test the function of microtubules during mitosis. Cells were collected with microalgae at Rochambeau and transferred to culture flasks incubated in dark at 28ºC. One flask contained sea water (internal control, un-treated cells), one contained colchicine 2mM (colchicine) and one was subjected to constant agitation (agitation). An aliquot was fixed every two hours from each treatment and also directly at the sampling site (external control).

Tables 2-4. Treatments which interfere with microtubule organization do not inhibit *Ostreopsis* cf. *ovata* cell division. Tables show percentage of cells in mitosis (table2), cytokinesis (table 3) and in division (mitosis and cytokinesis). The experiment was performed during a single night in the proliferative phase of 2020 bloom.

Table 2

Mitosis (%)				
Sampling time	External control	Internal control	Agitation	Colchicine
0:00	4,97	6,3	4,01	5,3
2:00	2,487	0,96	0,17	2,56
4:00	1,11	2	0,36	1,03
6:00	0,80	1,48	0,47	0,28

Table 3

Cytokinesis				
Sampling time	External control	Internal control	Agitation	Colchicine
0:00	2,02	1,57	1,78	1,95
2:00	1,95	1,29	2,70	3,15
4:00	3,06	2,86	1,43	2,51
6:00	1,74	2,22	1,258	2,67

Table 4

Division (mitosis + cytokinesis)				
Sampling time	External control	Internal control	Agitation	Colchicine
0:00	7	7,87	5,8	7,25
2:00	4,44	2,26	2,87	5,71
4:00	4,17	4,87	1,8	3,54
6:00	2,55	3,71	1,73	2,96

However, visual analysis of cell and nuclear morphology during cell division showed that in addition to the five morphotypes previously characterized for *O.* cf. *ovata* cells (interphase, pre-dividing, mitotic, cytokinetic and post-dividing cells), three new morphotypes were present in treated cells. These three new morphotypes were (i) mis-oriented karyokinesis, where the nucleus did not divide along the shorter transverse axis (Figure 38C); (ii) dorsal mitosis, when karyokinesis occurred in the dorsal region instead that in the cell center (Figure 38D); and (iii) mis-oriented cytokinesis, when the cell did not divide along the dorsal-ventral axis (Figures 38E, J).

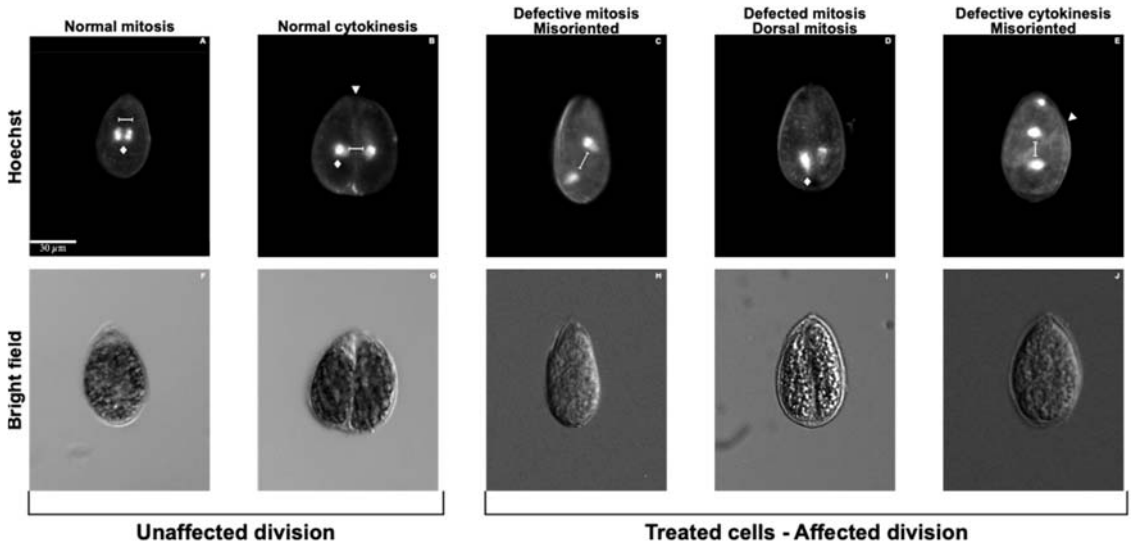

Figure 38. Morphotypes of mitotic an cytokinetic cells from *Ostreopsis* cf. *ovata* 2020 bloom treated with colchicine or subject to constant agitation.

A-E) Representative epifluorescent images of Hoechst 33342 stained cells and F-J) corresponding bright field images of colchicine treated cells. Nuclear position and presence of division plate were used for classification. Unaffected division grouped cells whose karyokinesis occurred in the cell center (arrows, A, B) along the short axis of the cell (bars A, B), and cytokinesis occurred along the longitudinal axis of the cell (arrowhead B, G). Affected division included cells undergoing karyokinesis at a different angle (bar, C) to the short axis of the cell (mis-oriented) and cells that divided with nucleus in dorsal position (arrows, D, dorsal mitosis) and cells undergoing cytokinesis at an angle with the longitudinal plane (E, J, defective cytokinesis).

Quantification of the different morphotypes in all analyzed conditions is reported in annex 2. The morphotypes 'mis-oriented' karyokinesis and 'dorsal mitosis' were grouped as 'defective mitosis'.

As shown in Figure 39A, the three mutant morphotypes were absent in the external control and appeared at low level (less than 10% of mitotic cells and less than 20% of cells in cytokinesis) in samples maintained in the laboratory in sea water only (internal control). In colchicine treated cells, instead, half of the population of mitotic cells showed defects in

mitosis after two hours of treatment (2:00 a.m.). The effect of colchicine on mitosis increased with time and by 6 hours of treatment more than 90% of cells undergoing mitosis showed either orientation defects or incorrect nuclear positioning (Figure 39A - Colchicine).

Similar results were obtained with agitation, with the exception that the effect was more pronounced at 2:00 a.m., when 95% of mitotic cells showed defective mitosis. The effect decreased with time and at 6:00 a.m. 40% of mitotic cells showed defects in mitosis (Figure 38A - Agitation).

Cytokinesis was also evaluated in the same samples. Cytokinesis occurred exclusively along the longitudinal axis in the external control (38B and 39B). In the presence of 2mM colchicine, instead, the plane of cytokinesis was mis-oriented (not along the dorsal-ventral axis, Figure 38E) in 30-50% of dividing cells, depending on length of treatment (Figure 39B). Cells with mis-oriented cytokinetic plates were observed also under constant agitation. Under these conditions, the number of misoriented cytokinetic events increased with time, reaching more than the 60% of the cytokinetic cells at 6:00 am (Figure 39B).

Taken together the results of this functional analysis show that repositioning of the nucleus to the cell center is not a prerequisite for mitosis or cytokinesis in *O.* cf. *ovata* cells. Moreover, although lack of microtubules in treated natural cells has not yet been confirmed by immunofluorescence, these results suggest that *O.* cf. *ovata* can undergo both mitosis and cytokinesis in the absence of microtubules, but microtubules are required for nuclear centering and proper orientation of the mitotic spindle along the transverse axis and of the cytokinetic plate along the longitudinal dorsal-ventral axis.

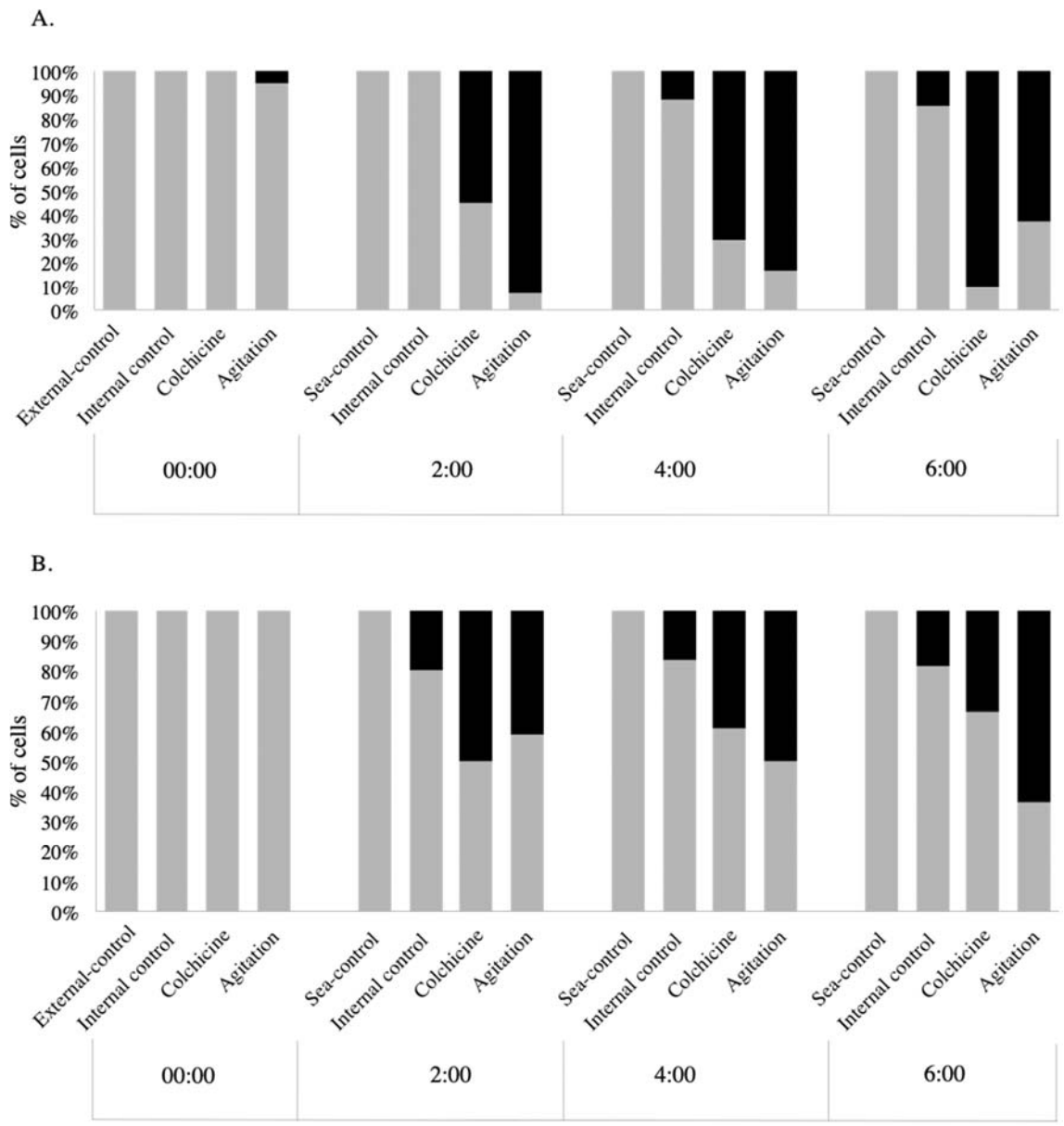

Figure 39. Interfering with microtubule organization results in defects in mitosis (A)and cytokinesis (B). Percentage of normal (grey) or abnormal (black) *O.* cf. *ovata* cells collected at midnight during the proliferative phase of the bloom and either maintained in sea water under static conditions (Internal control), or treated with 2mM colchicine (Colchicine) or incubated in sea water with constant agitation (Agitation). Cells were fixed every 2 hours from beginning of treatment and stained for Hoechst 33342 to analyze mitosis and cytokinesis. At each time point a sample was also collected from the sea and immediately fixed for Hoechst 33342 staining (Sea-control). Raw data associated with this graph are reported in annex 2.

3.3 Discussion

3.3.1 Dinomitosis and cytokinesis in *Ostreopsis* cf. *ovata*

Based on the observations described above a model of *O.* cf. *ovata* vegetative cycle can be proposed (Figure 40).

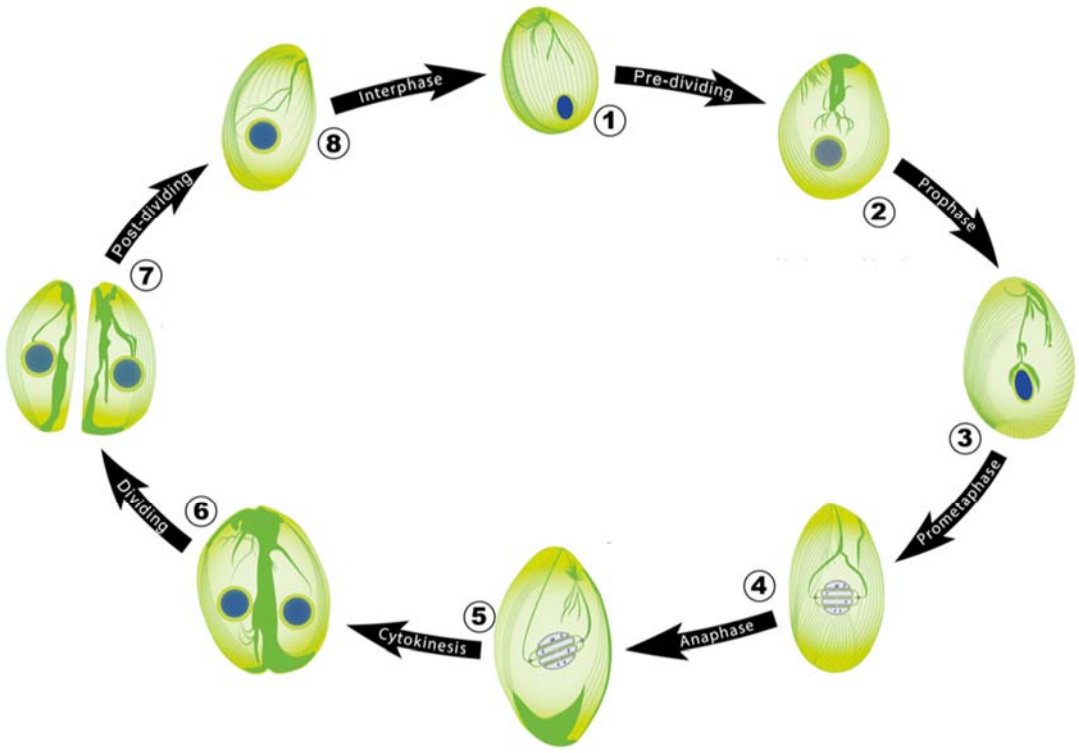

Figure 40. Vegetative cycle of *Ostreopsis* cf. *ovata*.
Graphic representation of the microtubular interaction with the nucleus through the different phases of the vegetative cycle of *O. cf. ovata*. Green – microtubules; blue – DNA. The numbers indicate the cell stage: 1-Interphase, 2 and 3 ventral bundles connect the nucleus and moved to the center (pre-dividing); 4-6 spindle microtubules are formed outside of the nucleus; 6 and 7 show the cytokinetic plate; 8 correspond to a post-dividing cells.

Ventral bundles of microtubules, which during interphase are present in the ventral part of the cell, grow and branch toward the nucleus, located in the dorsal area, as cells prepare for mitosis. The growing ventral bundle contacts the nucleus in its dorsal position and moves it to the cell center (pre-dividing). Upon central localization, the mitotic spindle forms from opposite poles of the nucleus (prophase), 6-7 spindle microtubule bundles transverse the nucleus along the short axis of the cell and chromosomes align on the equatorial plane (metaphase) in a metaphase-like plate. The microtubule mitotic spindle is formed progressively, from the ventral side of the nucleus towards the dorsal side. Spindle

microtubules interact on one side with the chromosomes and on the other side they meet at the kinetosome-like structure. The kinetosome-like structures connect the spindle to the cell ventral cortex through the desmoses, two fine microtubule fibers that in mitosis replace the pre-mitotic ventral bundle. As chromosome segregation continues, a cytokinetic plate starts to form the dorsal side, during anaphase. As the cytokinetic plate approaches the middle of the cell, the microtubule mitotic spindle depolymerizes leaving thin structures (telophase) that interact with the separated nuclei and which are inserted in the kinetosome, keeping the contact with the ventral area through the desmoses. While cytokinesis continues, new ventral bundles are formed in each daughter cells. The cytokinetic plate divides the cell along the longitudinal axis, giving rise to two daughter cells each with a nucleus in lateral position. The laterally positioned nucleus of post-dividing cells remains connected to the ventral bundles until its re-positions to the dorsal side.

The presence of cortical microtubules during mitosis and cytokinesis confirms the generalized idea that, differently from opisthokonts, dinoflagellates do not depolymerize microtubules during mitosis. In opisthokonts, cytoplasmic microtubules are used as a source of tubulin to organize the mitotic spindle. In dinoflagellates the source of tubulin that organizes the mitotic spindle is unknown. One possibility is that a subpopulation of cytoplasmic microtubules which has not been identified yet, depolymerizes during mitosis. Alternatively, expression of tubulin might be up-regulated during division, either at the transcriptional or translational level.

The basal bodies (which contain centrioles) organize the microtubular structure of both flagella from the ventral area in *O.* cf. *ovata* (Escalera et al., 2014). The ventral bundles and the desmoses emanate from the same area toward the nucleus, and during mitosis link the mitotic spindle poles to the ventral zone. These microtubular bundles that emanate from the basal body toward the nucleus are not exclusive to *O.* cf. *ovata.* Similar microtubule based structures have been described in different species of dinoflagellates. A single microtubular strand was found in *Ceratium tripos* (Dodge & Crawford, 1970) and in *Amphidinium poecilochroum* (Larsen, 1988) starting near the flagellar base and ending close to the nucleus. In *Katodinium glandulum*, a similar structure containing twenty-five microtubule rows was described to be present from the flagellar base to the vicinity of the nucleus (Wetherbee, 1975). Soyer (1977), also reported in *Prorocentrum micans* a cylinder of microtubules arising near the basal bodies, passing through the Golgi region and ending in the proximity of the nucleus. In the same species, Schnepf et al., (1990) identified two microtubular bands that extend from the flagellar base towards the cell sides during the early stages of division. In

1993, Perret et. al. and later Ausseil et. al. (2000), proposed that in *C. cohnii* and in other dinoflagellates that stop swimming during mitosis, the basal bodies that organize the microtubules of the flagella, are used to organize the microtubule desmoses which connect the basal body with the mitotic spindle poles, while the flagella are absent (Ausseil et al., 2000; Perret et al., 1993).

Dinoflagellates are not the only organisms where the basal body is associated with flagellar structures and intracytoplasmic microtubular bundles. The capacity to organize microtubular structures in opposite directions has been reported in *Chlamydomonas*, where the basal bodies are also associated with an MTOC that organizes the assembly of microtubules that extend and interact with the nucleus, and the flagella in the other direction (Silflow et al., 1999). In these organisms, γ-tubulin is associated with the basal body. In these cells γ-tubulin is localized in two to four discrete dots or rods and in weak patches in the basal body region, and has been associated with the assembly sites for cortical microtubules. In interphase, the protein labels two discrete dots in the basal body area as well as the general surrounding region. Before division, the cell re-absorbs both flagella. During cell division, two γ-tubulin containing dots separate and localize to opposite poles of the mitotic apparatus and are no longer visible at the flagellar basal bodies. They then migrate during cleavage to their initial position, in the basal body area. γ-tubulin is also observed in the cytokinetic furrow (Silflow et al., 1999).

Similarly, to what just described for *Chlamydomonas*, in *C. cohnii* which loses its flagella and stops swimming before mitosis, the mitotic spindle is organized from γ-tubulin containing centrosomes, while γ-tubulin free kinetosomes are present at the basal bodies and organize the desmoses (Ausseil et al., 2000).

Here I showed that in *Ostreopsis* γ-tubulin labels a zone in the ventral area, where the basal bodies are located, while it is absent from the spindle poles during mitosis. As γ-tubulin is an essential component of the centrioles, this observation suggests that, similarly to other core dinoflagellates (Drechsler & McAinsh, 2012), *O.* cf. *ovata* has acentriolar spindle poles. Based on my observations, γ-tubulin instead is present in the ventral area where the basal bodies are located and from where the microtubules of the flagellar apparatus, the ventral bundles and the desmoses are organized. As the presence of γ-tubulin at basal bodies is necessary for flagellar organization, it is interesting that the presence of flagella during cell division and a centriole organized spindle seem to be mutually exclusive. Indeed, in organisms, like *Chlamydomonas reinhardtii* and *C. cohnii,* which depolymerize their flagella

during cell division (mitosis and cytokinesis), γ-tubulin, which is no longer required at basal bodies, is repositioned to the spindle poles; whereas other core dinoflagellates, like *O.* cf. *ovata,* which maintain their flagella throughout the cell cycle and therefore maintain γ-tubulin at basal bodies during cell division, have acentriolar (γ-tubulin free) spindle poles.

Centrioles normally organize microtubules in one direction. As flagella protrude from the cell body towards the exterior, while ventral bundles and desmoses grow toward the inside of the cell, it is possible that centrioles duplicate during interphase and separate during mitosis, as suggested in some images of *O.* cf. *ovata* where γ and β-tubulin appear separated into two different areas on the ventral side of the cell (Figures 28K, 29B, 34J, 35B and 36L). Nevertheless, the pattern of γ-tubulin is not localized in specific dots (as it would be if labelling only centrioles) but distributed in the ventral area. In *Chlamydomonas reinhardtii*, it has been proposed that the patchy distribution of γ-tubulin in the basal body region is associated to the assembly of cortical microtubules. Similar reasons could explain the staining observed in *O.* cf. *ovata*, although more studies are required to confirm this observation.

To my knowledge, *O.* cf. *ovata* is the only dinoflagellate that repositions its nucleus to the cell center in preparation for division. A similar movement associated with mitosis however can be observed in *Chlamydomonas reinhardtii*. In this organism, the flagella are reabsorbed prior to division and during prophase two major microtubule fibers extend from the basal bodies toward the nucleus. Each fiber branches surrounding the nucleus which repositions from the middle of the cell to the apical side, where the basal bodies are located. These bundles remain connected to the basal bodies during interphase, as well as both flagella, suggesting that the basal bodies can organize both microtubule structures, as I propose for *O.* cf. *ovata*. Interestingly, the movement of the nucleus in *Chlamydomonas* relies not only on the mechanical action of microtubules but also on the contractile activity of centrin, a component of centrioles and basal bodies which shuttles along the microtubule bundles during the movement of the nucleus. Centrin is thought to provide contractility to the microtubule bundles to allow nuclear movement (Salisbury et al., 1988). It will be interesting to analyze the distribution of centrin, which is expressed in the *O.* cf. *ovata* transcriptome, during nuclear repositioning in *O.* cf. *ovata,* to determine whether a similar mechanism is acting in these cells.

Cytokinesis is also similar in both organisms, being based on microtubular structures that divide the cell along the longitudinal axis, although in *Chlamydomonas* cytokinesis starts from the side where the basal bodies are located, whereas in *O.* cf. *ovata* the

cytokinetic plate is formed on the opposite side of the flagellar basal bodies. In *Chlamydomonas* F-actin was associated with the initial formation of the cytokinetic furrows, however its complete removal only modestly delayed cytokinesis, suggesting that cytokinesis is actin-independent (Onishi et al., 2020). Although I did not address directly the role of actin in *O.* cf. *ovata* cytokinesis, I never observed actin accumulation in the cytokinetic plate, suggesting that microfilaments may also not be required for cytokinesis in this organism. In both cases cytokinesis, although microtubule based, is different from the microtubule-based division observed in plants where cytokinesis occurs centrifugally starting from the center of the cell.

In plants, no contractile actomyosin ring is observed during cytokinesis and it was suggested that the use of an actomyosin ring for cytokinesis might be restricted to yeasts, amoebas and animals. Based on earlier studies in *C. cohnii,* however, it was suggested that dinoflagellate may undergo cytokinesis with a mechanism similar to that observed in animals (Jérôme Ausseil et al., 1999; Guillén et al., 1998; E. Perret et al., 1993) using both actin and myosin II. The presence of microtubules at the site of cytokinesis in *O.* cf. *ovata* and *C. cohnii*, and the absence of actin at the same site in *O.* cf. *ovata* does not support such hypothesis. Moreover, Richards and Cavalier-Smith (2005) showed that myosin II is absent in bikonts (plants, chromists and protozoa).

3.3.2 Functional analysis of microtubules

Here I showed that in *O.* cf. *ovata* the nucleus interacts with a microtubule based ventral bundle during repositioning from the dorsal location, suggesting that this movement is carried out by microtubules. Consistently, I showed that in colchicine treated cells the nucleus often does not reposition and mitosis occurs in dorsal position. These results support the initial hypothesis that the ventral bundle is required for nuclear positioning but also suggest that this repositioning is not a prerequisite for nuclear division. Moreover, although these are only preliminary results that need to be further pursued, it is interesting to observe that all cells treated with colchicine were able to divide, suggesting that microtubules are not indispensable for nuclear division. Instead, as I observed in many dividing cells that the axis of mitotic and cytokinetic division was mis-oriented, microtubules seem to be required for the orientation of the mitotic and/or the cytokinetic division plane.

In animals and yeasts, treatment with microtubule depolymerizing drugs results in a delay in mitotic progression, arresting cells in pro-metaphase, by activation of the SAC (Chenevert et al., 2020; Endo et al., 2010). Surprisingly, in *O.* cf. *ovata*, treatment with

colchicine did not result in an increase in mitotic index, suggesting that these cells do not arrest in mitosis. This observation is in contrast with previous reports that indicated that the SAC is active in dinoflagellates (Yeung et al., 2000). A possible explanation for this discrepancy might be found in the design of my experiment. As discussed in chapter 2, cell division in *O.* cf. *ovata* is fast. It is therefore possible that, if the delay imposed by the microtubule depolymerization was of short duration, the sampling I performed was not sufficient to highlight such delay. However, it should be noted that in *C. cohnii,* mitotic delay was observed when cells were treated with nocodazole, whereas treatment with colchicine did not activate the SAC in *Alexandrium catenella* (Cho et al., 2011) and *Alexandrium tamarense* (Zhang et al., 2018). As the SAC response depends on the microtubule poison used (Collin et al., 2013; Di Fiore & Pines, 2010), it is not surprising that different results were obtained with nocodazole and colchicine and a comparison of the mitotic response to both drugs in the same species should be carried out.

Although the lack of microtubules should be confirmed in the functional experiments, another interesting observation was that *Ostreopsis* cells divide in the presence of colchicine, which fully depolymerizes microtubules, at least, in culture cells (Figure 26). Nuclear division in the absence of microtubules has already been reported in *Plasmodium* (Spreng et al., 2019) and in fission yeast (Castagnetti et al., 2010). In fission yeast it was shown that in the absence of spindle microtubules, cells can undergo nuclear division and enter S phase of the following cell cycle. The karyokinetic mechanism seems to rely on actin microfilament since actin depolymerization blocks nuclear division.

Proper positioning of the cell division plane is essential for the correct partitioning of cellular components and determinants. In the functional experiments described here, I also observed changes in the orientation of the axis of cytokinesis, suggesting that microtubules also play a role in the correct positioning of the cell division plane. Given the presence of a microtubule-based plate at the site of cytokinesis, this mis-orientation could be a direct consequence of the lack of microtubules during cytokinesis. Alternatively, the erroneous positioning of the cell division plane could be an indirect consequence of the mis-orientation of the axis of nuclear division. In animal cells the position of the division plane is dictated by the orientation and position of the mitotic spindle, to induce furrowing between the segregating chromosomes (Lu & Johnston, 2013). In some cells the signal comes from the spindle midzone inducing furrowing in the cortex nearest to the midzone (Strickland et al., 2005). In other cells instead the positional information comes from astral microtubules, which provide an inhibitory signal to the polar cortical region and therefore restrict furrowing to the

cell equator (Glotzer, 2004). In either cases the cell division plane is perpendicular to the spindle plane. In *O.* cf. *ovata* colchicine treated cells the division plane forms always between the dividing chromosomes suggesting that a relationship might exist between chromosome segregation and cytokinesis. However as microtubule asters have not been described in dinoflagellates it is more likely that the positional information originates from the nucleus, as observed in fission yeast (Akamatsu et al., 2014; Pollard & Wu, 2010).

3.3.3 Dinomitosis and post-translational modification of microtubules

Among the main post-translational modifications of microtubules, there are acetylation and tyrosination of tubulin. The enzymes responsible for both of these modifications are present in the *O.* cf. *ovata* reference transcriptome, suggesting that the modifications may be occurring in these cells. To confirm the presence of these modifications I used two antibodies, one that recognized tyrosinated tubulin and the other one against acetylated tubulin. Labeling of *O.* cf. *ovata* cells at different cell cycle stages with these two antibodies showed that both modifications occur in *O.* cf. *ovata* in different parts of the microtubule cytoskeleton.

Tyrosination occurs in a dynamic cycle and both tyrosinated and detyrosinated tubulin co-exist in the cell. Tubulin acetylation and detyrosination, often label similar structures; for example, both were shown to be enriched at spindle poles in animal cells (Barisic et al., 2015; K. W. Wolf & Spanel-Borowski, 1992). Detyrosinated tubulin has been associated with microtubule longevity, as detyrosinated microtubules depolymerize more slowly than tyrosinated ones, although detyrosination does not confer stability to microtubules (Song & Brady, 2015; Webster, 1990). Consistently, in *O.* cf. *ovata*, tyrosinated tubulin is found in the central spindle, a transient structure only present briefly in the cell while chromosomes are segregated; whereas tyrosinated tubulin is absent from the spindle poles. Acetylated tubulin instead is generally associated with more stable microtubules (Janke, 2014). In endothelial cells, acetylated tubulin stains the polar microtubule array, close to the spindle poles (K. Wolf, 1995). Similarly, in *O.* cf. *ovata* acetylated tubulin labeled microtubules at the poles of the spindle, likely in the kinetosome area from where the spindle microtubules are organized (Figures 34D, H, L, M, P; 35H). The ventral bundles also showed the presence of acetylated but not tyrosinated tubulin. This observation is consistent with the presence of the ventral bundle throughout the cell cycle and its proposed role in the movement of the nucleus prior to mitosis. The microtubules of the ventral bundle need to be stable and have to hold onto the nucleus until it is repositioned.

In animal cells, post-translational modifications of microtubules during cytokinesis have been observed in the mid-body, a microtubule based structure that connects the two daughter cells before abscission. In TC-7 (African green monkey) and PtK_1 (rat kangaroo) cells, the mid-body was stained by detyrosinated tubulin (Gundersen & Bulinski, 1986). Lacroix et al., (2010), showed that a different post-translational modification, glutamylation, occurs in the mid-body of Hela cells. In plants, acetylated microtubules are present in the pre-prophase band, a microtubular structure which is part of the cytokinetic machinery (Giannoutsou et al., 2012). In *O.* cf. *ovata*, the cytokinetic plate was indistinctly stained by both tyrosinated and acetylated tubulins, showing the co-existence of the two sub-populations of microtubule, one more stable possibly required to maintain the division plate while the new membrane and the new cell wall are formed, and one more dynamic possibly associated with the transport of vesicles necessary for the assembly of these new structures.

Although I focused my analysis of tubulin modification on mitotic structures, I could observe that cortical microtubules are also acetylated, whereas in most cases tyrosinated tubulin was absent from the cortical array. Interestingly, in *Trypanosoma*, cortical microtubules were also shown to be acetylated (Souto-Padron et al., 1993) and it was proposed that the post-translational modification of microtubule sub-populations may provide a mechanism whereby the cell discriminates between new and old microtubules, during cell division to allow the distribution of equivalent sets of microtubules between the two daughter cells (Sasse & Gull, 1988). Further studies will be required to establish whether a similar mechanism is at play in *Ostreopsis* cells.

Taken together these results show a highly dynamic microtubule apparatus during dinomitosis. In addition to tyrosination and acetylation, other post-translation modifications have been reported in animals and plants, which could be analyzed to obtain further insights into how microtubule dynamics orchestrate this interesting and unique kind of mitosis.

3.4 Material and methods

3.4.1 Cell cultures

All experiments with cultured cells were performed using strain MCV054 maintained as described in Chapter 2. Cells were fixed for staining during the proliferative phase (day 6 to 10) in order to obtain the greatest number of cells in division.

3.4.2 Actin staining and immunofluorescence

For immunofluorescence a protocol from Escalera et al., (2014) was modified. Cells were fixed in a fixative solution containing 80% cold methanol, 10% DMSO (Sigma-Aldrich) and 0,5 mM EGTA for at least 24 hours, at -20ºC. After fixation, samples were rehydrated progressively in PBS and finally incubated in PBT (PBS with 0.1% Triton X-100) for 15 minutes at room temperature (RT) to permeabilize the membrane. Cells were recovered by centrifugation, 5 minutes at 0.2 RCF, and then blocked for 30 minutes at room temperature in block solution (5% BSA in PBT), rinsed once with PBS and then incubated for three days at 4ºC in block solution with primary antibody. For microtubule staining, D66 anti β-tubulin antibody (mouse monoclonal antibody from *Lytechinus pictus*, Sigma-Aldrich, St.Louis, Missouri, US) was used at 1:400 dilution; for acetylated tubulin, T6793 antibody (Clone 6-11B-1, monoclonal mouse, Sigma-Aldrich, St.Louis, Missouri, US) was used at 1:400 dilution; for tyrosinated tubulin, YL1/2 antibody (ab6160; rat monoclonal, abcam) was used at 1:400 dilution; for γ-tubulin, T6557 antibody (Clone GTU-88, mouse, Sigma-aldrich), was used at 1:50 dilution.

After incubation with the primary antibody, cells were washed three times in PBT, and then incubated over-night at 4ºC in block solution with the appropriate secondary antibody at a 1:400 dilution (fluorescently-conjugated anti-mouse and anti-rat antibodies, Jackson ImmunoResearch). After over-night incubation, cells were washed twice with PBS, and then incubated for 10 minutes with Hoechst-33342 1µg/L (Sigma-Aldrich) to label the DNA, rinsed two more times with PBS and finally resuspended in 100-200 µl of PBS. 50 µl of cells were mixed with 50 µl of citiflour AF1 (Science Services) and mounted on slides for imaging.

Actin filaments were visualized using CytoPainter Phalloidin-iFluor 488 Reagent (ab176753, abcam). Cells were fixed in 4% PFA (F8775 from Sigma-Aldrich) for at least 24 hours at 4ºC, washed three times in PBS, permeabilized and blocked as described for immunofluorescence. After a 30 minute incubation in block solution, cells were incubated in PBT containing phalloidin at 1:400 dilution, for 1 hour at RT in the dark. Cells were then washed twice in PBS, and mounted as described above for imaging.

Images were acquired with a Leica SP8 microscope equipped with a 63X objective, which is part of the Plateforme d'Imagerie Microscopique (PIM) of the Institute de la mer de Villefranche sur mer. Images were analyzed with the software ImageJ-Fiji and Imaris.

3.4.3 Colchicine and agitation treatments

Cells collected the 26th of June during the proliferative phase of 2020 bloom were treated with colchicine or subject to agitation. The sampling started at mid night; approximately 3 g of macroalga were placed in individual cell culture flasks and placed in an incubator at 28ºC, the temperature of the sea water at time of sampling.

For colchicine treatment, colchicine (Sigma ref C9754-100MG) was resuspended in distillated water (20 mM) and used at a final concentration of 2mM in natural sea water. For agitation, the flask, containing macroalga and cells in 25 ml of natural sea water, was placed in an orbital rotator at 70 rpm. Cells were fixed in 2% PFA (Sigma-Aldrich) for 24 hours at 4ºC and then stained with Hoechst-33342 (Sigma-Aldrich) as described in Chapter 2.

Samples were examined with an inverted microscope Zeiss Imager equipped with bright field (BF), phase contrast and epifluorescence (EF) illumination and with a Zeiss Axiocam 506, present in the Plateforme d'Imagerie Microscopique.

3.4.4 Electron microscopy

Cells collected in the Bay of Villefranche were fixed in 4% glutaraldehyde-grade I (Simga-Aldrich) at room temperature and shipped to the Stazione Zoologica Anton Dohrn, Naples for processing. Cells were processed as described in Escalera, et al. (2014). Briefly, the pellet was rinsed four times with 0.1 M cacodylate buffer (pH7.5), centrifuging with a hand centrifuge for 1-2 min. After the last wash, 1 mL of a mix of 0.5% ferricyanide and 0.5% osmium tetroxide in 0.1 M cacodylate buffer (pH 7.5) was added to the pellet to increase the contrast. The sample was kept overnight at 4◦C, rinsed five times with 0.1 M cacodylate buffer (pH 7.5) and centrifuged as mentioned above. Cells were dehydrated in an ethanol series, further substituted by propylene oxide and embedded in Epon812 (TAAB, TAAB Laboratories Equipment Ltd, Berkshire, UK) at room temperature for 1 day and polymerized at 60◦C for 2 days. Resin blocks were sectioned with a MT X ultramicrotome (RMC products, Boeckeler, Tucson, AZ, USA). Sections were contrasted with 4% aqueous uranyl acetate for 30 min, rinsed once with a mix (1:1) of methanol and bidistilled water, twice with bidistilled water, placed on formvar-coated grids and observed with a Zeiss LEO 912AB TEM (Zeiss, Oberkochen, Germany).

Chapter 4

Transcriptomic analysis of *Ostreopsis* cf. *ovata* cell cycle

"The human mind has an invincible tendency to reduce the diverse to the identical …There are two tendencies in science; the tendency towards identification and generalization and the tendency towards the exploration of brute reality, accompanied by a recognition of the specificity of phenomena."

Aldous Huxley (1937), in Ends and Means

4.1 Introduction

Despite the ecological and economical cost caused by dinoflagellate HABs, which are mostly due to massive cell proliferation events, the mechanisms that underlie cell proliferation in dinoflagellates are still mostly unknown. Our knowledge of the eukaryotic cell division cycle, in fact, comes mainly from studies performed in plants, animals, and fungi (Burki, 2014).

About two decades ago, the bloom of genomic, transcriptomic and proteomic approaches in different organisms, has brought new insights in the understanding of cell cycle and cell proliferation in otherwise unaccessible organisms. However, even these approaches are unusually challenging in dinoflagellates because of their large genome size (LaJeunesse et al., 2005), the existence of multiple copies of genes (Bachvaroff & Place, 2008), the significant genetic variation in clonal cultures (Cho et al., 2011), the difficulties associated to their low proliferation rate (Tang, 1996) and because of the technical challenges associated with the extraction of genetic material in good quantity/quality relation from thecate dinoflagellates due to the presence of the theca (Akbar et al., 2018; Conesa et al., 2016).

Given the technical difficulties only very few dinoflagellate genomes have been sequenced. However, using transcriptome data, recent studies have started to reveal some of the molecules involved in the regulation of the dinoflagellate cell cycle, such as cyclins and CDKs (Gorman et al., 2020; Morse et al., 2016) and have begun to analyze the correlation between the expression profiles of these proteins and their functions (Cato et al., 2019a; Lin, 2011). As the information about the mechanisms controlling the cell cycle in dinoflagellates is limited, most studies rely on protein function comparisons against well studied model organisms on the assumption that protein function is conserved among proteins with similar sequences (homologue) (Koonin & Galperin, 2003). Hence, the search of homologues proteins provides a heuristic approach in elucidating the function of unknown proteins from

organisms with scarce experimental data, and provides a starting point to perform further analysis based on experimental tests.

In this chapter, I describe the *de novo* transcriptome which I generated for *O.* cf. *ovata*, strain MCV054 at three different points of the growth curve: lag-phase, proliferative phase and stationary phase. Raw read data from each sample were pooled to create a single assembly containing an enrichment of *O.* cf. *ovata* transcripts.

In order to identify factors involved in the vegetative cycle of *O.* cf. *ovata*, I searched for homologs of cell cycle genes from three species (herein called reference species): *Saccharomyces cerevisiae, Plasmodium falciparum and Chlamydomonas reinhardtii* (Figure 41). Budding yeast *S. cerevisiae* was selected because its cell cycle components are well described and the mechanisms underlying regulation of cell cycle is well understood in this organism. *P. falciparum* was selected as a representative species from the apicomplexans, a sister group of dinoflagellates, which has an available annotated genome. An annotated genome is also available for *C. reinhardtii*. This green alga was selected for the similarities in the mitotic and cytokinetic process shared with *O.* cf. *ovata*, as described in chapter 3.

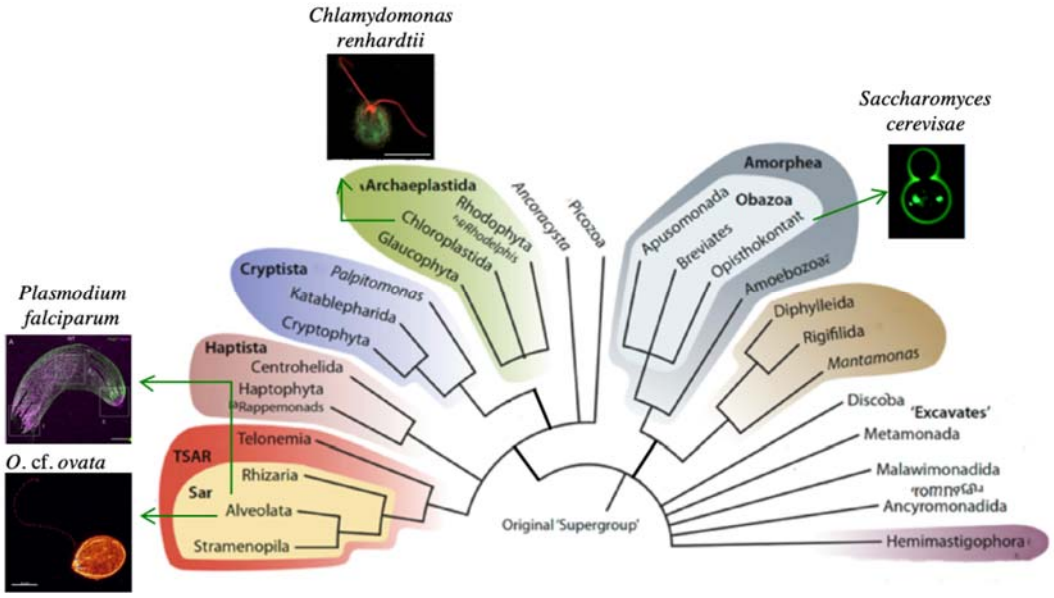

Figure 41. Phylogenetic tree of eukaryotes indicating the position of the reference species and of *Ostreopsis* cf. *ovata*.

Representative images of selected species: *O.* cf. *ovata*: Chenvert, J. personal communication. *P. falciparum* from Okamoto & Keeling, 2014. *C. renhardtii* from Wang et al., 2013. *S. cerevisiae* from Distler et al., 2001. The eukaryotic tree was adapted from Burki et al., 2020.

In this chapter I will first introduce our current understanding of the cell cycle and how it is regulated in different eukaryotes, including dinoflagellates. I will focus in particular on mitosis, describing how mitotic entry, mitotic progression and mitotic exit are regulated. I will then describe the comparative analysis I performed to identify *O.* cf. *ovata* homologs of the cell cycle genes identified in the three reference species mentioned above. For this, I used a conservative strategy, called reciprocal best hits (Hodges et al., 2010; Ward N & Moreno-Hagelsieb, 2014). This approach allowed to generate a list of proteins that are potentially involved in *O.* cf. *ovata* cell cycle. Based on these findings, I propose a potential mechanism for the control of mitotic entry in *O.* cf. *ovata*, I generated a hypothetical model of the dinoflagellate kinetochore, a pathway of the mitotic exit network in *O.* cf. *ovata*, and I describe further components of cytokinesis and basal bodies.

To determine whether any of the identified cell cycle genes are differentially expressed in interphase and mitosis, I generated metatranscriptomic datasets from samples during the day (interphase), the evening (pre-dividing) and at night (mitosis) in 2019 bloom. Using the reference transcriptome, to extract the *O.* cf. *ovata* transcripts from the metatranscriptomes and Kallisto and Sleuth to quantify differentially expressed transcripts, I could show that some cyclins, kinetochore components, basal body and cytokinetic proteins are regulated during *O.* cf. *ovata* cell division, suggesting that *O.* cf. *ovata* cell cycle is partially regulated at the transcriptional level. Finally, based on the transcriptomic activity of cyclins and the presence of kinases in *O.* cf. *ovata*, I propose a basic regulatory network of *O.* cf. *ovata* vegetative cycle.

4.1.1 The eukaryotic cell cycle

The eukaryotic cell cycle (Figure 42), as previously mentioned, includes interphase, divided in G1, S-phase and G2, and mitosis. During G1 the cell grows, duplicates most organelles, and accumulates components necessary for the following steps of the cell cycle. S-phase is characterized by the synthesis of the DNA with the duplication of sister chromatids. Duplicated sister chromatids are held together by cohesin, a protein complex composed of four proteins: Smc1 and 3 and Scc1 and 3 (Leman & Noguchi, 2014). Following DNA synthesis, in G2, the cell continues to grow and produces more components needed for mitosis and cell division. Following interphase cells enter in M-phase, which includes mitosis and cytokinesis. During mitosis, removal of cohesins by separase (Espl1 in yeast) leads to the separation of sister chromatids that are segregated to opposite poles by the mitotic spindle.

Once chromosomes are properly segregated, the cell divides giving rise to two daughter cells by cytokinesis (Cooper, 2000).

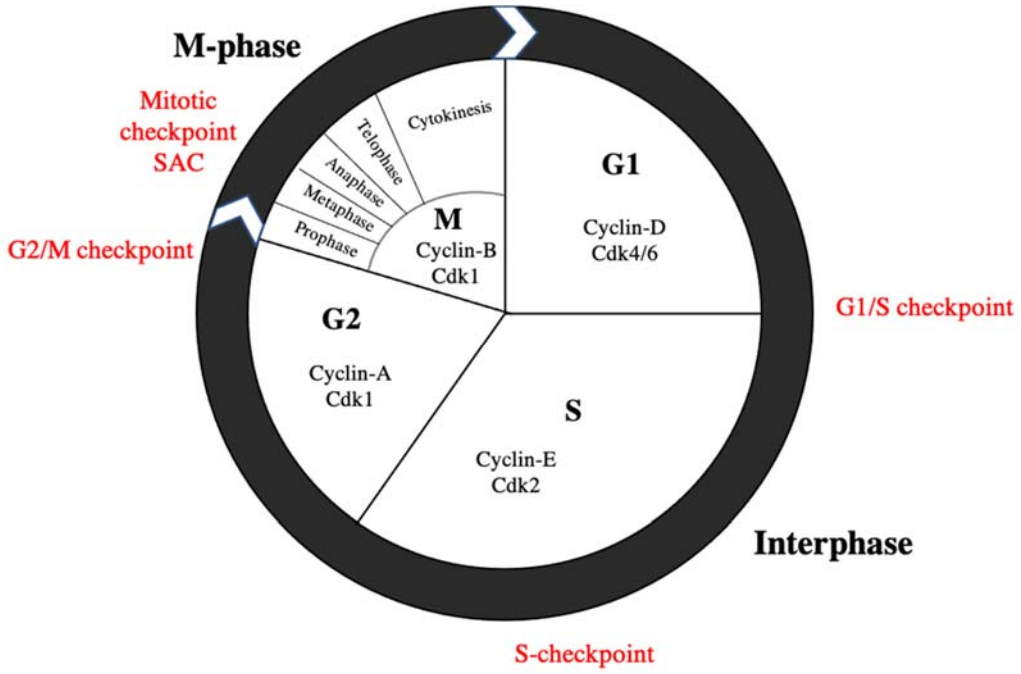

Figure 42. The cell cycle in opisthokonta.
Schematic representation of the cell cycle phases and associated main regulatory Cdk-Cyclin complexes. Interphase includes G1, S-phase and G2; M-phase includes mitosis and cytokinesis. Mitosis is sub-divided in: prophase, metaphase, anaphase, telophase. Cell cycle transitions are regulated by cyclins and CDKs. In G1, cyclin-D and Cdk4/6 are required to initiate the cell cycle. Cyclin-E is expressed during S-phase and associates with Cdk2. Cdk1 associates with Cyclin-A in G2 and then with Cyclin-B during mitosis. Checkpoints (indicated in red) control cell cycle transitions and ensure completion of specific events of the cell cycle before progression to subsequent stages.

Cell cycle transitions are regulated by cyclin-dependent kinases, CDKs, a family of serine/threonine kinases whose enzymatic activity depends on binding to a regulatory subunit, called Cyclin. Although initially identified for their role in cell cycle regulation, CDKs are also involved in transcription in response to extracellular stimuli. CDKs involved in the regulation of transcription usually bind only one specific Cyclin, whose protein level remains constant throughout the cell cycle. CDKs involved in cell cycle regulation instead can bind a variety of cyclins, whose levels oscillate during the cell cycle. Three subfamilies of CDKs, Cdk1, Cdk2 and Cdk4, are involved in the regulation of the cell cycle (Malumbres, 2014). However, Cdk1 is the only CDK essential for the cell cycle in mammals and yeast, whereas the other CDKs (Cdk2, Cdk4 in mammals and Pho85 in budding yeast) are not essential, although they are required for survival under stress conditions and in meiosis (Huang et al.,

2002).

Based on a combination of studies performed in several model organisms it is now generally accepted that in G1, cyclin-D and E are mainly associated with Cdk4 (Keenan et al., 2004); cyclin-E associates with Cdk2 during S-phase to promote DNA replication; cyclin-A then binds to Cdk2 and Cdk1 to allow S-phase progression and the onset of mitosis; and cyclin B associates with Cdk1 to allow mitotic entry and mitotic progression (Fisher, 2011; Malumbres, 2014) (Figure 42). The availability of the different cyclins, which controls both the activity of CDKs and the specificity of target recognition, allows timely initiation of cell cycle events. Cyclin levels change during the cell cycle owing to protein synthesis and degradation (Figure 42 and 43). Accumulation of cyclins is controlled both at the level of transcription and of translation.

In addition to the regulatory interaction between CDKs and cyclins, the catalytic activity of CDKs is controlled by other mechanisms that include sub-cellular localization, activating and inhibitory phosphorylation and binding to CDK inhibitory (CKIs) proteins (Rhind & Russell, 2012). Most CDK family members possess inhibitory and activating phosphorylation sites. For example, Cdk1 is inhibited by phosphorylation of threonine 14 (Thr14) and tyrosine 15 (Tyr15), while it is activated by phosphorylation of threonine 161 (Thr161). Phosphorylation at Thr14 and Tyr15 by the Wee1 and Myt1 interferes with proper ATP alignment, whereas T-loop phosphorylation at Thr161 by CDK activating kinases (CAKs) improves substrate binding and complex stability to enable full Cdk activation (Atherton-Fessler et al., 1994; Pavletich, 1999).

The transition in interphase requires the activity of an important transcription factor, E2F, which is controlled by the protein Rb. Cdk-4/6 and Cdk2, in association with their respective catalytic partners, cyclin-D and E, are responsible for phosphorylation of Rb, thereby alleviating its inhibition on E2F and allowing the activation of genes necessary for promoting S phase entry and DNA synthesis (Lim & Kaldis, 2013). By modulating the activity of G1 kinases, CKIs are also indirectly involved in regulating the expression of E2F-responsive genes (Ravitz & Wenner, 1997).

Eukaryotic cells also coordinate the transition between different cell cycle phases, to ensure that each one is properly completed before moving on to the following phase. This control is ensured by surveillance mechanisms called checkpoints (Figure 42). Two checkpoints between G1 to S and between G2 to M, ensure that the cell has properly duplicated its DNA and has reached a minimal size required for cell division. Another checkpoint known as the mitotic checkpoint, or the Spindle Assembly Checkpoint (SAC) is

active during mitosis to ensure the equal distribution of chromatids to daughter cells (Barnum & O'Connell, 2014).

The regulation of the cell cycle by cyclins and CDKs is common to all eukaryotes (Lents & Baldassare, 2016), however, some differences have been identified between organisms probably to adapt to the specific requirements of their life cycles.

Differently from animals and fungi (opisthokonts), in the green algae, *C. reinhardtii* the cell cycle is characterized by a prolonged G1 phase in which cells can enlarge up to 10-folds. Depending on the cell size reached at the end of G1, *C. reinhardtii* cells then undergo successive rounds of rapidly alternating DNA synthesis and mitoses (S/M) to produce between 2 and 32 daughter cells (2n) that hatch out of the mother cell. This kind of division is known as multiple fission and is regulated through a diurnal cycle, with cell division being suppressed during the day, when cells grow, and rapid division cycles occurring at night (Bisova et al., 2005). *Chlamydomonas* has eleven cyclins, of which five are involved in the cell cycle: an A-type cyclin (Cyc-A1) present in all phases, a B-type cyclin (Cyc-B1) expressed in M, and three D-type cyclins (Cyc-D1 to 3) expressed in G1/S (Prochnik et al., 2010). Three CDKs are present in *Chlamydomonas:* CdkA in G1/S, CdkB1 in G2/M, and CdkD1 present throughout the cell cycle (Cross & Umen, 2015). Despite the similarities in the molecular machinery shared between animals and *Chlamydomonas*, such as cyclins and CDKs however, their cellular function is not always conserved. Mutational analysis carried out in synchronized culture cells, for example, showed that CdkA, the homologue of Cdk1, is required in S/M transition but not for mitosis, while CdkB promotes mitosis (Tulin & Cross, 2015).

In apicomplexan parasites, such as *P. falciparum,* the cell cycle is a complex process with a single parasite replicating to form two to tens of thousands of individuals, depending on species, life cycle stage and host. The apicomplexan cell cycle, similarly to that of *C. reinhardtii,* comprises just three main phases: G1, S, and M; while G2 phase is very brief or absent (White & Suvorova, 2018). Apicomplexa have only three cyclins: Cyc1, Cyc3 and Cyc4, and seven CDKs including CDK-related kinases: PK5, PK6, Mrk1, Crk-1, Crk-3, Crk-5 and Crk-4. None of the apicomplexan cyclins is homologous to canonical cell-cycle cyclins (e.g., mammalian Cyc D, E and A) and their levels are stable throughout the cell cycle; the *Plasmodium* cell cycle is thought not to be regulated by conventional waves of cyclin/CDK activity (Matthews et al., 2018; White & Suvorova, 2018). Analysis of Cyc1 knockdown cells, however, showed that Cyc1 is required for proper cytokinesis. The CDK Mrk1 and the

CAK Mat1 are also involved in cytokinesis and both are able to bind to Cyc1 (Jirage et al., 2010). Crk5, which can be activated *in vitro* by Cyc1 and Cyc4, instead is important for the progression through interphase, whereas Pk6 is important in S-phase (Matthews et al., 2018). Crk-1 and Crk-3, are predicted to have a role in transcriptional regulation and thus in cell growth and proliferation. The function and regulation of Pk5, the homolog of the central cell cycle regulator Cdk1 in animal and yeasts, remains unclear.

4.1.2 Dinoflagellate cell cycle – Cyclins and CDKs

Our understanding of cell cycle progression in dinoflagellates is very limited and fragmented, due to technical and historical reasons. I will summarize below the information currently available.

The master kinase Cdk1 was identified in *C. cohnii* (Rodriguez et al., 1993), in *Gambierdiscus toxicus* (Dolah et al., 1995), in *Karenia brevis* (Barbier et al., 2003), in *L. polyedrum* and *Symbiodinium* (Morse et al., 2016b). In *Gambierdiscus toxicus* Cdk1 was shown to remain at constant level throughout the cell cycle but its histone H1 kinase activity was highest in M-phase cells, suggesting that dinoflagellate Cdk1 behaves similarly to canonical yeast Cdk1 (Bertomeu et al., 2007).

A homologue of Cyclin B, the mitotic partner of Cdk1, has been described in *C. cohnii*, *Karenia brevis* (Barbier et al., 2003) and in A*lexandrium fundyense* (Zhuang et al., 2013). In *Karenia brevis* (Barbier et al., 2003) Cyclin B was shown to localize in both cytoplasmic and nuclear compartments and to bind directly to Cdk1. In *Alexandrium fundyense* the abundance of Cyclin B transcripts was shown to increase up to 6 folds in the G2/M phase compared to other cell cycle phases *(*Zhuang et al., 2013).

G1/S cyclins instead were identified in *Lingulodinium polyedrum* (LpCyc1) (Bertomeu & Morse, 2004) and in *Prorocentrum donghaiense* (Shi et al., 2017). In the latter, transcripts encoding G1/S cyclin were shown to increase 26 folds in late G1 phase and to drop in early S phase.

Extensive studies that allowed the identification of more cell cycle components have been performed recently with the application of bioinformatics approaches that allow genome wide analysis. Using transcriptomic data available for *Lingulodinium polyedrum* and *Symbiodinium* spp, Morse et al, (2016) analyzed the presence of budding yeast cell cycle regulators in these two dinoflagellate species. This study identified three CDKs homologs Cdk1, Cdk5 and Cdk8, and cyclins of both the A and B type.

Recently, using the published genome of *Breviolum minutum* (known as *Symbiodinium minutum*) homologues to *H. sapiens*, *P. falciparum*, and *T. gondii* cell cycle genes were identified in this dinoflagellate. This study identified ten putative CDKs: Cdk 1-3, 4/6, 5, 7, 9, 11; and fifteen putative cyclins, from which seven were classified as mitotic cyclins: A, B1, B2, B3, E, D and F. Analysis of the expression of these genes (RT-qPCR) during the cell cycle (identified by flow cytometry analysis), however, showed that cyclin-B2 peaks during S phase which suggests a function in the G1/S transition. Cdk1 mRNA level instead was high both during S phase and in G2/M. No significant changes were observed for other CDKs. As the expression of both Cdk1 and cyclin-B2 was elevated at the G1/S transition, it was suggested that in dinoflagellates cyclin-B2/Cdk1 might drive S-phase progression, much like cyclin-A/Cdk2 in mammals. Moreover, Cdk1 was also regulated during the G2/M transition, suggesting a pleiotropic role during the cell cycle (Cato et al., 2019a).

Phylogenetic analysis of cell-cycle regulatory proteins in several species belonging to the Symbiodiniaceae further showed that three of the four CDKs (Cdk G/H/J) identified in *S. minutum* (Cato et al., 2019) are also present in other Symbiodiniaceae species (Gorman et al., 2020). The most common CDK identified in Symbiodiniaceae was an alveolate-specific CDK (CdkB). According to the authors, the CdkB is homologous to the metazoan Cdk1.

This study also identified proteins related to eukaryotic cell-cycle as cyclins-A, B, D and G/I, and transcriptional cyclin-L, along with proteins related to plant cyclin-D, protist/plant P/U-type cyclin and cyclin Y, as well as genes related to Cyc-2 and mitotic Cyc-6 from the sister taxon Apicomplexa. The role of these proteins in dinoflagellates remains unknown.

4.1.3 Mitosis

Chromosome segregation during mitosis relies in all known eukaryotes on a bipolar spindle, a complex microtubule structure. In animal cells the spindle is usually organized by centrosomes, complex structures embedded in spindle poles. In animals centrosomes are essential for faithful chromosome segregation, although in some systems, such as chicken and fly embryos, they were shown not to be essential for cell division itself (Meraldi, 2016). The centrosomes compromise over 100 proteins and consist of two barrel-shaped centrioles embedded in a matrix of proteins known as the pericentriolar material, which serves as a platform for protein complexes that regulate organelle trafficking, protein degradation and spindle assembly. Then, centrosomes function as MTOCs that concentrate tubulin and serve

to organize spindle microtubules during chromosome segregation (Woodruff et al., 2014). The centrioles duplicate and mature during interphase, and then separate at the onset of mitosis and migrate to opposite poles to organize the spindle. One of the most important components of the centriole is γ-tubulin. In animals, γ-tubulin is concentrated at the MTOCs where it associates with the minus end of microtubules. γ-tubulin can also be found in the cytoplasm and can be mobilized from the centrosome during microtubule nucleation (Wiese & Zheng, 2006).

Entering mitosis, mitosis promoting factor

Mitotic entry and mitotic progression require only one CDK, Cdk1, and two cyclins: Cyclin-A and Cyclin-B. Cyclin-A can also interact with Cdk2, while cyclin-B interacts exclusively with Cdk1 (John et al., 2001). Activation of CDK to allow timely progression through mitosis relies on the accumulation of cyclin-A and cyclin-B. Cyclin-A accumulates starting from S-phase, while Cyclin-B accumulates in G2. Cyclin-A/Cdk2 activity is required to promote transcription of cyclin-B, explaining their sequential accumulation. As Cyclin B accumulates during G2, the concentration of the Cdk1-Cyclin-B complex increases in the cytoplasm. Phosphorylation of Cdk1 on Thr14 and Tyr15, by Wee1 and Myt1, maintains the complex inactive and avoids untimely mitotic entry. At the end of G2, the Cdk1-CyclinB complex is activated by dephosphorylation by the phosphatase Cdc25, allowing onset of mitosis (Atherton-Fessler et al., 1994; Lim & Kaldis, 2013; Pavletich, 1999).
The degradation of cyclin-A and B triggers the metaphase to anaphase transition and mitotic exit. Degradation of both cyclins requires the activity of the Anaphase Promoting Complex or Cyclosome, APC/C (Figure 43).

APC/C

APC/C is a multiprotein E3 ubiquitin ligase composed of 13 to 15 sub-units which ubiquitinates proteins marking them for degradation by the proteasome. Three enzymes, E1, E2 and E3 are involved in ubiquitination of target proteins with E3 providing target specificity and transferring of the ubiquitin moiety from the E2 conjugating enzyme to the target proteins. The E3 ligase involved in degradation of mitotic targets is APC/C. Two ancillary subunits are known to activate APC/C: Cdc20 and Cdh1. (Hégarat et al., 2016; Wieser & Pines, 2015). Cdc20 associates with APC/C from the metaphase-to-anaphase transition (APC/C^{Cdc20}) and induces the degradation of Cyclin-B1 and of Securin (encoded by Pds1 in *S. cerevisiae*), an inhibitor of Separase (Lara-Gonzalez et al., 2012). In metaphase,

Separase, released from the inhibitory activity of Securin, cleaves the Scc1 subunit of cohesion allowing separation of sister chromatids (Wieser & Pines, 2015) (Figure 43). The reduction in Cdk1 activity due to APC/C^{cdc20} dependent degradation of cyclin B, releases Cdh1 inhibition allowing its association with APC/C (APC/C^{Cdh1}) from anaphase until late G1 phase, to allow mitotic exit (Hégarat et al., 2016).

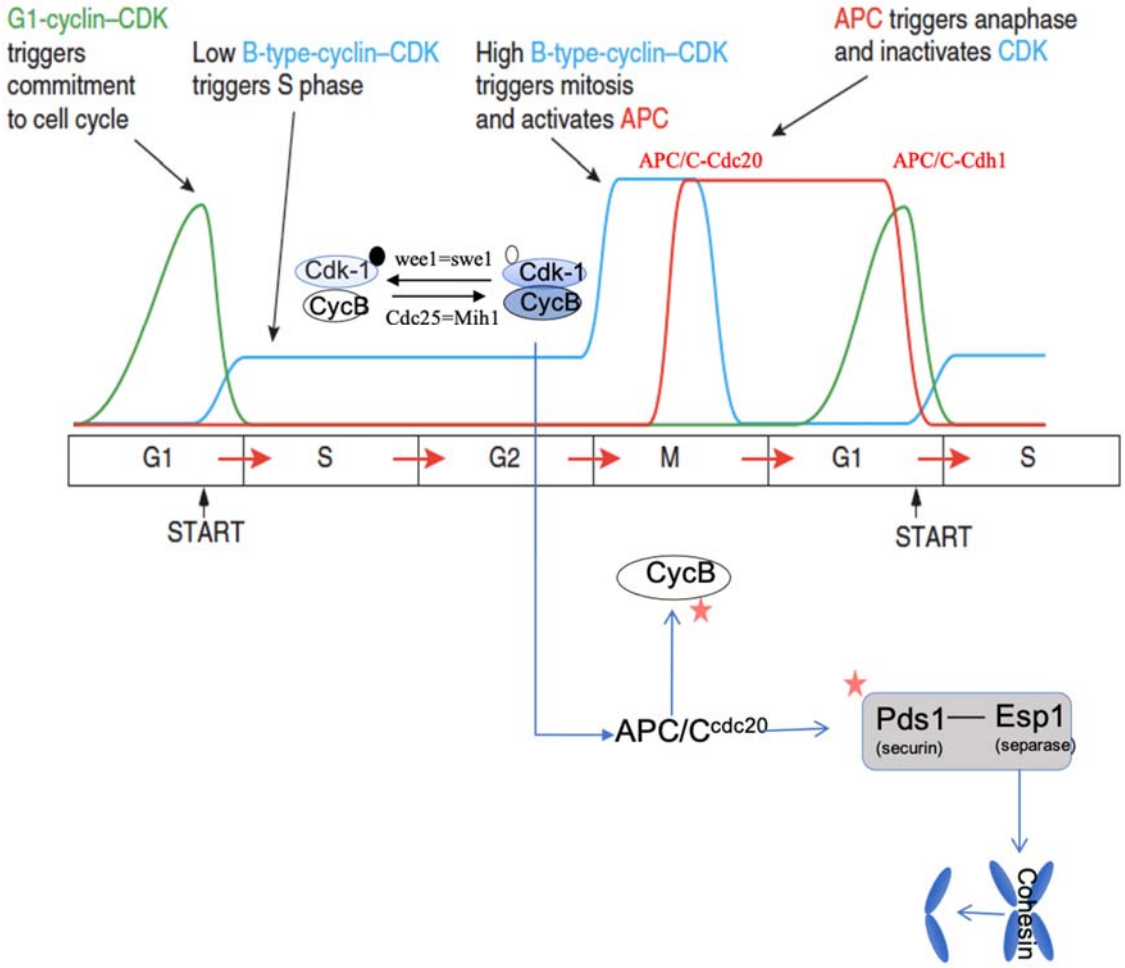

Figure 43. Cyclin dependent kinases control cell cycle transitions.
G1-cyclin/CDK complex is required to initiate the cell cycle and to activate the cyclin-B/CDK complex. Low level of Cyclin-B/CDK activity is permissive for S phase. Cdk1 phosphorylation (black circle) by Wee1 prevents its full activation, preventing premature mitosis. Full Cdk1 activation depends on the phosphatase Cdc25. Active Cyclin-B/Cdk1 triggers mitosis and activates APC/C. APC/C associates with Cdc20 and by ubiquitination (red star) marks Cyclin-B for degradation, resulting in a drop in CDK activity and mitotic exit. In addition, APC/C-Cdc20 ubiquitinates securin (Pds1) releasing separase (Esp1) which cleaves cohesis and allows chromosome segregation. Figure adapted from Rhind & Russell, 2012.

Spindle Assembly Checkpoint

The spindle assembly checkpoint, or SAC, delays chromosome segregation by preventing APC/C activation until all chromosomes are properly attached to spindle microtubules. Hence, SAC delays the metaphase to anaphase transition avoiding errors in chromosome segregation and the generation of aneuploid cells (Ciliberto & Shah, 2013).

Six proteins make up the core SAC: Mad1, Mad2, Mad3/BubR1; Bub1, Bub3; Mps1 (Figure 44) (Weiss & Winey, 1996). Mps1 and Bub1 are the only two kinases. Mad3 and Bub1 are paralog genes meaning that they arose by gene duplication. This duplication happened at least nine independent times in eukaryotic evolution from an ancestral gene usually referred to as MadBub (Hooff et al., 2017; Tromer et al., 2016).

SAC components are generally well conserved in eukaryotes. Opisthokonts and *C. reinhardtii* have all components, whereas Bub3 is missing in the genome of the dinoflagellate *S. minutum.* The only known exception is *P. falciparum* where none of the SAC components has been identified (Hooff et al., 2017).

Unattached kinetochores are the trigger for SAC activation. In the absence of spindle microtubules, Mps1 is recruited to unattached kinetochores where it allows the recruitment of all other SAC components. Upon kinetochore localization Mad1 and Mad2 associate in a tetramer that acts as a 'template' for the transformation of Mad2 from 'open' to 'closed' configuration. Closed-Mad2 interacts with Cdc20 and together with Mad3/BubR1 and Bub3 forms an inhibitory complex known as the mitotic checkpoint complex (MCC) which prevents APC/C activation both by sequestering Cdc20 and by direct binding to APC/C (Jia et al., 2013; Sudakin et al., 2001).

Following kinetochore-microtubule interaction, SAC is inactivated. Such inactivation requires the protein $p31^{comet}$. $p31^{comet}$ interacts with the Mad1-Mad2 complex. $p31^{comet}$ is able to remove Mad2 from the mitotic checkpoint (Westhorpe et al., 2011). $p31^{comet}$ interacts as well with TRIP13 preventing the generation of new closed Mad2 (Yang et al., 2007). Removal of SAC proteins from kinetochores also relies on dynein (Silva et al., 2014), which removes Mad2, Mad3, Mad1, Bub1 and Bub3 from attached kinetochores towards the spindle poles.

The Kinetochore

Kinetochores are multiprotein complexes required for chromosome-spindle interaction. In opisthokonts more than 100 components have been described. The kinetochore components can be organized in four layers identifiable by electron microscopy: the inner plate and the middle layer which form the inner kinetochore, and the outer plate and the corona which form the outer kinetochore (Cheeseman & Desai, 2008).

The inner kinetochore assembles at a specific region of the chromosomes known as the centromere which consist of small repeated DNA sequences called microsatellites, associated with the histone H3 variant, Cenp-A. Cenp-A interacts and recruits the other components of the inner kinetochore forming the constitutive centromere associated network or CCAN, which remains associated with centromeres during the entire cell cycle. Sixteen proteins are present in the CCAN and are organized in sub-complex: the Cenp-H/I sub-complex (Cenp-H/-I/-K/-L/-M/-N), the Cenp-O class protein (COMA sub-complex (Cenp-O/-P/-Q/-U), Cenp-R), the Cenp-T/W sub-complex (Cenp-T/-W/-S/-X) and Cenp-C (Suzuki et al., 2014). These proteins are conserved in opisthokonts (Figure 44), but are absent in *C. reinhardtii*, in *P. falciparum*, and in *S. minitum* with the exception of Cenp A, C and E (Hooff et al., 2017).

Aurora, Borealin, Incenp and Survivin also interact with the inner kinetochore and play a key role in bipolar spindle attachment by acting as a "sensor" of connection between the centromere and the spindle (Lampson & Cheeseman, 2011).

In prophase, CenpA and the CCAN induce the assembly of the outer kinetochore, which consists of a network known as KMN network, which has three main components: Knl1, Mis12 and Ndc80. Knl1 binds to Zwint1; Mis12 associates with Nnf1, Nsl1 and Dsn1 (Mis12 complex); and Ndc80 binds to Nuf2, Spc24 and Spc25 in the Ndc80 complex. The KMN complex is present in ophisthokonts while only the Ndc80 complex is present in the genome of *S. minutum*; only Knl1 is conserved in *C. reinhardtii*, and *P. falciparum* has only Ndc80 (Hooff et al., 2017).

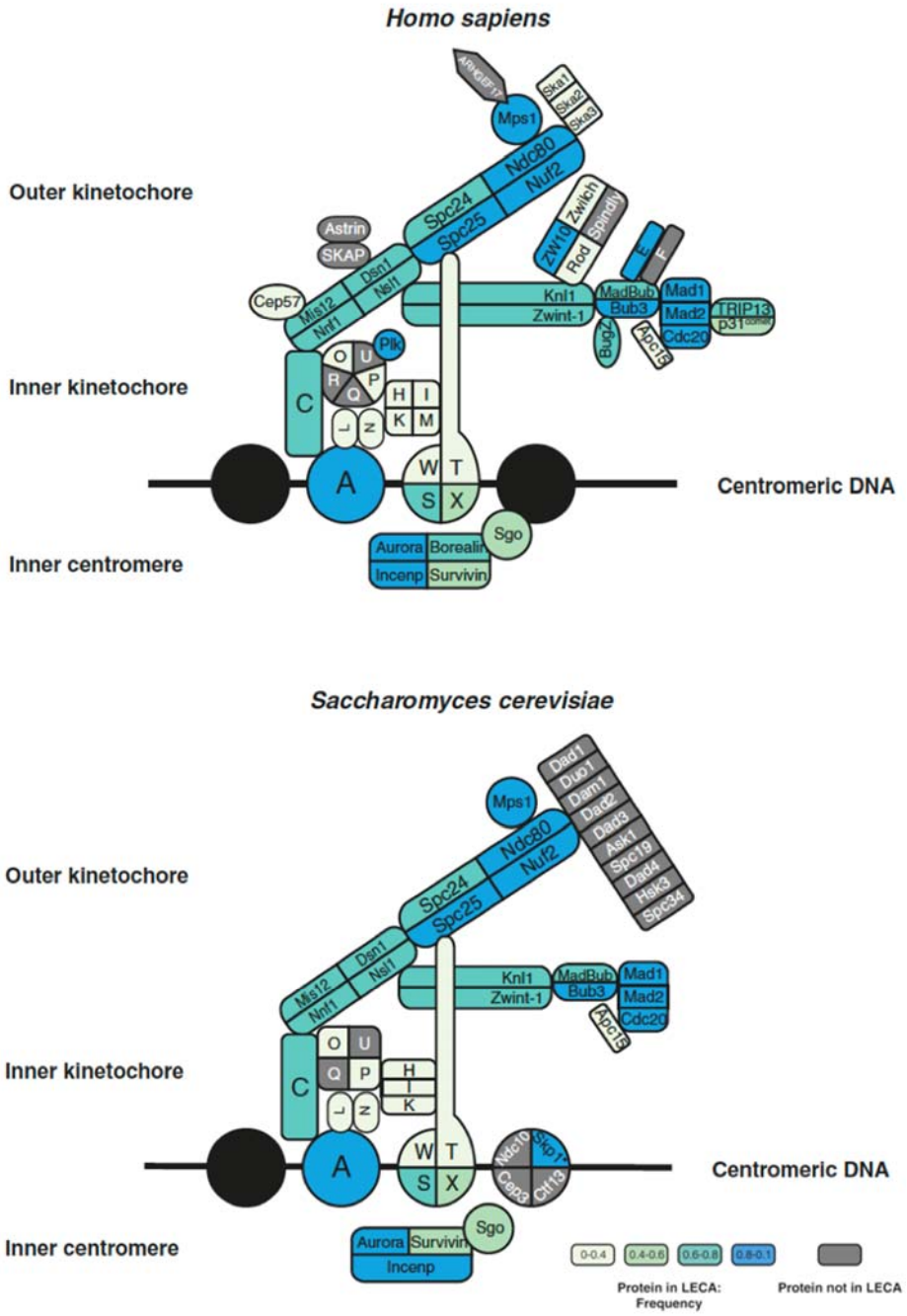

Figure 44. Kinetochore organization in humans and yeasts.
The colors of the proteins indicate the probability of each protein to be present in kinetochores in LECA and their occurrence frequency across eukaryotes (further details can be found in Materials and methods of van Hooff et al., 2017). Figure from van Hooff et al., 2017.

The KMN network recruits the protein Zwint allowing the localization of the Rod-ZW10-Zwilch (RZZ) complex. This complex which is absent in yeast and *Chlamydomonas reinhardtii,* is partially conserved in *P. falciparum* and *S. minutum* (only Zw10), and is present in animal cells (Hooff et al., 2017); it is required to recruit the minus end motor

dynein to kinetochores. Dynein, the well conserved kinesin Cenp-E and the KMN network are directly involved in the interaction with spindle microtubules.

Kinetochores that are not attached to spindle microtubules have an additional layer termed the fibrous corona. The corona expands into crescents around the unattached outer kinetochore, to facilitate the capture of kinetochores by incoming microtubules. The fibrous corona is formed by the RZZ complex and the SAC proteins, Mad1/Mad2, whose function is to sense and signal unattached kinetochores. Additionally, the outer components of the CCAN, Cenp-E and Cenp-F localize to the corona and capture incoming microtubules to initiate the binding of the kinetochores to microtubules (McHugh & Welburn, 2017).

In dinoflagellates chromosome segregation occurs within an intact nucleus with a cytoplasmic spindle. As it is thought that in these organisms, the kinetochore spindle microtubules interaction is indirect due to the presence of the nuclear membrane, the presence of canonical kinetochores is controversial (Bhaud et al., 2000). Electron microscopy studies showed the presence of dark and dense material in the nuclear membrane in contact with spindle microtubules in some species of *Syndinium* (Ris & Kubai, 1974), *Amphidinium* (Oakley & Dodge, 1974), and in *C. cohnii* (Bhaud et al., 2000) (Figure 45). This structure was called a kinetochore-like structure (Oakley & Dodge, 1976a). Analysis of *S. minutum* (Shoguchi et al., 2013) genome revealed the presence of some kinetochore proteins.

In the primitive dinoflagellate *Oxyrrhis marina*, which differently from core dinoflagellates, has an intranuclear spindle, electron microscopy analysis has not identified kinetochore like structures suggesting that this organism does not assemble kinetochores (Kato et al., 2000).

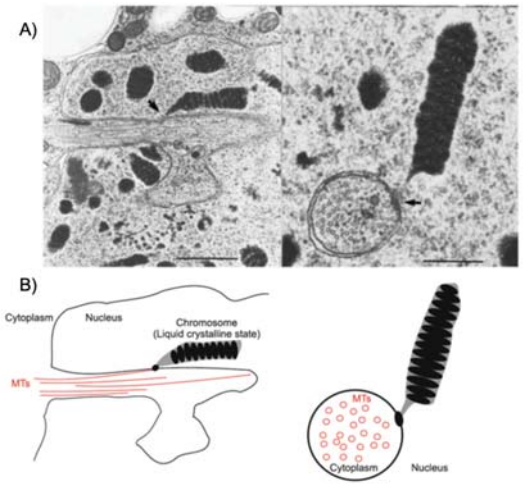

Figure 45. Kinetochore-like structures in dinoflagellates.
A) Electron microscopy pictures of mitotic *Crypthecodinium cohnii* chromosomes associated with the nuclear membrane. The kinetochore-like structure embedded in the nuclear membrane makes contact with extranuclear spindle microtubules (arrows). Scale bars are 0.8 µm (left), 0.3 µm (right). B) Schematic representation of EM pictures in A). Figure adapted from Drinnenberg & Akiyoshi, 2017

Mitotic Exit Network, the MEN

In budding yeast, mitotic exit is controlled by the Mitotic Exit Network (MEN) (Figure 46), which also controls spindle orientation and initiates cytokinesis (Baro et al., 2017).

Central to the function of the MEN cascade is Cdc14, a phosphatase which counteracts the activity of Cdk1. Just as the activation of Cdk1 triggers mitotic entry, its downregulation is required for exit from mitosis. Cdc14 activity is also important to dephosphorylate and activate various Cdk1 targets, the Cdk1 inhibitor Sic1, the transcription factor Swi5 and the APC/C co-activator Cdh1, all required for mitotic exit.

The activity of Cdc14 is tightly regulated. During most of the cell cycle, Cdc14 is sequestered in the nucleolus in a complex with its inhibitor Net1 (also known as Cfi1). Net1 anchors Cdc14, and together with Sir2 they form the RENT complex. After anaphase onset Cdc14 is released from the nucleolus into the nucleus and the cytoplasm. Two events control this switch: the activation of the MEN cascade and the activation of the Cdc Fourteen Early Anaphase Release (FEAR) network (Baro et al., 2017). The MEN was the first network to be identified in budding yeast to control anaphase onset (Howell et al., 2020). Tem1, a small GTPase associated with the spindle pole bodies, the yeast centrosome equivalent, is maintained inactive by the two component GAP, Bfa1-Bub2 until anaphase onset. The kinase Kin4, which is confined in the mother cell, inhibits the polo kinase Cdc5, whose activity is required to inhibit Bfa1 and ultimately activate Tem1. Inactivation of Bfa1 occurs upon movement of a spindle pole across the bud neck in anaphase following spindle elongation. In the bud, where Kin4 is absent, Cdc5-mediated phosphorylation of Bfa1 activates Tem1. This activation is further increased by the activator Lte1, whose activity is also restricted to the bud. In mid-anaphase, therefore, active Tem1 recruits Cdc15 to the SPB and activates Dbf2-Mob1. Dbf2-Mob2 in turn phosphorylate Net1, which release Cdc14 from the nucleolus (Baro et al., 2017).

Differently from the MEN network, the FEAR network only releases Cdc14 into the nucleus (Yellman & Roeder, 2015). Once all chromosomes are correctly attached to the mitotic spindle, separase (Esp1) becomes activated due to the degradation of its inhibitor securin (Pds1) by the APC/C^{Cdc20}. Active, Esp1 cleaves the cohesin complex, allowing chromosome segregation and in parallel in association with Zds1, downregulates the phosphatase PP2A - Cdc55, allowing phosphorylation of Net1 by Cdk1 and subsequent release of Cdc14 from the RENT complex in early anaphase (Figure 46) (Lee et al., 2005).

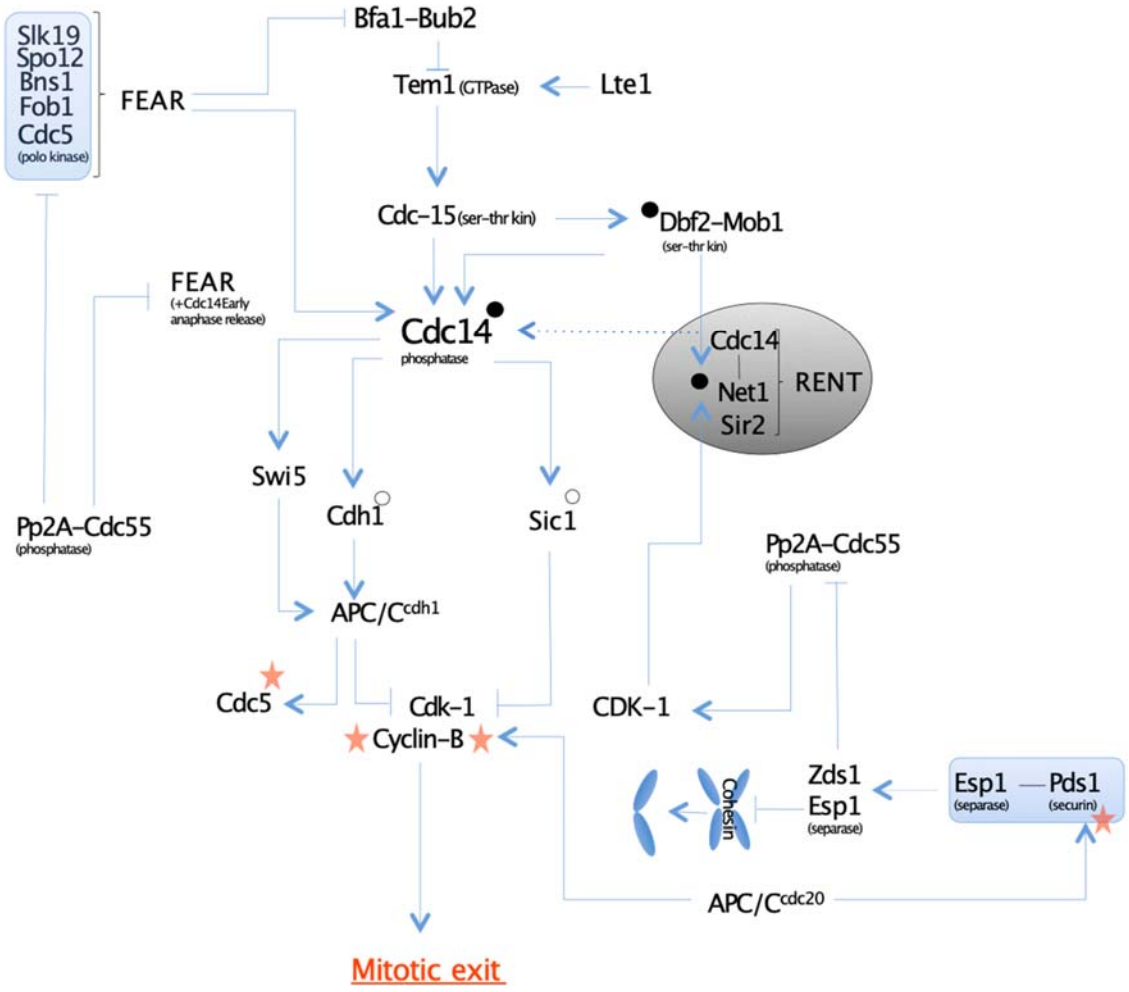

Figure 46. Mitotic Exit Network in budding yeast.
Schematic representation of the main interactions controlling mitotic exit in budding yeast. Black circles represent phosphorylation, while empty circles are unphosphorylated proteins. The gray oval represents the nucleolus. Red stars indicate ubiquitination. Dotted arrows indicate relocalization of proteins to different cellular locations.

4.1.4 Basal body

The basal body is a MTOC, which historically is found at the base of cilia and flagella. In apicomplexans parasites, only the male gamete, known as the microgamete, assembles basal bodies and flagella; whereas the other stages (the invasive asexual stages), have essentially lost the flagellar apparatus (Francia et al., 2015). In the flagellate stages, *Plasmodium* assemble *de novo* its basal body which is required to build a new flagellum. The formation of the flagellum is known as exflagellation, a process that occurs during microgametogenesis. The flagellum is formed from the basal body, which contain a cartwheel protein, Sas-6 and the tubulin nucleating protein, γ-tubulin. Sas-6 knock-out parasites do not

produce motile cells (Marques et al., 2015). In addition to Sas-6 and γ-tubulin, other important components reported are α and β- tubulin; δ- and ε-tubulin; Sas4/Cpap, and Bld10/Cep135. Proteomic analysis of *Plasmodium* microgametes, shows a lack of intraflagellar transport (IFT) machinery and of most BBsome. The IFT is formed by several proteins that give a bidirectional motility along axonemal microtubules, essential for the formation and maintenance of most eukaryotic cilia and flagella. The BBSome is an octameric protein complex, essential component of the basal body in animals and involved in trafficking cargo proteins (Hodges et al., 2010).

In *C. reinhardtii* which is considered a good model to study basal bodies given its haploidic life, the annotated genome and the ease of synchronization of culture cells (Dutcher & O'Toole, 2016), the mature basal body contains a ring of amorphous material below the cartwheel. The cartwheel also has spokes that require the proteins Bld12 and Sas-6 for its correct formation, while the spoke tips require Cep135/Bld10 to stabilizes the 9-fold symmetry of the centriole (Hiraki et al., 2007; Hirono, 2014).

The composition of the basal bodies varies in different organisms and extensive effort has been put into defining the basic components of these MTOCs. The difficulties are to determine whether an individual protein has a role only as basal body component; furthermore, the function of some proteins varies among organisms. Despite these difficulties an ancestral basal body has been reconstructed based on a comparative study of 45 proteomes of organisms from the major eukaryotic groups (Hodges et al., 2010). This study identified 14 proteins present in at least 4 of the major taxonomic groups, corresponding to the 'core basal body' (Figure 47). These proteins are: ε-tubulin which is required for the basal body/centriole morphogenesis (Dutcher et al., 2002); δ-tubulin which is required for the proper assembly of the flagella in the basal body (Fromherz, 2004); the most ubiquitous proteins were: Centrin-2, an essential centriolar component in the duplication of the centriole; WDR16 whose function is unknown although it has been identified as a component of the basal body; Sas-4 and Sas-6 which are involved in the attachment of microtubules to the central centriolar cylinder and are essential for the cartwheel formation. The remaining core basal body proteins are seven proteins that included centriolar components as centriolin, proteins involved in the orientation of the basal bodies as Vfl1 and structural components plus flagellar transport associated proteins as Poc1 and 5, Cep164, Dip13, Cep76 and Cep135.

In *C. reinhardtii* all core basal body proteins are present, whereas only four core components (centrin, Wdr16, Sas-4 and 6) and Dip13 and Cep76 are conserved in *Plasmodium falciparum* (Hodges et al., 2010).

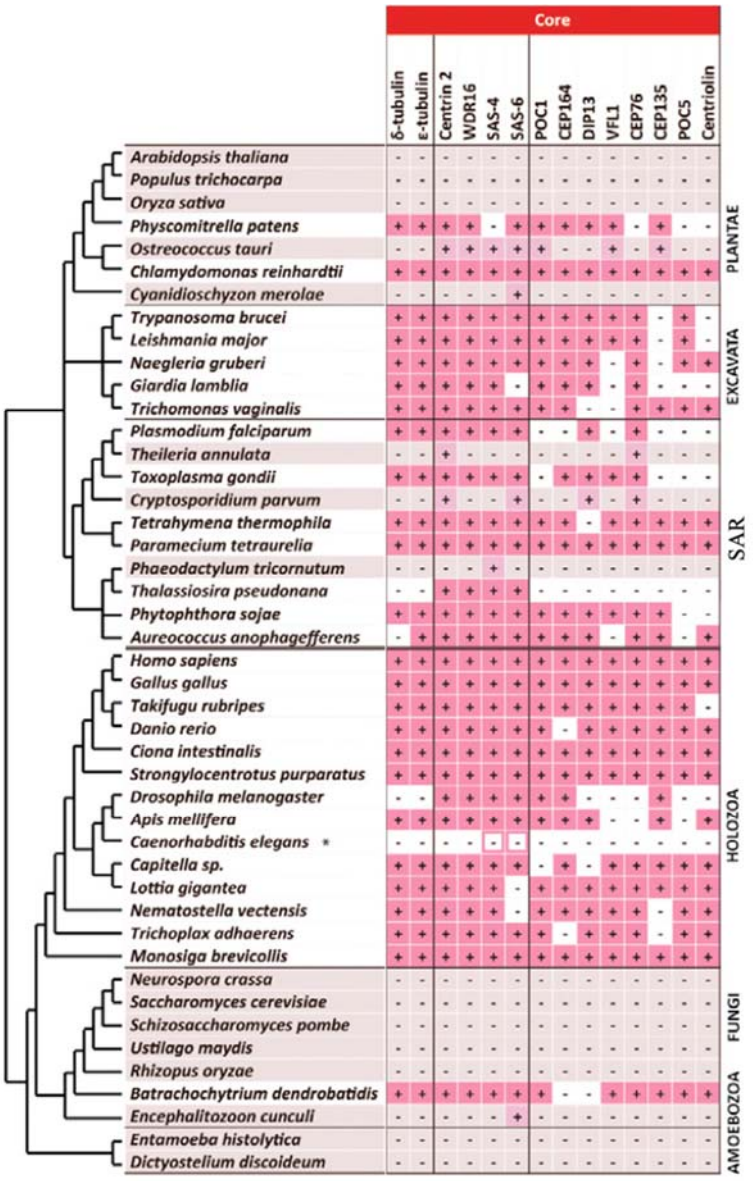

Figure 47. Distribution of centriolar and centrosomal proteins among eukaryotes.
Protein homologues were identified in 45 eukaryotic genomes, including 29 ciliated species (white) and 16 non-ciliated species (highlighted in pink). The presence of homologue(s) is indicated by a plus symbol (+). 'Core' proteins are conserved ancestral centriolar proteins. 'Ancestral' proteins are those present among extant eukaryotes. Figure adapted from Hodges, et. al (2010).

4.2 Results

In this chapter, I describe the bioinformatics approach I undertook to identify a set of proteins potentially involved in the control of *O.* cf. *ovata* cell division. To perform this analysis, I have generated an enriched *de novo* transcriptome corresponding to different phases of the growth curve of culture *O.* cf. *ovata* cells (MCV054).

Using a reciprocal best hit approach (Ward & Moreno-Hagelsieb, 2014), I then identified the *O.* cf. *ovata* homologs of a set of proteins involved in mitotic division in three reference species, *S. cerevisiae*, *C. reinhardtii*, and *P. falciparum*. I analyzed proteins involved in cell division: components of the basal body; proteins that control mitotic division (mitotic promoting factors, APC/C, SAC, kinetochore and MEN), molecular components of cytokinesis; and the major controllers of the cell cycle.

I then asked whether the identified genes were regulated at transcriptional level during interphase and mitosis and during bloom development. To this end I generated meta-transcriptomic datasets corresponding to different stages of the *O.* cf. *ovata* bloom: proliferative, stationary, senescence and at the end of the bloom as well as day (interphase) and night (mitosis) samples. This analysis showed that several factors involved in the mitotic cycle, including mitotic cyclins, kinetochore, basal body and SAC components, are conserved in *O.* cf. *ovata* and differentially expressed suggesting transcriptional control of the cell cycle in dinoflagellates.

4.2.1 *Ostreopsis* cf. *ovata* reference transcriptome production and general characteristics

To investigate the genes involved in control of mitotic progression in *O.* cf. *ovata*, I decided to generate a *de novo* transcriptome, referred to as reference transcriptome, of strain MCV054.

The first step in the process was the generation of high quality total RNA from cultured cells. RNA extraction in thecate dinoflagellates requires breakage of the cellulose theca (Rosic & Hoegh-Guldberg, 2010), but most techniques are extremely aggressive and result in RNA shearing and loss of RNA quality. I therefore tested different extraction protocols to generate high quality total RNA in sufficient amount. The tested protocols included incubation in TRI-reagent (Sigma-Aldrich) either at room temperature or at 90ºC, glass beads beating, manual grinding, fast freezing in liquid nitrogen and a combination of TRI-reagent (Sigma-Aldrich) with any of the mechanical treatments. Individual treatments and a combination of incubation with TRI-reagent (Sigma-Aldrich) and manual grinding, did not allow extraction of enough total RNA. Fast freezing alone or in combination with TRI-reagent incubation instead resulted in degradation of the RNA.

Optimal results were obtained by incubation with TRI-reagent at room temperature for 5 minutes (Sigma-Aldrich) combined with bead beating at 4000 rpm for 40 seconds to break the cellulose theca, followed by extraction with a RiboPure^{TM} (Ambion) kit. Using this optimized protocol, I could extract around 2 μg of high-quality total RNA from approximately

700.000 cells. I used this standardized protocol to extract RNA from *O.* cf. *ovata* cells at three phases of the growth curve (described in Chapter 2): lag phase prior to the beginning of proliferation (day 6), proliferative phase (day 12) and stationary phases (day 18). Triplicates were generated for each time point. The nine samples were sent to BGI Transcriptome Sequencing services (China), for library construction and sequencing using the DNBseq sequencing technology. BGI services included filtering of the raw reads and removal of adaptor sequences, contamination and low-quality reads from raw reads. After cleaning, a total of 66-68 million contigs were obtained from each RNA-Seq (table 5).

Table 5. Reference transcritpome assembly statistics.
The table provides information for the 9 samples corresponding to different phases of the growth curve for *O.* cf. *ovata* strain MCV054. Q20(%) is the sequencing quality score of a given base and indicates the probability of 1 error every 100 nucleotides.

Phase of the growth curve	Clean Reads	Clean bases	Read length (bp)	Q20(%)
Lag phase, n-1	68,000,434	6,800,043,400	100	97.51%
Lag phase, n-2	67,390,962	6,739,096,200	100	97.62%
Lag phase, n-3	67,436,436	6,743,643,600	100	97.46%
Proliferative, n-1	67,056,980	6,705,698,000	100	97.89%
Proliferative, n-2	66,342,750	6,634,275,000	100	97.50%
Proliferative, n-3	66,946,716	6,694,671,600	100	97.63%
Stationary, n-1	67,052,198	6,705,219,800	100	98.02%
Stationary, n-2	67,905,852	6,790,585,200	100	97.75%
Stationary, n-3	66,873,538	6,687,353,800	100	97.77%

Raw read data from all conditions and triplicates were pooled to create the reference transcriptome. Then, the library was assembled using Trinity, resulting in 220667 transcripts with a GC percentage of 61.02 and an average contig length of 825.26 nucleotides. To remove contaminations from other species, especially bacteria, I filtered the obtained sequences by querying them against the NCBI-NR database and keeping only the sequences that matched to Dinophyceae. This resulted in a total of 23.206 *Ostreopsis* sequences. These sequences were translated using Transdecoder and the obtained protein sequences were annotated using PANTHER. I retrieved a total of 17171 annotated sequences, of which 4443 (25.8%) were orphan proteins.

4.2.2 Search for homologous proteins

To identify the genes involved in control of the mitotic cycle in *O.* cf. *ovata* I took a conservative approach called reciprocal best-hit strategy. I first identified all *O.* cf. *ovata*

homologs of the proteins present in the proteomes of three reference organisms: *Saccharomyces cerevisiae (*obtained from uniprot.org), *Chlamydomonas reinhardtii (*obtained from plantdg.org) and *Plasmodium falciparum (*obtained from plasmodb.org). This strategy generated pairs of homologs between *O.* cf. *ovata* (identified by an ID number) and each reference organism (identified by the name and ID number of the protein as indicated in the corresponding database).

Using the databases uniprot.org, plasmodb.org and plantdg.org I then identified all proteins known to be involved in cell cycle, mitosis and cytokinesis as well as components of the basal body in the three reference organisms. I curated this list manually and added information and components available in the literature. Based on their function in the reference species, the identified proteins were then classified in: proteins forming the basal body; cell cycle regulators; mitotic proteins and cytokinetic components. Mitotic proteins were further divided into (i) mitosis promoting factors, (ii) APC/C components, (iii) SAC components, (iv) kinetochore components and (v) members of the MEN. I then analyzed which of these proteins were present in the *O.* cf. *ovata* homolog database I had created.

I identified 69 homologous proteins of the 319 yeast proteins (21.6% homologous, Figure 48A, and in annex 3- table 1), 86 homologous proteins of the 224 proteins of *C. reinhardtii* (38.4%; Figure 48B, annex 3- table 2), and 93 homologous proteins of the 202 proteins of *P. falciparum* (46%; in Figure 48C, annex 3- table 3). The pie charts in Figure 48 shows the distribution of the *O.* cf. *ovata* homologs present in each cell cycle category. *O.* cf. *ovata* shares more homologous proteins from the basal body and for cytokinesis with *C. reinhardtii* than with *P. falciparum*. This is not surprising as *P. falciparum* has a rather specialized basal body used only in the male gamete and yeast have no basal body. Mitotic components and cell cycle regulators instead were better conserved between *P. falciparum* and *O.* cf. *ovata* (table on Figure 48C). This result is also not surprising considering that these are both alveolate species and are therefore relatively close to each other from a phylogenetic perspective.

Taken together this analysis identifies 209 *O.* cf. *ovata* proteins potentially involved in cell cycle regulation (annex 3 – table 4). In the following sections, I will describe these conserved proteins in more details, in relation with their function during the mitotic cycle.

A) % of conserved proteins in *S. cerevisiae*

Saccharomyces cerevisiae - 319 proteins				
	Mitosis	Cytokinesis	Cyclins	Basal Body
Total of searched proteins	199	102	18	0
Orthologous in Ostreopsis	40	22	7	0
% of conserved proteins	20.1%	21.5%	38.8%	0.0%

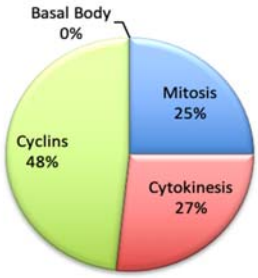

B) % of conserved proteins in C. reinhartii

Chlamydomonas reinhardtii - 224 proteins				
	Mitosis	Cytokinesis	Cyclins	Basal Body
Total of searched proteins	101	22	29	72
Orthologous in Ostreopsis	20	13	4	50
% of conserved proteins	18.00%	59%	13.80%	69.40%

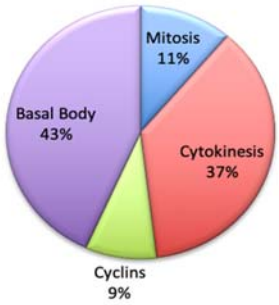

C) % of conserved proteins in *P. falciparum*

Plasmodium falciparum- 201 proteins				
	Mitosis	Cytokinesis	Cyclins	Basal Body
Total of searched proteins	82	57	34	28
Orthologous in Ostreopsis	47	24	14	8
% of conserved proteins	58.5%	42%	41,1%	28.5%

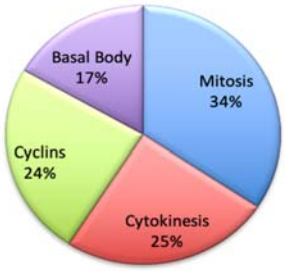

Figure 48. Quantification of shared cell cycle homologs
between *O.* cf. *ovata* and A) *Saccharomyces cerevisiae*, B) *Chlamydomonas reinhardtii* and C) *Plasmodium falciparum*. Proteins are classified according to their functions. Pie charts show distribution of conserved cell cycle proteins in each category.

4.2.3 Basal body

As basal bodies are absent in budding yeast, for this analysis I used only *P. falciparum* and *C. reinhardtii* proteins. 72 basal bodies proteins were identified in *C. reinhardtii*, which has historically been used as a model organism for ciliogenesis and flagellogenesis and whose basal body has been therefore extensively characterized. Only 28 proteins instead were identified in *P. falciparum,* which assembles the flagellum only in the male gametes. Of these proteins, 14 were previously identified in a comparative study across 45 eukaryotic species as the core components of centrioles in basal bodies and centrosomes (Figure 47) (Hodges et al., 2010). These proteins are: δ- and ε–tubulin, Centrin 2, Centriolin, Bld10/Cep135, Cep164, Cep76, Dip13, Poc1, Poc5, Sas4, Sas6, Vfl1 and Wdr16/Daw1. All 14 core proteins are present in *C. reinhardtii*.

55 basal body proteins were identified in *O.* cf. *ovata* of which 50 are shared with *C. reinhardtii* (annex 3, table 5) and 8 with *P. falciparum*, only three proteins were shared between the three organisms. In *O.* cf. *ovata* I identified 7 of the 14 core basal body components: Centrin-2, Sas4, Sas6, Poc1, Dip13, SVfl1, and Cep76. Additionally, δ- and ε–tubulin were found using PANTHER annotation.

Sas4, Sas6 and Poc1 were identified in different organisms by functional analysis as proteins required to assemble the microtubules at basal bodies (Dutcher & O'Toole, 2016); Sas-6 is also required for the formation of the cartwheel structure (Nakazawa et al., 2007) and together with Centrin has been shown to be required for basal body duplication in *C. reinhardtii* (Dutcher & O'Toole, 2016). Together with tubulin, which I also identified, these proteins are likely to be essential components of the basal body in *O.* cf. *ovata.*

Other proteins, which are not considered as part of the core basal body components, were also present in *O.* cf. *ovata* and are listed in annex 3, table 5.

4.2.4 Mitosis

One hundred and twelve proteins involved in mitosis were analyzed (annex 3, table 6). To simplify the analysis, these proteins were classified in 7 subgroups based on their function: mitotic progression, APC/C, chromosome associated proteins, nuclear pore, MEN, kinetochore, SAC (including spindle components), and the MTOC. Cyclins and CDKs, are listed separately as cell cycle regulators (table 7, annex 3).

Here, I present the major cell cycle components that are conserved in *O.* cf. *ovata* in relation with their role in mitosis as described in the reference species.

Mitotic entry, mitotic progression and APC/C

Cdk1 is the main kinase controlling mitotic entry and mitotic progression. In *O.* cf. *ovata* Ov-Cdk1 was identified. The Ov-Cdk1 contains the PSTAIRE sequence, a well-conserved motif essential for cyclin binding (Morgan, 1997). I also identified homologs of the three mitotic cyclins, cyclin B (Ov-ClB 1, 2 and 4 in yeast), which control Cdk1 activity during mitosis. The presence of both Ov-Cdk1 and Ov-ClB suggests that control of mitotic entry may follow the same control as in opisthokonts (Figure 49). During interphase Cdk1 activity is inhibited by Wee1-mediated phosphorylation. Activation of Cdk1 at mitotic entry requires its dephosphorylation by the phosphatase Cdc25. Wee1, but not Cdc25, was identified in the reference transcriptome, suggesting some similarities in the mechanism that controls mitotic entry through Ov-Cdk1 activation.

The decrease in Cdk1 activity at mitotic exit is regulated by degradation of Cyclin-B by APC/C. APC/C is activated in metaphase by binding to Cdc20 and later in mitosis by interaction with Cdh1 (Visintin, 1997). Most of the APC/C components, with the exception of of APC/C 7 and 9 (table 6, annex 3) are present in *O.* cf. *ovata*. Cdh1 was also present in the reference transcriptome. Surprisingly, I could not retrieve an homolog of Cdc20, whose presence was instead previously reported in other two dinoflagellate species, *S. minitum* (Hooff et al., 2017) and *Lingulodinium polyedra* (Morse et al., 2016b). As the reciprocal best hit strategy I used is recognized as conservative (Hodges et al., 2010), I searched the reference transcriptome for Cdc20 using a basic BLAST search and retrieved a *O.* cf. *ovata* ID. Clustal Omega 2.1 alignment of the retrieved sequence with *S. minitum* Cdc20 showed 70% sequence similarity (Figure 1 of annex 3), supporting the presence of Cdc20 in *O.* cf. *ovata*. Thus, the mechanism controlling CDK activity in mitosis appears to be conserved in *O.* cf. *ovata* (Figure 49).

Chromosome associated proteins

Dinoflagellate chromosomes are not organized around nucleosomes and for a long time were therefore thought not to have histones. Histones were later identified in *Pyrocystis lunula* and *Alexandrium tamarense* (Hackett et al., 2004; O. K. Okamoto & Hastings, 2003) and analysis of the *O.* cf. *ovata* reference transcriptome confirmed that all core histones (H2A, H2B, H3 and H4) are also conserved in this species.

I also found other 22 proteins involved in chromosome organization and segregation. I focused particularly on the cohesion complex which is required to hold together sister chromatids prior to segregation in anaphase and the condensin complex which is thought to stabilize chromosome organization and promote condensation. Both complexes contain proteins of the structural maintenance of chromosome (SMC) family. 4 out of 6 SMC proteins are conserved in *O.* cf. *ovata:* Ov-Smc1-4.

Smc2 and Smc4 are part of the condensin complex (Jessberger, 2002). Two additional non-SMC condensins: Cnd1 and Cnd2 (Iwasaki et al., 2015) required for the conversion of interphase chromatin into mitotic-like condensed chromosomes in yeast (Sutani et al., 1999) are also present in *O.* cf. *ovata*.

Smc1 and Smc3 are part of the cohesin complex and form a heterodimer which together with Scc1 arranges in a ring-like structure which holds together sister chromatids before segregation. Surprisingly neither Scc1, nor its meiotic counterpart, Rec8, are present in *O.* cf. *ovata*. In addition to these core cohesion components, other factors are associated with

the cohesion complex (Wap1 and Pds5). Of those, Pds5 (Wang et al., 2002), which stabilizes centromeric cohesion prior to chromosome segregation and is required for cohesion removal and the metaphase-anaphase transition, is conserved in *O.* cf. *ovata*.

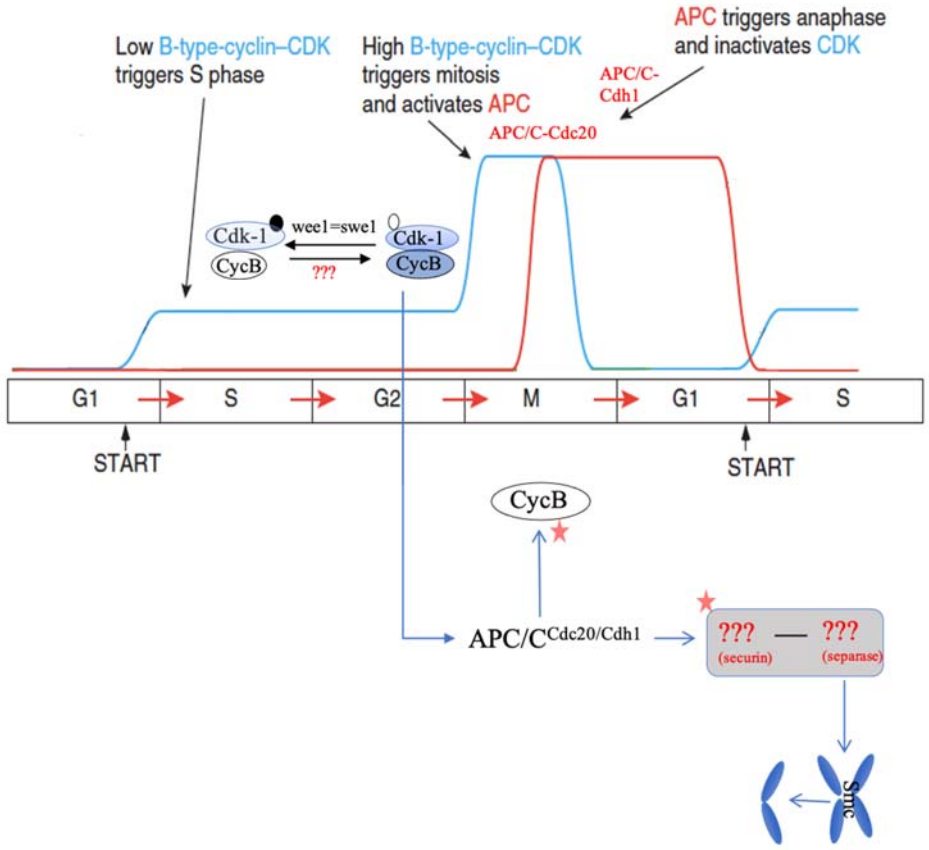

Figure 49. Hypothetical control of mitosis in *Ostreopsis* cf. *ovata*.
The major events of mitosis are shown in relation with the regulation of successive waves of Ov-Cdk/Ov-cyclin-B and APC/C activity. The cell cycle initiates in interphase with low levels of Ov-cyclin-B associated with Ov-Cdk1. The low level of Ov-cyclin-B/Cdk1 activity promotes S-phase, but phosphorylation (black circle) by Ov-Wee1 prevents full activation, and premature mitosis. Full Ov-Cdk1 activation is allowed by an unidentified phosphatase. Active Ov-cyclinB/Cdk1 complex triggers mitosis and activates Ov-APC/C. Ov-APC/C associates with Ov-Cdc20 and triggers anaphase and feeds back to inactivate Ov-cyclin-B/Cdk1 activity through ubiquitination (red star) and consequent degradation of Ov-cyclinB; Ov-cyclinB degradation continues with Ov-APC/C^{Cdh1}. In addition, Ov-APC/C^{Cdc20} triggers chromosome segregation through ubiquitination of unknown targets. Finally, full inactivation of Ov-Cdk1 allows exit from mitosis and the re-establishment of interphase chromosomes.

Kinetochore and the SAC

Proper chromosome segregation in animals and yeast cells requires kinetochores, multi-protein structures assembled on the centromeric region of the chromosome and which mediate interactions with spindle microtubules. Components of the kinetochore have been

identified in different eukaryotic organisms. A recent study analyzed 70 kinetochore proteins in 90 phylogenetically distant organisms, including the dinoflagellate S. *minutum* (Hooff et al., 2017). Based on this study, Tromer et al. (2019) proposed a model of the kinetochore of the last eukaryotic common ancestor (LECA), herein called core kinetochore, which contains 52 of the 70 analyzed proteins.

As the presence of kinetochores in dinoflagellate is controversial, I searched the reference transcriptome for homologs of the 70 kinetochore proteins identified by Hooff et al. (2017) as well as of all proteins which were annotated as kinetochore proteins in uniprot.org, plantdg.org and plasmodb.org for the three reference species. For this analysis I also included kinetochore proteins identified in humans where comprehensive studies have allowed the identification of all kinetochore components and a well-annotated genome is available.

Of the analyzed kinetochore proteins, 52 proteins were present in *O.* cf. *ovata*, whose identities are reported in table 6 of annex 3. 36 of the 52 identified *O.* cf. *ovata* proteins are shared with the LECA core kinetochore.

The 36 core kinetochore proteins found in *O.* cf. *ovata* include: 9 APC/C subunits (Ov-Apc1-5, 10, 11, 13 and 15), 4 components of the nuclear pore complex (Ov-Tpr, Ov-Nup85, Ov-Nup107 and Ov-Nup170); 5 SAC components (Ov-Mad1, Ov-Mad2, Ov-Bub3, Ov-Mps1, and the SAC target Ov-Cdc20); 3 components of the Ndc80 complex (Ov-Ndc80, Ov-Nuf2 and Ov-Spc25); the kinesin Ov-Cenp-E and the microtubule associated protein Ov-Cenp-F; 2 RZZ components (Ov-Rod and Ov-Zw10); Ov-Cep57, Ov-Bugz, and Ov-Pch2; 3 components of the chromosomal passenger complex, CPC (Ov-Aurora, Ov-Borealin and Ov-Incenp); two CCAN components (Ov-CenpA and Ov-CenpC); the kinase Ov-Plk1; 2 CBF3 complex components required for centromeric DNA recognition (Ov-Skp1 and Ov-Cbf3c), and Ov-Spt4. The five SAC proteins together with Ov-Cenp-E and F, Ov-Cep57, Ov-Ndc80, Ov-Nuf2, Ov-Rod, Ov-Spc25, Ov-Bugz, Ov-Zw10 and Ov-Pch2 form the outer kinetochore (14 proteins); while the inner kinetochore includes 9 proteins: Ov-Aurora, Ov-Borealin, Ov-Cbf3c, Ov-CenpA and C, Ov-Incenp, Ov-Skp1, Ov-Spt4 and Ov-Plk1. Mapping of the conserved *O.* cf. *ovata* core components onto the budding yeast kinetochore suggested from the analysis of Hooff, et. al., (2017), is presented in Figure 50C.

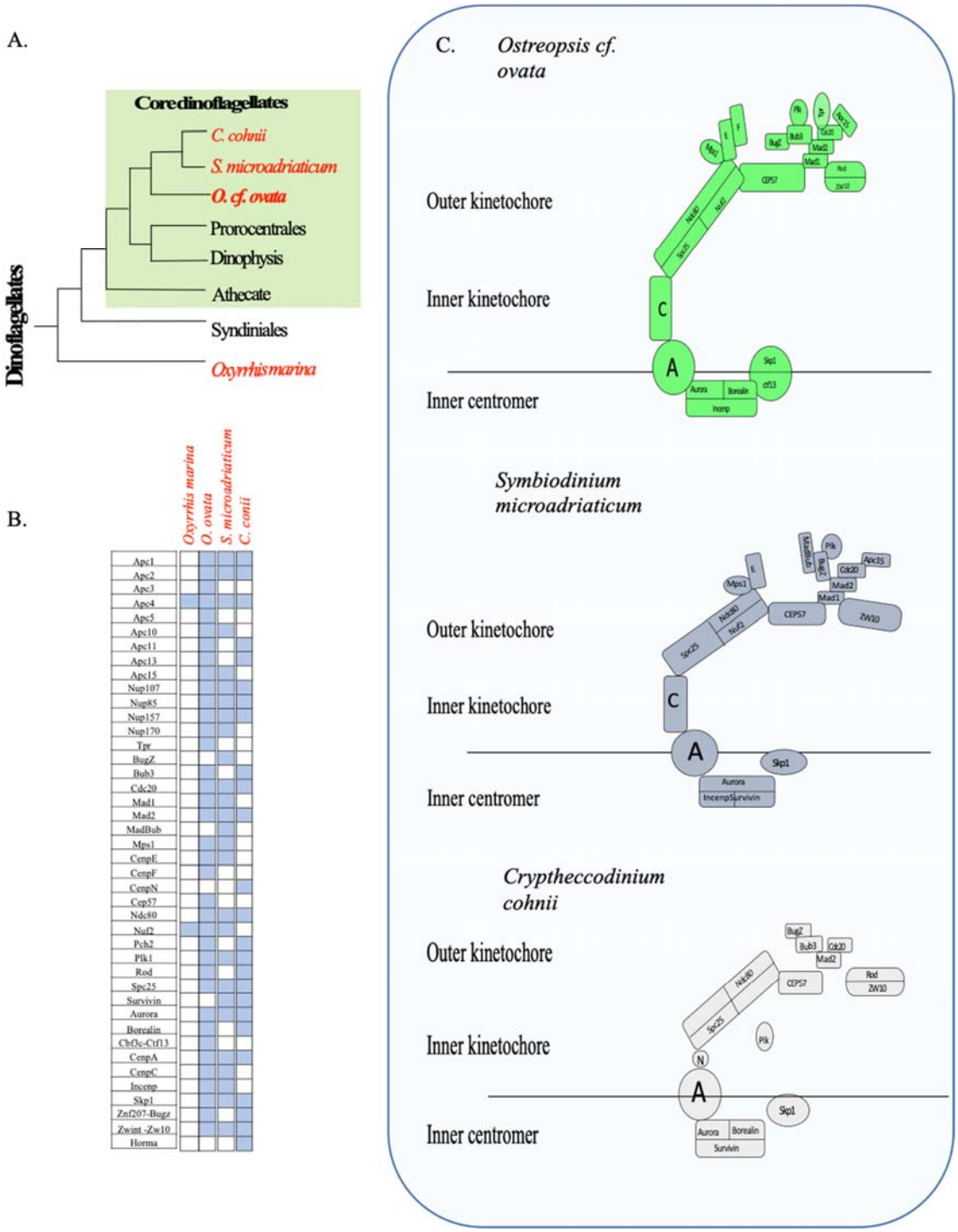

Figure 50. Dinoflagellate kinetochores.

A) Phylogenetic tree of dinoflagellates indicating the position of the four species (red) used in the analysis. B) Kinetochore proteins whose presence/absence was analyzed in dinoflagellates. Blue square indicates presence of homologous proteins in the indicated species. C) Schematic representation of hypothetical kinetochores in the 3 dinoflagellate species that have kinetochore-like structures.

This analysis also retrieved 16 additional *O.* cf. *ovata* kinetochore proteins, which are not part of the LECA core kinetochore. Among these proteins, four additional APC/C subunits (Ov-Cdc16, Ov-Cdc23, Ov-Cdc27 and Ov-Fap18) and 4 nuclear pore complex components (Ov-Nup107, Ov-Nup85, Ov-Tpr and Ov-Nup170) were identified. Additional proteins which are not directly part of the kinetochore but which localize at kinetochores during mitosis and are involved in microtubules-driven chromosome segregation in mitosis, such as dynein, Kar-3 and Dynamin, are also conserved in *O.* cf. *ovata* (annex 3, table 6).

Having identified a potential core kinetochore in *O.* cf. *ovata*, I then asked whether this was specific to this species or was conserved in other dinoflagellates. Using the same strategy described above to identify *O.* cf. *ovata* kinetochore components I therefore looked for homologs of kinetochore proteins in three other dinoflagellate species (Figure 50A): *C. cohnii*, which has kinetochore-like structures identified by electron microscopy and has available transcriptomic data; *Symbiodinium microadriaticum* a species with an annotated genome, and *Oxyrrhis marina,* the most primitive dinoflagellate.

Consistently with the lack of visible kinetochore structures by electron microscopy (Cachon et al., 1979; Gao & Li, 1986), kinetochore proteins were absent in *O. marina*, with the exception of Apc4 and Nuf2 (Figure 50B).

As indicated in Figure 50B, 27 core kinetochore proteins were present in *S. microadriaticum* and 25 in *C. cohnii*, suggesting conservation of a basic kinetochore structure in core dinoflagellates. A possible reconstruction of the kinetochore in the three species is reported in Figure 50C. Comparison of the kinetochore proteins present among the three species identified 14 shared proteins: the APC components Apc1 and Apc2, most of the NUP components (Nup107, Nup85, and Nup157), Cdc20, Mad2, the KMN components Ndc80 and Spc25, Aurora, CenpA, Skp1 Zwint and Plk1.

Interestingly, these conserved proteins include components of the KMN network, (Ndc80, Nuf2 and Spcs25) and of the RZZ complex (Rod and Zw10), involved in the attachment with spindle microtubules, as well as the inner kinetochore proteins CenpA required to direct kinetochore assembly at centromeres and Skp1, required for centromeric DNA recognition (Cleveland et al., 2003). The presence of these two functional complexes suggests that kinetochore function in chromosome-spindle microtubule interaction is conserved in dinoflagellates, despite the presence of an interposed nuclear membrane.

The CPC components Aurora, Borealin and Incenp were also identified in two of the three species. In mitosis this complex localizes at inner centromeres and is required to regulate proper kinetochore microtubule interaction and to activate SAC signaling in the

presence of erroneous attachments. In yeast and animal cells the CPC relocalizes to the cell equator at the metaphase-anaphase transition to promote cytokinesis (Kitagawa & Lee, 2015). It will be interesting to analyze the dynamic localization of those proteins during mitosis in *O.* cf. *ovata* to determine whether they are associated with kinetochore-like structures and whether they relocalize to the site of cytokinesis following chromosome segregation.

Mitotic exit network in *Ostreopsis* cf. *ovata*, a basic network.

The MEN pathway regulates Cdc14 activity, a phosphatase required for mitotic exit in budding yeast cells. The FEAR pathway provides an alternative way of controlling Cdc14 in anaphase when Cdk1 activity is still high (Játiva et al., 2019). Search of homologs of MEN/FEAR components in *O.* cf. *ovata* (Figure 51) retrieved the phosphatase Cdc14, the kinase Dbf2 which in yeast activates Cdc14 (Mah et al., 2001), and its regulatory subunit Mob1; the phosphatase PP2A-Cdc55 which dephosphorylates Cdk1 targets to allow mitotic exit and whose activity is silenced by Cdk1 itself (Moyano-Rodriguez & Queralt, 2019), and the kinase Cdc5, essential to activate Cdc14 through the inhibition of Bfa1 (Geymonat et al., 2003). As already indicated in the previous sections, all subunits of APC/C^{Cdc20} whose activity is required in yeast to cleave securin (Pds1) and cyclin-B and which in involved in the FEAR pathway, were conserved in *O.* cf. *ovata*. However, Pds1 and Separase, the enzyme regulated by securin, are both absent in *O.* cf. *ovata* transcriptome. Bfa1, Bub2, Tem1 and Lte1, which control activation of the MEN pathway and are associated with the yeast spindle pole bodies (Burke, 2009), and members of the RENT complex, which is involved in maintaining cdc14 in the nucleolus, were also absent.

The absence of most MEN/FEAR components does not support a role for this pathway in control of mitotic exit in dinoflagellates. Alternatively, a simplified mechanism for mitotic exit control could be envisaged (Figure 51) that will be further described in discussion.

Figure 51. Hypothetical mitotic exit network in *Ostreopsis* cf. *ovata*.
Schematic representation of the main interactions of the mitotic exit network in *O.* cf. *ovata*. Black circles represents phosphorylation, while empty circles are unphosphorylated proteins. Red stars represent ubiquitination. Red question marks indicate components not identified in *O.* cf. *ovata* transcriptome.

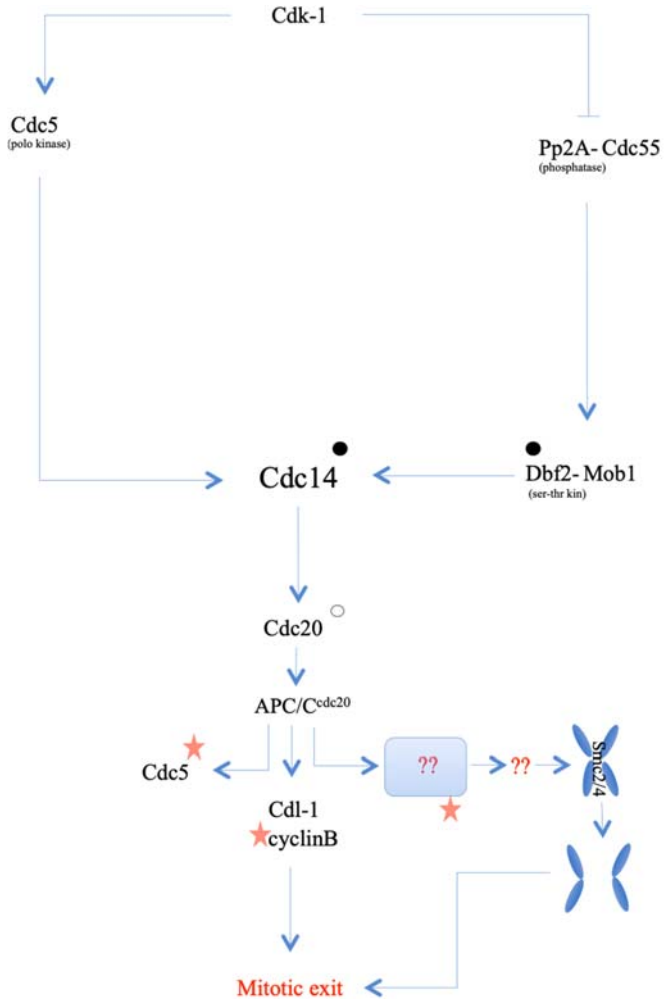

4.2.5 Cytokinesis

Cytokinesis, the final step of cell division, which physically separates the two daughter cells, relies on very different mechanisms in different organisms and is regulated by organism specific signals. It is therefore difficult to precisely define proteins that are generally involved in cytokinesis. Therefore, I analyzed proteins that are known to be involved in cytokinesis in budding yeast, which divides using an actomyosin ring. As I have shown that in *O.* cf. *ovata* a microtubule-based plate assembles at the site of cytokinesis and that an actomyosin ring instead does not appear to be involved, I also searched for proteins involved in cytokinesis in the green alga *C. rehinardii* that uses a microtubule-based cytokinesis (Cross & Umen, 2015).

A few proteins, which have been described as involved in cytokinesis in *P. falciparum,* were also included.

Of the analyzed proteins, 63 were conserved in *O.* cf. *ovata* (table 7 in annex 3). These proteins can be subdivided in classes based on their functions: basal body components (12 proteins), proteins involved in microtubule-based movement (5 proteins), proteins involved in vesicular trafficking and membrane assembly (10 proteins), proteins involved in progression of cytokinesis (36 proteins).

Cytoskeletal components and their associated proteins (Ov-α-tubulin, Ov-β-tubulin, Ov-actin and Ov-actin-related proteins as Ov-Arp2/3 and Ov-Cofilin) and proteins involved in vesicular trafficking (Ov-Vps members) were shared between all species.

Analysis of the myosin genes retrieved 20 different *O.* cf. *ovata* myosin transcripts (table 6). Consistently with previous bioinformatic studies, which showed that Myosin II is absent in all organisms outside of Opisthokonta and Amoebozoa (Richards & Cavalier-Smith, 2005), myosin II, the main myosin isoform responsible for cytokinesis in animal and fungi (Glotzer, 2017), was absent. Thus, this result support my previous observation that in *O.*cf. *ovata* cytokinesis is not driven by an actomyosin ring, but by a cytokinetic plate made of microtubules.

Table 6. Panther annotation of Myosin proteins identified in *Ostreopsis* cf. *ovata* transcriptome.
The left column contains the transcript IDs from *O.* cf. *ovata*, the middle column contains the Panther IDs that corresponds to the proteins shown in the right column.

***Ostreopsis* cf. ovata ID**	**Panther ID**	**Panther name**
TRINITY_DN1203_c0_g4_i1	PTHR13140:SF706	DILUTE CLASS UNCONVENTIONAL MYOSIN, ISOFORM C
TRINITY_DN12282_c0_g3_i1	PTHR23160	MYOSIN HEAVY CHAIN-RELATED
TRINITY_DN1329_c0_g2_i1	PTHR45615:SF40	MYOSIN HEAVY CHAIN, NON-MUSCLE
TRINITY_DN19372_c0_g1_i1	PTHR13140:SF706	DILUTE CLASS UNCONVENTIONAL MYOSIN, ISOFORM C
TRINITY_DN23105_c0_g1_i2	PTHR21448	SMOOTH MUSCLE MYOSIN HEAVY CHAIN-RELATED
TRINITY_DN23690_c1_g2_i1	PTHR13140:SF706	DILUTE CLASS UNCONVENTIONAL MYOSIN, ISOFORM C
TRINITY_DN2371_c0_g3_i3	PTHR13140:SF550	MYOSIN IIIA
TRINITY_DN2476_c0_g1_i3	PTHR23048	MYOSIN LIGHT CHAIN 1, 3
TRINITY_DN25689_c0_g1_i8	PTHR45615:SF40	MYOSIN HEAVY CHAIN, NON-MUSCLE
TRINITY_DN29034_c0_g1_i2	PTHR23160	MYOSIN HEAVY CHAIN-RELATED
TRINITY_DN31042_c0_g1_i1	PTHR45615:SF40	MYOSIN HEAVY CHAIN, NON-MUSCLE
TRINITY_DN3380_c0_g4_i1	PTHR45615:SF40	MYOSIN HEAVY CHAIN, NON-MUSCLE
TRINITY_DN46825_c0_g1_i1	PTHR45615:SF40	MYOSIN HEAVY CHAIN, NON-MUSCLE
TRINITY_DN4758_c0_g4_i1	PTHR13140:SF706	DILUTE CLASS UNCONVENTIONAL MYOSIN, ISOFORM C
TRINITY_DN48189_c0_g2_i1	PTHR23160	MYOSIN HEAVY CHAIN-RELATED
TRINITY_DN508_c0_g2_i1	PTHR45615:SF23	MYOSIN-11
TRINITY_DN6025_c0_g1_i3	PTHR13140:SF706	DILUTE CLASS UNCONVENTIONAL MYOSIN, ISOFORM C
TRINITY_DN642_c1_g4_i1	PTHR24347:SF393	MYOSIN, LIGHT CHAIN KINASE 5
TRINITY_DN6677_c0_g6_i1	PTHR45615:SF40	MYOSIN HEAVY CHAIN, NON-MUSCLE
TRINITY_DN9370_c1_g1_i1	PTHR22692	MYOSIN VII, XV

4.2.6 Cyclins and cell cycle progression

As the focus of my analysis was on mitosis, I did not analyze in great details the proteins involved in cell cycle progression. However, I checked if CDKs, cyclins and major cell cycle regulators, which control progression through different cell cycle stages were present in *O.* cf. *ovata*.

24 cell cycle regulators were identified in *O.* cf. *ovata* and are presented in table 8 of annex 3. For homologs of *P. falciparum* and *C. reinhardtii* often little information is available as the proteins were also identified by sequence comparison to yeast counterparts.

In *O.* cf. *ovata* I identified four of the six budding yeast cyclins, ClB1, ClB3, ClB4 and ClB6; two out of three *Plasmodium* cyclins, Cyc1 and Cyc4, and two of the *Chlamydomonas* cyclins: Cyc-A, and a cyclin whose function was reported as unknown. None of these cyclins was directly associated with G1 phase. In my preliminary analysis the only *O.* cf. *ovata* protein associated exclusively with G1 phase, was the transcriptional repressor Ov-Whi5 whose homologue in yeast negatively regulates SBF-mediated expression of G1/S genes (Costanzo et al., 2004; Robbins et al., 2017). SBF inhibition is relieved by CDK mediated phosphorylation of Whi5 to allow transcription of genes necessary for the G1/S transition (Costanzo et al., 2004). The lack of G1 cyclins suggests that this role may have been acquired by another cyclin. Examples of change in cyclin function have already been reported. For example, Cyc1 in *Plasmodium* is necessary for cytokinesis (Robbins et al., 2017), whereas its ortholog, cyclin H in humans, is required for G1/S. Alternatively different CDK-cyclin complexes may not be required and instead quantitative differences in the activity of a single CDK-cyclin complex may regulate cell cycle transitions, as postulated for fission yeast Cdk1-cyclinB (Cdc2-Cdc1) (Fisher & Nurse, 1996).

In yeast, ClB 5 and 6 are required for progression through S-phase and correct DNA replication (Palou et al., 2010). ClB6 is present in *O.* cf. *ovata*. Surprisingly, a study performed in the dinoflagellate *S. minitum,* showed that ClB2, which I did not find in *O.* cf. *ovata,* peaks in S-phase (Cato et al., 2019b). Pho85/Cdk5, a cyclin dependent kinase that was involved in G1/S control in budding yeast is also present in *O.* cf. *ovata.*

In animal cells, cyclin A in association with Cdk2 controls the onset of S-phase and stimulates DNA synthesis. In association with cdk1, cyclin A instead drives early mitotic events, such as chromosome condensation and nuclear envelope breakdown. Cyclin-A is also present in *O.* cf. *ovata,* but no Cdk2 was identified, suggesting a conservation of the role of cyclinA-Cdk1 in mitotic entry, but not in S-phase. The mitotic role of the Cdk1-CyclinA (CdkA-CycA) complex in mitotic entry is also conserved in *C. reinhardtii* (Bertoni, 2018). As

mentioned at the beginning of this section (mitotic entry) Cdk1 and mitotic cyclin B are also conserved and probably involved in control of mitotic progression.

4.2.7 Meta-transcriptome RNA and quality control

Having identified a large number of genes which are potentially involved in control of the cell cycle and of cell proliferation, I then to ask whether their expression was regulated during the bloom in relation to changes in proliferation regime and also at different stages of the cell cycle. I therefore generated metatrascriptomic data corresponding to bloom phases and times. For this analysis I prepared total RNA from wild type bloom samples during the proliferative phase, at the peak of the bloom, during senescence and at the end of the bloom. I also prepared total RNA from samples collected during the day (12:00), in the evening (20:00) and at night (4:00). As I had shown that cell division occurs exclusively at night (chapter 2), I assumed that day samples contained mostly *O.* cf. *ovata* cells in interphase, whereas evening samples were enriched in pre-dividing cells and night samples were enriched in mitotic and dividing cells. Microscopic analysis of Hoechst 33342 stained samples corresponding to day, evening and night confirmed this assumption (Figure 54A), although the enrichment of predividing and dividing cells was never above $1/5^{th}$ of the population. The sample collected at 12:00 showed almost exclusively interphase cells. The sample collected in the evening showed 20% pre-dividing cells, while the sample collected at 4:00 contained 10% of pre-dividing cells and 8% of cells undergoing mitosis or cytokinesis.

For each time point, I produced triplicates and 21 RNA samples were sent for sequencing to BGI. Two of the 21 initial samples, corresponding to a senescence sample and a day sample, however were excluded due to RNA degradation. Following sequencing, raw data were treated as described for the reference transcriptome. Between 73 and 76 million contigs were obtained from each sample with a mean GC content of 54.2 (table 7).

A meta-transcriptome represents the total RNA expressed by all the different species co-occurring in the sample. Therefore, I used the reference transcriptome to map the transcripts corresponding to *O.* cf. *ovata* and calculated the percentage of reads mapped to *Ostreopsis*. The change in relative amount of *O.* cf. *ovata* RNA over the total RNA present in each sample, followed the same trend of the cell concentrations observed during the bloom (Figure 52A). During the proliferative phase, 14.1% of the RNA present in the metatranscriptome was from *O.* cf. *ovata*; it increased to 40% in peak samples and then decreased to 34% in the senescence samples and dropped to 7.6% at the end of the bloom.

Following meta-transcriptomes quantification using kallisto, I performed a Principal Component Analysis (PCA) in order to compare the samples, and check that the biological replicates showed the expected similarity compared to different bloom stages. PCA plots of the normalized log-transformed count data show the correlation in terms of gene expression levels among all the samples in 2-D graph space (Figure 52B). The result of the distribution of samples showed a good correlation between most of the replicates. However, as two samples corresponding to the end phase were separated from the other samples in the PCA, I decided to use a conservative analysis in the comparison of transcripts that were differentially expressed, defining a cut-off for the p and q value <0.01.

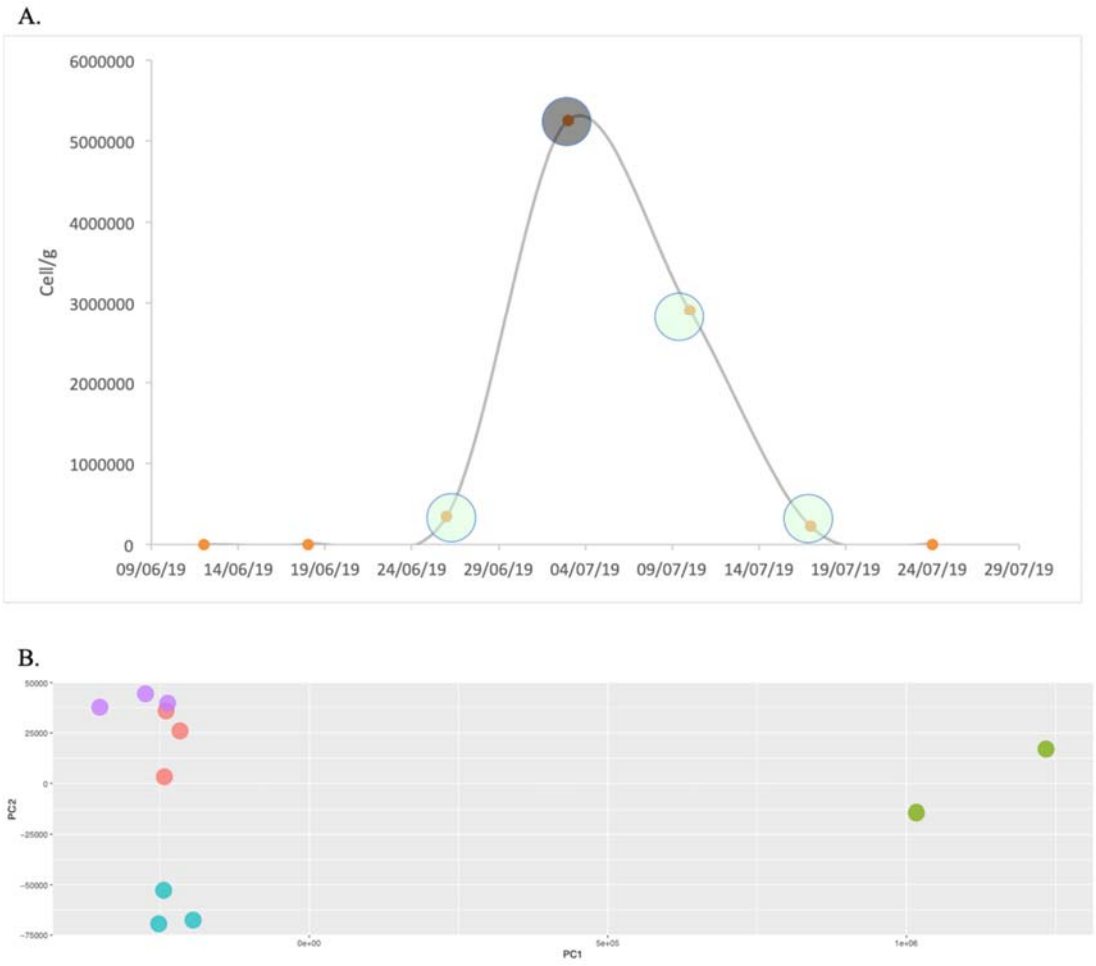

Figure 52. Meta-transcriptomic samples from *Ostreopsis* cf. *ovata* 2019 bloom.
A) Quantification of cell concentration during *O.* cf. *ovata* 2019 bloom. Green circles shows when the samples for metatranscriptomic were collected during the bloom. The grey circle at the peak of the bloom indicates when the day, evening and night samples were collected to compare between cells in interphase, pre-dividing and division. B) PCA map showing correlation in terms of gene expression levels among all the samples in 2-D graph space. Red circles = triplicate samples from proliferative phase; green circles = samples from the peak; blue circles = senescence; purple circle = end phase.

Table 7. Transcriptome assembly statistics for bloom samples.
Day, evening and night samples were collected the same day. Q20(%) is the sequencing quality score of a given base and indicates the probability of 1 error every 100 nucleotides. Numbers 1 to 3 in the Sample ID column means triplicates. Senescence and Day samples were processed only duplicates.

Sample ID	Clean Reads	Clean bases	Read length (bp)	Q20(%)
Proliferative-1	75,269,038	7,526,903,800	100	96.90%
Proliferative-2	73,411,738	7,341,173,800	100	97.02%
Proliferative-3	73,315,664	7,331,566,400	100	96.92%
Peak-1	74,816,754	7,481,675,400	100	97.19%
Peak-2	74,508,784	7,450,878,400	100	97.11%
Peak-3	73,414,512	7,341,451,200	100	96.77%
Senescence-1	73,812,998	7,381,299,800	100	96.75%
Senescence-2	73,847,990	7,384,799,000	100	96.90%
End-1	75,576,922	7,557,692,200	100	97.48%
End-2	73,506,292	7,350,629,200	100	97.43%
End-3	75,787,252	7,578,725,200	100	97.53%
Day-1	72,935,260	7,293,526,000	100	97.57%
Day-2	74,149,488	7,414,948,800	100	97.50%
Evening-1	73,705,624	7,370,562,400	100	97.41%
Evening-2	73,848,046	7,384,804,600	100	97.55%
Eveninig-3	75,628,144	7,562,814,400	100	97.19%
Night-1	75,133,618	7,513,361,800	100	97.11%
Night-2	74,896,262	7,489,626,200	100	96.84%
Night-3	75,509,186	7,550,918,600	100	97.12%

4.2.8 High transcriptional control of *Ostreopsis* cf. *ovata* during the bloom. Meta-transcriptome analysis.

Differential gene expression in *O.* cf. *ovata* was analyzed during the bloom, considering a p and q value < 0.001. As shown in Figure 53, this analysis showed high levels of transcriptional regulation: 8068 transcripts were differentially expressed between the proliferative phase and the stationary phase (Figure 53A); 8155 between the proliferative phase and senescence, (Figure 53B); 1440 between the proliferative phase and the end of the bloom (Figure 53C); 10690 between stationary phase and senescence (Figure 53D); 8985 between the stationary phase and the end of the bloom (Figure 53E); and 4649 between senescence and the end of the bloom (Figure 53F). Although it is generally accepted that in dinoflagellates many processes are regulated at the translational rather than transcriptional level (Wisecaver & Hackett, 2011), this analysis shows that a significant number of genes are regulated at the level of transcription during bloom development.

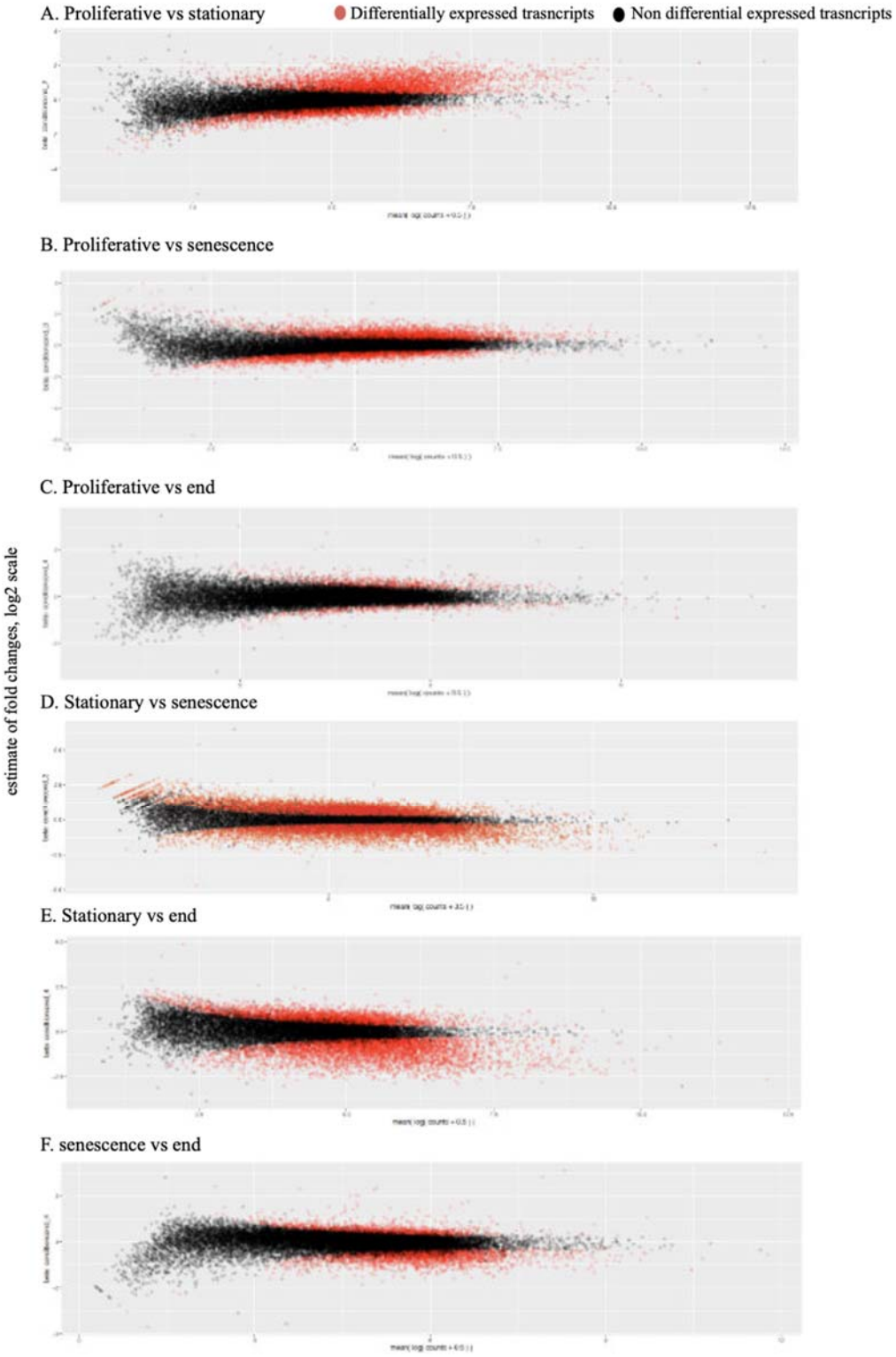

Figure 53. Differential gene expression analysis of the meta-transcriptomic samples.
A) Plot of differentially expressed genes between proliferative and stationary phases; B) proliferative phase and senescence; C) proliferative phase and end of bloom; D) stationary phase and senescence; E) stationary phase and end of bloom; F) senescence and end of bloom. Differentially expressed transcripts are shown in red. Up-regulated transcripts are above zero while downregulated transcripts are below zero (Y axis – estimate of fold changes, log2 scale). X axis shows values in log10 scale.

4.2.9 Transcriptional control of *Ostreopsis* cf. *ovata* during the cell cycle.

In order to identify the transcripts that are transcriptionally regulated during *O.* cf. *ovata* vegetative cycle, I analyzed the transcripts whose expression changed during a 24 hours cycle (day, evening and night).

The PCA plot (Figure 54) showed that most of the samples clustered close to each other with the exception of one day sample. As this sample is broadly separated in the PCA plot, I used a stricter cut-off <0.001 for the differential gene expression analysis (Figure 55).

Figure 54. Meta-transcriptome samples for *Ostreopsis* cf. *ovata* cell cycle analysis.
A) Quantification of different *O.* cf. *ovata* morphotypes in day (12:00 – interphase, left), evening (20:00 – pre-dividing, middle) and night (4:00 – dividing, right) samples for metatrascriptomic analysis. B) PCA plot of metatranscriptomic data generated form day, evening and night sample. Red circles correspond to day samples (12:00); green circles correspond to triplicates of evening samples (20:00); blue circles correspond to triplicates of night sample (4:00).

The comparison between day and evening showed 5489 differential expressed transcripts, of which 2327 were downregulated in the evening and 3162 up-regulated (Figure 55A).

During the night, 3646 transcripts were downregulated and 2977 were up-regulated relative to the day. In total, 6623 transcripts were differential expressed in this comparison

(Figure 55B). Comparison of evening and night samples identified only 241 differentially expressed transcripts, of which 96 were downregulated during the night and 145 were upregulated (Figure 55C). This analysis showed that the main changes at transcriptional level occur in the day to night transition, whereas evening and night samples were relatively similar. Of these 241 transcripts, almost 80% (193) were common transcripts differentially expressed between the pairs 'day vs evening' and 'day vs night'. None of the 48 remaining transcripts was related with cell division.

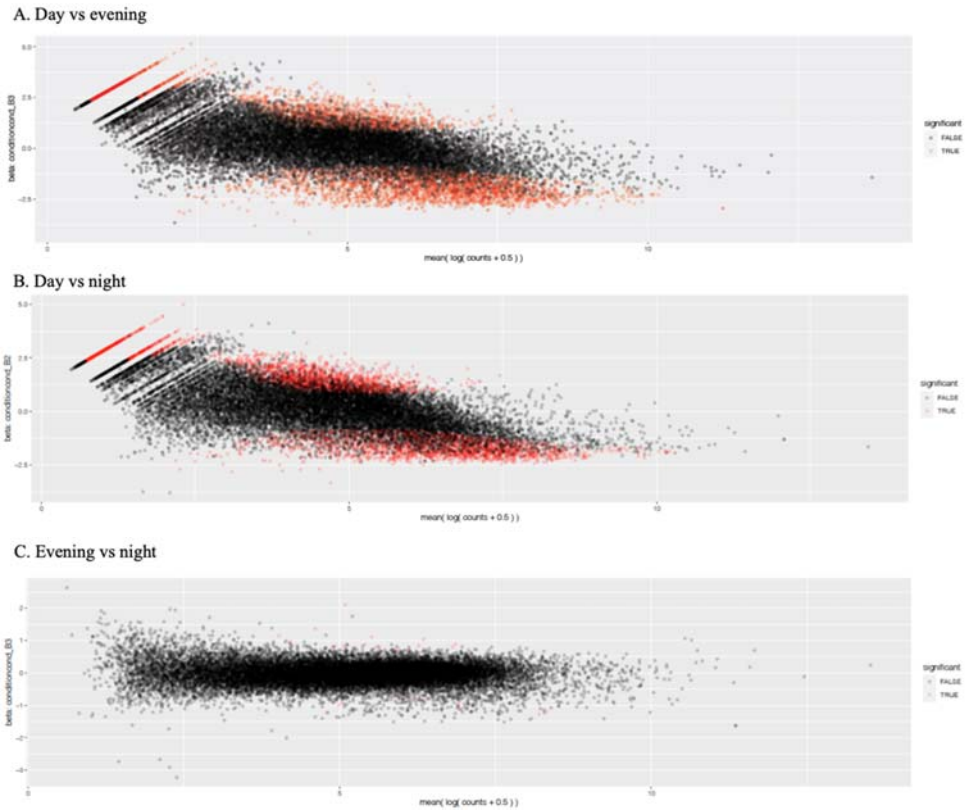

Figure 55. Differential gene expression analysis of the meta-transcriptomic samples for day, evening and night.
A) Plot of differentially expressed genes between day and evening; B) between day and night; C) between evening and night. Differentially expressed transcripts are shown in red, using a cut-off value < 0.001. Up-regulated transcripts are above zero while down regulated transcripts are below zero. X-axis shows values in log2 scale.

I then analyzed whether any of the 209 *O.* cf. *ovata* cell cycle proteins I had identified in my analysis of the reference transcriptome, were differentially expressed during the 24 hours cycle.

Although the evening and night samples contain mostly interphase cells (80%), the comparison between metatranscriptomic datasets showed that 66 transcripts (31.6%) of the *O.*

cf. *ovata* cell cycle components were differentially expressed between day and evening. Of those, 32 transcripts were upregulated in the evening samples. 58 (28%) transcripts encoding *O.* cf. *ovata* cell cycle components were differential expressed between day and night. These 58 proteins include most of the components (50) that are differential expressed between evening and day, and of those 28 were up-regulated. The complete list of differential expressed transcripts identified in this analysis is presented in table 9, annex 3.

Cyc-A was up-regulated in the evening but not in the night samples (Figure 56A), whereas both evening and night samples showed up-regulation of ClB4 (Figure 56B, C) and down regulation of ClB1 (Figure 56D, E).

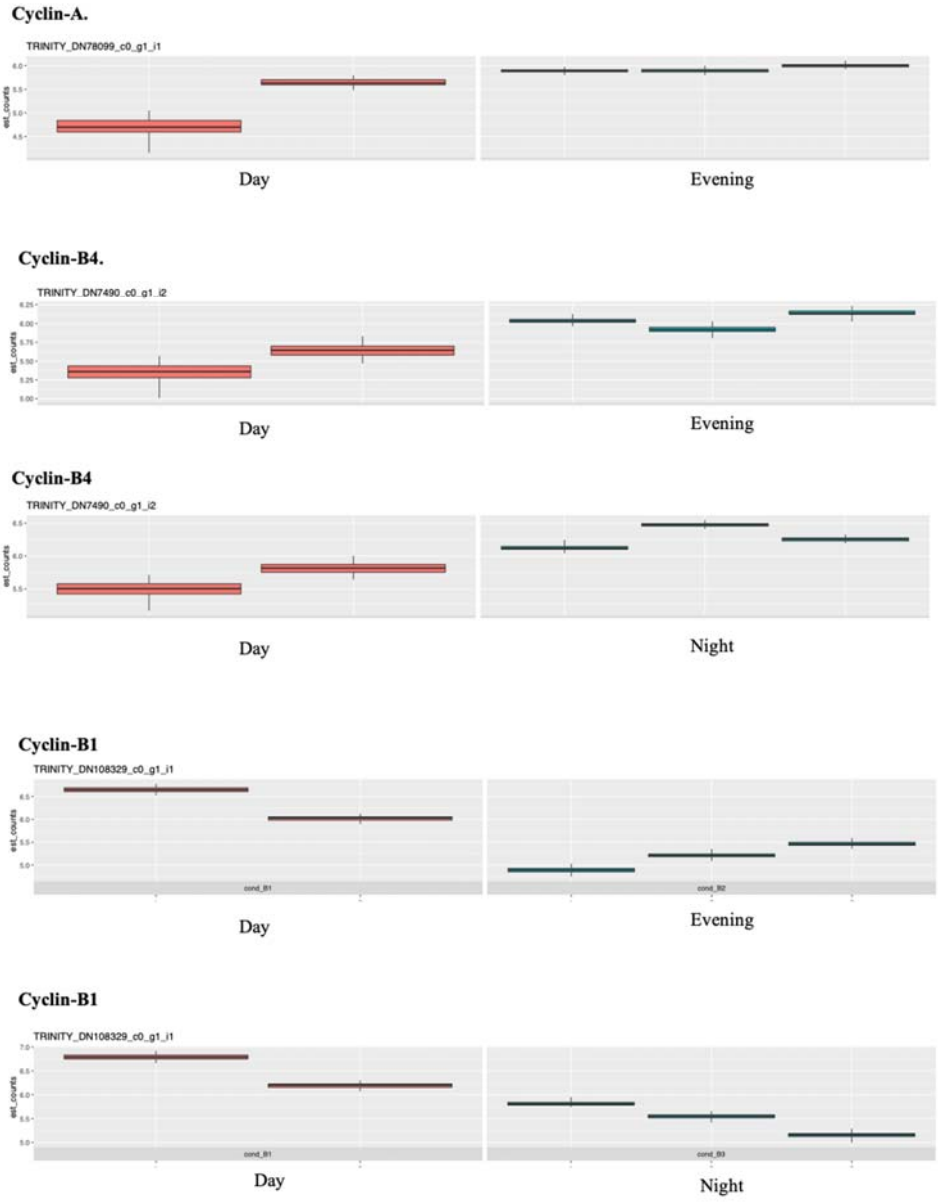

Figure 56. Quantification of transcript levels for cyclins which were identified as differentially expressed. For cyclin-A transcripts were quantified in all day (left A) and evening (right A) samples, whereas for cyclin B4 and B1, transcripts were quantified in all day (left B-D), evening (right B and D) and night (right C and E).

Nuclear pore proteins associated with the kinetochore (Nup107, Nup170, Nup85 and Tpr) and most core kinetochore components, including SAC proteins (Cbf3c, Skp1, Cep57, Ndc80, Nuf2, Spc25, Mad1 and Mps1; Figure 57) are also up-regulated both in evening and night samples (pre-dividing and dividing cells). Surprisingly instead two subunits of APC/C (Apc13, Apc15) and the APC/C activator Cdh1, were down-regulated in both samples.

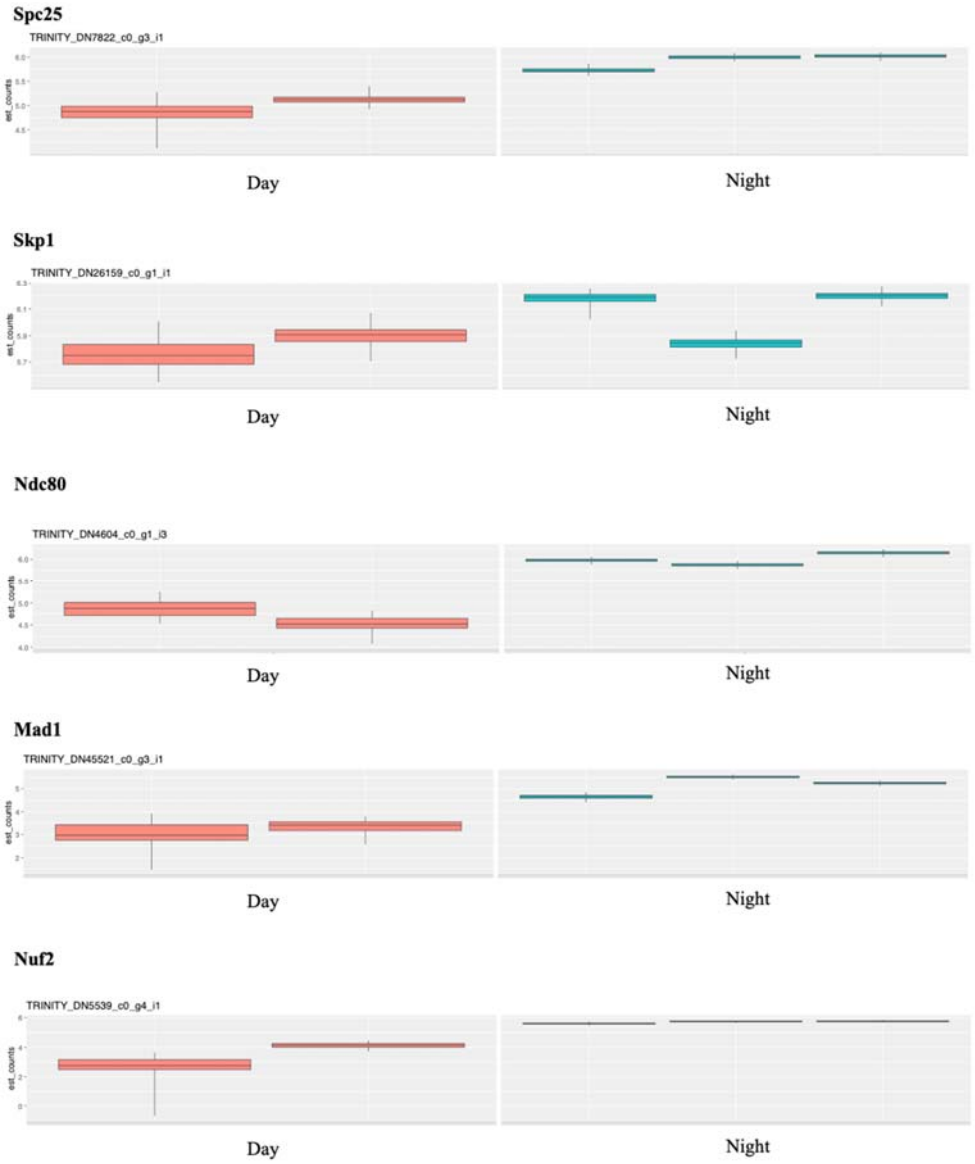

Figure 57. Quantification of transcript levels for kinetochore components which were identified as differentially expressed between day and night. For each component transcripts were quntified in all day (left) and night (right) samples

This analysis suggests that transcription of several cell cycle regulators may be controlled as cells prepare for mitosis (evening, pre-dividing cells), while the regulation between pre-dividing to dividing cells does not seems to be controlled by transcriptional activity. Alternatively, as pre-dividing and dividing cells did not show important differences in transcriptional landscape, pre-dividing cells may be already committed to mitosis in terms of transcriptional regulation.

4.3. Discussion

In this chapter, I described the assembly and characterization of a *de novo* transcriptome for *O.* cf. *ovata* with the aim to produce a database of proteins involved in mitotic control in dinoflagellates. Recently another *de novo* transcriptome of *O.* cf. *ovata* was published (Verma, et al., 2019) which was used to analyze pathways involved in toxin production. A comparison of the two *Ostreopsis* transcriptomes would be useful to validate the analysis and the tools generated here, but the sequences only become available recently preventing me from performing such comparative analysis.

4.3.1 *Ostreopsis* cf. *ovata* cell cycle

Analysis of cell cycle regulated genes highly relies on synchronization of the cell cycle to obtain population of cells going through the same stage of the cell cycle at the same time. As synchronization protocols have not yet been optimized for *O.* cf. *ovata*, the best chance of obtaining cells in pre-dividing stage or undergoing division was to collect cells during the bloom when cell division occurs exclusively at night. However, the wild population was still heterogenous. Considering that just 8% of cells were dividing at night and 20% were in the pre-dividing stage in the evening, the majority of cells were always in interphase. However, recently Cato et al. (2019), analyzed changes in expression of putative cell cycle genes by RT-PCR in a non-homogenous cultures of *S. minutum*, which reached 65% of cells in G1/S and 46% in G2/M, respectively, as determined by flow cytometry. Despite the heterogeneity of the cultures the authors were able to identify CycB2/Cdk1 as regulator of G1/S phase; other cyclins were identified: Cyclin-A, two more Cyclins-B: CycB1 and CycB3, and other Cyclins as P, L, and Y.

Based on this premises, I therefore reasoned that the day sample is representative of interphase cells; the evening sample, which is enriched in pre-dividing cells, is representative of cell between G2 and early mitosis; and the night sample, which is enriched in cells in division (bi-nucleated cells), will allow to identify genes regulated during M-phase (mitosis

and cytokinesis). Using these data sets I identified five cyclins (Ov-ClB1, 2, 4 and 6 and Ov-cyclin A), two CDKs (Ov-Cdc28/Cdk1 and Ov-Pho85/cdk5) and one G1-specific transcriptional repressor (Ov-Whi5). The same cyclins and CDKs were also identified, using a similar approach in other two dinoflagellate species, *Lingulodinium polyedrum* and *Symbiodinium sp.* (Morse et al., 2016b). In all three species, no G1 cyclins were identified. Whi5, a repressor of the transcription factor SBF (de Bruin et al., 2004), instead was only present in *O.* cf. *ovata*.

Differently from yeasts, the CDKs were expressed at constant levels in all samples. As in yeast Pho85 is associated with control of G1 and S-phase and Whi5 was shown to be a target of active Pho85, I suggest that Ov-Pho85 is the CDK controlling G1/S in *O.* cf. *ovata*.

Ov-ClB1, whose homolog in *S. cerevisae* is associated with mitosis, is up-regulated during the day in *O.* cf. *ovata*, suggesting that this cyclin may be associated with interphase rather than mitosis in this organism. Other examples of cyclins accomplishing different function from the one initially reported have been already identified. In *P. falciparum* Cyc-1 was identified as necessary for cytokinesis whereas in yeast its homologue cyclin-H is required for transcriptional control and in complementation experiments PfCyc-1 rescues triple Cln1, 2, 3 (G1 cyclins) budding yeast deletion mutants (Robbins et al., 2017). Alternatively ClB1 may be involved in control of mitosis and its transcript which accumulates during interphase is under translational control resulting in accumulation of the protein only when the cell prepares for mitosis.

ClB2, which is proposed as a regulator in G1/S in *S. minitum* instead, peaks during mitosis in budding yeast (Cato et al., 2019). ClB6 regulates S-phase in yeast and it was reported to be expressed during S-phase in *L. polyedrum* and *Symbiodinium sp* (Morse et al., 2016). Given the presence of ClB6 in *O.* cf. *ovata,* it is reasonable to assume that it plays a similar role in dinoflagellate S-phase control. A similar argument can be used for ClB2. Precise analysis of cyclin transcriptional profile during the cell cycle would be required to confirm this assumption, as the single meta-trascriptomic dataset corresponding to interphase (day) does not allow to distinguish genes regulated during different stages of interphase.

Interestingly, Ov-CycA was up-regulated only in the evening sample and not in the night sample, whereas Ov-ClB4 was up-regulated both in evening and night samples, suggesting that Ov-CycA may regulate mitotic entry, whereas Ov-ClB4 may be the mitotic B-cyclin. The homologue of Ov-CycA was also found in *Chlamydomonas*, where it is involved in G2/M transition (Bertoni, 2018).

Based on this analysis and integrating the results of the differential expression analysis, therefore, I propose that *O.* cf. *ovata* cell cycle is controlled by CDKs and associated cyclins as shown in Figure 58. In this model Ov-Pho85 and Ov-Cdk1 control transitions during different phases of interphase, but given that I have produced only one dataset corresponding to interphase I cannot distinguish between G1, S and G2. Based on studies in the reference organisms, however it is possible to suggest that Ov-Pho85 controls G1, that Ov-Whi5 regulates G1 transcription and that cyclins Ov-ClB6 and/or ClB2 probably in association with Ov-Pho85 control S-phase. G2 that is proposed to correlate with evening samples, could be controlled by Ov-CycA/Cdk1; and M-phase could be controlled by Ov-ClB4/Ov-Cdk1.

Cyclin-1, although present in *O.* cf. *ovata,* was omitted from the diagram because in *O.* cf. *ovata* Cyclin-1 is up-regulated only in the evening sample, but its *P. falciparum* homolog is required for cytokinesis and its yeast homolog cyclin-H controls transcription.

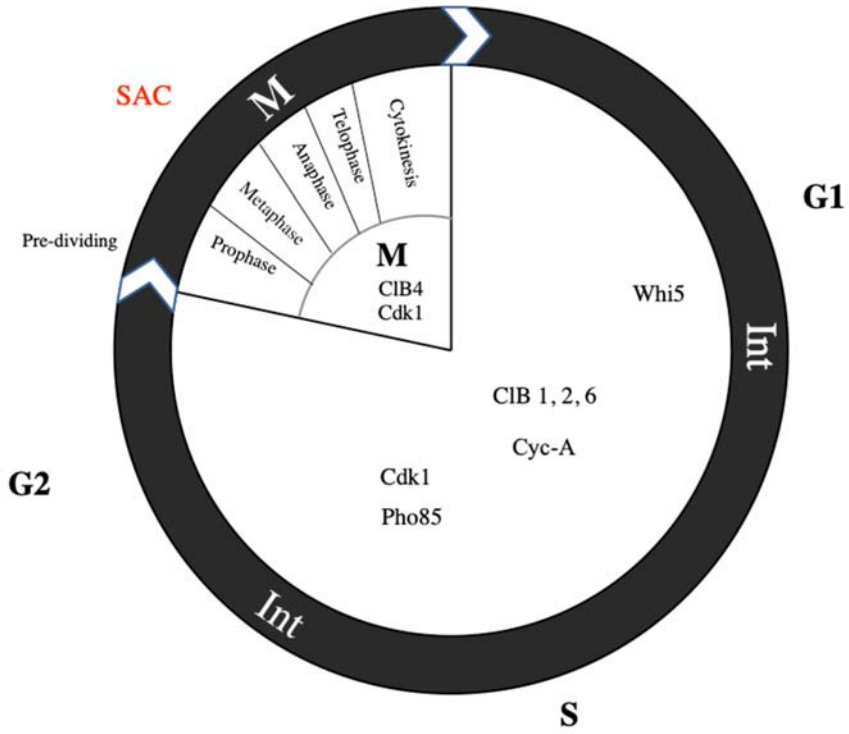

Figure 58. Cell cycle in *Ostreopsis* cf. *ovata*.
Two main phases of *O.* cf. *ovata* cell cycle are indicated: Interphase (Int) and M-phase (M). It is assumed that as other dinoflagellate, *O.* cf. *ovata* has a canonical cell cycle with G1, S and G2 in interphase. The major events of the cell cycle are regulated by cyclins and CDKs proteins. The diagram shows cyclins hypothetically regulating interphase in combination with the two CDKs Pho85 and Cdk1. Cyclin-A, ClB1, 2 and 6; the CDKs Pho85 and Cdk1, and the transcriptional factor Whi5 were identified as regulators of interphase. ClB4, which is up-regulated in evening and night samples, is proposed to bind Cdk1 to regulate mitosis. Pre-dividing cells which are defined by central nuclear position, are suggested to be in prophase (mitosis).

4.3.2 Control of mitotic entry in *Ostreopsis* cf. *ovata*

Mitotic entry requires activation of the Cdk1-Cyclin-B complex. During interphase the complex is kept inactive by Wee1-dependent phosphorylation of Cdk1 on Thr14 and Tyr15 (Den Haese et al., 1995). When the conditions are appropriate for initiation of mitosis, the phosphatase Cdc25 relieves Cdk1-CyclinB inhibition by removal of the two inhibitory phosphates (Kumagai & Dunphy, 1992). Although, as mentioned above Cdk1 and Cyclin B are conserved in *O.* cf. *ovata,* only Wee1, but not Cdc25, could be found. Cdc25 was also absent in other two dinoflagellates, *S. minitum* (Cato et al., 2019) and *Lingulodinium polyedrum* (Morse et al., 2016b), suggesting that either the gene was lost in dinoflagellates, or it originated after the emergence of the dinoflagellate lineage. Analysis of the *O.* cf. *ovata* Cdk1 protein sequence also showed lack of conservation of the two Wee1 phosphorylation sites in Cdk1. As shown in Figure 2 of annex 3, Tyr15 and Thr14 are replaced by Ala14 and Phe15, respectively, in Cdk1 from *O.* cf. *ovata*. Although it is formally possible that Cdk1 is phosphorylated on different residues in dinoflagellates and that a phosphatase other that Cdc25 counteracts Wee1 function, it is interesting to notice that Cdc25 is also missing in plants and green algae. In plants, lack of Cdc25 is associated with the presence of a unique class of CDKs, known as B-type CDKs, which lack the canonical cyclin-binding domain PSTAIRE and instead have a divergent PPTALRE motif (Boudolf et al., 2006). In plants, a canonical CdkA controls S-phase, while CdkB controls mitosis. CdkB is absent in G1 cells and CdkB transcripts accumulate in G2, suggesting transcriptional control of mitotic CdkB. It was suggested that transcription of CdkB is under the control of CdkA to allow timely accumulation of mitotic CdkB activity (Tulin & Cross, 2015). A similar mechanism might be working in dinoflagellates. The idea that dinoflagellates possess other kind of cyclin dependent kinases has been already suggested for *S. minitum*, where phylogenetic analysis of CDKs revealed the presence of four CDKs, of which CRKBm3 was reported to peak during division and likely, controlling mitosis (Cato et al., 2019a). Careful phylogenetic analysis of the *O.* cf. *ovata* CDKs will reveal the presence of different families of CDKs, as observed in plants and other dinoflagellates and will help with dissecting the mechanism controlling mitotic entry in *O.* cf. *ovata*.

4.3.3 Kinetochore in dinoflagellates

During mitosis, chromosome segregation relies on the assembly of a bipolar mitotic spindle and the interaction of chromosomes with spindle microtubules through multiprotein complexes known as kinetochores. In core-dinoflagellates kinetochore-like structures have

been identified by electron microscopy (Bhaud et al., 2000; Oakley & Dodge, 1976b). However, recently, Cuadrado et. al., (2019) proposed that, as kinetochores have not been defined in dinoflagellates, dinomitosis may occur in the absence of canonical kinetochores, by the attachment of the telomeric region of the chromosome to the nuclear envelope (Cuadrado et al., 2019).

However, this hypothesis is probably incorrect and the molecular composition of the dinoflagellates kinetochore is starting to be elucidated (Drinnenberg & Akiyoshi, 2017). A multi species study of the kinetochore in eukaryotes identified several kinetochore components in the genome of *S. minutum* (Hooff et al., 2017). Additionally, Yeung et al. (2000) showed SAC activation in *C. cohnii*, which in yeasts and animal cells, requires the presence of functional kinetochores.

Here, I analyzed the conservation of kinetochore components in three dinoflagellate species and found that functional complexes are entirely conserved, such as the Ndc80 complex (Ndc80-Spc25-Nuf2), which is required for microtubule binding, the SAC complex which is required to monitor kinetochore-spindle interaction, and the DNA binding part of the CCAN (CenpA). These results support the presence of a functional kinetochore in dinoflagellates defined by molecular components that interact on one side with microtubules and on the other side with centromeric DNA. A model of the dinoflagellate kinetochore is proposed in Figure 50. In this model, the components that are closer to the DNA (CCAN complex and the inner centromeric proteins) are associated with the nuclear membrane inside the nucleus; whereas the microtubule interacting proteins (Ndc80 and SAC components) are outside the nucleus. As the dinoflagellate kinetochore-like structure is observed inside of the nuclear membrane, either novel scaffolding proteins have been recruited to the dinoflagellate kinetochore to connect the DNA associated complex with the microtubule binding complex, or some of the conserved proteins have acquired domains that allow insertion into the nuclear membrane. Careful analysis of the domain composition of the identified proteins could provide clues to distinguish between these two hypotheses.

Ov-Apc13 and Ov-Apc15 were both down-regulated during division (evening and night samples), as well as the APC/C activator Ov-Cdh1. This is a puzzling result as APC/C^{Cdh1} is usually active from anaphase and during G1. However, this result is consistent with previous observations in NIH3T3 cells where Fizzy-related (Cdh1) mRNA was observed to be unstable from early mitosis (prometaphase) through to G1 and to accumulate again in S and G2 (Inbal et al., 1999), although the protein was shown to be present at constant levels throughout the cell cycle (Fang et al., 1998). No mechanism has been so far suggested to

explain this discrepancy and to understand the reason this gene is controlled at the level of transcription but not at the protein level.

Optimization of synchronization protocols will be extremely important to dissect the cell cycle function and regulation of all these components in *O.* cf. *ovata*.

4.3.4 Mitotic exit in *Ostreopsis* cf. *ovata*

Exit from mitosis is the final cell cycle transition that results in resetting of the interphase state and beginning of a new cell cycle. From a biochemical point of view this transition requires inactivation of Cdk through the degradation of its activator Cyclin-B. Additionally dephosphorylation and inactivation of Cdk mitotic targets is required to reset the interphase state.

A pathway to mitotic exit in *O.* cf. *ovata* is proposed based on the homologs of the yeast MEN pathway (Figure 51). In budding yeast, the activation and regulation of MEN relies on the activity of GTPases - Tem1 and Bfa1, Bub2, Kel1 and Cdc15 (Scarfone & Piatti, 2015), proteins associated with spindle poles and aster microtubules (Baro et al., 2017). Those proteins are all missing in *O.* cf. *ovata*, as well as all members of the FEAR complex except for Cdc5.

The lack of these regulatory proteins poses the question of what activates the phosphatase Cdc14 to control mitotic exit in dinoflagellates. One possibility is that Cdc14 is activated by the polo kinase Cdc5, which in turn is activated by Cdk1 (Rodriguez-Rodriguez et al., 2016). Activation of Cdc14 is also achieved through down-regulation of Pp2A-Cdc55 activity, which counteracts Cdk1-mediated phosphorylation. As Dbf2-Mob1 is inactivated by Pp2A-Cdc55, down-regulation of this phosphatase results in Mob1 activation and subsequent Cdc14 release from the nucleolus. Given the lack of Net1 and other components of the RENT, however, a different mechanism would have to maintain Cdc14 in the nucleolus and control Cdc14 activity during interphase.

A streamlined mechanism for mitotic exit however could be envisaged, whereby Cdc14 activation relies on Cdk1 activity. Active Cdc14 would in turn dephosphorylate Cdc20, allowing its binding to APC/C. APC/C^{Cdc20} mediated degradation of ClB4 would then in turn result in inactivation of Cdk1 and mitotic exit (Figure 51). The essential role of phosphatases in mitotic exit has been proven in many eukaryotes. However, whereas in yeasts inhibition of Cdc14 is sufficient to block mitotic exit, in vertebrates, mitotic exit is blocked only by treatment with okadaic acid a pan-phosphatase inhibitor, indicating the effect of several phosphatases (Vandré & Wills, 1992). Several isoforms of PP1 and PP2A-B56 have been

shown to be required for timely mitotic exit in animal cells and a complex regulatory mechanism has been dissected (Moura & Conde, 2019). So far, I focused on the yeast pathway, but identification of homologs of those phosphatases and their regulators and characterization of their patterns of expression in *O.* cf. *ovata* will provide further insights into the regulatory mechanisms involved in mitotic exit in dinoflagellates.

4.3.5 Basal body

Several basal body components, including structural proteins (the Flagellar Basal Body components Fbb 9, 11, 17, 18; the Bbs5 and the Cfap20); proteins related to the transport of components through the basal body as the IFT complex (Absalon et al., 2008); and proteins whose function is related with the cartwheel structure of the axoneme and the MTOC were identified in *O.* cf. *ovata*. Most of these proteins were down-regulated at night; except for the MTOC and axoneme-related proteins which were up-regulated during the evening and at night. In *Chlamydomonas reinhardtii*, mutations in MTOC proteins, such as Sas6, Centrin, Cep70, γ-tubulin, and ε-tubulin, result in defects in basal body duplication, which normally occurs during mitosis (Dutcher & O'Toole, 2016). As these proteins are also up-regulated during mitosis in *O.* cf. *ovata*, it could be suggested that in *O.* cf. *ovata* the basal body duplication occurs during mitosis; consistently, as basal body proteins, associated with the maturation of the basal body, are up-regulated during the day, basal body maturation probably occurs during interphase in *O.* cf. *ovata*.

4.3.6 Cytokinesis

I have shown that cytokinesis in *O.* cf. *ovata* relies on microtubules with dynamics that distinguish it both from the actomyosin based cytokinesis of animals and yeasts, but also from the microtubule-based cytokinesis of plants and protist parasites. Like dinomitosis, cytokinesis in dinoflagellates has been very poorly studied. Moreover, as most of the proteins usually implicated in cytokinesis have pleiotropic function, like basic cytoskeletal components, motors and proteins involved in vesicular trafficking, it is difficult to infer a molecular mechanism, which underlies this process. The identification of a microtubule rich structure at the site of cytokinesis and the lack of myosin II in *O.* cf. *ovata*, as in most bikonts (Richards & Cavalier-Smith, 2005), however allows to exclude an actomyosin based mechanism.

During cytokinesis plants assemble a microtubule-based phragmoplast, which forms in the center of the cell and then grows towards the poles (centrifugally). In *O.* cf. *ovata* instead,

I showed that the cytoskeletal plate forms from the dorsal area towards the ventral side. An MTOC is therefore likely to be localized at the dorsal side to initiate cytokinesis. This is different from green algae where the cytokinetic microtubule-based structure is assembled from the basal bodies. Notwithstanding these differences, up-regulation of γ-tubulin, which I observed in *O.* cf. *ovata*, could be required to sustain the high microtubule polymerization associated with mitosis and cytokinesis. Indeed, analysis of γ-tubulin distribution (chapter 3, Figure 36) supports this hypothesis of the presence of an MTOC at the dorsal side of the cell where the cytokinetic plate forms.

Membrane trafficking is involved in cytokinesis whether it is based on acto-myosin ring constriction or on microtubular structures, like phragomplasts (Gerien & Wu, 2018). The conservation of proteins related with vesicle trafficking in *O.* cf. *ovata* could extend the conservation of the membrane trafficking and membrane building during cytokinesis to dinoflagellates.

4.3.7 Transcriptional control of the cell cycle

The high number of transcripts differentially expressed at different phases of the bloom indicates an active transcriptional control during *O.* cf. *ovata* bloom, which is in contrast with the generally accepted idea that dinoflagellates have low transcriptional regulation (Bayer et al., 2012b; Wisecaver & Hackett, 2011). Indeed, microarray analysis of genes under circadian control showed 5%–20% of transcripts regulated in *Neurospora crassa*, 10% in *Arabidopsis thaliana*, 5%–10% in mouse and 30%–65% in the cyanobacteria *Synechococcus elongates* (Ito et al., 2009; Woelfle & Johnson, 2006), but only 3% in the dinoflagellate *Polyedra lunula*, and 0.7% in *Karenia brevis* (Roy & Morse, 2013). Similarly, no transcriptomic response toward phosphorus limitation was observed in *K. brevis* whereas changes were observed at the post-translational level (Akbar et al., 2018; Morey et al., 2011). In the same organism, the RNA expression of polyketide synthases, enzymes required for toxin production, did not change over the diel cycle despite evidence that toxin production was associated with certain diel phases or cell cycle stages in dinoflagellates (Van Dolah et al., 2007).

These and many other studies indicate low transcriptional activity in dinoflagellates and suggest that control of gene expression in dinoflagellates may be achieved instead by control of translation and/or protein stability. However, high transcriptional activity has been also observed in certain studies. Interestingly, similarly to what I observed with *O.* cf. *ovata*, meta-transcriptomic analysis of *Prorocentrum donghaiense* bloom (Yu et al., 2020) identified

5696 differentially expressed transcripts, when comparing night and day samples. Classification of these transcripts showed up-regulation mainly of phagotrophic and "environmental communication" genes, as well as nutrient uptake, energy metabolism and carbohydrate metabolism during the night. Interestingly, the authors also reported some transcripts related with mitosis, such as Cyclin-A, Cyclin-B, Cdk1 and transcripts indicated as "cell cycle checkpoint". APC/C 6, 10, 11 were instead up-regulated during the day.

Analysis of transcripts expressed at different phases of the growth curve in *Karenia brevis* culture, identified nearly 3000 differentially expressed transcripts, with the main categories associated with energy acquisition, ribosome biogenesis, gene expression, stress adaptation, calcium signaling, and putative brevetoxin biosynthesis (Morey et al., 2011).

The lack of specific studies that directly address transcriptional control at the genome wide level does not allow to conclude how much transcriptional regulation weights in dinoflagellates biology and in particular in the control of cell cycle. However, my study identified 6623 differentially expressed transcripts corresponding to roughly 30% of the annotated transcriptome, suggesting significant transcriptional control in *O.* cf. *ovata*. Among those 58 of the 209 transcripts (35,4%), encoding proteins involved in cell division, were differentially expressed. Gene ontology analysis of all differentially expressed transcripts will be useful to determine which biological processes are regulated at the transcriptional level at different cell cycle stages and at different phases of the bloom.

Interestingly, I observed very few differentially expressed genes between evening and night samples (241 transcripts), suggesting that the transition from pre-dividing to dividing cells is not subject to transcriptional control. A question which should be addressed however is whether predividing cells, identified by nuclear repositioning to the cell center, are in interphase or have already entered mitosis. The similar transcriptional landscape between the two populations suggests that pre-dividing cells have already committed to mitosis. Indeed, as already discussed, most mitotic cyclins are up-regulated in both evening and night samples, whereas early mitotic cyclin-A is only expressed in the evening samples, further supporting that predividing cells are early mitotic cells, possibly in prophase. It would be interesting to analyze whether specific markers of prophase associate with pre-dividing cells. Currently the difficulty lies with the identification of such markers as most events occurring in prophase, such as chromosome condensation, phosphorylation of histone H3, nuclear envelope breakdown, centrosome separation (Hans & Dimitrov, 2001) and so on do not take place in dinoflagellates. As Cdk1 activation is associated with mitotic commitment, a first concrete

indication of the cell cycle stage of pre-dividing cells could be obtained by comparing levels of histone H1 kinase activity in interphase, pre-dividing and dividing cells.

This preliminary study has uncovered several transcripts, which are potentially associated with cell proliferation. Aside from improving our understanding of the biology of dinoflagellates, identification of differentially expressed genes associated with cell division and cell proliferation could provide useful molecular markers to detect and quantify bloom development, overcoming the tedious and time-consuming microscopic visual analysis currently used to monitor *Ostreopsis* blooms.

4.4 Material and methods

For the bioinformatic analysis included in this thesis, I used the server from the Laboratoire de Biologie du Développement de Villefranche sur mer, I4 service: http://lbdv.obs-vlfr.fr/fr/recherche/services_a_la_recherche/bio_informatique.html; as well as ABIMS cluster, using the bioinformatics infrastructure from the Station Biologique de Roscoff: http://abims.sb-roscoff.fr/ and https://crimson.oca.eu/fr/mesocentre-sigamm.

The assembly of the transcriptome was performed with the help of the group 'Evolution de génomes et de protéines animales' at the Laboratoire de Biologie du Développement de Villefranche (LBDV/UMR7009). I did the rest of the analysis.

4.4.1 Sample collection

Total RNA extracted from the strain MCCV-054 was used to produce the reference transcriptome. 150 ml of cells grown in L1 media were used to extract RNA during the lag-phase (day 6), the proliferative phase (day 12) and the stationary phase (day 18).

The samples used for the meta-transcriptome were collected during the 2019 bloom: proliferative phase, the 26th of June at 9:00 am; peak phase, 3rd of July at 9:00 am; senescence the 12th of July at 9:00 am; and end of the bloom the 17th of July at 9:00 am. These samples were collected using an optimized sampling method which allows to sample large number of cells, described in Jauzein, et al (2017). Briefly, a device containing an artificial substrate (a net) was placed in the water column (Figure 59) for 24 hours. Then the artificial substrate was placed inside a 2-liter bottle filled with sea water to recover the collected cells (Jauzein et al., 2017).

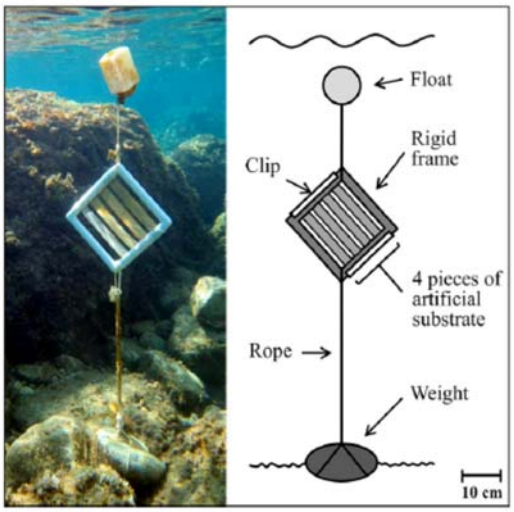

Figure 59. Set-up used for deployment of artificial substrates in the field.
A picture showing the deployment of artificial substrates during an *Ostreopsis* bloom in Villefranche Bay (France) is given on the left side. This picture shows the incubation of four types of substrates, characterized by four different porosities (from 50 µm to 1.15 mm), that were hold on a unique rigid frame. It is schematized on the right side in order to detail each piece of the assembly. Image from Jauzein, et al, 2016.

At the peak of the bloom (04.07.19), samples were collected at three different times of the day at 12:00, 20:00 and 4:00 am. In this case, 10-15 g of macroalgae were placed in 2-liter bottles, filled with sea water and immediately transported to the laboratory. From each bottle, 10 ml were fixed in PFA 2% (Sigma) at 4ºC for at least 24 hours for cell cycle characterization by Hoechst 33342 as described in chapter 2. The rest of the cells were used for RNA extraction.

No reagents were added to preserve the quality of the RNA.

4.4.2 RNA extraction

Cell pellets were obtained by filtration through 5 µm membrane filters of mixed cellulose esters (Millipore) using a manifold apparatus.

Cells were collected from filter and placed in 1ml of TRI-reagent (Sigma-Aldrich) and incubated on ice for five minutes. Glass beads (sephadex g-25, Sigma Aldrich), ~ 3 g, were added to each tube. Cells were broken by beating in a 220 V bead beater at 4000 rpm for 40 s. RNA was then extracted using a RiboPure^{TM} (Ambion) kit following the manufacturer's instructions.

Any residual DNA was removed by treatment with DNase I (Q1 DNAse, Promega) for 1h at 37 °C (2 units per sample) followed by purification with the RNeasy minElute Cleanup kit (Qiagen).

RNA was stored at -80°C until further analyses. RNA purity, quantity and integrity were assessed for each sample using a Nanodrop ND-1000 and 2100 Bioanalyser.

4.4.3 Generation of the reference transcriptome and annotation

RNA samples were sent to BGI-Tech, China to produce the libraries using DNBSEQ™ technology platforms generating 100 base pair (bp) paired end reads.

After sequencing, reads were assembled *de novo* with Trinity v. 2.4.0 (Grabherr et al., 2011) using default parameters. Contigs assemblies from the nine samples of the culture cells were pooled together to generate the reference transcriptome.

The group 'Genome and protein evolution in animals' searched all the *Ostreopsis* sequences against the NCBI-NR database using diamond blast, saving the best hit. These sequences were then cleaned from non-Dinophyceae sequences by querying and extracting the NCBI best hits.

The transcriptome was translated to protein sequences using open reading frames (ORF's) of a minimum of 90 amino acids using Transdecoder v. 3.0.1 (https://github.com/TransDecoder/TransDecoder/wiki; last accessed July 2019)

PantherScore2,1.pl script with the panther hidden Markov model library was used to annotate the transcriptome. This script launches hmmsearch against all HMMs in the panther database and chooses the correct result based on panthers scoring model. The PANTHER14.1 database was used to extract the results.

The panther database and scoring tool can be downloaded from: http://pantherdb.org/downloads/index.jsp

Meta-transcriptome

As for the reference transcriptome, library generation and sequencing were performed by BGI Tech, China.

After sequencing, the abundances of *O. cf. ovata* transcripts in the metatranscriptome were quantified using kallisto, which allows to use a pseudoalignment mapped with the reference transcritpome (Bray et al., 2016), resulting in counts of transcripts that belong to *O.* cf. *ovata*. Raw read counts were transformed to FPKM (fragments per kilobase of exon per million fragments mapped). The process was performed launching a Unix command using the server of the institute:

```
for i in $(ls -1 ../../common/19metatranscriptomes/Clean/);do kallisto quant -i ../../common/Richard_data/ostreopsis/ostreopsis_ref_transcriptome.idx -o 19metatranscriptomes_kallisto_$i -t 40 -b 100
```

../../common/19metatranscriptomes/Clean/$i/*gz 1>19_meta_stdout_$i 2>19_meta_stderr_$i ;done

I used the R package Sleuth to perform the gene expression analysis using a False Discovery Rate, FDR ≤ 0.01.

4.4.4 Reciprocal best hits and reference lists

I used the script described by R. Copley in: https://rcply.github.io/rbh_orthologs.html

This strategy is based on the premise that, when two sets of sequences (i.e. proteomes) are compared, homologous pair of sequences should be closer to each other than they are to anything else. So, 2 database searches are required to check that this relationship holds:

- Protein X (from genome B) vs (all proteins from genome A) gives best hit Protein Y.
- Protein Y (from genome A) vs (all proteins from genome B) gives best hit Protein X

Then, I used 'ssearch' from the FASTA package which retrieves files in which the first column of output contains the identifier of the searched 'query' sequence and the second column, the database hit. Using the commands below, the '-m 8' option specifies this sort of tabular output; '-b 1' specifies just the best hit; '-E 0.1' is an E-value threshold to be safe against really spurious hits that happen to be also be 'reciprocal'. The 2nd command below, inverts the order of the 'query' and 'database' protein sets, turning the 'query' of the first command into the 'database' and the 'database' into the 'query'. The output files were named differently to keep the track later.

```
ssearch36 -m 8 -b 1 -E 0.1 proteins_a proteins_b > proteins_a_vs_proteins_b_ssearch.txt
ssearch36 -m 8 -b 1 -E 0.1 proteins_b proteins_a > proteins_b_vs_proteins_a_ssearch.txt
```

From the first file (a vs b), I extracted just the identifiers, which are in the first two columns, and sort them in alphabetical order:

```
awk '{print $1,$2 }' proteins_a_vs_proteins_b_ssearch.txt | sort -u > a_vs_b.txt
```

For the 2nd file (b vs a), I inverted the identifiers so that I can compare the two files later. This is done by inverting the field specifiers in the awk command $2 and $1:

```
awk '{ print $2,$1 }' proteins_b_vs_proteins_a_ssearch.txt | sort -u > b_vs_a.txt
```

Each line consists of a pair of sequences. Then, it is a matter to find the lines that are in common between the two files. To do this, I used unix:

```
comm -12 a_vs_b.txt b_vs_a.txt > rbh_ortholog_pairs.txt
```

The -12 switch suppresses lines that are only found in file 1 or 2.
The file 'rbh_ortholog_pairs.txt' should now contain a list of reciprocal best hits, which are often used as an approximate set of homologs.

The proteomes were obtained from:
Saccharomyces cerevisiae obtained from uniprot.org; *Plasmodium falciparum* (obtained from plasmodb.org) and *Chlamydomonas reinhardtii* (obtained from plantgdb.org)

Chapter 5

General discussion and future prospective

The increase in the frequency and distribution of toxic bloom events has pushed scientific interest towards understanding the underlying biological processes responsible for the increase in cell population associated with algal blooms. Although cell migration has been recognized as a contributing factor to local increase in cell concentration (Burkholder et al., 2006), the clustering of unicellular organisms alone is unlikely to produce massive tides without associated increase in cell division. *Ostreopsis* species are among the most common species causing HABs in tropical and subtropical areas (Parsons et al., 2012; Rhodes, 2011) and *O.* cf. *ovata* which undergoes yearly seasonal blooms in the Bay of Villefranche, near the Institute de la Mer where I performed my PhD, provides a perfect case study to determine the contribution of cell proliferation to HABs *in situ* and to dissect the underlying molecular mechanisms, given that cell cultures have been established in the laboratory.

Analysis of the occurrence of *O.* cf. *ovata* cell proliferation during the bloom, described in Chapter 2, confirmed that, in the wild, cell division occurs exclusively at night. During the proliferative phase only 30% of cells divided every night, allowing the inference that the whole population doubles every 3 days, which is consistent with the net growth rate measured for *O.* cf. *ovata* during the bloom. It is generally accepted that this low-rate of division is attributable to the dinoflagellate low photosynthetic metabolism (Tang, 1996). However, other factors may contribute to the long cell cycle duration in these organisms. As dinoflagellate have typically large genomes, one factor that could influence cell cycle duration is the time required to duplicate large quantities of DNA (Gornik et al., 2019). Indeed, continuous DNA synthesis was observed in some species of dinoflagellates (Cato et al., 2019a; Filfilan & Sigee, 1977; Galleron & Durrand, 1979), suggesting a very prolonged S-phase.

Despite this peculiarity and their extremely divergent nuclear organization, dinoflagellates are thought to follow the typical eukaryote cell cycle with G1, S, G2 and M phases. Recent studies also showed that master regulators of the cell cycle, such as cyclins and CDKs, are conserved in dinoflagellates, although their function remains mostly speculative and supported only by analogies with opisthokonts (Morse et al., 2016b). Yet, the role of analogies in science has been broadly used as a heuristic approach to generate testable hypothesis about unknown mechanisms. It is in this light, that during my PhD work, I used

this approach, to determine whether genes and underlying mechanisms known to control cell cycle progression, mitosis and cytokinesis in established model organisms could be identified in *O.* cf. *ovata* and could be used to understand mitotic control in dinoflagellates. Although I have only begun to unveil the complex network of regulatory mechanisms that controls cell cycle and mitosis in dinoflagellates, the confirmation that *O.* cf. *ovata* divides during the night and the morphological characterization of cells in division allowed me to correlate the expression of genes potentially involved in cell cycle regulation with specific transitions in the cycle.

By integrating results obtained from the cytological characterization of the vegetative cycle of *O.* cf. *ovata* presented in Chapter 3 with the transcriptomic and metatranscriptomic analysis presented in Chapter 4, I can propose a first model of the mitotic cycle in this dinoflagellate. In this hypothetical model interphase, recognized morphologically by the basal-basal position of the nucleus, is proposed regulated by four cyclins, Ov-ClB1, 2, 6 and Ov-CycA, in complexes with two CDKs, Ov-Cdk1 and Ov-Pho85, and by the transcriptional regulator Ov-Whi5; these proteins control progression through S-phase, and regulate transcription and cell growth.

During interphase, the ventral microtubule bundle grows towards the nucleus and re-positions it to the middle of the cell where M-phase takes place. The central re-positioning of the nucleus was initially identified as a predividing stage and was not associated with mitosis (Bravo et al., 2012). However, the identification of mitotic specific proteins in metatrascriptomic samples enriched in pre-dividing cells suggests that the pre-dividing morphotype corresponds instead to an early phase of mitosis and that re-positioning of the nucleus may be linked with mitotic commitment. Further studies using specific mitotic markers will allow to determine when cells commit to mitosis and how different cell cycle phases are related to the different morphotypes. However, given the particular characteristics of the dinokaryon and of dinomitosis, most events which characterize mitotic entry in other eukaryotes, such as chromosome condensation, centrosome separation and histone H3 phosphorylation (Cooper, 2000), just to mention a few, do not take place in dinoflagellates and therefore the first challenge will be to identify specific markers to define the different phases of mitosis.

Following DNA replication, Ov-ClB4 and Ov-Cdk1 are suggested to trigger mitotic entry and mitotic progression. During mitosis chromosomes are segregated by microtubules that are attached on one side to acentriolar centrosomes and on the other side to kinetochores. The kinetochore of *O.* cf. *ovata* has never been imaged. However by extension of electron

microscopy studies in other species, such as *C. cohnii* (Kubai & Ris, 1969; Eric Perret et al., 1991), it is proposed that the kinetochore in *O.* cf. *ovata* is embedded in the nuclear membrane, linking the spindle microtubules with the chromosomes across the nuclear envelope. Analysis of the reference transcriptome of *O.* cf. *ovata* confirmed the presence of several kinetochore components. As the goal of kinetochores is to associate chromosomes and spindle microtubules, it is interesting that most of the Ov-Ndc80 complex, which is required for interaction with spindle microtubules, is conserved in *O.* cf. *ovata*. Similarly CENP-A, which provides the epigenetic mark for kinetochore assembly (Black & Cleveland, 2011) is also present. More difficult will be to identify intermediate proteins that link the two functional complexes across the nuclear envelope.

Remarkably, most SAC components were also identified suggesting that, as for yeast and animal cell chromosome segregation may be controlled by this checkpoint signaling pathway. Berdalet et al., (2017) showed that *O.* cf. *ovata* cells grown under constant agitation, stop dividing earlier than control cells grown in stationary conditions, which supports the presence of an active SAC resulting in an arrest in mitosis. However, an alternative explanation could be considered whereby lack of a functional SAC would result in progression through cell division without correct chromosome segregation, producing aneuplod cells with reduced viability. My preliminary functional studies using microtubule depolymerizing drugs and agitation support this second hypothesis that contrary to what suggested in other dinoflagellates (Yeung et al., 2000), SAC is not functional in *O.* cf. *ovata*.

A functional SAC is absent also in other organisms such as in *Trypanosoma brucei* (Akiyoshi & Gull, 2013; Ploubidou et al., 1999) and in *Giardia intestinalis* (Markova et al., 2016), which in the absence of mitotic spindles divide without any delay and even replicate their DNA before dying. Differently from *O.* cf. *ovata*, these organisms were shown to lack most SAC components, with the exception of Mad2. Experiments carried out in *Trypanosoma brucei* however showed that Mad2 associates with the basal body and suggested that the original function of this protein might be in control of basal body segregation and not in mitotic checkpoint control (Akiyoshi & Gull, 2013). This ancestral function may be conserved in *O.* cf. *ovata* and further characterization of the subcellular localization of SAC proteins will shed light on the function of SAC proteins in dinoflagellates.

Following chromosome segregation, a microtubule based cytokinetic plate forms and divides the cell along the longitudinal axis. The absence of an actomyosin ring is not surprising, as myosin-II is absent in most unikonts (Richards & Cavalier-Smith, 2005) and

here I have confirmed its absence in *O.* cf. *ovata*. However, other aspects of cytokinesis observed in this dinoflagellate were of interest.

Differently from most other previously studied eukaryotes the axis of cytokinesis aligns with the long axis of the cell. Moreover, differently from the microtubule-based cytokinesis observed in plants, where the microtubule based phragmoplast forms from the cell center towards the cell wall, in *O.* cf. *ovata* the cytokinetic plate appears to form asymmetrically from the dorsal side. This is similar to what was observed in *Trypanosoma brucei* where cytokinesis occurs unidirectionally from the anterior end of the cell along the long axis of the cell (Kohl et al., 1999; Vaughan & Gull, 2003). In *Trypanosoma brucei*, the CPC have been observed to relocalize from the central spindle to the anterior tip of the cell to initiate cytokinesis (Li et al., 2008). As I identified several components of the CPC in *O.* cf. *ovata* (Ov-Aurora, Ov-Borealin and Ov-Incenp), it will be interesting to analyze their localization in mitotic and cytokinetic cells to determine their potential implication in positioning the site of cytokinesis in *O.* cf. *ovata*.

Finally, treatment with the microtubule depolymerizing drug colchicine results in deviation of the plane of cell division from the long axis, suggesting that microtubules are required for proper positioning of the cell division site. Moreover as mis-oriented cytokinesis occurs within few hours of colchicine treatment this experiment suggests that the site of cell division in *O.* cf. *ovata* is not selected in G1 as in budding yeast, but either in late G2 as in fission yeast, or during mitosis as in animals.

A major difficulty to the use of *O.* cf. *ovata* as a model to study cell cycle control in dinoflagellates, is the lack of protocols to synchronize cells in culture. To overcome this problem I have used wild samples which I showed to divide exclusively at night, providing a source of semi-syncronized population. However, the seasonality of the bloom does not provide a constant source of cells and limits functional studies to a brief and intense period of the year. Notwithstanding the difficulties, synchronized cultures would allow to obtain a more detailed characterization of the mitotic phases. For example, it would be interesting to determine if the central positioning of the nucleus, before the spindle is formed, correlates with active Ov-Cdk1, or with an increase in Ov-cyclin-A which peaks in the metatranscriptomic analysis only during the evening, period of pre-dividing enrichment. Moving on from this initial description, testing of different hypotheses will soon encounter technical difficulties. It is hard to imagine how cell cycle studies could be done without the optimization of synchronization and transformation protocols. Successful synchronization

protocols exist for *C. cohnii* (Wong & Whiteley, 1996). This protocol is based on differences in size and motility between cells at different cell cycle stages, with G1 cells being small and non motile. Based on my observations a similar protocol cannot be applied to *O.* cf. *ovata*, as I did not observe loss of flagella at any stage of the cycle, not even in mitosis. An alternative procedure is the one used to synchronize phototrophic algae which has been successfully used in *Alexandrium minutum* (Figueroa et al., 2007) and *Prorocentrum donghaiense* (D.-Z. Wang et al., 2013). This method is based on the exposure of cells to light–dark cycles; the culture cells are incubated in darkness during 48h and then returned to the normal light:dark cycle (Figueroa et al., 2007). The group of Dr Lemée has tried this method, but unfortunately cells either died or formed cysts that did not undergo excystment. A third possibility could be the use of cell cycle inhibitors as nocodazole or colchicine, which depolymerize microtubules and in yeast and animal arrest cells in mitosis due to activation of the SAC. However, preliminary tests showed that nocodazole does not arrest cells in mitosis, possibly because it always precipitates when added in the culture media and becomes trapped in the mucus, visible as a white and viscous material. Colchicine instead dissolved in the medium and successfully depolymerized microtubules, but it did not efficiently arrest cell cycle progression.

The use of semi-synchronous cells is still an alternative to explore the dinoflagellate cell cycle, as it was shown in *S. minutum* (Cato et al., 2019a) and as I showed in this thesis. The correlation between different phases of the cell cycle with the expression of proteins is useful to generate predictions but also to identify markers to monitor *O.* cf. *ovata* HABs. In the case of *O.* cf. *ovata*, I have proposed that Ov-Cdk1 or cyclins as Ov-ClB4 and Ov-CycA could be related with mitosis. If confirmed, considering that mitosis is the main process responsible of *O.* cf. *ovata* blooms, quantifying the level of expression of these proteins during several nights at different phases of the bloom would reveal whether thresholds of expression are associated with changes in proliferation during the bloom. Those transitions and their associated markers could be then used to monitor bloom development *in situ*.

This could be complemented with other proteins whose expression correlates with other phases of the bloom, as it could be the case of apoptotic markers during the senescence of HABs. Identification of such molecular markers associated with different cell cycle and bloom phases, could be used as strategy to monitor bloom development and to reduce the economic losses due to *O.* cf. *ovata* HABs.

References

Absalon, S., Blisnick, T., Kohl, L., Toutirais, G., Doré, G., Julkowska, D., Tavenet, A., & Bastin, P. (2008). Intraflagellar Transport and Functional Analysis of Genes Required for Flagellum Formation in Trypanosomes. *Molecular Biology of the Cell*, *19*(3), 929–944. https://doi.org/10.1091/mbc.e07-08-0749

Accoroni, S., Colombo, F., Pichierri, S., Romagnoli, T., Marini, M., Battocchi, C., Penna, A., & Totti, C. (2012). Ecology of *Ostreopsis* cf. *Ovata* Blooms in the Northwestern Adriatic Sea. *Cryptogamie, Algologie*, *33*(2), 191–198. https://doi.org/10.7872/crya.v33.iss2.2011.191

Accoroni, S., Glibert, P. M., Pichierri, S., Romagnoli, T., Marini, M., & Totti, C. (2015). A conceptual model of annual Ostreopsis cf. Ovata blooms in the northern Adriatic Sea based on the synergic effects of hydrodynamics, temperature, and the N:P ratio of water column nutrients. *Harmful Algae*, *45*, 14–25.

Accoroni, S., Percopo, I., Cerino, F., Romagnoli, T., Pichierri, S., Perrone, C., & Totti, C. (2015). Allelopathic interactions between the HAB dinoflagellate Ostreopsis cf. Ovata and macroalgae. *Harmful Algae*, *49*, 147–155. https://doi.org/10.1016/j.hal.2015.08.007

Accoroni, S., Romagnoli, T., Colombo, F., Pennesi, C., Di Camillo, C. G., Marini, M., Battocchi, C., Ciminiello, P., Dell'Aversano, C., Dello Iacovo, E., Fattorusso, E., Tartaglione, L., Penna, A., & Totti, C. (2011). Ostreopsis cf. ovata bloom in the northern Adriatic Sea during summer 2009: Ecology, molecular characterization and toxin profile. *Marine Pollution Bulletin*, *62*(11), 2512–2519. https://doi.org/10.1016/j.marpolbul.2011.08.003

Accoroni, S., Romagnoli, T., Penna, A., Capellacci, S., Ciminiello, P., Dell'Aversano, C., Tartaglione, L., Abboud-Abi Saab, M., Giussani, V., Asnaghi, V., Chiantore, M., & Totti, C. (2016). *Ostreopsis fattorussoi* sp. Nov. (Dinophyceae), a new benthic toxic *Ostreopsis* species from the eastern Mediterranean Sea. *Journal of Phycology*, *52*(6), 1064–1084. https://doi.org/10.1111/jpy.12464

Accoroni, S., Romagnoli, T., Pichierri, S., & Totti, C. (2014). New insights on the life cycle stages of the toxic benthic dinoflagellate Ostreopsis cf. Ovata. *Harmful Algae*, *34*, 7–16. https://doi.org/10.1016/j.hal.2014.02.003

Akamatsu, M., Berro, J., Pu, K.-M., Tebbs, I. R., & Pollard, T. D. (2014). Cytokinetic nodes in fission yeast arise from two distinct types of nodes that merge during interphase. *Journal of Cell Biology*, *204*(6), 977–988. https://doi.org/10.1083/jcb.201307174

Akbar, M., Ahmad, A., Usup, G., & Bunawan, H. (2018). RNA-Seq as an Emerging Tool for Marine Dinoflagellate Transcriptome Analysis: Process and Challenges. *Processes*, *6*(1), 5. https://doi.org/10.3390/pr6010005

Akiyoshi, B., & Gull, K. (2013). Evolutionary cell biology of chromosome segregation: Insights from trypanosomes. *Open Biology*, *3*(5), 130023. https://doi.org/10.1098/rsob.130023

Amzil, Z., Sibat, M., Chomerat, N., Grossel, H., Marco-Miralles, F., Lemee, R., Nezan, E., & Sechet, V. (2012). Ovatoxin-a and Palytoxin Accumulation in Seafood in Relation to Ostreopsis cf. Ovata Blooms on the French Mediterranean Coast. *Marine Drugs*, *10*(12), 477–496. https://doi.org/10.3390/md10020477

Anderson, D.M., & Morel, F. M. M. (1979). The seeding of two red tide blooms by the germination of benthic Gonyaulax tamarensis hypnocysts. *Estuarine and Coastal Marine Science*, *8*(3), 279–293. https://doi.org/10.1016/0302-3524(79)90098-7

Anderson, Donald M., Cembella, A. D., & Hallegraeff, G. M. (2012). Progress in Understanding Harmful Algal Blooms: Paradigm Shifts and New Technologies for Research, Monitoring, and Management. *Annual Review of Marine Science*, *4*(1), 143–176. https://doi.org/10.1146/annurev-marine-120308-081121

Anderson, Donald M., Glibert, P. M., & Burkholder, J. M. (2002). Harmful algal blooms and eutrophication: Nutrient sources, composition, and consequences. *Estuaries*, *25*(4), 704–726. https://doi.org/10.1007/BF02804901

Arias, A., Saiz, E., & Calbet, A. (2020). Towards an Understanding of Diel Feeding Rhythms in Marine Protists: Consequences of Light Manipulation. *Microbial Ecology*, *79*(1), 64–72. https://doi.org/10.1007/s00248-019-01390-y

Atherton-Fessler, S., Liu, F., Gabrielli, B., Lee, M. S., Peng, C. Y., & Piwnica-Worms, H. (1994). Cell cycle regulation of the p34cdc2 inhibitory kinases. *Molecular Biology of the Cell*, *5*(9), 989–1001. https://doi.org/10.1091/mbc.5.9.989

Ausseil, Jérôme, Soyer-Gobillard, M.-O., Géraud, M.-L., Bhaud, Y., Baines, I., Preston, T., & Moreau, H. (1999). Characterization of p80, a Novel Nuclear and Cytoplasmic Protein in Dinoflagellates. *Protist*, *150*(2), 197–211. https://doi.org/10.1016/S1434-4610(99)70022-2

Ausseil, Jérome, Soyer-Gobillard, M.-O., Géraud, M.-L., Bhaud, Y., Perret, E., Barbier, M., Albert, M., Plaisance, L., & Moreau, H. (2000). Dinoflagellate centrosome: Associated proteins old and new. *European Journal of Protistology*, *36*(1), 1–19. https://doi.org/10.1016/S0932-4739(00)80017-6

Bachvaroff, T. R., Gornik, S. G., Concepcion, G. T., Waller, R. F., Mendez, G. S., Lippmeier, J. C., & Delwiche, C. F. (2014). Dinoflagellate phylogeny revisited: Using ribosomal proteins to resolve deep branching dinoflagellate clades. *Molecular Phylogenetics and Evolution*, *70*, 314–322. https://doi.org/10.1016/j.ympev.2013.10.007

Bachvaroff, T. R., & Place, A. R. (2008). From Stop to Start: Tandem Gene Arrangement, Copy Number and Trans-Splicing Sites in the Dinoflagellate Amphidinium carterae. *PLoS ONE*, *3*(8), e2929. https://doi.org/10.1371/journal.pone.0002929

Balasubramanian, M. K., Bi, E., & Glotzer, M. (2004). Comparative Analysis of Cytokinesis in Budding Yeast, Fission Yeast and Animal Cells. *Current Biology*, *14*(18), R806–R818. https://doi.org/10.1016/j.cub.2004.09.022

Ballantine, D. L., Tosteson, T. R., & Bardales, A. T. (1988). Population dynamics and toxicity of natural populations of benthic dinoflagellates in southwestern Puerto Rico. *Journal of Experimental Marine Biology and Ecology*, *119*(3), 201–212. https://doi.org/10.1016/0022-0981(88)90193-1

Banse, K. (1982). Cell volumes, maximal growth rates of unicellular algae and ciliates, and the role of ciliates in the marine pelagial1,2: Growth of algae and ciliates. *Limnology and Oceanography*, *27*(6), 1059–1071. https://doi.org/10.4319/lo.1982.27.6.1059

Barbier, M., Leighfield, T. A., Soyer-Gobillard, M.-O., & Van Dolah, F. M. (2003). Permanent expression of a cyclin B homologue in the cell cycle of the dinoflagellate Karenia brevis. *The Journal of Eukaryotic Microbiology*, *50*(2), 123–131. https://doi.org/10.1111/j.1550-7408.2003.tb00246.x

Barisic, M., Silva e Sousa, R., Tripathy, S. K., Magiera, M. M., Zaytsev, A. V., Pereira, A. L., Janke, C., Grishchuk, E. L., & Maiato, H. (2015). Microtubule detyrosination guides chromosomes during mitosis. *Science*, *348*(6236), 799–803. https://doi.org/10.1126/science.aaa5175

Barlow, S. B., & Triemer, R. E. (1988). The mitotic apparatus in the dinoflagellateAmphidinium carterae. *Protoplasma*, *145*(1), 16–26. https://doi.org/10.1007/BF01323252

Barnum, K. J., & O'Connell, M. J. (2014). Cell Cycle Regulation by Checkpoints. In E. Noguchi & M. C. Gadaleta (Eds.), *Cell Cycle Control* (Vol. 1170, pp. 29–40). Springer New York. https://doi.org/10.1007/978-1-4939-0888-2_2

Baro, B., Queralt, E., & Monje-Casas, F. (2017). Regulation of Mitotic Exit in Saccharomyces cerevisiae. In F. Monje-Casas & E. Queralt (Eds.), *The Mitotic Exit Network* (Vol. 1505, pp. 3–17). Springer New York. https://doi.org/10.1007/978-1-4939-6502-1_1

Bathe, M., & Chang, F. (2010). Cytokinesis and the contractile ring in fission yeast: Towards a systems-level understanding. *Trends in Microbiology*, *18*(1), 38–45. https://doi.org/10.1016/j.tim.2009.10.002

Bayer, T., Aranda, M., Sunagawa, S., Yum, L. K., DeSalvo, M. K., Lindquist, E., Coffroth, M. A., Voolstra, C. R., & Medina, M. (2012a). Symbiodinium Transcriptomes: Genome Insights into the Dinoflagellate Symbionts of Reef-Building Corals. *PLoS ONE*, *7*(4), e35269. https://doi.org/10.1371/journal.pone.0035269

Bayer, T., Aranda, M., Sunagawa, S., Yum, L. K., DeSalvo, M. K., Lindquist, E., Coffroth, M. A., Voolstra, C. R., & Medina, M. (2012b). Symbiodinium Transcriptomes: Genome Insights into the Dinoflagellate Symbionts of Reef-Building Corals. *PLoS ONE*, *7*(4), e35269. https://doi.org/10.1371/journal.pone.0035269

Berdalet, E. (1992). Effects of turbulence on the marine dinoflagellate *Gymnodinium nelsonii*. *Journal of Phycology*, *28*(3), 267–272. https://doi.org/10.1111/j.0022-3646.1992.00267.x

Berdalet, E., Tester, P., Chinain, M., Fraga, S., Lemée, R., Litaker, W., Penna, A., Usup, G., Vila, M., & Zingone, A. (2017). Harmful Algal Blooms in Benthic Systems: Recent Progress and Future Research. *Oceanography*, *30*(1), 36–45. https://doi.org/10.5670/oceanog.2017.108

Berdalet, E., Fleming, L. E., Gowen, R., Davidson, K., Hess, P., Backer, L. C., Moore, S. K., Hoagland, P., & Enevoldsen, H. (2016). Marine harmful algal blooms, human health and wellbeing: Challenges and opportunities in the 21st century. *Journal of the Marine Biological Association of the United Kingdom*, *96*(1), 61–91. https://doi.org/10.1017/S0025315415001733

Berdalet, E., Peters, F., Koumandou, V. L., Roldán, C., Guadayol, Ò., & Estrada, M. (2007). Species-specific physiological response of dinoflagellates to quantified small-scale turbulence [1]. *Journal of Phycology*, *43*(5), 965–977. https://doi.org/10.1111/j.1529-8817.2007.00392.x

Berdieva, M., Pozdnyakov, I., Matantseva, O., Knyazev, N., & Skarlato, S. (2018). Actin as a cytoskeletal basis for cell architecture and a protein essential for ecdysis in *Prorocentrum minimum* (Dinophyceae, Prorocentrales): Actin cytoskeleton in *P. minimum* cell. *Phycological Research*, *66*(2), 127–136. https://doi.org/10.1111/pre.12214

Bertomeu, T., & Morse, D. (2004). Isolation of a dinoflagellate mitotic cyclin by functional complementation in yeast. *Biochemical and Biophysical Research Communications*, *323*(4), 1172–1183. https://doi.org/10.1016/j.bbrc.2004.09.008

Bertomeu, T., Rivoal, J., & Morse, D. (2007). A dinoflagellate CDK5-like cyclin-dependent kinase. *Biology of the Cell*, *99*(9), 531–540. https://doi.org/10.1042/BC20070018

Bertoni, G. (2018). Cell Cycle Regulation by Chlamydomonas Cyclin-Dependent Protein Kinases. *The Plant Cell*, *30*(2), 271–271. https://doi.org/10.1105/tpc.18.00103

Bhaud, Y., Guillebault, D., Lennon, J., Defacque, H., Soyer-Gobillard, M. O., & Moreau, H. (2000). Morphology and behaviour of dinoflagellate chromosomes during the cell cycle and mitosis. *Journal of Cell Science*, *113*(7), 1231–1239.

Bhaud, YVONNE, Salmon, J.-M., & SOYER-GOBILLARD, M.-O. (1991). The Complex Cell Cycle of the Dinoflagellate Protoctist Crypthecodinium Cohnii as Studied In Vivo and by Cytofluorimetry. *Journal of Cell Science*, *100*(3), 675.

Bianco I, Sangiorgi V, Penna A, Guerrini F, Pistocchi R, Zaottini E, Congestri R, (2007). *Ostreopsis ovata* in benthic aggregates along the Latium Coast (middle Tyrrhenian Sea), p. 29 (abstract). In: Proc. Int. Symp. on Algal Toxins, Trieste, Italy.

Bisova, K., Krylov, D. M., & Umen, J. G. (2005). Genome-Wide Annotation and Expression Profiling of Cell Cycle Regulatory Genes in *Chlamydomonas reinhardtii*. *Plant Physiology*, *137*(2), 475–491. https://doi.org/10.1104/pp.104.054155

Black, B. E., & Cleveland, D. W. (2011). Epigenetic Centromere Propagation and the Nature of CENP-A Nucleosomes. *Cell*, *144*(4), 471–479. https://doi.org/10.1016/j.cell.2011.02.002

Blanfune, A., Cohu, S., Mangialajo, L., Lemée, R., & Thibaut, T. (2012). Preliminary Assessments of the Impact of *Ostreopsis* cf. *Ovata* (Dinophyceae) Development on Macroinvertebrates in the North Western Mediterranean

Sea. *Cryptogamie, Algologie*, *33*(2), 129–136. https://doi.org/10.7872/crya.v33.iss2.2011.129

Bloodgood, R. A. (2009). From Central to Rudimentary to Primary: The History of an Underappreciated Organelle Whose Time Has Come.The Primary Cilium. In *Methods in Cell Biology* (Vol. 94, pp. 2–52). Elsevier. https://doi.org/10.1016/S0091-679X(08)94001-2

Bohrmann B, Hainder M, Kellenberger E: (1993). Concentration evaluation of chromatin in unstained resinembedded sections by means of low-dose ratiocontrast imaging in STEM. *Ultramicroscopy* 49: 235–251.

Boudolf, V., Inze, D., & Deveylder, L. (2006). What if higher plants lack a CDC25 phosphatase? *Trends in Plant Science*, *11*(10), 474–479. https://doi.org/10.1016/j.tplants.2006.08.009

Bravo, I., & Figueroa, R. I. (2014). Towards an Ecological Understanding of Dinoflagellate Cyst Functions. *Microorganisms*, *2*(1), 11–32. https://doi.org/10.3390/microorganisms2010011

Bravo, I., Isabel Figueroa, R., Garcés, E., Fraga, S., & Massanet, A. (2010). The intricacies of dinoflagellate pellicle cysts: The example of Alexandrium minutum cysts from a bloom-recurrent area (Bay of Baiona, NW Spain). *Deep Sea Research Part II: Topical Studies in Oceanography*, *57*(3–4), 166–174. https://doi.org/10.1016/j.dsr2.2009.09.003

Bravo, I., Vila, M., Casabianca, S., Rodriguez, F., Rial, P., Riobó, P., & Penna, A. (2012). Life cycle stages of the benthic palytoxin-producing dinoflagellate Ostreopsis cf. Ovata (Dinophyceae). *Harmful Algae*, *18*, 24–34. https://doi.org/10.1016/j.hal.2012.04.001

Bray N.L., Pimentel H., Melsted P., and Pachter L. (2016) Near-optimal probabilistic RNA-seq quantification, Nature Biotechnology 34, 525–527. doi:10.1038/nbt.3519

Breslow, D. K., & Holland, A. J. (2019). Mechanism and Regulation of Centriole and Cilium Biogenesis. *Annual Review of Biochemistry*, *88*(1), 691–724. https://doi.org/10.1146/annurev-biochem-013118-111153

Bricheux, G., Mahoney, D. G., & Gibbs, S. P. (1992). Development of the pellicle and thecal plates following ecdysis in the dinoflagellateGlenodinium foliaceum. *Protoplasma*, *168*(3–4), 159–171. https://doi.org/10.1007/BF01666262

Brosnahan, M. L., Fischer, A. D., Lopez, C. B., Moore, S. K., & Anderson, D. M. (2020). Cyst-forming dinoflagellates in a warming climate. *Harmful Algae*, *91*, 101728. https://doi.org/10.1016/j.hal.2019.101728

Burke, D. J. (2009). Interpreting spatial information and regulating mitosis in response to spindle orientation. *Genes & Development*, *23*(14), 1613–1618. https://doi.org/10.1101/gad.1826409

Burkholder, J. M., Azanza, R. V., & Sako, Y. (2006). The Ecology of Harmful Dinoflagellates. In Edna Granéli & J. T. Turner (Eds.), *Ecology of Harmful Algae* (Vol. 189, pp. 53–66). Springer Berlin Heidelberg. http://link.springer.com/10.1007/978-3-540-32210-8_5

Burkholder, JoAnn M., Glibert, P. M., & Skelton, H. M. (2008). Mixotrophy, a major mode of nutrition for harmful algal species in eutrophic waters. *Harmful Algae*, *8*(1), 77–93. https://doi.org/10.1016/j.hal.2008.08.010

Burki, F. (2014). The Eukaryotic Tree of Life from a Global Phylogenomic Perspective. *Cold Spring Harbor Perspectives in Biology*, *6*(5), a016147–a016147. https://doi.org/10.1101/cshperspect.a016147

Burki, Fabien, Roger, A. J., Brown, M. W., & Simpson, A. G. B. (2020). The New Tree of Eukaryotes. *Trends in Ecology & Evolution*, *35*(1), 43–55. https://doi.org/10.1016/j.tree.2019.08.008

Cachon, J., Cachon, M., & Salvano, P. (1979). The nuclear division of Oxyrrhis marina: An example of the role played by the nuclear envelope in chromosome segregation. *Archiv Für Protistenkunde*, *122*(1–2), 43–54. https://doi.org/10.1016/S0003-9365(79)80019-6

Cachon, M., Cachon, J., Cosson, J., Greuet, C., & Huitorel, P. (1991). Dinoflagellate flagella adopt various conformations in response to different needs. *Biology of the Cell*, *71*(1–2), 175–182. https://doi.org/10.1016/0248-4900(91)90063-S

Carnicer, O., García-Altares, M., Andree, K. B., Tartaglione, L., Dell'Aversano, C., Ciminiello, P., de la Iglesia, P., Diogène, J., & Fernández-Tejedor, M. (2016). Ostreopsis cf. ovata from western Mediterranean Sea: Physiological responses under different temperature and salinity conditions. *Harmful Algae*, *57*, 98–108. https://doi.org/10.1016/j.hal.2016.06.002

Castagnetti, S., Oliferenko, S., & Nurse, P. (2010). Fission Yeast Cells Undergo Nuclear Division in the Absence of Spindle Microtubules. *PLoS Biology*, *8*(10), e1000512. https://doi.org/10.1371/journal.pbio.1000512

Cato, M. L., Jester, H. D., Lavertu, A., Lyman, A., Tallent, L. M., & Mitchell, G. C. (2019a). Genome-Wide Analysis of Cell Cycle-Regulating Genes in the Symbiotic Dinoflagellate *Breviolum minutum*. *G3: Genes|Genomes|Genetics*, *9*(11), 3843–3853. https://doi.org/10.1534/g3.119.400363

Cato, M. L., Jester, H. D., Lavertu, A., Lyman, A., Tallent, L. M., & Mitchell, G. C. (2019b). Genome-Wide Analysis of Cell Cycle-Regulating Genes in the Symbiotic Dinoflagellate *Breviolum minutum*. *G3: Genes|Genomes|Genetics*, *9*(11), 3843–3853. https://doi.org/10.1534/g3.119.400363

Cavalier-Smith, T., & Chao, E. E. (2004). Protalveolate phylogeny and systematics and the origins of Sporozoa and dinoflagellates (phylum Myzozoa nom. Nov.). *European Journal of Protistology*, *40*(3), 185–212. https://doi.org/10.1016/j.ejop.2004.01.002

Cembella, A. D. (2003). Chemical ecology of eukaryotic microalgae in marine ecosystems. *Phycologia*, *42*(4), 420–447. https://doi.org/10.2216/i0031-8884-42-4-420.1

Cembella, A., & John, U. (2006). Molecular Physiology of Toxin Production and Growth Regulation in Harmful Algae. In Edna Granéli & J. T. Turner (Eds.), *Ecology of Harmful Algae* (Vol. 189, pp. 215–227). Springer Berlin Heidelberg. https://doi.org/10.1007/978-3-540-32210-8_17

Charlson, R. J., Lovelock, J. E., Andreae, M. O., & Warren, S. G. (1987). Oceanic phytoplankton, atmospheric sulphur, cloud albedo and climate. *Nature*, *326*(6114), 655–661. https://doi.org/10.1038/326655a0

Chatton, E. (1920). Les péridiniens parasites. Morphologie, reproduction,éthologie. Arch. Zool. Exp. Gen.59, 1-475.

Cheeseman, I. M., & Desai, A. (2008). Molecular architecture of the kinetochore–microtubule interface. *Nature Reviews Molecular Cell Biology*, *9*(1), 33–46. https://doi.org/10.1038/nrm2310

Cheffings, T. H., Burroughs, N. J., & Balasubramanian, M. K. (2016). Actomyosin Ring Formation and Tension Generation in Eukaryotic Cytokinesis. *Current Biology*, *26*(15), R719–R737. https://doi.org/10.1016/j.cub.2016.06.071

Chenevert, J., Roca, M., Besnardeau, L., Ruggiero, A., Nabi, D., McDougall, A., Copley, R. R., Christians, E., & Castagnetti, S. (2020). The Spindle Assembly Checkpoint Functions during Early Development in Non-Chordate Embryos. *Cells*, *9*(5), 1087. https://doi.org/10.3390/cells9051087

Cho, Y., Ogawa, M., Hirota, M., & Oshima, Y. (2011). Effects of mitomycin C and colchicine on toxin production and cell cycle regulation in the dinoflagellate Alexandrium tamarense. *Harmful Algae*, *10*(3), 235–244. https://doi.org/10.1016/j.hal.2010.10.003

Chomérat, N., Bilien, G., Derrien, A., Henry, K., Ung, A., Viallon, J., Darius, H. T., Mahana iti Gatti, C., Roué, M., Hervé, F., Réveillon, D., Amzil, Z., & Chinain, M. (2019). Ostreopsis lenticularis Y. Fukuyo (Dinophyceae, Gonyaulacales) from French Polynesia (South Pacific Ocean): A revisit of its morphology, molecular phylogeny and toxicity. *Harmful Algae*, *84*, 95–111. https://doi.org/10.1016/j.hal.2019.02.004

Ciliberto, A., & Shah, J. (2013). Cell Cycle Signaling, Spindle Assembly Checkpoint. In W. Dubitzky, O. Wolkenhauer, K.-H. Cho, & H. Yokota (Eds.), *Encyclopedia of Systems Biology* (pp. 317–321). Springer New York. https://doi.org/10.1007/978-1-4419-9863-7_44

Cleveland, D. W., Mao, Y., & Sullivan, K. F. (2003). Centromeres and Kinetochores: From Epigenetics to Mitotic Checkpoint Signaling. *Cell*, *112*(4), 407–421. https://doi.org/10.1016/S0092-8674(03)00115-6

Cohu, S., & Lemée, R. (2012). Vertical distribution of the toxic epibenthic dinoflagellates Ostreopsis cf. ovata, Prorocentrum lima and Coolia monotis in the NW Mediterranean Sea. Cahiers de Biologie Marine. 53. 373-380.

Cohu, S., Mangialajo, L., Thibaut, T., Blanfuné, A., Marro, S., & Lemée, R. (2013). Proliferation of the toxic dinoflagellate Ostreopsis cf. Ovata in relation to depth, biotic substrate and environmental factors in the North West Mediterranean Sea. *Harmful Algae*, *24*, 32–44. https://doi.org/10.1016/j.hal.2013.01.002

Collin, P., Nashchekina, O., Walker, R., & Pines, J. (2013). The spindle assembly checkpoint works like a rheostat rather than a toggle switch. *Nature Cell Biology*, *15*(11), 1378–1385. https://doi.org/10.1038/ncb2855

Conesa, A., Madrigal, P., Tarazona, S., Gomez-Cabrero, D., Cervera, A., McPherson, A., Szcześniak, M. W., Gaffney, D. J., Elo, L. L., Zhang, X., & Mortazavi, A. (2016). A survey of best practices for RNA-seq data analysis. *Genome Biology*, *17*(1), 13. https://doi.org/10.1186/s13059-016-0881-8

Coombs, G. H. (Ed.). (1998). *Evolutionary relationships among protozoa*. Kluwer Acad.

Cooper, G.M. (2000). The Eukaryotic Cell Cycle. Cell Mol. Approach 2nd Ed.

Costanzo, M., Nishikawa, J. L., Tang, X., Millman, J. S., Schub, O., Breitkreuz, K., Dewar, D., Rupes, I., Andrews, B., & Tyers, M. (2004). CDK Activity Antagonizes Whi5, an Inhibitor of G1/S Transcription in Yeast. *Cell*, *117*(7), 899–913. https://doi.org/10.1016/j.cell.2004.05.024

Costas, E., Gil, S. G., Aguilera, A., & Lopez-Rodas, V. (1993). Effects of mitotic growth factors on growth rates in marine dinoflagellates. *Phycologia*, *32*(5), 351–355. https://doi.org/10.2216/i0031-8884-32-5-351.1

Costas, Eduardo, Gil, S. G., Aguilera, A., & Rodas, V. L. (1993). An apparent growth factor modulation of marine dinoflagellate excystment. *Journal of Experimental Marine Biology and Ecology*, *166*(2), 241–249. https://doi.org/10.1016/0022-0981(93)90222-A

Cross, F. R., & Umen, J. G. (2015). The Chlamydomonas cell cycle. *The Plant Journal: For Cell and Molecular Biology*, *82*(3), 370–392. https://doi.org/10.1111/tpj.12795

Cuadrado, Á., De Bustos, A., & Figueroa, R. I. (2019). Chromosomal markers in the genus Karenia: Towards an understanding of the evolution of the chromosomes, life cycle patterns and phylogenetic relationships in dinoflagellates. *Scientific Reports*, *9*(1), 3072. https://doi.org/10.1038/s41598-018-35785-7

Dagenais-Bellefeuille, S., Bertomeu, T., & Morse, D. (2008). S-Phase and M-Phase Timing Are under Independent Circadian Control in the Dinoflagellate *Lingulodinium*. *Journal of Biological Rhythms*, *23*(5), 400–408. https://doi.org/10.1177/0748730408321749

Dagenais-Bellefeuille, S., & Morse, D. (2013). Putting the N in dinoflagellates. *Frontiers in Microbiology*, *4*. https://doi.org/10.3389/fmicb.2013.00369

Davidson, K., Gowen, R. J., Harrison, P. J., Fleming, L. E., Hoagland, P., & Moschonas, G. (2014). Anthropogenic nutrients and harmful algae in coastal waters. *Journal of Environmental Management*, *146*, 206–216. https://doi.org/10.1016/j.jenvman.2014.07.002

Davy, S. K., Allemand, D., & Weis, V. M. (2012). Cell Biology of Cnidarian-Dinoflagellate Symbiosis. *Microbiology and Molecular Biology Reviews*, *76*(2), 229–261. https://doi.org/10.1128/MMBR.05014-11
de Bruin, R. A. M., McDonald, W. H., Kalashnikova, T. I., Yates, J., & Wittenberg, C. (2004). Cln3 Activates G1-Specific Transcription via Phosphorylation of the SBF Bound Repressor Whi5. *Cell*, *117*(7), 887–898. https://doi.org/10.1016/j.cell.2004.05.025

Den Haese, G. J., Walworth, N., Carr, A. M., & Gould, K. L. (1995). The Wee1 protein kinase regulates T14 phosphorylation of fission yeast Cdc2. *Molecular Biology of the Cell*, *6*(4), 371–385. https://doi.org/10.1091/mbc.6.4.371

Di Fiore, B., & Pines, J. (2010). How cyclin A destruction escapes the spindle assembly checkpoint. *Journal of Cell Biology*, *190*(4), 501–509. https://doi.org/10.1083/jcb.201001083

Dierssen, H., McManus, G. B., Chlus, A., Qiu, D., Gao, B.-C., & Lin, S. (2015). Space station image captures a red tide ciliate bloom at high spectral and spatial resolution. *Proceedings of the National Academy of Sciences*, *112*(48), 14783–14787. https://doi.org/10.1073/pnas.1512538112

Distler, M., Kulkarni, A., Rai, R., & Cooper, T. G. (2001). Green Fluorescent Protein-Dal80p Illuminates up to 16 Distinct Foci That Colocalize with and Exhibit the Same Behavior as Chromosomal DNA Proceeding through the Cell Cycle of Saccharomyces cerevisiae. *Journal of Bacteriology*, *183*(15), 4636–4642. https://doi.org/10.1128/JB.183.15.4636-4642.2001

Dodge, J. D., & Crawford, R. M. (1970). The morphology and fine structure of *ceratium hirundinella* (dinophyceae) [1]. *Journal of Phycology*, *6*(2), 137–149. https://doi.org/10.1111/j.1529-8817.1970.tb02372.x

Dolah, F. M., Leighfield, T. A., Sandel, H. D., & Hsu, C. K. (1995). Cell division in the dinoflagellate gambierdiscus toxicus is phased to the diurnal cycle and accompanied by activation of the cell cycle regulatory protein, cdc2 kinase1. *Journal of Phycology*, *31*(3), 395–400. https://doi.org/10.1111/j.0022-3646.1995.00395.x

Drechsler, H., & McAinsh, A. D. (2012). Exotic mitotic mechanisms. *Open Biology*, *2*(12). https://doi.org/10.1098/rsob.120140

Drinnenberg, I. A., & Akiyoshi, B. (2017). Evolutionary Lessons from Species with Unique Kinetochores. In B. E. Black (Ed.), *Centromeres and Kinetochores* (Vol. 56, pp. 111–138). Springer International Publishing. https://doi.org/10.1007/978-3-319-58592-5_5

Driscoll, W. W., Hackett, J. D., & Ferrière, R. (2016). Eco-evolutionary feedbacks between private and public goods: Evidence from toxic algal blooms. *Ecology Letters*, *19*(1), 81–97. https://doi.org/10.1111/ele.12533

Drouet, K. (2021). *Impact de la température sur la biogéographie et la phénologie des dinoflagellés benthiques toxiques du genre Ostreopsis en Méditérranée et en Atlantique* [Thesis, Sorbonne Université]. http://www.theses.fr/s263039

Dutcher, S. K., Morrissette, N. S., Preble, A. M., Rackley, C., & Stanga, J. (2002). ε-Tubulin Is an Essential Component of the Centriole. *Molecular Biology of the Cell*, *13*(11), 3859–3869. https://doi.org/10.1091/mbc.e02-04-0205

Dutcher, S. K., & O'Toole, E. T. (2016). The basal bodies of Chlamydomonas reinhardtii. *Cilia*, *5*(1), 18. https://doi.org/10.1186/s13630-016-0039-z

Ehler, L. L., & Dutcher, S. K. (1998). Pharmacological and genetic evidence for a role of rootlet and phycoplast microtubules in the positioning and assembly of cleavage furrows in Chlamydomonas reinhardtii. *Cell Motility and the Cytoskeleton*, *40*(2), 193–207. https://doi.org/10.1002/(SICI)1097-0169(1998)40:2<193::AID-CM8>3.0.CO;2-G

Ellegaard, M., Figueroa, R. L., & Versteegh, G. J. M. (2013). Dinoflagellate life cycles, strategy and diversity: Key foci for future research. In J. M. Lewis, F. Marret, & L. R. Bradley (Eds.), *Biological and Geological Perspectives of Dinoflagellates* (pp. 249–261). Geological Society of London. https://doi.org/10.1144/TMS5.24

Endo, K., Mizuguchi, M., Harata, A., Itoh, G., & Tanaka, K. (2010). Nocodazole induces mitotic cell death with apoptotic-like features in *Saccharomyces cerevisiae*. *FEBS Letters*, *584*(11), 2387–2392. https://doi.org/10.1016/j.febslet.2010.04.029

Escalera, L., Benvenuto, G., Scalco, E., Zingone, A., & Montresor, M. (2014). Ultrastructural Features of the Benthic Dinoflagellate Ostreopsis cf. Ovata (Dinophyceae). *Protist*, *165*(3), 260–274. https://doi.org/10.1016/j.protis.2014.03.001

Eshun-Wilson, L., Zhang, R., Portran, D., Nachury, M. V., Toso, D. B., Löhr, T., Vendruscolo, M., Bonomi, M., Fraser, J. S., & Nogales, E. (2019). Effects of α-tubulin acetylation on microtubule structure and stability. *Proceedings of the National Academy of Sciences*, *116*(21), 10366–10371. https://doi.org/10.1073/pnas.1900441116

Falkowski, P. G. (2004). The Evolution of Modern Eukaryotic Phytoplankton. *Science*, *305*(5682), 354–360. https://doi.org/10.1126/science.1095964

Fang, G., Yu, H., & Kirschner, M. W. (1998). Direct Binding of CDC20 Protein Family Members Activates the Anaphase-Promoting Complex in Mitosis and G1. *Molecular Cell*, *2*(2), 163–171. https://doi.org/10.1016/S1097-2765(00)80126-4

Fang, H., Klages, N., Baechler, B., Hillner, E., Yu, L., Pardo, M., Choudhary, J., & Brochet, M. (2017). Multiple short windows of calcium-dependent protein kinase 4 activity coordinate distinct cell cycle events during Plasmodium gametogenesis. *ELife*, *6*, e26524. https://doi.org/10.7554/eLife.26524

Fast, N.M. et al. 2002. Re-examining alveolate evolution using multiple protein molecular phylogenies. J. Eukaryot. Microbiol. 49:30-37.

Faust, M. A. (1999). Three new Ostreopsis species (Dinophyceae): O. marinus sp. nov., O. belizeanus sp. nov., and O. caribbeanus sp. nov. *Phycologia*, *38*(2), 92–99. https://doi.org/10.2216/i0031-8884-38-2-92.1

Faust, M. A., & Morton, S. L. (1995). Morphology and ecology of the marine dinoflagellate ostreopsis labens sp. Nov. (dinophyceae)1. *Journal of Phycology*, *31*(3), 456–463. https://doi.org/10.1111/j.0022-3646.1995.00456.x

Field, C. B. (1998). Primary Production of the Biosphere: Integrating Terrestrial and Oceanic Components. *Science*, *281*(5374), 237–240. https://doi.org/10.1126/science.281.5374.237

Figueroa, R. I., Garcés, E., & Bravo, I. (2007). Comparative study of the life cycles of *Alexandrium tamutum* and *Alexandrium minutum* (Gonyaulacales, Dinophyceae) in culture [1]. *Journal of Phycology*, *43*(5), 1039–1053. https://doi.org/10.1111/j.1529-8817.2007.00393.x

Filfilan, S. A., & Sigee, D. C. (1977). Continuous DNA replication in the nucleus of the dinoflagellate Prorocentrum micans (Ehrenberg). *Journal of Cell Science*, *27*, 81–90.

Finegan, T. M., & Bergstralh, D. T. (2019). Division orientation: Disentangling shape and mechanical forces. *Cell Cycle (Georgetown, Tex.)*, *18*(11), 1187–1198. https://doi.org/10.1080/15384101.2019.1617006

Fisher, D. (2011). Control of DNA Replication by Cyclin-Dependent Kinases in Development. In J. Z. Kubiak (Ed.), *Cell Cycle in Development* (pp. 201–217). Springer Berlin Heidelberg. https://doi.org/10.1007/978-3-642-19065-0_10

Fisher, D. L., & Nurse, P. (1996). A single fission yeast mitotic cyclin B p34cdc2 kinase promotes both S-phase and mitosis in the absence of G1 cyclins. *The EMBO Journal*, *15*(4), 850–860.

Fırat-Karalar, E. N., & Stearns, T. (2014). The centriole duplication cycle. *Philosophical Transactions of the Royal Society B: Biological Sciences*, *369*(1650), 20130460. https://doi.org/10.1098/rstb.2013.0460

Francia, M. E., Dubremetz, J.-F., & Morrissette, N. S. (2015). Basal body structure and composition in the apicomplexans Toxoplasma and Plasmodium. *Cilia*, *5*(1), 3. https://doi.org/10.1186/s13630-016-0025-5

Francia, M. E., & Striepen, B. (2014). Cell division in apicomplexan parasites. *Nature Reviews Microbiology*, *12*(2), 125–136. https://doi.org/10.1038/nrmicro3184

Fromherz, S. (2004). Mutations in -tubulin promote basal body maturation and flagellar assembly in the absence of -tubulin. *Journal of Cell Science*, *117*(2), 303–314. https://doi.org/10.1242/jcs.00859

Fukuda, Y., & Suzaki, T. (2015). Unusual Features of Dinokaryon, the Enigmatic Nucleus of Dinoflagellates. In S. Ohtsuka, T. Suzaki, T. Horiguchi, N. Suzuki, & F. Not (Eds.), *Marine Protists* (pp. 23–45). Springer Japan. https://doi.org/10.1007/978-4-431-55130-0_2

Fukuyo, Y. (1981). Taxonomical study on benthic dinoflagellates collected in coral reefs. *NIPPON SUISAN GAKKAISHI*, *47*(8), 967–978. https://doi.org/10.2331/suisan.47.967

Galleron, C., & Durrand, A. M. (1979). Cell cycle and DNA synthesis in a marine dinoflagellateAmphidinium

carterae. *Protoplasma*, *100*(2), 155–165. https://doi.org/10.1007/BF01283926

Gao, X. P., & Li, J. Y. (1986). Nuclear division in the marine dinoflagellate Oxyrrhis marina. *Journal of Cell Science*, *85*, 161–175.

Garcés, E., Delgado, M., Masó, M., & Camp, J. (1998). Life history and in situ growth rates of alexandrium taylori (dinophyceae, pyrrophyta). *Journal of Phycology*, *34*(5), 880–887. https://doi.org/10.1046/j.1529-8817.1998.340880.x

Gavelis, G. S., Herranz, M., Wakeman, K. C., Ripken, C., Mitarai, S., Gile, G. H., Keeling, P. J., & Leander, B. S. (2019). Dinoflagellate nucleus contains an extensive endomembrane network, the nuclear net. *Scientific Reports*, *9*(1). https://doi.org/10.1038/s41598-018-37065-w

Geelen, D., & Inzé, D. (2006). Dynamics and Structure of the Preprophase Band and the Phragmoplast. In T. Nagata, K. Matsuoka, & D. Inzé (Eds.), *Tobacco BY-2 Cells: From Cellular Dynamics to Omics* (Vol. 58, pp. 23–40). Springer Berlin Heidelberg. https://doi.org/10.1007/3-540-32674-X_2

Gerien, K. S., & Wu, J.-Q. (2018). Molecular mechanisms of contractile-ring constriction and membrane trafficking in cytokinesis. *Biophysical Reviews*, *10*(6), 1649–1666. https://doi.org/10.1007/s12551-018-0479-3

Geymonat, M., Spanos, A., Walker, P. A., Johnston, L. H., & Sedgwick, S. G. (2003). In Vitro Regulation of Budding Yeast Bfa1/Bub2 GAP Activity by Cdc5. *Journal of Biological Chemistry*, *278*(17), 14591–14594. https://doi.org/10.1074/jbc.C300059200

Giannoutsou, E., Galatis, B., Zachariadis, M., & Apostolakos, P. (2012). Formation of an endoplasmic reticulum ring associated with acetylated microtubules in the angiosperm preprophase band. *Cytoskeleton*, *69*(4), 252–265. https://doi.org/10.1002/cm.21020

Gillies, T. E., & Cabernard, C. (2011). Cell division orientation in animals. *Current Biology: CB*, *21*(15), R599-609. https://doi.org/10.1016/j.cub.2011.06.055

Glotzer, M. (2004). Cleavage furrow positioning. *Journal of Cell Biology*, *164*(3), 347–351. https://doi.org/10.1083/jcb.200310112

Glotzer, M. (2017). Cytokinesis in Metazoa and Fungi. *Cold Spring Harbor Perspectives in Biology*, *9*(10), a022343. https://doi.org/10.1101/cshperspect.a022343

Gómez, F. (2015). Hoppenrath, M., Murray, S.A., Chomérat, N. and Horiguchi, T. 2014. Marine Benthic Dinoflagellates—Unveiling Their Worldwide Biodiversity. Kleine Senckenberg-Reihe, Band 54, Schweizerbart, Stuttgart, Germany ISBN 978-3-510-61402-8, 276 pp., 19.90 Euro, a. *Limnology and Oceanography Bulletin*, *24*(2), 62–62. https://doi.org/10.1002/lob.10009

Gómez, F., López-García, P., & Moreira, D. (2011). Molecular phylogeny of dinophysoid dinoflagellates: the systematic position of oxyphysis oxytoxoides and the dinophysis hastata group (dinophysales, dinophyceae)1: molecular phylogeny of dinophysales. *Journal of Phycology*, *47*(2), 393–406. https://doi.org/10.1111/j.1529-8817.2011.00964.x

Gorman, L. M., Wilkinson, S. P., Kitchen, S. A., Oakley, C. A., Grossman, A. R., Weis, V. M., & Davy, S. K. (2020). Phylogenetic analysis of cell-cycle regulatory proteins within the Symbiodiniaceae. *Scientific Reports*, *10*(1), 20473. https://doi.org/10.1038/s41598-020-76621-1

Gornik, S. G., Hu, I., Lassadi, I., & Waller, R. F. (2019). The Biochemistry and Evolution of the Dinoflagellate Nucleus. *Microorganisms*, *7*(8), 245. https://doi.org/10.3390/microorganisms7080245

Gould, S. B., Tham, W.-H., Cowman, A. F., McFadden, G. I., & Waller, R. F. (2008). Alveolins, a New Family of Cortical Proteins that Define the Protist Infrakingdom Alveolata. *Molecular Biology and Evolution*, *25*(6), 1219–1230. https://doi.org/10.1093/molbev/msn070

Grabherr, M. G., Haas, B. J., Yassour, M., Levin, J. Z., Thompson, D. A., Amit, I., Adiconis, X., Fan, L., Raychowdhury, R., Zeng, Q., Chen, Z., Mauceli, E., Hacohen, N., Gnirke, A., Rhind, N., di Palma, F., Birren, B.

W., Nusbaum, C., Lindblad-Toh, K., … Regev, A. (2011). Full-length transcriptome assembly from RNA-Seq data without a reference genome. *Nature Biotechnology*, *29*(7), 644–652. https://doi.org/10.1038/nbt.1883

Granéli, E., & Turner, J. T. (2006). An Introduction to Harmful Algae. In Edna Granéli & J. T. Turner (Eds.), *Ecology of Harmful Algae* (Vol. 189, pp. 3–7). Springer Berlin Heidelberg. https://doi.org/10.1007/978-3-540-32210-8_1

Granéli, Edna, & Turner, J. T. (Eds.). (2006). *Ecology of Harmful Algae* (Vol. 189). Springer Berlin Heidelberg. http://link.springer.com/10.1007/978-3-540-32210-8

Griffith, A. W., & Gobler, C. J. (2020). Harmful algal blooms: A climate change co-stressor in marine and freshwater ecosystems. *Harmful Algae*, *91*, 101590. https://doi.org/10.1016/j.hal.2019.03.008

Grimaud, G. M., Mairet, F., Sciandra, A., & Bernard, O. (2017). Modeling the temperature effect on the specific growth rate of phytoplankton: A review. *Reviews in Environmental Science and Bio/Technology*, *16*(4), 625–645. https://doi.org/10.1007/s11157-017-9443-0

Guidi, F., Pezzolesi, L., & Vanucci, S. (2018). Microbial dynamics during harmful dinoflagellate *Ostreopsis* cf. *ovata* growth: Bacterial succession and viral abundance pattern. *MicrobiologyOpen*, *7*(4), e00584. https://doi.org/10.1002/mbo3.584

Guillén, N., Carlier, M.-F., Brugerolle, G., Tardieux, I., & Ausseil, J. (1998). L'actine cytosquelettique et ses protéines associées. Quelques exemples chez les protistes. *Parasite*, *5*(2), 107–117. https://doi.org/10.1051/parasite/1998052107

Gundersen, G. G., & Bulinski, J. C. (1986). Distribution of tyrosinated and nontyrosinated alpha-tubulin during mitosis. *Journal of Cell Biology*, *102*(3), 1118–1126. https://doi.org/10.1083/jcb.102.3.1118

Guy, R. C. (2014). Red Tide. In *Encyclopedia of Toxicology* (pp. 65–66). Elsevier. https://doi.org/10.1016/B978-0-12-386454-3.00919-2

Habermann, E. (1989). Palytoxin acts through Na+, K+-ATPase. *Toxicon*, *27*(11), 1171–1187. https://doi.org/10.1016/0041-0101(89)90026-3

Hackett, J. D., Anderson, D. M., Erdner, D. L., & Bhattacharya, D. (2004). Dinoflagellates: A remarkable evolutionary experiment. *American Journal of Botany*, *91*(10), 1523–1534. https://doi.org/10.3732/ajb.91.10.1523

Hallegraeff, G. M. (1993). A review of harmful algal blooms and their apparent global increase. *Phycologia*, *32*(2), 79–99. https://doi.org/10.2216/i0031-8884-32-2-79.1

Hallegraeff, Gustaaf M. (2010). Ocean climate change, phytoplankton community responses, and harmful algal blooms: a formidable predictive challenge. *Journal of Phycology*, *46*(2), 220–235. https://doi.org/10.1111/j.1529-8817.2010.00815.x

Hammarton, T. C. (2019). Who Needs a Contractile Actomyosin Ring? The Plethora of Alternative Ways to Divide a Protozoan Parasite. *Frontiers in Cellular and Infection Microbiology*, *9*, 397. https://doi.org/10.3389/fcimb.2019.00397

Hans, F., & Dimitrov, S. (2001). Histone H3 phosphorylation and cell division. *Oncogene*, *20*(24), 3021–3027. https://doi.org/10.1038/sj.onc.1204326

Hansen, P. J. (2011). The Role of Photosynthesis and Food Uptake for the Growth of Marine Mixotrophic Dinoflagellates1: mixotrophy in marine dinoflagellates. *Journal of Eukaryotic Microbiology*, *58*(3), 203–214. https://doi.org/10.1111/j.1550-7408.2011.00537.x

Hardin, W. R., Li, R., Xu, J., Shelton, A. M., Alas, G. C. M., Minin, V. N., & Paredez, A. R. (2017). Myosin-independent cytokinesis in *Giardia* utilizes flagella to coordinate force generation and direct membrane trafficking. *Proceedings of the National Academy of Sciences*, *114*(29), E5854–E5863. https://doi.org/10.1073/pnas.1705096114

Hastings, J. (2013). Circadian Rhythms in Dinoflagellates: What Is the Purpose of Synthesis and Destruction of Proteins? *Microorganisms*, *1*(1), 26–32. https://doi.org/10.3390/microorganisms1010026

Hégarat, N., Rata, S., & Hochegger, H. (2016). Bistability of mitotic entry and exit switches during open mitosis in mammalian cells. *BioEssays*, *38*(7), 627–643. https://doi.org/10.1002/bies.201600057

Heimann, K., Klerks, P. L., & Hasenstein, K. H. (2009). Involvement of actin and microtubules in regulation of bioluminescence and translocation of chloroplasts in the dinoflagellate Pyrocystis lunula. *Botanica Marina*, *52*(2). https://doi.org/10.1515/BOT.2009.010

Herzog, M., Soyer, M. O., & Daney de Marcillac, G. (1982). A high level of thymine replacement by 5-hydroxymethyluracil in nuclear DNA of the primitive dinoflagellate Prorocentrum micans E. *European Journal of Cell Biology*, *27*(2), 151–155.

Hinchliff, C. E., Smith, S. A., Allman, J. F., Burleigh, J. G., Chaudhary, R., Coghill, L. M., Crandall, K. A., Deng, J., Drew, B. T., Gazis, R., Gude, K., Hibbett, D. S., Katz, L. A., Laughinghouse, H. D., McTavish, E. J., Midford, P. E., Owen, C. L., Ree, R. H., Rees, J. A., … Cranston, K. A. (2015). Synthesis of phylogeny and taxonomy into a comprehensive tree of life. *Proceedings of the National Academy of Sciences*, *112*(41), 12764–12769. https://doi.org/10.1073/pnas.1423041112

Hiraki, M., Nakazawa, Y., Kamiya, R., & Hirono, M. (2007). Bld10p Constitutes the Cartwheel-Spoke Tip and Stabilizes the 9-Fold Symmetry of the Centriole. *Current Biology*, *17*(20), 1778–1783. https://doi.org/10.1016/j.cub.2007.09.021

Hirono, M. (2014). Cartwheel assembly. *Philosophical Transactions of the Royal Society B: Biological Sciences*, *369*(1650), 20130458. https://doi.org/10.1098/rstb.2013.0458

Hirsh, J. K., & Wu, C. H. (1997). Palytoxin-induced single-channel currents from the sodium pump synthesized by in vitro expression. *Toxicon*, *35*(2), 169–176. https://doi.org/10.1016/S0041-0101(96)00136-5

Hoagland, P., & Scatasta, S. (2006). The Economic Effects of Harmful Algal Blooms. In Edna Granéli & J. T. Turner (Eds.), *Ecology of Harmful Algae* (Vol. 189, pp. 391–402). Springer Berlin Heidelberg. https://doi.org/10.1007/978-3-540-32210-8_30

Hodges, M. E., Scheumann, N., Wickstead, B., Langdale, J. A., & Gull, K. (2010). Reconstructing the evolutionary history of the centriole from protein components. *Journal of Cell Science*, *123*(9), 1407–1413. https://doi.org/10.1242/jcs.064873

Honsell, G., Bonifacio, A., De Bortoli, M., Penna, A., Battocchi, C., Ciminiello, P., Dell'Aversano, C., Fattorusso, E., Sosa, S., Yasumoto, T., & Tubaro, A. (2013). New Insights on Cytological and Metabolic Features of Ostreopsis cf. ovata Fukuyo (Dinophyceae): A Multidisciplinary Approach. *PLoS ONE*, *8*(2), e57291. https://doi.org/10.1371/journal.pone.0057291

Hooff, J. J., Tromer, E., Wijk, L. M., Snel, B., & Kops, G. J. (2017). Evolutionary dynamics of the kinetochore network in eukaryotes as revealed by comparative genomics. *EMBO Reports*, *18*(9), 1559–1571. https://doi.org/10.15252/embr.201744102

Howell, R. S. M., Klemm, C., Thorpe, P. H., & Csikász-Nagy, A. (2020). Unifying the mechanism of mitotic exit control in a spatiotemporal logical model. *PLOS Biology*, *18*(11), e3000917. https://doi.org/10.1371/journal.pbio.3000917

Huang, D., Moffat, J., & Andrews, B. (2002). Dissection of a Complex Phenotype by Functional Genomics Reveals Roles for the Yeast Cyclin-Dependent Protein Kinase Pho85 in Stress Adaptation and Cell Integrity. *Molecular and Cellular Biology*, *22*(14), 5076–5088. https://doi.org/10.1128/MCB.22.14.5076-5088.2002

Inbal, N., Listovsky, T., & Brandeis, M. (1999). The mammalian Fizzy and Fizzy-related genes are regulated at the transcriptional and post-transcriptional levels. *FEBS Letters*, *463*(3), 350–354. https://doi.org/10.1016/S0014-5793(99)01640-3

Berdieva, M., Safonov, P., Institute of Cytology, Russian Academy of Sciences, Matantseva, O., & Institute of Cytology, Russian Academy of Sciences. (2019). Ultrastructural aspects of ecdysis in the naked dinoflagellate Amphidinium carterae. *Protistology*, *13*(2). https://doi.org/10.21685/1680-0826-2019-13-2-2

Ito, H., Mutsuda, M., Murayama, Y., Tomita, J., Hosokawa, N., Terauchi, K., Sugita, C., Sugita, M., Kondo, T., & Iwasaki, H. (2009). Cyanobacterial daily life with Kai-based circadian and diurnal genome-wide transcriptional control in Synechococcus elongatus. *Proceedings of the National Academy of Sciences*, *106*(33), 14168–14173. https://doi.org/10.1073/pnas.0902587106

Iwasaki, O., Tanizawa, H., Kim, K.-D., Yokoyama, Y., Corcoran, C. J., Tanaka, A., Skordalakes, E., Showe, L. C., & Noma, K. (2015). Interaction between TBP and Condensin Drives the Organization and Faithful Segregation of Mitotic Chromosomes. *Molecular Cell*, *59*(5), 755–767. https://doi.org/10.1016/j.molcel.2015.07.007

Janke, C. (2013). Mysterious modification of tubulin. *Nature Reviews Molecular Cell Biology*, *14*(11), 692–692. https://doi.org/10.1038/nrm3685

Janke, C. (2014). The tubulin code: Molecular components, readout mechanisms, and functions. *Journal of Cell Biology*, *206*(4), 461–472. https://doi.org/10.1083/jcb.201406055

Janke, C., & Magiera, M. M. (2020). The tubulin code and its role in controlling microtubule properties and functions. *Nature Reviews Molecular Cell Biology*, *21*(6), 307–326. https://doi.org/10.1038/s41580-020-0214-3

Janouškovec, J., Gavelis, G. S., Burki, F., Dinh, D., Bachvaroff, T. R., Gornik, S. G., Bright, K. J., Imanian, B., Strom, S. L., Delwiche, C. F., Waller, R. F., Fensome, R. A., Leander, B. S., Rohwer, F. L., & Saldarriaga, J. F. (2017). Major transitions in dinoflagellate evolution unveiled by phylotranscriptomics. *Proceedings of the National Academy of Sciences*, *114*(2), E171–E180. https://doi.org/10.1073/pnas.1614842114

Játiva, S., Calabria, I., Moyano-Rodriguez, Y., Garcia, P., & Queralt, E. (2019). Cdc14 activation requires coordinated Cdk1-dependent phosphorylation of Net1 and PP2A–Cdc55 at anaphase onset. *Cellular and Molecular Life Sciences*, *76*(18), 3601–3620. https://doi.org/10.1007/s00018-019-03086-5

Jauzein, C., Couet, D., Blasco, T., & Lemée, R. (2017). Uptake of dissolved inorganic and organic nitrogen by the benthic toxic dinoflagellate Ostreopsis cf. Ovata. *Harmful Algae*, *65*, 9–18. https://doi.org/10.1016/j.hal.2017.04.005

Jessberger, R. (2002). The many functions of smc proteins in chromosome dynamics. *Nature Reviews Molecular Cell Biology*, *3*(10), 767–778. https://doi.org/10.1038/nrm930

Jia, L., Kim, S., & Yu, H. (2013). Tracking spindle checkpoint signals from kinetochores to APC/C. *Trends in Biochemical Sciences*, *38*(6), 302–311. https://doi.org/10.1016/j.tibs.2013.03.004

Jirage, D., Chen, Y., Caridha, D., O'Neil, M. T., Eyase, F., Witola, W. H., Mamoun, C. B., & Waters, N. C. (2010). The malarial CDK Pfmrk and its effector PfMAT1 phosphorylate DNA replication proteins and co-localize in the nucleus. *Molecular and Biochemical Parasitology*, *172*(1), 9–18. https://doi.org/10.1016/j.molbiopara.2010.03.009

John, P. C. L., Mews, M., & Moore, R. (2001). Cyclin/cdk complexes: Their involvement in cell cycle progression and mitotic division. *Protoplasma*, *216*(3–4), 119–142. https://doi.org/10.1007/BF02673865

Kamijo, K., Ohara, N., Abe, M., Uchimura, T., Hosoya, H., Lee, J.-S., & Miki, T. (2006). Dissecting the role of Rho-mediated signaling in contractile ring formation. *Molecular Biology of the Cell*, *17*(1), 43–55. https://doi.org/10.1091/mbc.e05-06-0569

Kato, K. H., Moriyama, A., Itoh, T. J., Yamamoto, M., Horio, T., & Huitorel, P. (2000). Dynamic changes in microtubule organization during division of the primitive dinoflagellate Oxyrrhis marina. *Biology of the Cell*, *92*(8–9), 583–594. https://doi.org/10.1016/S0248-4900(00)01106-0

Katz, L. A. (2001). Evolution of nuclear dualism in ciliates: A reanalysis in light of recent molecular data. *International Journal of Systematic and Evolutionary Microbiology*, *51*(4), 1587–1592.

https://doi.org/10.1099/00207713-51-4-1587

Keeling, P. J. (2004). Diversity and evolutionary history of plastids and their hosts. *American Journal of Botany*, *91*(10), 1481–1493. https://doi.org/10.3732/ajb.91.10.1481

Keenan, S. M., Lents, N. H., & Baldassare, J. J. (2004). Expression of Cyclin E Renders Cyclin D-CDK4 Dispensable for Inactivation of the Retinoblastoma Tumor Suppressor Protein, Activation of E2F, and G1-S Phase Progression. *Journal of Biological Chemistry*, *279*(7), 5387–5396. https://doi.org/10.1074/jbc.M310383200

Kitagawa, M., & Lee, S. H. (2015). The chromosomal passenger complex (CPC) as a key orchestrator of orderly mitotic exit and cytokinesis. *Frontiers in Cell and Developmental Biology*, *3*, 14. https://doi.org/10.3389/fcell.2015.00014

Kiφrboe, T., & Titelman, J. (1998). Feeding, prey selection and prey encounter mechanisms in the heterotrophic dinoflagellate *Noctiluca scintillans*. *Journal of Plankton Research*, *20*(8), 1615–1636. https://doi.org/10.1093/plankt/20.8.1615

Kohl, L., Sherwin, T., & Gull, K. (1999). Assembly of the paraflagellar rod and the flagellum attachment zone complex during the Trypanosoma brucei cell cycle. *The Journal of Eukaryotic Microbiology*, *46*(2), 105–109. https://doi.org/10.1111/j.1550-7408.1999.tb04592.x

Kohli, G. S., John, U., Figueroa, R. I., Rhodes, L. L., Harwood, D. T., Groth, M., Bolch, C. J. S., & Murray, S. A. (2015). Polyketide synthesis genes associated with toxin production in two species of Gambierdiscus (Dinophyceae). *BMC Genomics*, *16*(1), 410. https://doi.org/10.1186/s12864-015-1625-y

König, J., Frankel, E. B., Audhya, A., & Müller-Reichert, T. (2017). Membrane remodeling during embryonic abscission in Caenorhabditis elegans. *The Journal of Cell Biology*, *216*(5), 1277–1286. https://doi.org/10.1083/jcb.201607030

Koonin, E. V., & Galperin, M. Y. (2003). *Sequence - Evolution - Function: Computational Approaches in Comparative Genomics*. Kluwer Academic. http://www.ncbi.nlm.nih.gov/books/NBK20260/

Koufopanou, V. (1994). The Evolution of Soma in the Volvocales. *The American Naturalist*, *143*(5), 907–931. JSTOR.

Kremp, A. (2013). Diversity of dinoflagellate life cycles: Facets and implications of complex strategies. In J. M. Lewis, F. Marret, & L. R. Bradley (Eds.), *Biological and Geological Perspectives of Dinoflagellates* (pp. 197–205). Geological Society of London. https://doi.org/10.1144/TMS5.18

Kubai, D. F., & Ris, H. (1969). DIVISION IN THE DINOFLAGELLATE GYRODINIUM COHNII (SCHILLER). *Journal of Cell Biology*, *40*(2), 508–528. https://doi.org/10.1083/jcb.40.2.508

Kumagai, A., & Dunphy, W. G. (1992). Regulation of the cdc25 protein during the cell cycle in Xenopus extracts. *Cell*, *70*(1), 139–151. https://doi.org/10.1016/0092-8674(92)90540-S

Kwok, A. C. M., & Wong, J. T. Y. (2003). Cellulose Synthesis Is Coupled to Cell Cycle Progression at G_1 in the Dinoflagellate *Crypthecodinium cohnii*. *Plant Physiology*, *131*(4), 1681–1691. https://doi.org/10.1104/pp.102.018945

Lacroix, B., van Dijk, J., Gold, N. D., Guizetti, J., Aldrian-Herrada, G., Rogowski, K., Gerlich, D. W., & Janke, C. (2010). Tubulin polyglutamylation stimulates spastin-mediated microtubule severing. *Journal of Cell Biology*, *189*(6), 945–954. https://doi.org/10.1083/jcb.201001024

LaJeunesse, T. C., Lambert, G., Andersen, R. A., Coffroth, M. A., & Galbraith, D. W. (2005). Symbiodinium (pyrrhophyta) genome sizes (dna content) are smallest among dinoflagellates1. *Journal of Phycology*, *41*(4), 880–886. https://doi.org/10.1111/j.0022-3646.2005.04231.x

Lampson, M. A., & Cheeseman, I. M. (2011). Sensing centromere tension: Aurora B and the regulation of kinetochore function. *Trends in Cell Biology*, *21*(3), 133–140. https://doi.org/10.1016/j.tcb.2010.10.007

Landsberg, J. H. (2002). The Effects of Harmful Algal Blooms on Aquatic Organisms. *Reviews in Fisheries Science*, *10*(2), 113–390. https://doi.org/10.1080/20026491051695

Landsberg, J., Van Dolah, F., & Doucette, G. (2005). Marine and Estuarine Harmful Algal Blooms: Impacts on Human and Animal Health. In S. Belkin & R. R. Colwell (Eds.), *Oceans and Health: Pathogens in the Marine Environment* (pp. 165–215). Springer US. https://doi.org/10.1007/0-387-23709-7_8

Langousis, G., & Hill, K. L. (2014). Motility and more: The flagellum of Trypanosoma brucei. *Nature Reviews. Microbiology*, *12*(7), 505–518. https://doi.org/10.1038/nrmicro3274

Lara-Gonzalez, P., Westhorpe, F. G., & Taylor, S. S. (2012). The spindle assembly checkpoint. *Current Biology: CB*, *22*(22), R966-980. https://doi.org/10.1016/j.cub.2012.10.006

Larsen, J. (1988). An ultrastructural study of Amphidinium poecilochroum (Dinophyceae), a phagotrophic dinoflagellate feeding on small species of cryptophytes. *Phycologia*, *27*(3), 366–377. https://doi.org/10.2216/i0031-8884-27-3-366.1

Lassus, P. (Ed.). (2016). *Toxic and harmful microalgae of the world ocean*. International Society for the Study of Harmful Algae-ISSHA ; United Nations Educational, Scientific and Cultural Organisation.

Leander, B. S. and P. J. Keeling. 2004. Early evolutionary history of dinoflagellates and apicomplexans (Alveolata) inferred from HSP90 and actin phylogenies. J. Phycol. 40:341-250

Lee, K. S., Park, J.-E., Asano, S., & Park, C. J. (2005). Yeast polo-like kinases: Functionally conserved multitask mitotic regulators. *Oncogene*, *24*(2), 217–229. https://doi.org/10.1038/sj.onc.1208271.

Leman, A. R., & Noguchi, E. (2014). Linking chromosome duplication and segregation via sister chromatid cohesion. *Methods in molecular biology* (Clifton, N.J.), 1170, 75–98. https://doi.org/10.1007/978-1-4939-0888-2_5

Lemée, R., Mangialajo, L., Cohu, S., Amzil, Z., Blanfune, A., Chomerat, N., Ganzin, N., Gasparini, S., Grossel, H., Guidi-Guivard, L., Hoareau, L., Duff, F. le, Marro, S., Simon, N., Nezan, E., Pedrotti, M.-L., Sechet, V., Soliveres, O., & Thibaut, T. (2012). Interactions between Scientists, Managers and Policy Makers in the Framework of the French MediOs Project on *Ostreopsis* (2008–2010). *Cryptogamie, Algologie*, *33*(2), 137–142. https://doi.org/10.7872/crya.v33.iss2.2011.137

Lents, N. H., & Baldassare, J. J. (2016). Cyclins and Cyclin-Dependent Kinases. In *Encyclopedia of Cell Biology* (pp. 423–431). Elsevier. https://doi.org/10.1016/B978-0-12-394447-4.30057-8

Leveson A, Wong F, Wong JT. (1997). Cyclins in a dinoflagellate cell cycle. Mol Mar Biol Biotechnol. Sep;6(3):172-9. PMID: 9284557.

Levi-Setti, R., Gavrilov, K. L., & Rizzo, P. J. (2008). Divalent cation distribution in dinoflagellate chromosomes imaged by high-resolution ion probe mass spectrometry. *European Journal of Cell Biology*, *87*(12), 963–976. https://doi.org/10.1016/j.ejcb.2008.06.002

Li, Z., Lee, J. H., Chu, F., Burlingame, A. L., Günzl, A., & Wang, C. C. (2008). Identification of a Novel Chromosomal Passenger Complex and Its Unique Localization during Cytokinesis in Trypanosoma brucei. *PLoS ONE*, *3*(6), e2354. https://doi.org/10.1371/journal.pone.0002354

Lim, S., & Kaldis, P. (2013). Cdks, cyclins and CKIs: Roles beyond cell cycle regulation. *Development*, *140*(15), 3079–3093. https://doi.org/10.1242/dev.091744

Lin, S. (2006). The smallest dinoflagellate genome is yet to be found: a comment on lajeunesse et al. “symbiodinium (pyrrhophyta) genome sizes (dna content) are smallest among dinoflagellates”1. *Journal of Phycology*, *42*(3), 746–748. https://doi.org/10.1111/j.1529-8817.2006.00213.x

Lin, S. (2011). Genomic understanding of dinoflagellates. *Research in Microbiology*, *162*(6), 551–569. https://doi.org/10.1016/j.resmic.2011.04.006

Llaveria, G., & Berdalet, E. (2009). *Effects of small-scale turbulence on dinoflagellate ecophysiology* [Universitat Politècnica de Catalunya]. http://hdl.handle.net/10261/40987. Thesis

Lowe, C. D., Keeling, P. J., Martin, L. E., Slamovits, C. H., Watts, P. C., & Montagnes, D. J. S. (2011). Who is Oxyrrhis marina? Morphological and phylogenetic studies on an unusual dinoflagellate. *Journal of Plankton Research*, *33*(4), 555–567. https://doi.org/10.1093/plankt/fbq110

Lu, M. S., & Johnston, C. A. (2013). Molecular pathways regulating mitotic spindle orientation in animal cells. *Development*, *140*(9), 1843–1856. https://doi.org/10.1242/dev.087627

Mabrouk, L., Hamza, A., Brahim, M. B., & Bradai, M.-N. (2011). Temporal and depth distribution of microepiphytes on Posidonia oceanica (L.) Delile leaves in a meadow off Tunisia: Temporal and depth distribution of microepiphytes. *Marine Ecology*, *32*(2), 148–161. https://doi.org/10.1111/j.1439-0485.2011.00432.x

Mah, A. S., Jang, J., & Deshaies, R. J. (2001). Protein kinase Cdc15 activates the Dbf2-Mob1 kinase complex. *Proceedings of the National Academy of Sciences*, *98*(13), 7325–7330. https://doi.org/10.1073/pnas.141098998

Malumbres, M. (2014). Cyclin-dependent kinases. *Genome Biology*, *15*(6), 122. https://doi.org/10.1186/gb4184

Mangialajo, L., Bertolotto, R., Cattaneo-Vietti, R., Chiantore, M., Grillo, C., Lemee, R., Melchiorre, N.,

Martin MA, Osmani SA, Oakley BR. (1997) The role of gamma-tubulin in mitotic spindle formation and cell cycle progression in Aspergillus nidulans. J Cell Sci. Mar;110 (Pt 5):623-33. PMID: 9092944.

Maruta H, Greer K, Rosenbaum JL. (1986). The acetylation of alpha-tubulin and its relationship to the assembly and disassembly of microtubules. *J Cell Bio*l. 103(2):571-9. doi: 10.1083/jcb.103.2.571. PMID: 3733880; PMCID: PMC2113826.

Moretto, P., Povero, P., & Ruggieri, N. (2008). The toxic benthic dinoflagellate Ostreopsis ovata: Quantification of proliferation along the coastline of Genoa, Italy. *Marine Pollution Bulletin*, *56*(6), 1209–1214. https://doi.org/10.1016/j.marpolbul.2008.02.028

Marcinko, C. L. J., Allen, J. T., Poulton, A. J., Painter, S. C., & Martin, A. P. (2013). Diurnal variations of dinoflagellate bioluminescence within the open-ocean north-east Atlantic. *Journal of Plankton Research*, *35*(1), 177–190. https://doi.org/10.1093/plankt/fbs081

Markova, K., Uzlikova, M., Tumova, P., Jirakova, K., Hagen, G., Kulda, J., & Nohynkova, E. (2016). Absence of a conventional spindle mitotic checkpoint in the binucleated single-celled parasite Giardia intestinalis. *European Journal of Cell Biology*, *95*(10), 355–367. https://doi.org/10.1016/j.ejcb.2016.07.003

Marques, S. R., Ramakrishnan, C., Carzaniga, R., Blagborough, A. M., Delves, M. J., Talman, A. M., & Sinden, R. E. (2015). An essential role of the basal body protein SAS -6 in *P lasmodium* male gamete development and malaria transmission. *Cellular Microbiology*, *17*(2), 191–206. https://doi.org/10.1111/cmi.12355

Matthews, H., Duffy, C. W., & Merrick, C. J. (2018). Checks and balances? DNA replication and the cell cycle in Plasmodium. *Parasites & Vectors*, *11*(1), 216. https://doi.org/10.1186/s13071-018-2800-1

Mazuski, C., & Herzog, E. D. (2015). Circadian Rhythms: To Sync or Not To Sync. *Current Biology*, *25*(8), R337–R339. https://doi.org/10.1016/j.cub.2015.02.032

McHugh, T., & Welburn, J. P. I. (2017). Dynein at kinetochores: Making the connection. *Journal of Cell Biology*, *216*(4), 855–857. https://doi.org/10.1083/jcb.201703054

McKay, H. F., & Burgess, D. R. (2011). 'Life is a Highway': Membrane Trafficking During Cytokinesis. *Traffic*, *12*(3), 247–251. https://doi.org/10.1111/j.1600-0854.2010.01139.x

McKean, P. G. (2003). Coordination of cell cycle and cytokinesis in Trypanosoma brucei. *Current Opinion in Microbiology*, *6*(6), 600–607. https://doi.org/10.1016/j.mib.2003.10.010

Meitinger, F., & Palani, S. (2016). Actomyosin ring driven cytokinesis in budding yeast. *Seminars in Cell & Developmental Biology*, *53*, 19–27. https://doi.org/10.1016/j.semcdb.2016.01.043

Mendes Pinto, I., Rubinstein, B., & Li, R. (2013). Force to divide: Structural and mechanical requirements for actomyosin ring contraction. *Biophysical Journal*, *105*(3), 547–554. https://doi.org/10.1016/j.bpj.2013.06.033

Meraldi, P. Centrosomes in spindle organization and chromosome segregation: a mechanistic view. (2016). *Chromosome Res* 24, 19–34. https://doi.org/10.1007/s10577-015-9508-2

Meunier, S., & Vernos, I. (2012). Microtubule assembly during mitosis—From distinct origins to distinct functions? *Journal of Cell Science*, *125*(Pt 12), 2805–2814. https://doi.org/10.1242/jcs.092429

Minc, N., Burgess, D., & Chang, F. (2011). Influence of cell geometry on division-plane positioning. *Cell*, *144*(3), 414–426. https://doi.org/10.1016/j.cell.2011.01.016

Mineyuki, Y. (1999). The Preprophase Band of Microtubules: Its Function as a Cytokinetic Apparatus in Higher Plants. In *International Review of Cytology* (Vol. 187, pp. 1–49). Elsevier. https://doi.org/10.1016/S0074-7696(08)62415-8

Monti, M., & Cecchin, E. (2012). Comparative Growth of Three Strains of *Ostreopsis ovata* at Different Light Intensities with Focus on Inter-Specific Allelopathic Interactions. *Cryptogamie, Algologie*, *33*(2), 113–119. https://doi.org/10.7872/crya.v33.iss2.2011.113

Moon, E., Nam, S. W., Shin, W., Park, M. G., & Coats, D. W. (2015). Do All Dinoflagellates have an Extranuclear Spindle? *Protist*, *166*(5), 569–584. https://doi.org/10.1016/j.protis.2015.08.005

Moore, R. E., & Scheuer, P. J. (1971). Palytoxin: A New Marine Toxin from a Coelenterate. *Science*, *172*(3982), 495–498. https://doi.org/10.1126/science.172.3982.495

Moore, Richard E., & Bartolini, G. (1981). Structure of palytoxin. *Journal of the American Chemical Society*, *103*(9), 2491–2494. https://doi.org/10.1021/ja00399a093

Morey, J. S., Monroe, E. A., Kinney, A. L., Beal, M., Johnson, J. G., Hitchcock, G. L., & Van Dolah, F. M. (2011). Transcriptomic response of the red tide dinoflagellate, Karenia brevis, to nitrogen and phosphorus depletion and addition. *BMC Genomics*, *12*(1), 346. https://doi.org/10.1186/1471-2164-12-346

Morgan, D. O. (1997). CYCLIN-DEPENDENT KINASES: Engines, Clocks, and Microprocessors. *Annual Review of Cell and Developmental Biology*, *13*(1), 261–291. https://doi.org/10.1146/annurev.cellbio.13.1.261

Morse, D., Daoust, P., & Benribague, S. (2016a). A Transcriptome-based Perspective of Cell Cycle Regulation in Dinoflagellates. *Protist*, *167*(6), 610–621. https://doi.org/10.1016/j.protis.2016.10.002

Moura, M., & Conde, C. (2019). Phosphatases in Mitosis: Roles and Regulation. *Biomolecules*, *9*(2), 55. https://doi.org/10.3390/biom9020055

Moyano-Rodriguez, Y., & Queralt, E. (2019). PP2A Functions during Mitosis and Cytokinesis in Yeasts. *International Journal of Molecular Sciences*, *21*(1), 264. https://doi.org/10.3390/ijms21010264

Munday, R. (2006). Toxicological requirements for risk assessment of shellfish contaminants: A review. *African Journal of Marine Science*, *28*(2), 447–449. https://doi.org/10.2989/18142320609504195

Munday, Rex. (2011). Palytoxin toxicology: Animal studies. *Toxicon*, *57*(3), 470–477. https://doi.org/10.1016/j.toxicon.2010.10.003

Murata, T., & Wada, M. (1991). Effects of centrifugation on preprophase-band formation in Adiantum protonemata. *Planta*, *183*(3), 391–398. https://doi.org/10.1007/BF00197738

Murray, S., Ip, C. L.-C., Moore, R., Nagahama, Y., & Fukuyo, Y. (2009). Are Prorocentroid Dinoflagellates Monophyletic? A Study of 25 Species Based on Nuclear and Mitochondrial Genes. *Protist*, *160*(2), 245–264.

https://doi.org/10.1016/j.protis.2008.12.004

Musacchio, A., & Salmon, E. D. (2007). The spindle-assembly checkpoint in space and time. *Nature Reviews Molecular Cell Biology*, *8*(5), 379–393. https://doi.org/10.1038/nrm2163

Nakazawa, Y., Hiraki, M., Kamiya, R., & Hirono, M. (2007). SAS-6 is a Cartwheel Protein that Establishes the 9-Fold Symmetry of the Centriole. *Current Biology*, *17*(24), 2169–2174. https://doi.org/10.1016/j.cub.2007.11.046

Nascimento, S. M., Corrêa, E. V., Menezes, M., Varela, D., Paredes, J., & Morris, S. (2012). Growth and toxin profile of Ostreopsis cf. Ovata (Dinophyta) from Rio de Janeiro, Brazil. *Harmful Algae*, *13*, 1–9. https://doi.org/10.1016/j.hal.2011.09.008

Nash, E. A., Barbrook, A. C., Edwards-Stuart, R. K., Bernhardt, K., Howe, C. J., & Nisbet, R. E. R. (2007). Organization of the Mitochondrial Genome in the Dinoflagellate Amphidinium carterae. *Molecular Biology and Evolution*, *24*(7), 1528–1536. https://doi.org/10.1093/molbev/msm074

Ninčević Gladan, Ž., Arapov, J., Casabianca, S., Penna, A., Honsell, G., Brovedani, V., Pelin, M., Tartaglione, L., Sosa, S., Dell'Aversano, C., Tubaro, A., Žuljević, A., Grbec, B., Čavar, M., Bužančić, M., Bakrač, A., & Skejić, S. (2019). Massive Occurrence of the Harmful Benthic Dinoflagellate Ostreopsis cf. Ovata in the Eastern Adriatic Sea. *Toxins*, *11*(5), 300. https://doi.org/10.3390/toxins11050300

Nishihama, R., & Machida, Y. (2001). Expansion of the phragmoplast during plant cytokinesis: A MAPK pathway may MAP it out. *Current Opinion in Plant Biology*, *4*(6), 507–512. https://doi.org/10.1016/S1369-5266(00)00208-9

Norris, D. R., Bomber, J. W., & Balech, E. (1985). Benthic dinoflagellates associated with ciguatera from the Florida Keys. I. Ostreopsis heptagona sp. nov. In Toxic dinoflagellates, 39-44.

Not, F., Siano, R., Kooistra, W. H. C. F., Simon, N., Vaulot, D., & Probert, I. (2012). Diversity and Ecology of Eukaryotic Marine Phytoplankton. In *Advances in Botanical Research* (Vol. 64, pp. 1–53). Elsevier. https://doi.org/10.1016/B978-0-12-391499-6.00001-3

Nuzzo, L. (1999). Different excystment patterns in two calcareous cyst-producing species of the dinoflagellate genus Scrippsiella. *Journal of Plankton Research*, *21*(10), 2009–2018. https://doi.org/10.1093/plankt/21.10.2009

Oakley, B. R., & Dodge, J. D. (1974). Kinetochores associated with the nuclear envelope in the mitosis of a dinoflagellate. *The Journal of Cell Biology*, *63*(1), 322–325.

Oakley, B. R., & Dodge, J. D. (1976a). Mitosis and cytokinesis in the dinoflagellate Amphidinium carterae. *Cytobios*, *17*(65), 35–46.

Oakley, B. R., & Dodge, J. D. (1976b). Mitosis and cytokinesis in the dinoflagellate Amphidinium carterae. *Cytobios*, *17*(65), 35–46.

Okamoto, N., & Keeling, P. (2014). A Comparative Overview of the Flagellar Apparatus of Dinoflagellate, Perkinsids and Colpodellids. *Microorganisms*, *2*(1), 73–91. https://doi.org/10.3390/microorganisms2010073

Okamoto, O. K., & Hastings, J. W. (2003). Genome-wide analysis of redox-regulated genes in a dinoflagellate. *Gene*, *321*, 73–81. https://doi.org/10.1016/j.gene.2003.07.003

Onishi, M., Umen, J. G., Cross, F. R., & Pringle, J. R. (2020). Cleavage-furrow formation without F-actin in *Chlamydomonas*. *Proceedings of the National Academy of Sciences*, *117*(31), 18511–18520. https://doi.org/10.1073/pnas.1920337117

O'Toole, E. T., & Dutcher, S. K. (2014). Site-specific basal body duplication in Chlamydomonas. *Cytoskeleton (Hoboken, N.J.)*, *71*(2), 108–118. https://doi.org/10.1002/cm.21155

Paerl, H. W., & Huisman, J. (2008). CLIMATE: Blooms Like It Hot. *Science*, *320*(5872), 57–58. https://doi.org/10.1126/science.1155398

Paerl, Hans W., Hall, N. S., & Calandrino, E. S. (2011). Controlling harmful cyanobacterial blooms in a world experiencing anthropogenic and climatic-induced change. *Science of The Total Environment*, *409*(10), 1739–1745. https://doi.org/10.1016/j.scitotenv.2011.02.001

Palou, G., Palou, R., Guerra-Moreno, A., Duch, A., Travesa, A., & Quintana, D. G. (2010). Cyclin Regulation by the S Phase Checkpoint. *Journal of Biological Chemistry*, *285*(34), 26431–26440. https://doi.org/10.1074/jbc.M110.138669

Pagano M, Pepperkok R, Verde F, Ansorge W, Draetta G. (1992). Cyclin A is required at two points in the human cell cycle. EMBO J. Mar;11(3):961-71. PMID: 1312467; PMCID: PMC556537.

Paoletti, A., & Chang, F. (2000). Analysis of mid1p, a Protein Required for Placement of the Cell Division Site, Reveals a Link between the Nucleus and the Cell Surface in Fission Yeast. *Molecular Biology of the Cell*, *11*(8), 2757–2773. https://doi.org/10.1091/mbc.11.8.2757

Parsons, M. L., Aligizaki, K., Bottein, M.-Y. D., Fraga, S., Morton, S. L., Penna, A., & Rhodes, L. (2012). Gambierdiscus and Ostreopsis: Reassessment of the state of knowledge of their taxonomy, geography, ecophysiology, and toxicology. *Harmful Algae*, *14*, 107–129. https://doi.org/10.1016/j.hal.2011.10.017

Parsons, M. L., & Preskitt, L. B. (2007). A survey of epiphytic dinoflagellates from the coastal waters of the island of Hawai'i. *Harmful Algae*, *6*(5), 658–669. https://doi.org/10.1016/j.hal.2007.01.001

Patron, N. J., Waller, R. F., Archibald, J. M., & Keeling, P. J. (2005). Complex Protein Targeting to Dinoflagellate Plastids. *Journal of Molecular Biology*, *348*(4), 1015–1024. https://doi.org/10.1016/j.jmb.2005.03.030

Pavaux, A.-S. (2019). *Ecologie chimique du dinoflagellé toxique Ostreopsis cf. Ovata en Méditerranée Nord Occidentale*. http://www.theses.fr/2019SORUS292/document. Thesis

Pavaux, A.-S., Berdalet, E., & Lemée, R. (2020). Chemical Ecology of the Benthic Dinoflagellate Genus Ostreopsis: Review of Progress and Future Directions. *Frontiers in Marine Science*, *7*, 498. https://doi.org/10.3389/fmars.2020.00498

Pavletich, N. P. (1999). Mechanisms of cyclin-dependent kinase regulation: Structures of cdks, their cyclin activators, and cip and INK4 inhibitors. *Journal of Molecular Biology*, *287*(5), 821–828. https://doi.org/10.1006/jmbi.1999.2640

Pearson, C. G., & Winey, M. (2009). Basal Body Assembly in Ciliates: The Power of Numbers. *Traffic*, *10*(5), 461–471. https://doi.org/10.1111/j.1600-0854.2009.00885.x

Peris, L., Thery, M., Fauré, J., Saoudi, Y., Lafanechère, L., Chilton, J. K., Gordon-Weeks, P., Galjart, N., Bornens, M., Wordeman, L., Wehland, J., Andrieux, A., & Job, D. (2006). Tubulin tyrosination is a major factor affecting the recruitment of CAP-Gly proteins at microtubule plus ends. *Journal of Cell Biology*, *174*(6), 839–849. https://doi.org/10.1083/jcb.200512058

Perret, E., Davoust, J., Albert, M., Besseau, L., & Soyer-Gobillard, M. O. (1993). Microtubule organization during the cell cycle of the primitive eukaryote dinoflagellate Crypthecodinium cohnii. *Journal of Cell Science*, *104 (Pt 3)*, 639–651.

Perret, Eric, Albert, M., Bordes, N., Bornens, M., & Soyer-Gobillard, M.-O. (1991). Microtubular spindle and centrosome structures during the cell cycle in a dinoflagellate Crypthecodinium cohnii B.: An immunocytochemical study. *Biosystems*, *25*(1–2), 53–65. https://doi.org/10.1016/0303-2647(91)90012-A

Pickett-Heaps, J. D. (1979). Electron Microscopy and The Phylogeny of Green Algae and Land Plants. *American Zoologist*, *19*(2), 545–554. https://doi.org/10.1093/icb/19.2.545.

Piperno G, LeDizet M, Chang XJ. (1987). Microtubules containing acetylated alpha-tubulin in mammalian cells in culture. *J Cell Biol*. Feb;104(2):289-302. doi: 10.1083/jcb.104.2.289.

Pistocchi, R., Pezzolesi, L., Guerrini, F., Vanucci, S., Dell'Aversano, C., & Fattorusso, E. (2011). A review on the effects of environmental conditions on growth and toxin production of Ostreopsis ovata. *Toxicon*, *57*(3), 421–428. https://doi.org/10.1016/j.toxicon.2010.09.013

Ploubidou, A., Robinson, D. R., Docherty, R. C., Ogbadoyi, E. O., & Gull, K. (1999). Evidence for novel cell cycle checkpoints in trypanosomes: Kinetoplast segregation and cytokinesis in the absence of mitosis. *Journal of Cell Science*, *112 (Pt 24)*, 4641–4650.

Pollard, T. D., & O'Shaughnessy, B. (2019). Molecular Mechanism of Cytokinesis. *Annual Review of Biochemistry*, *88*(1), 661–689. https://doi.org/10.1146/annurev-biochem-062917-012530

Pollard, T. D., & Wu, J.-Q. (2010). Understanding cytokinesis: Lessons from fission yeast. *Nature Reviews Molecular Cell Biology*, *11*(2), 149–155. https://doi.org/10.1038/nrm2834

Pollingher, U., & Zemel, E. (1981). In situ and experimental evidence of the influence of turbulence on cell division processes of *Peridinium cinctum* forma *westii* (Lemm.) Lefèvre. *British Phycological Journal*, *16*(3), 281–287. https://doi.org/10.1080/00071618100650301

Pozdnyakov, I., & Skarlato, S. (n.d.). *Dinoflagellate amphiesma at different stages of the life cycle*. 9.
Preble, A. M., Giddings, T. H., & Dutcher, S. K. (2001). Extragenic bypass suppressors of mutations in the essential gene BLD2 promote assembly of basal bodies with abnormal microtubules in Chlamydomonas reinhardtii. *Genetics*, *157*(1), 163–181.

Prince, E. K., Myers, T. L., & Kubanek, J. (2008). Effects of harmful algal blooms on competitors: Allelopathic mechanisms of the red tide dinoflagellate Karenia brevis. *Limnology and Oceanography*, *53*(2), 531–541. https://doi.org/10.4319/lo.2008.53.2.0531

Prochnik, S. E., Umen, J., Nedelcu, A. M., Hallmann, A., Miller, S. M., Nishii, I., Ferris, P., Kuo, A., Mitros, T., Fritz-Laylin, L. K., Hellsten, U., Chapman, J., Simakov, O., Rensing, S. A., Terry, A., Pangilinan, J., Kapitonov, V., Jurka, J., Salamov, A., … Rokhsar, D. S. (2010). Genomic analysis of organismal complexity in the multicellular green alga Volvox carteri. *Science (New York, N.Y.)*, *329*(5988), 223–226. https://doi.org/10.1126/science.1188800

Qiao, R., Weissmann, F., Yamaguchi, M., Brown, N. G., VanderLinden, R., Imre, R., Jarvis, M. A., Brunner, M. R., Davidson, I. F., Litos, G., Haselbach, D., Mechtler, K., Stark, H., Schulman, B. A., & Peters, J.-M. (2016). Mechanism of APC/C ^{CDC20} activation by mitotic phosphorylation. *Proceedings of the National Academy of Sciences*, *113*(19), E2570–E2578. https://doi.org/10.1073/pnas.1604929113

Quod, J. P. (1994). *Ostreopsis mascarenensis* sp. Nov. (Dinophyceae) dinoflagellé toxique associé á la ciguatéra dans l'Ocean Indien. Cryptogamie, Algologie.

Ravitz, M. J., & Wenner, C. E. (1997). Cyclin-Dependent Kinase Regulation during G1 Phase and Cell Cycle Regulation by TGF-ß. In *Advances in Cancer Research* (Vol. 71, pp. 165–207). Elsevier. https://doi.org/10.1016/S0065-230X(08)60099-8

Rhind, N., & Russell, P. (2012). Signaling Pathways that Regulate Cell Division. *Cold Spring Harbor Perspectives in Biology*, *4*(10), a005942–a005942. https://doi.org/10.1101/cshperspect.a005942

Rhodes, L. (2011). World-wide occurrence of the toxic dinoflagellate genus Ostreopsis Schmidt. *Toxicon*, *57*(3), 400–407. https://doi.org/10.1016/j.toxicon.2010.05.010

Riaz, S., & Sui, Z. (2018). Molecular Cloning, Transcriptome Profiling, and Characterization of Histone Genes in the Dinoflagellate Alexandrium pacificum. *Journal of Microbiology and Biotechnology*, *28*(7), 1185–1198. https://doi.org/10.4014/jmb.1802.01075

Riaz, S., Sui, Z., Niaz, Z., Khan, S., Liu, Y., & Liu, H. (2018). Distinctive Nuclear Features of Dinoflagellates with A Particular Focus on Histone and Histone-Replacement Proteins. *Microorganisms*, *6*(4), 128. https://doi.org/10.3390/microorganisms6040128

Richards, T. A., & Cavalier-Smith, T. (2005). Myosin domain evolution and the primary divergence of

eukaryotes. *Nature*, *436*(7054), 1113–1118. https://doi.org/10.1038/nature03949

Richlen, M. L., Morton, S. L., Barber, P. H., & Lobel, P. S. (2008). Phylogeography, morphological variation and taxonomy of the toxic dinoflagellate Gambierdiscus toxicus (Dinophyceae). *Harmful Algae*, *7*(5), 614–629. https://doi.org/10.1016/j.hal.2007.12.020

Ris, H., & Kubai, D. F. (1974). An unusual mitotic mechanism in the parasitic protozoan Syndinium sp. *Journal of Cell Biology*, *60*(3), 702–720. https://doi.org/10.1083/jcb.60.3.702

Rizzo PJ. (2003). Those amazing dinoflagellate chromosomes. *Cell Res*. Aug;13(4):215-7. doi: 10.1038/sj.cr.7290166. PMID: 12974611.

Robbins, J. A., Absalon, S., Streva, V. A., & Dvorin, J. D. (2017). The Malaria Parasite Cyclin H Homolog PfCyc1 Is Required for Efficient Cytokinesis in Blood-Stage Plasmodium falciparum. *MBio*, *8*(3), mBio.00605-17, e00605-17. https://doi.org/10.1128/mBio.00605-17

Roberts, K. R., & Roberts, J. E. (1991). The flagellar apparatus and cytoskeleton of the dinoflagellates. In M. Melkonian, R. A. Andersen, & E. Schnepf, *The Cytoskeleton of Flagellate and Ciliate Protists* (pp. 105–122). Springer Vienna. https://doi.org/10.1007/978-3-7091-6714-4_10

Rodriguez, M., Cho, J. W., Sauer, H. W., & Rizzo, P. J. (1993). Evidence For the Presence of A Cdc2-Like Protein Kinase In the Dinoflagellate Crypthecodinium Cohnii. *The Journal of Eukaryotic Microbiology*, *40*(1), 91–96. https://doi.org/10.1111/j.1550-7408.1993.tb04887.x

Rodriguez-Rodriguez, J.-A., Moyano, Y., Játiva, S., & Queralt, E. (2016). Mitotic Exit Function of Polo-like Kinase Cdc5 Is Dependent on Sequential Activation by Cdk1. *Cell Reports*, *15*(9), 2050–2062. https://doi.org/10.1016/j.celrep.2016.04.079

Rosic, N. N., & Hoegh-Guldberg, O. (2010). A method for extracting a high-quality RNA from Symbiodinium sp. *Journal of Applied Phycology*, *22*(2), 139–146. https://doi.org/10.1007/s10811-009-9433-x

Roy, S., & Morse, D. (2013). Transcription and Maturation of mRNA in Dinoflagellates. *Microorganisms*, *1*(1), 71–99. https://doi.org/10.3390/microorganisms1010071

Rudlaff, R. M., Kraemer, S., Marshman, J., & Dvorin, J. D. (2020). Three-dimensional ultrastructure of Plasmodium falciparum throughout cytokinesis. *PLOS Pathogens*, *16*(6), e1008587. https://doi.org/10.1371/journal.ppat.1008587

Saldarriaga, J. F., & 'Max' Taylor, F. J. R. (2017). Dinoflagellata. In J. M. Archibald, A. G. B. Simpson, & C. H. Slamovits (Eds.), *Handbook of the Protists* (pp. 625–678). Springer International Publishing. https://doi.org/10.1007/978-3-319-28149-0_22

Salisbury, J. L., Baron, A. T., & Sanders, M. A. (1988). The centrin-based cytoskeleton of Chlamydomonas reinhardtii: Distribution in interphase and mitotic cells. *Journal of Cell Biology*, *107*(2), 635–641. https://doi.org/10.1083/jcb.107.2.635

Sasse, R., & Gull, K. (1988). Tubulin post-translational modifications and the construction of microtubular organelles in Trypanosoma brucei. *Journal of Cell Science*, *90 (Pt 4)*, 577–589.

Scalco, E., Brunet, C., Marino, F., Rossi, R., Soprano, V., Zingone, A., & Montresor, M. (2012). Growth and toxicity responses of Mediterranean Ostreopsis cf. Ovata to seasonal irradiance and temperature conditions. *Harmful Algae*, *17*, 25–34. https://doi.org/10.1016/j.hal.2012.02.008

Scarfone, I., & Piatti, S. (2015). Coupling spindle position with mitotic exit in budding yeast: The multifaceted role of the small GTPase Tem1. *Small GTPases*, *6*(4), 196–201. https://doi.org/10.1080/21541248.2015.1109023

Schmidt, J. (1901). Flora of Koh Chang. Contributions to the knowledge of the vegetation in the Gulf of Siam. Preliminary Report on the Botanical Results of the Danish Expedition to Siam 1899-1900. Bianco Luno.

Schnepf, E. (1988). Cytochalasin D inhibits completion of cytokinesis and affects theca formation in dinoflagellates. *Protoplasma*, *143*(1), 22–28. https://doi.org/10.1007/BF01282955

Schnepf, Eberhard, & ElbräChter, M. (1999). Dinophyte chloroplasts and phylogeny—A review. *Grana*, *38*(2–3), 81–97. https://doi.org/10.1080/00173139908559217

Schnepf, Eberhard, Winter, S., Storck, I., & Quader, H. (1990). A complementary experimental study of cell division in the dinoflagellate Prorocentrum micans. *European Journal of Protistology*, *25*(3), 234–242. https://doi.org/10.1016/S0932-4739(11)80175-6

Sekida, S., Takahira, M., Horiguchi, T., & Okuda, K. (2012). Effects of high pressure in the armored dinoflagellate scrippsiella hexapraecingula (peridiniales, dinophyceae): changes in thecal plate pattern and microtubule assembly1: changes in thecal plate pattern. *Journal of Phycology*, *48*(1), 163–173. https://doi.org/10.1111/j.1529-8817.2011.01094.x

Sellner, K. G., Doucette, G. J., & Kirkpatrick, G. J. (2003). Harmful algal blooms: Causes, impacts and detection. *Journal of Industrial Microbiology and Biotechnology*, *30*(7), 383–406. https://doi.org/10.1007/s10295-003-0074-9

Shears, N. T., & Ross, P. M. (2009). Blooms of benthic dinoflagellates of the genus Ostreopsis; an increasing and ecologically important phenomenon on temperate reefs in New Zealand and worldwide. *Harmful Algae*, *8*(6), 916–925. https://doi.org/10.1016/j.hal.2009.05.003

Sheng, J., Malkiel, E., Katz, J., Adolf, J., Belas, R., & Place, A. R. (2007). Digital holographic microscopy reveals prey-induced changes in swimming behavior of predatory dinoflagellates. *Proceedings of the National Academy of Sciences*, *104*(44), 17512–17517. https://doi.org/10.1073/pnas.0704658104

Shi, X., Ma, M., & Lin, S. (2017). Cell Cycle-Dependent Expression Dynamics of G1/S Specific Cyclin, Cellulose Synthase and Cellulase in the Dinoflagellate Prorocentrum donghaiense. *Frontiers in Microbiology*, *8*, 1118. https://doi.org/10.3389/fmicb.2017.01118

Shida, T., Cueva, J. G., Xu, Z., Goodman, M. B., & Nachury, M. V. (2010). The major -tubulin K40 acetyltransferase TAT1 promotes rapid ciliogenesis and efficient mechanosensation. *Proceedings of the National Academy of Sciences*, *107*(50), 21517–21522. https://doi.org/10.1073/pnas.1013728107

Shikata, T., Matsunaga, S., Nishide, H., Sakamoto, S., Onistuka, G., & Yamaguchi, M. (2015). Diurnal vertical migration rhythms and their photoresponse in four phytoflagellates causing harmful algal blooms: Phytoflagellate vertical migration rhythms. *Limnology and Oceanography*, *60*(4), 1251–1264. https://doi.org/10.1002/lno.10095

Shoguchi, E., Shinzato, C., Kawashima, T., Gyoja, F., Mungpakdee, S., Koyanagi, R., Takeuchi, T., Hisata, K., Tanaka, M., Fujiwara, M., Hamada, M., Seidi, A., Fujie, M., Usami, T., Goto, H., Yamasaki, S., Arakaki, N., Suzuki, Y., Sugano, S., … Satoh, N. (2013). Draft assembly of the Symbiodinium minutum nuclear genome reveals dinoflagellate gene structure. *Current Biology: CB*, *23*(15), 1399–1408. https://doi.org/10.1016/j.cub.2013.05.062

Silflow, C. D., Liu, B., LaVoie, M., Richardson, E. A., & Palevitz, B. A. (1999). Gamma-tubulin in Chlamydomonas: Characterization of the gene and localization of the gene product in cells. *Cell Motility and the Cytoskeleton*, *42*(4), 285–297. https://doi.org/10.1002/(SICI)1097-0169(1999)42:4<285::AID-CM3>3.0.CO;2-Z

Silva, P. M. A., Reis, R. M., Bolanos-Garcia, V. M., Florindo, C., Tavares, Á. A., & Bousbaa, H. (2014). Dynein-dependent transport of spindle assembly checkpoint proteins off kinetochores toward spindle poles. *FEBS Letters*, *588*(17), 3265–3273. https://doi.org/10.1016/j.febslet.2014.07.011

Smayda, T. J., & Reynolds, C. S. (2003). Strategies of marine dinoflagellate survival and some rules of assembly. *Journal of Sea Research*, *49*(2), 95–106. https://doi.org/10.1016/S1385-1101(02)00219-8

Song, Y., & Brady, S. T. (2015). Post-translational modifications of tubulin: Pathways to functional diversity of microtubules. *Trends in Cell Biology*, *25*(3), 125–136. https://doi.org/10.1016/j.tcb.2014.10.004

Souto-Padron, T., Cunha e Silva, N. L., & Souza, W. de. (1993). Acetylated alpha-tubulin in Trypanosoma cruzi: Immunocytochemical localization. *Memórias Do Instituto Oswaldo Cruz*, *88*(4), 517–528. https://doi.org/10.1590/S0074-02761993000400004

Soyer, M.-O., & Haapala, O. K. (1974). Structural changes of dinoflagellate chromosomes by pronase and ribonuclease. *Chromosoma*, *47*(2), 179–192. https://doi.org/10.1007/BF00331805

Soyer, M.-O. (1977). Mise en évidence et rôle des microtubules paranucléaires chez Prorocentrum micans E. (Dinoflagellé libre) C. R. Acad. Sci. Paris, Sér. D, 285. pp. 693-696

Soyer, M.-O., Géraud M.L., Coulaud D., Barray M., Théveny B., Révet B., Delain E. (1990) Location of B-and Z-DNA in the chromosomes of a primitive eukaryote dinoflagellate. *J. Cell Biol.* 111:293–304. doi: 10.1083/jcb.111.2.293.

Soyer, M.-O., Ausseil, J., & Géraud, M.-L. (1996). Nuclear and cytoplasmic actin in dinoflagellates. *Biology of the Cell*, *87*(1–2), 17–35. https://doi.org/10.1111/j.1768-322X.1996.tb00963.x

Soyer, M.-O., Besseau, L., Géraud, M.-L., Guillebault, D., Albert, M., & Perret, E. (2002). Cytoskeleton and mitosis in the dinoflagellate Crypthecodinium cohnii: Immunolocalization of P72, an HSP70-related protein. *European Journal of Protistology*, *38*(2), 155–170. https://doi.org/10.1078/0932-4739-00871

Soyer, M.-O. (2006). Edouard Chatton (1883-1947) and the dinoflagellate protists: Concepts and models. *International Microbiology: The Official Journal of the Spanish Society for Microbiology*, *9*(3), 173–177.

Spector, D. L. (Ed.). (1984). *Dinoflagellates*. Academic Press.

Spector, D. L., & Triemer, R. E. (1981). Chromosome structure and mitosis in the dinoflagellates: An ultrastructural approach to an evolutionary problem. *Biosystems*, *14*(3–4), 289–298. https://doi.org/10.1016/0303-2647(81)90035-6

Spreng, B., Fleckenstein, H., Kübler, P., Di Biagio, C., Benz, M., Patra, P., Schwarz, U. S., Cyrklaff, M., & Frischknecht, F. (2019). Microtubule number and length determine cellular shape and function in *Plasmodium*. *The EMBO Journal*, *38*(15). https://doi.org/10.15252/embj.2018100984

Stires, J. C., & Latz, M. I. (2018). Contribution of the cytoskeleton to mechanosensitivity reported by dinoflagellate bioluminescence. *Cytoskeleton*, *75*(1), 12–21. https://doi.org/10.1002/cm.21392

Stolte, W., & Garcés, E. (2006). Ecological Aspects of Harmful Algal In Situ Population Growth Rates. In Edna Granéli & J. T. Turner (Eds.), *Ecology of Harmful Algae* (pp. 139–152). Springer Berlin Heidelberg. https://doi.org/10.1007/978-3-540-32210-8_11

Strassert, J. F. H., Jamy, M., Mylnikov, A. P., Tikhonenkov, D. V., & Burki, F. (2019). New Phylogenomic Analysis of the Enigmatic Phylum Telonemia Further Resolves the Eukaryote Tree of Life. *Molecular Biology and Evolution*, *36*(4), 757–765. https://doi.org/10.1093/molbev/msz012

Strickland, L. I., Donnelly, E. J., & Burgess, D. R. (2005). Induction of Cytokinesis Is Independent of Precisely Regulated Microtubule Dynamics. *Molecular Biology of the Cell*, *16*(10), 4485–4494. https://doi.org/10.1091/mbc.e05-04-0305

Striepen, B., Jordan, C. N., Reiff, S., & van Dooren, G. G. (2007). Building the perfect parasite: Cell division in apicomplexa. *PLoS Pathogens*, *3*(6), e78. https://doi.org/10.1371/journal.ppat.0030078

Strom, S. L., & Morello, T. A. (1998). Comparative growth rates and yields of ciliates and heterotrophic dinoflagellates. *Journal of Plankton Research*, *20*(3), 571–584. https://doi.org/10.1093/plankt/20.3.571

Sudakin, V., Chan, G. K. T., & Yen, T. J. (2001). Checkpoint inhibition of the APC/C in HeLa cells is mediated by a complex of BUBR1, BUB3, CDC20, and MAD2. *Journal of Cell Biology*, *154*(5), 925–936. https://doi.org/10.1083/jcb.200102093

Sutani, T., Yuasa, T., Tomonaga, T., Dohmae, N., Takio, K., & Yanagida, M. (1999). Fission yeast condensin

complex: Essential roles of non-SMC subunits for condensation and Cdc2 phosphorylation of Cut3/SMC4. *Genes & Development*, *13*(17), 2271–2283. https://doi.org/10.1101/gad.13.17.2271

Suzuki, A., Badger, B. L., Wan, X., DeLuca, J. G., & Salmon, E. D. (2014). The Architecture of CCAN Proteins Creates a Structural Integrity to Resist Spindle Forces and Achieve Proper Intrakinetochore Stretch. *Developmental Cell*, *30*(6), 717–730. https://doi.org/10.1016/j.devcel.2014.08.003

Sweeney, B. M. (1982). Interaction of the Circadian Cycle with the Cell Cycle in *Pyrocystis fusiformis*. *Plant Physiology*, *70*(1), 272–276. https://doi.org/10.1104/pp.70.1.272

Szyk, A., Deaconescu, A. M., Piszczek, G., & Roll-Mecak, A. (2011). Tubulin tyrosine ligase structure reveals adaptation of an ancient fold to bind and modify tubulin. *Nature Structural & Molecular Biology*, *18*(11), 1250–1258. https://doi.org/10.1038/nsmb.2148

Tamura, M., Shimada, S., & Horiguchi, T. (2005). Galeidiniium rugatum gen. Et sp. Nov. (dinophyceae), a new coccoid dinoflagellate with a diatom endosymbiont1: dinoflagellate with a diatom endosymbiont. *Journal of Phycology*, *41*(3), 658–671. https://doi.org/10.1111/j.1529-8817.2005.00085.x

Talbert, P., Henikoff, S. (2012). Chromatin: Packaging without Nucleosomes. *Curr. biol. 22(24):*R1040-3. doi: 10.1016/j.cub.2012.10.052.

Tang, E. P. Y. (1996). Why do dinoflagellates have lower growth rates?1. *Journal of Phycology*, *32*(1), 80–84. https://doi.org/10.1111/j.0022-3646.1996.00080.x

Tanimoto, Y., Yamaguchi, H., Yoshimatsu, T., Sato, S., & Adachi, M. (2013). Effects of temperature, salinity and their interaction on growth of toxic Ostreopsis sp. 1 and Ostreopsis sp. 6 (Dinophyceae) isolated from Japanese coastal waters. *Fisheries Science*, *79*(2), 285–291. https://doi.org/10.1007/s12562-013-0597-6

Tawong, W., Yoshimatsu, T., Yamaguchi, H., & Adachi, M. (2015). Effects of temperature, salinity and their interaction on growth of benthic dinoflagellates Ostreopsis spp. From Thailand. *Harmful Algae*, *44*, 37–45. https://doi.org/10.1016/j.hal.2015.02.011

Ternon, E., Paix, B., Thomas, O. P., Briand, J.-F., & Culioli, G. (2020). Exploring the Role of Macroalgal Surface Metabolites on the Settlement of the Benthic Dinoflagellate Ostreopsis cf. Ovata. *Frontiers in Marine Science*, *7*, 683. https://doi.org/10.3389/fmars.2020.00683

Tester, P. A., Litaker, R. W., & Berdalet, E. (2020). Climate change and harmful benthic microalgae. *Harmful Algae*, *91*, 101655. https://doi.org/10.1016/j.hal.2019.101655

Tichadou, L., Glaizal, M., Armengaud, A., Grossel, H., Lemée, R., Kantin, R., Lasalle, J.-L., Drouet, G., Rambaud, L., Malfait, P., & de Haro, L. (2010). Health impact of unicellular algae of the *Ostreopsis* genus blooms in the Mediterranean Sea: Experience of the French Mediterranean coast surveillance network from 2006 to 2009. *Clinical Toxicology*, *48*(8), 839–844. https://doi.org/10.3109/15563650.2010.513687

Tippit, D. H., & Pickett-Heaps, J. D. (1976). Apparent amitosis in the binucleate dinoflagellate Peridinium balticum. *Journal of Cell Science*, *21*(2), 273–289.

Tognetto, L., Bellato, S., Moro, I., & Andreoli, C. (1995). Occurrence of Ostreopsis ovata (Dinophyceae) in the Tyrrhenian Sea during Summer 1994. *Botanica Marina*, *38*(1–6). https://doi.org/10.1515/botm.1995.38.1-6.291

Totti, C., Accoroni, S., Cerino, F., Cucchiari, E., & Romagnoli, T. (2010). Ostreopsis ovata bloom along the Conero Riviera (northern Adriatic Sea): Relationships with environmental conditions and substrata. *Harmful Algae*, *9*(2), 233–239. https://doi.org/10.1016/j.hal.2009.10.006

Tromer, E., Bade, D., Snel, B., & Kops, G. J. P. L. (2016). Phylogenomics-guided discovery of a novel conserved cassette of short linear motifs in BubR1 essential for the spindle checkpoint. *Open Biology*, *6*(12), 160315. https://doi.org/10.1098/rsob.160315

Tulin, F., & Cross, F. R. (2015). Cyclin-Dependent Kinase Regulation of Diurnal Transcription in Chlamydomonas. *The Plant Cell*, *27*(10), 2727–2742. https://doi.org/10.1105/tpc.15.00400

Uzbekov, R. E. (Ed.). (2018). *Flagella and cilia: Types, structure and functions*. Nova Science Publishers.
Van Dolah, F. M., Lidie, K. B., Morey, J. S., Brunelle, S. A., Ryan, J. C., Monroe, E. A., & Haynes, B. L. (2007). Microarray analysis of diurnal- and circadian-regulated genes in the florida red-tide dinoflagellate *Karenia brevis* (dinophyceae) [1]. *Journal of Phycology*, *43*(4), 741–752. https://doi.org/10.1111/j.1529-8817.2007.00354.x

van Oostende-Triplet, C., Guillet, D., Triplet, T., Pandzic, E., Wiseman, P. W., & Geitmann, A. (2017). Vesicle Dynamics during Plant Cell Cytokinesis Reveals Distinct Developmental Phases. *Plant Physiology*, *174*(3), 1544–1558. https://doi.org/10.1104/pp.17.00343

Vandré, D. D., & Wills, V. L. (1992). Inhibition of mitosis by okadaic acid: Possible involvement of a protein phosphatase 2A in the transition from metaphase to anaphase. *Journal of Cell Science*, *101 (Pt 1)*, 79–91.

Vanucci, S., Pezzolesi, L., Pistocchi, R., Ciminiello, P., Dell'Aversano, C., Iacovo, E. D., Fattorusso, E., Tartaglione, L., & Guerrini, F. (2012). Nitrogen and phosphorus limitation effects on cell growth, biovolume, and toxin production in Ostreopsis cf. Ovata. *Harmful Algae*, *15*, 78–90. https://doi.org/10.1016/j.hal.2011.12.003

Vardi, A., Berman-Frank, I., Rozenberg, T., Hadas, O., Kaplan, A., & Levine, A. (1999). Programmed cell death of the dinoflagellate Peridinium gatunense is mediated by CO2 limitation and oxidative stress. *Current Biology*, *9*(18), 1061–1064. https://doi.org/10.1016/S0960-9822(99)80459-X

Vaughan, S., & Gull, K. (2003). The trypanosome flagellum. *Journal of Cell Science*, *116*(Pt 5), 757–759. https://doi.org/10.1242/jcs.00287

Vaughan, S., & Gull, K. (2015). Basal body structure and cell cycle-dependent biogenesis in Trypanosoma brucei. *Cilia*, *5*, 5. https://doi.org/10.1186/s13630-016-0023-7

Vaulot, D., Olson, R. J., & Chisholm, S. W. (1986). Light and dark control of the cell cycle in two marine phytoplankton species. *Experimental Cell Research*, *167*(1), 38–52. https://doi.org/10.1016/0014-4827(86)90202-8

Verma, A., Barua, A., Ruvindy, R., Savela, H., Ajani, P. A., & Murray, S. A. (2019). The Genetic Basis of Toxin Biosynthesis in Dinoflagellates. *Microorganisms*, *7*(8), 222. https://doi.org/10.3390/microorganisms7080222

Verma, A., Kohli, G. S., Harwood, D. T., Ralph, P. J., & Murray, S. A. (2019). Transcriptomic investigation into polyketide toxin synthesis in *Ostreopsis* (Dinophyceae) species. *Environmental Microbiology*, *21*(11), 4196–4211. https://doi.org/10.1111/1462-2920.14780

Vicker, M. G., Becker, J., Gebauer, G., Schill, W., & Rensing, L. (1988). Circadian Rhythms of Cell Cycle Processes in the Marine Dinoflagellate Gonyaulax Polyedra. *Chronobiology International*, *5*(1), 5–17. https://doi.org/10.3109/07420528809078548

Vidyarathna, N. K., & Granéli, E. (2013). Physiological responses of Ostreopsis ovata to changes in N and P availability and temperature increase. *Harmful Algae*, *21–22*, 54–63. https://doi.org/10.1016/j.hal.2012.11.006

Vila, M., Garcés, E., & Masó, M. (2001). Potentially toxic epiphytic dinoflagellate assemblages on macroalgae in the NW Mediterranean. *Aquatic Microbial Ecology*, *26*, 51–60. https://doi.org/10.3354/ame026051

Villanueva, M. A., Arzápalo-Castañeda, G., & Castillo-Medina, R. E. (2014). The actin cytoskeleton organization and disorganization properties of the photosynthetic dinoflagellate *Symbiodinium kawagutii* in culture. *Canadian Journal of Microbiology*, *60*(11), 767–775. https://doi.org/10.1139/cjm-2014-0325

Visintin, R. (1997). CDC20 and CDH1: A Family of Substrate-Specific Activators of APC-Dependent Proteolysis. *Science*, *278*(5337), 460–463. https://doi.org/10.1126/science.278.5337.460

Visser, P. M., Verspagen, J. M. H., Sandrini, G., Stal, L. J., Matthijs, H. C. P., Davis, T. W., Paerl, H. W., & Huisman, J. (2016). How rising CO2 and global warming may stimulate harmful cyanobacterial blooms. *Harmful Algae*, *54*, 145–159. https://doi.org/10.1016/j.hal.2015.12.006

Wake, D. (2016). *Encyclopedia of Evolutionary Biology*. Elsevier Science. http://public.ebookcentral.proquest.com/choice/publicfullrecord.aspx?p=4523082

Waller, R. F., & Kořený, L. (2017). Plastid Complexity in Dinoflagellates: A Picture of Gains, Losses, Replacements and Revisions. In *Advances in Botanical Research* (Vol. 84, pp. 105–143). Elsevier. https://doi.org/10.1016/bs.abr.2017.06.004

Wang, D.-Z., Zhang, Y.-J., Zhang, S.-F., Lin, L., & Hong, H.-S. (2013). Quantitative Proteomic Analysis of Cell Cycle of the Dinoflagellate Prorocentrum donghaiense (Dinophyceae). *PLoS ONE*, *8*(5), e63659. https://doi.org/10.1371/journal.pone.0063659

Wang, L., Piao, T., Cao, M., Qin, T., Huang, L., Deng, H., Mao, T., & Pan, J. (2013). Flagellar regeneration requires cytoplasmic microtubule depolymerization and kinesin-13. *Journal of Cell Science*, *126*(6), 1531–1540. https://doi.org/10.1242/jcs.124255

Wang, L.-H., Liu, Y.-H., Ju, Y.-M., Hsiao, Y.-Y., Fang, L.-S., & Chen, C.-S. (2008a). Cell cycle propagation is driven by light–dark stimulation in a cultured symbiotic dinoflagellate isolated from corals. *Coral Reefs*, *27*(4), 823–835. https://doi.org/10.1007/s00338-008-0434-z

Wang, S.-W., Read, R. L., & Norbury, C. J. (2002). Fission yeast Pds5 is required for accurate chromosome segregation and for survival after DNA damage or metaphase arrest. *Journal of Cell Science*, *115*(Pt 3), 587–598.

Ward, N., & Moreno-Hagelsieb, G. (2014). Quickly finding orthologs as reciprocal best hits with BLAT, LAST, and UBLAST: How much do we miss? *PloS One*, *9*(7), e101850. https://doi.org/10.1371/journal.pone.0101850

Watson, S. B., Whitton, B. A., Higgins, S. N., Paerl, H. W., Brooks, B. W., & Wehr, J. D. (2015). Harmful Algal Blooms. In *Freshwater Algae of North America* (pp. 873–920). Elsevier. https://doi.org/10.1016/B978-0-12-385876-4.00020-7

Webster, D. R. (1990). Detyrosination of alpha tubulin does not stabilize microtubules in vivo [published erratum appears in J Cell Biol 1990 Sep;111(3):1325-6]. *The Journal of Cell Biology*, *111*(1), 113–122. https://doi.org/10.1083/jcb.111.1.113

Weiss, E., & Winey, M. (1996). The Saccharomyces cerevisiae spindle pole body duplication gene MPS1 is part of a mitotic checkpoint. *Journal of Cell Biology*, *132*(1), 111–123. https://doi.org/10.1083/jcb.132.1.111

Werner, M., Munro, E., & Glotzer, M. (2007). Astral signals spatially bias cortical myosin recruitment to break symmetry and promote cytokinesis. *Current Biology: CB*, *17*(15), 1286–1297. https://doi.org/10.1016/j.cub.2007.06.070

Westhorpe, F. G., Tighe, A., Lara-Gonzalez, P., & Taylor, S. S. (2011). P31comet-mediated extraction of Mad2 from the MCC promotes efficient mitotic exit. *Journal of Cell Science*, *124*(22), 3905–3916. https://doi.org/10.1242/jcs.093286

Wetherbee, R. (1975). The fine structure of ceratium tripos, a marine armored dinoflagellate. *Journal of Ultrastructure Research*, *50*(1), 77–88. https://doi.org/10.1016/S0022-5320(75)90010-6

Wetherbee R, Platt SJ, Beech PL, Pickett-Heaps JD, (1988). Flagellar transformation in the heterokont Epipyxis pulchra (Chrysophy-ceae): direct observations using image enhanced light microscopy. Protoplasma 145: 47–54

White, M. W., & Suvorova, E. S. (2018). Apicomplexa Cell Cycles: Something Old, Borrowed, Lost, and New. *Trends in Parasitology*, *34*(9), 759–771. https://doi.org/10.1016/j.pt.2018.07.006

Wiese, C., & Zheng, Y. (2006). Microtubule nucleation: -Tubulin and beyond. *Journal of Cell Science*, *119*(20), 4143–4153. https://doi.org/10.1242/jcs.03226

Wieser, S., & Pines, J. (2015). The Biochemistry of Mitosis. *Cold Spring Harbor Perspectives in Biology*, *7*(3), a015776. https://doi.org/10.1101/cshperspect.a015776

Wisecaver, J. H., & Hackett, J. D. (2011). Dinoflagellate Genome Evolution. *Annual Review of Microbiology*, *65*(1), 369–387. https://doi.org/10.1146/annurev-micro-090110-102841

Wloka, C., & Bi, E. (2012). Mechanisms of cytokinesis in budding yeast. *Cytoskeleton (Hoboken, N.J.)*, *69*(10), 710–726. https://doi.org/10.1002/cm.21046

Woelfle, M. A., & Johnson, C. H. (2006). No Promoter Left Behind: Global Circadian Gene Expression in Cyanobacteria. *Journal of Biological Rhythms*, *21*(6), 419–431. https://doi.org/10.1177/0748730406294418

Wolf, K. (1995). Acetylation of α-tubilin in different bovine cell types: Implications for microtubule dynamics in interphase and mitosis. *Cell Biology International*, *19*(1), 43–52. https://doi.org/10.1006/cbir.1995.1006

Wolf, K. W., & Spanel-Borowski, K. (1992). The interphase microtubule cytoskeleton of five different phenotypes of microvessel endothelial cell cultures derived from bovine corpus luteum. *Tissue & Cell*, *24*(3), 347–354. https://doi.org/10.1016/0040-8166(92)90051-8

Wong, J. T. Y., & Kwok, A. C. M. (2005). Proliferation of dinoflagellates: Blooming or bleaching. *BioEssays*, *27*(7), 730–740. https://doi.org/10.1002/bies.20250

Wong, J. T. Y., & Whiteley, A. (1996). An improved method of cell cycle synchronisation for the heterotrophic dinoflagellate Crypthecodinium cohnii Biecheler analyzed by flow cytometry. *Journal of Experimental Marine Biology and Ecology*, *197*(1), 91–99. https://doi.org/10.1016/0022-0981(95)00146-8

Woodruff, J. B., Wueseke, O., & Hyman, A. A. (2014). Pericentriolar material structure and dynamics. *Philosophical Transactions of the Royal Society B: Biological Sciences*, *369*(1650), 20130459. https://doi.org/10.1098/rstb.2013.0459

Yamaguchi, H., Tomori, Y., Tanimoto, Y., Oku, O., & Adachi, M. (2014). Evaluation of the effects of light intensity on growth of the benthic dinoflagellate Ostreopsis sp. 1 using a newly developed photoirradiation-culture system and a novel regression analytical method. *Harmful Algae*, *39*, 48–54. https://doi.org/10.1016/j.hal.2014.06.011

Yamaguchi, H., Yoshimatsu, T., Tanimoto, Y., Sato, S., Nishimura, T., Uehara, K., & Adachi, M. (2012). Effects of temperature, salinity and their interaction on growth of the benthic dinoflagellate *Ostreopsis* cf. *ovata* (Dinophyceae) from Japanese coastal waters: Growth features of Japanese *O.* cf. *ovata*. *Phycological Research*, *60*(4), 297–304. https://doi.org/10.1111/j.1440-1835.2012.00660.x

Yang, M., Li, B., Tomchick, D. R., Machius, M., Rizo, J., Yu, H., & Luo, X. (2007). P31comet blocks Mad2 activation through structural mimicry. *Cell*, *131*(4), 744–755. https://doi.org/10.1016/j.cell.2007.08.048

Yellman, C. M., & Roeder, G. S. (2015). Cdc14 Early Anaphase Release, FEAR, Is Limited to the Nucleus and Dispensable for Efficient Mitotic Exit. *PLOS ONE*, *10*(6), e0128604. https://doi.org/10.1371/journal.pone.0128604

Yeung, P. K. K., New, D. C., Leveson, A., Yam, C. H., Poon, R. Y. C., & Wong, J. T. Y. (2000). The Spindle Checkpoint in the Dinoflagellate Crypthecodinium cohnii. *Experimental Cell Research*, *254*(1), 120–129. https://doi.org/10.1006/excr.1999.4749

Yu, L., Zhang, Y., Li, M., Wang, C., Lin, X., Li, L., Shi, X., Guo, C., & Lin, S. (2020). Comparative metatranscriptomic profiling and microRNA sequencing to reveal active metabolic pathways associated with a dinoflagellate bloom. *Science of The Total Environment*, *699*, 134323. https://doi.org/10.1016/j.scitotenv.2019.134323

Zaccaroni, A., & Scaravelli, D. (2008). Toxicity of Sea Algal Toxins to Humans and Animals. In V. Evangelista, L. Barsanti, A. M. Frassanito, V. Passarelli, & P. Gualtieri (Eds.), *Algal Toxins: Nature, Occurrence, Effect and Detection* (pp. 91–158). Springer Netherlands. https://doi.org/10.1007/978-1-4020-8480-5_4

Zapata, M., Fraga, S., Rodríguez, F., & Garrido, J. (2012). Pigment-based chloroplast types in dinoflagellates. *Marine Ecology Progress Series*, *465*, 33–52. https://doi.org/10.3354/meps09879

Zhang, S.-F., Zhang, Y., Lin, L., & Wang, D.-Z. (2018). ITRAQ-Based Quantitative Proteomic Analysis of a Toxigenic Dinoflagellate Alexandrium catenella and Its Non-toxigenic Mutant Exposed to a Cell Cycle Inhibitor Colchicine. *Frontiers in Microbiology*, *9*, 650. https://doi.org/10.3389/fmicb.2018.00650

Zhuang, Y., Zhang, H., & Lin, S. (2013). Cyclin B gene and its cell cycle-dependent differential expression in the toxic dinoflagellate Alexandrium fundyense Atama Group I/Clade I. *Harmful Algae*, *26*, 71–79. https://doi.org/10.1016/j.hal.2013.04.002

Zingone, A., Montresor, M., & Marino, D. (1998). Morphological variability of the potentially toxic dinoflagellate *Dinophysis sacculus* (Dinophyceae) and its taxonomic relationships with *D. pavillardii* and *D. acuminata*. *European Journal of Phycology*, *33*(3), 259–273. https://doi.org/10.1080/09670269810001736763

Zingone, A., & Oksfeldt Enevoldsen, H. (2000). The diversity of harmful algal blooms: A challenge for science and management. *Ocean & Coastal Management*, *43*(8–9), 725–748. https://doi.org/10.1016/S0964-5691(00)00056-9

Annexes

Annex 1. Article to be submitted

Vertical distributions of *Ostreopsis* cf. *ovata* in NW Mediterranean Sea: impact on monitoring strategy

Anne-Sophie Pavaux [1*], David Velasquez[2], Kevin Drouet[1], Anais Lebrun[1], Alan Hiroux[1], Sophie Marro[1], Elisabeth Christians[2], Stefania Castagnetti[2], Rodolphe Lemée[1]

[1] Sorbonne Université, CNRS, Laboratoire d'Océanographie de Villefranche, LOV, F-06230, Villefranche-sur-Mer, France ;
[2] Sorbonne Université, CNRS, Laboratoire de Biologie du Développement de Villefranche-sur-Mer (LBDV), Sorbonne Université, 06230 Villefranche-sur-Mer, France ;

* Correspondence: annesophie.pavaux@gmail.com;

Highlights:

- *Ostreopsis* cf. *ovata* abundances vary over a 24-hour cycle
- Cell concentration peaks at different times depending on depth
- Cells division occurs during the night
- Daily variation has a great impact on monitoring strategy

Abstract:

Ostreopsis cf. *ovata* is a benthic and epiphytic dinoflagellate very common in tropical and temperate coastal areas, particularly in the Mediterranean Sea. This benthic dinoflagellate has also already been described as present free in the water column or aggregated at the sea water surface. However, the mechanisms of its resuspension have been poorly documented. To study this resuspension, a high-frequency temporal monitoring was conducted in the Villefranche bay (France) to determine the abundance of (1) epibenthic cells attached to macroalgae, (2) planktonic cells in the water column and (3) cells aggregated at the sea water surface. This monitoring was realized over 3 consecutive years (2018, 2019 and 2020) and at different phase of the bloom (exponential – 2020, peak – 2019 and decline phase – 2018). Strong variations in *O.* cf. *ovata* abundances was observed over a 24-hour cycle with a peak of abundances during the day and a strong decrease at night for all the 3 years monitored except in 2020 when the benthic abundances did not differ significantly between night and day. Moreover, the peak of abundance was first reached for epibenthic cells and later for planktonic and sea-surface cells. An increase in the size of both planktonic and epibenthic cells was also observed along the day, probably due to cell growth following their divisions during the night.

Monitoring of *O.* cf. *ovata* is currently based on a single sampling per day without precise indications of time of sampling and shows great variability in *O.* cf. *ovata* abundance. Our observations of daily variations in cell abundance along the water column clearly indicates that time and place of sampling constitute a great source of variability in the determination of *O.* cf. *ovata* abundance and have to be considered when designing new monitoring strategies to reduce variability and to harmonize data acquisition.

Key words: *Ostreopsis* cf. *ovata*, monitoring, cell division, vertical distribution

1. Introduction

Over the past decades, reports of *Ostreopsis* cf. *ovata* blooms have increased worldwide, both in terms of their geographical distribution and of their intensity and frequency (Accoroni et al., 2020, 2012; Cohu et al., 2011; Nascimento et al., 2012a, 2012b, 2020; Pfannkuchen et al., 2012; Tibiriçá et al., 2019). Blooms of *O*. cf. *ovata* have become more regular in temperate areas and notably in the Mediterranean Sea where they were associated with numerous human intoxications and hospitalisations caused by toxins produced by *O.* cf. *ovata* (Brescianini et al., 2006; Del Favero et al., 2012; Durando et al., 2007; Gallitelli et al., 2005; Illoul et al., 2012; Kermarec et al., 2008; Pavaux et al., 2020; Sansoni et al., 2003; Tichadou et al., 2010; Vila et al., 2016).

Ostreopsis cf. *ovata* is predominantly described as a benthic dinoflagellate, growing as epiphyte on macroalgae (or other abiotic substrates as rocks), thanks to the production of a complex mucilaginous matrix, increasing the adherence of cells on the substrates (Escalera et al., 2014; Honsell et al., 2013). Few papers have previously described *O*. cf. *ovata* as present free in the water column (Mangialajo et al., 2011; Pavaux et al., 2020; Vila et al., 2001) or even aggregated at the water surface (Jauzein et al., 2018; Vila et al., 2001). Due to this vertical distribution, the monitoring of *O*. cf. *ovata* is based on both planktonic and benthic samples (Cohu et al., 2011). Such vertical resuspension could strongly affect the monitoring of *O.* cf. *ovata*, already highly challenging by the absence of worldwide harmonization of the sampling method and the patchy distribution of this dinoflagellate. However, mechanisms underlying this vertical resuspension remain poorly documented, even if thermal winds or hydrodynamism has been described as factors favouring this phenomenon (Mangialajo et al., 2011; Vila et al., 2016). An exogen migration leading to such a vertical distribution has never been studied for *O.* cf. *ovata* although active migration has been already determined for other dinoflagellates such as *Alexandrium tamarense* or *Prorocentrum redfieldi* (Eppley et al., 1968; Hasle, 1950; Ralston et al., 2007; Staker and Bruno, 1980). Indeed, active vertical migration is an important adaptation of many dinoflagellates to (i) retrieve subsurface nutrients (Cullen, 1985; Fauchot et al., 2005), (ii) to avoid irradiance (Ault, 2000; Happey-Wood, 1976), and (iii) to overcome energetic turbulence near the surface (Smayda, 1997; Sullivan et al., 2003) conferring potential ecological advantages to dinoflagellates, over passives organisms (Ralston et al., 2007). For many dinoflagellates, vertical migration depends on complex mechanisms based on light and nutrient distribution as well as the nutritional state of the organisms. According to Ralston et al. (2007), generalization of factors explaining vertical migrations remain difficult because of intraspecific variability leading to different migration strategies or even no migration at all. Olsson and Granéli (1991) have also suggested a link between cell division and vertical migration since phased cell division could occur at depth to minimize grazing pression.

The aim of this study is thus to better characterize the resuspension of *O*. cf. *ovata* in the water column, using high temporal frequency monitoring of *O.* cf. *ovata* abundances at 3 different depths (on macroalgae, in the water column and at the sea water surface. Life cycle of *O.* cf. *ovata* cells (mitotic asexual division) was studied in the collected natural samples of *O*. cf. *ovata*, as it could be linked to the resuspension. Finally, consequences of this resuspension on monitoring strategies were discussed in order to improve these strategies.

2. Materials and methods

2.1. Sampling site

Samples were collected in a small creek of the Villefranche Bay (Rochambeau), French Mediterranean coast (Figure 1 - 43°41′34.83″ N and 7°18′31.66″ E). This site is characterized by a sheltered rocky coast with calm weather condition during summer months favourable for *Ostreopsis* cf. *ovata* blooms (Gémin et al., 2020; Jauzein et al., 2017;

Mangialajo et al., 2011). Three stations (A, B, C), with at least 1 m between them, were selected for sampling due to (i) their accessibility, even during the night, and (ii) the quantity and quality of the macroalgal substrate. Samples were collected during three consecutive summers (2018, 2019 and 2020): each site was sampled once a week, early in the morning, from the beginning of June until the end of August in order to monitor *O.* cf. *ovata* abundances. For each site, epibenthic and planktonic abundances were monitored as described in Cohu et al. (2013). Epibenthic abundances in both summer 2018 and 2019 are presented in the Figure 2.

In addition of this summer monitoring, a high temporal frequency monitoring was performed at three point around the station B since it was the most accessible station at night. Briefly, samples were collected every 4 hours, day and night, for 3 consecutive days in order to follow the resuspension of *O.* cf. *ovata* cells. In 2018, sampling was carried out between the 18th of July at 8:00 pm and the 21st of July at 8:00 pm, just after the peak of *O.* cf. *ovata* bloom (Figure 2a). In 2019, samples were collected during the peak of the bloom, between the 5th of July 8:00 pm and the 8th of July 8:00 pm (Figure 2b). In 2020, samples were collected during the exponential phase of the bloom, between the 6th of July 8:00 pm and the 9th of July 8:00 pm (Figure 2c). Three different types of samples were collected to estimate epibenthic, planktonic and sea water surface abundances of *Ostreopsis* cf. *ovata* respectively: (i) Macroalgae (fresh weight = 3.57 ± 2.1 g) collected at 50 cm depth following the method described by Cohu et al. (2013); (ii) planktonic samples at 30 cm depth and (iii) samples from the surface of the sea (from here on referred to as surface sample) to estimate mucilaginous aggregates of cells floating at the sea surface. Surface sea-water samples were collected first, followed by planktonic samples and macroalgae, which were collected last to avoid resuspension of *O.* cf. *ovata* cells during sampling. The most representative macroalgae of the site were sampled usually *Dictyota* sp. Lamouroux and occasionally *Halopteris scoparia* Sauvageau or *Padina pavonica* Thivy. Sea water temperature and salinity were measured at time of each sampling.

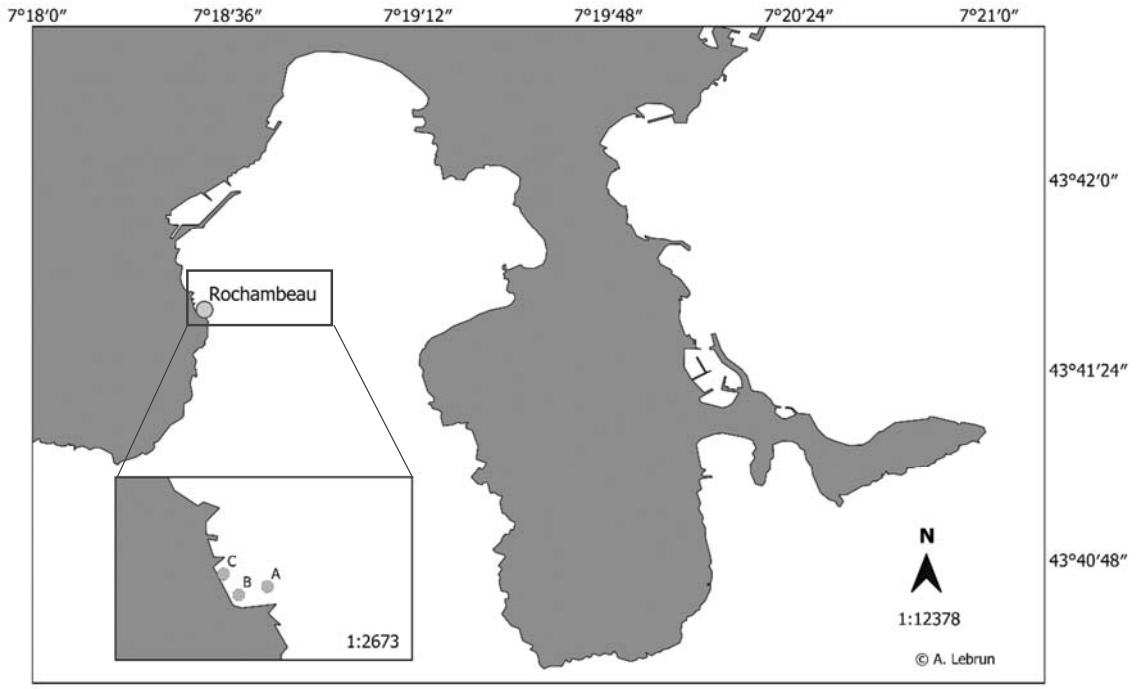

Figure 1 : Sampling sites at Rochambeau (Villefranche-sur-Mer, Mediterranean coast - 43°41′34.83″ N and 7°18′31.66″ E)

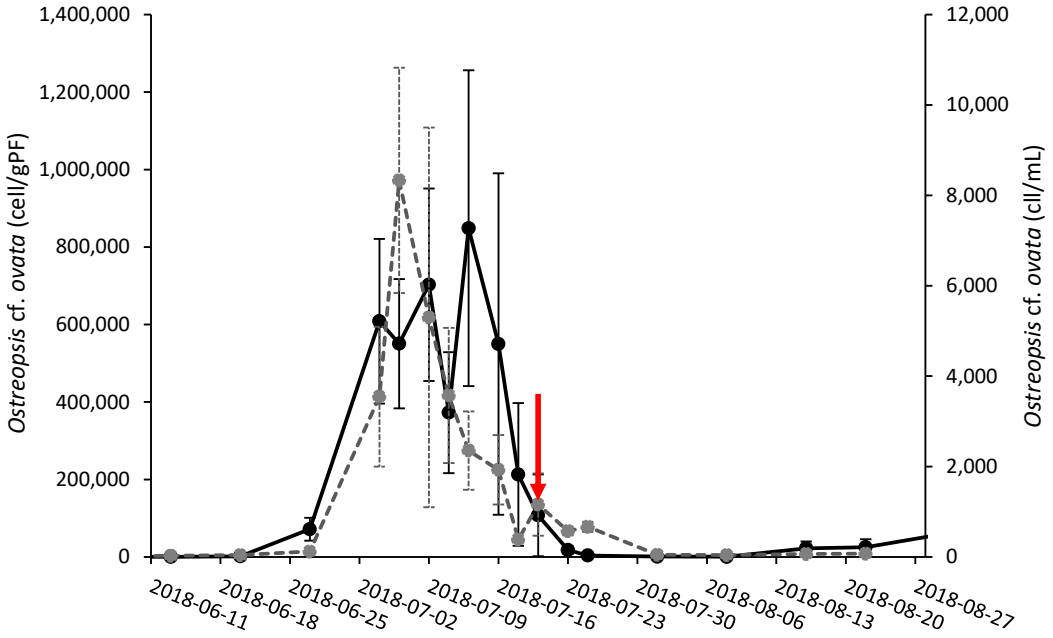
1,400,000
1,200,000
1,000,000
800,000
600,000
400,000
200,000
0
Ostreopsis cf. ovata (cell/gPF)
12,000
10,000
8,000
6,000
4,000
2,000
0
Ostreopsis cf. ovata (cll/mL)
2018-06-11
2018-06-18
2018-06-25
2018-07-02
2018-07-09
2018-07-16
2018-07-23
2018-07-30
2018-08-06
2018-08-13
2018-08-20
2018-08-27

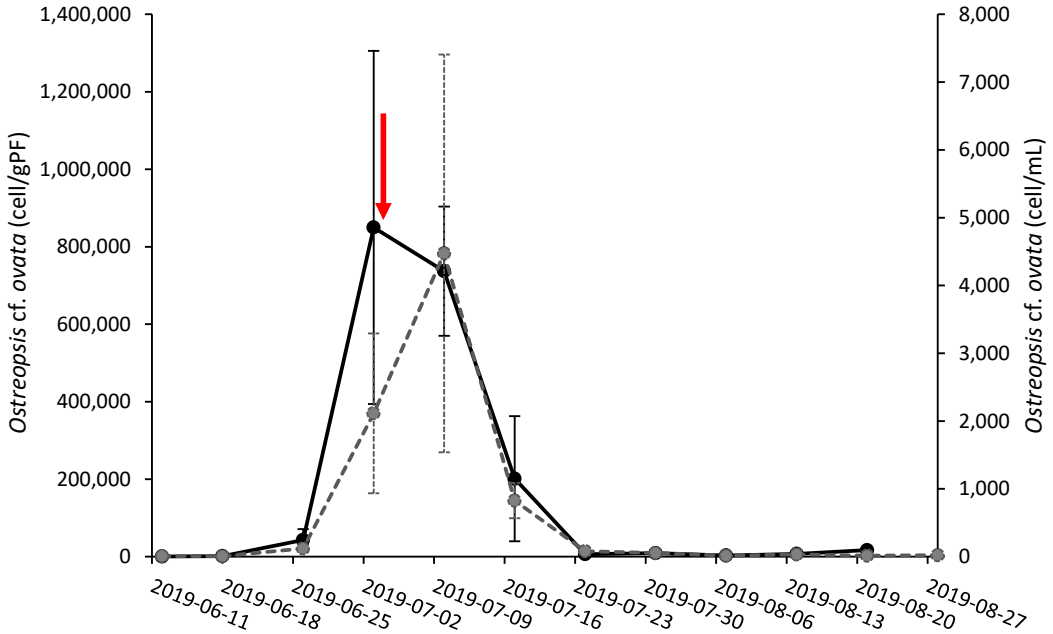
1,400,000
1,200,000
1,000,000
800,000
600,000
400,000
200,000
0
Ostreopsis cf. ovata (cell/gPF)
8,000
7,000
6,000
5,000
4,000
3,000
2,000
1,000
0
Ostreopsis cf. ovata (cell/mL)
2019-06-11
2019-06-18
2019-06-25
2019-07-02
2019-07-09
2019-07-16
2019-07-23
2019-07-30
2019-08-06
2019-08-13
2019-08-20
2019-08-27

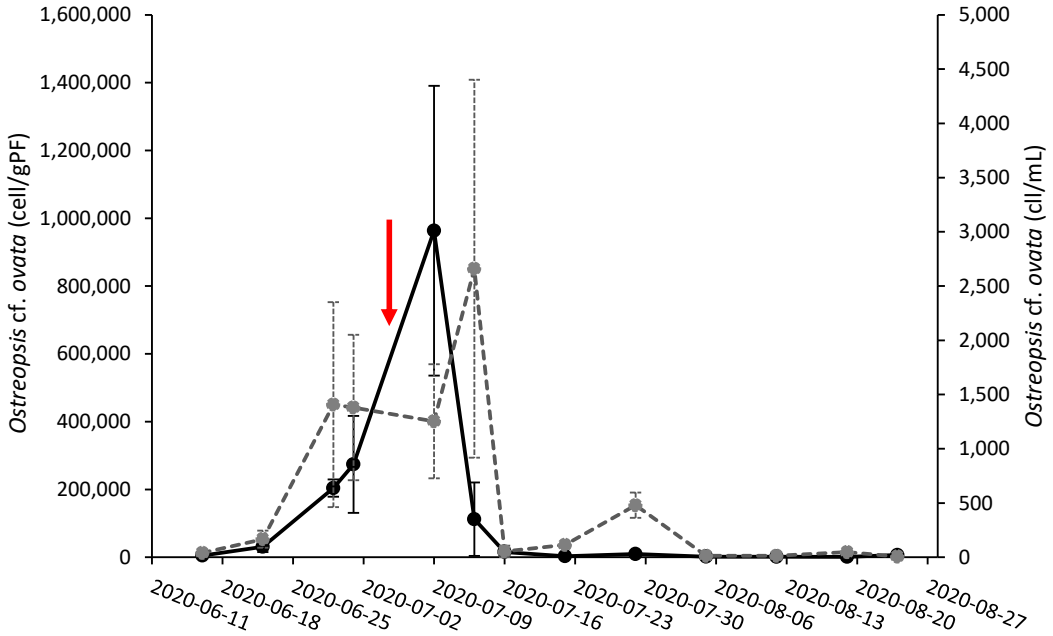

Figure 2 : Abundances of epibenthic and planktonic *Ostreopsis* cf. *ovata* cells at Rochambeau site (Villefranche-sur-Mer, France) in 2018 (a), 2019 (b) and 2020 (c). In 2018, high frequency time resolution samples were collected after the peak of the bloom, whereas in 2019 during the peak. In 2020, sampling was carried out at the exponential phase of the bloom. Red arrows point to time of high frequency sampling.

2.2. Samples processing

2.2.1. Determination of *Ostreopsis* cf. *ovata* abundances and size

Planktonic and surface samples were fixed with acidic lugol (4% v/v) and counted using an inverted microscope (Axiovert 40 CFL, Zeiss) following the Utermöhl method (Utermöhl, 1958) to estimate abundances (in number of cells.mL^{-1}). Macroalgae (= epibenthic samples) were treated following the method described by Cohu et al. (2013). Epibenthic abundance of *O.* cf. *ovata* was estimated under microscope (Axiovert 40 CFL, Zeiss) using Sedgwick rafter counting chamber and expressed as number of cells per gram of fresh weight of macroalgae (cells.gFW^{-1}). For both counting methods, at least 200 cells of O. cf. ovata were counted I each sample. Size of *O.* cf. *ovata* cells was measured for the 2019 benthic and planktonic samples. The length of the dorsoventral axis of a total number of 14 000 cells (i.e. 200 cells per sample) collected between the 7th of July 8:00 PM and the 8th of July 8:00 PM was measured.

2.2.2. Study of *Ostreopsis* cf. *ovata* division cycle

In 2019 (between the 5th of July at 8:00 AM and the 8th of July at 08:00 AM), 10 mL subsamples were taken from macroalgal samples (after a gentle agitation and before lugol fixation) to determine *O.* cf. *ovata* cell cycle stages. These aliquots of epibenthic cells samples were fixed in 1% formaldehyde (F8775, Sigma-Aldrich) over-night. Cells were then washed 3 times with 1x Phosphate Buffered Saline (PBS, Sigma-Aldrich) and stained with 1µg.L^{-1} Hoechst-33342 (Sigma-Aldrich) for 20 minutes at room temperature. A total of 34, 327 cells were examined using an epifluorescence microscope (Imager-A2, Zeiss) equipped with a Axiocam 506 camera (Zeiss). Nuclear position was used to determine 3 different cell cycle stages as described by Bravo et al. (2012): non-dividing cells, dividing cells (including

karyokinetic cells and cytokinetic cells) and post-dividing cells. Data are expressed as a percentage of cells in each stage, using the following equation:

$$\%\ of\ cells\ in\ x\ phase_{t1} = \frac{number\ of\ cells\ in\ x\ phase_{\ t1} * 100}{number\ of\ total\ cells\ observed_{\ t1}}$$

2.3. Statistical analysis

Normality of data and equality of variances across groups was verified using the Shapiro test and the Bartlett test, respectively. One-way ANOVA analysis was performed to study the influence of depth and time of sampling on *Ostreopsis* cf. *ovata* abundance. When the ANOVA analysis showed significant difference ($p<0.05$), a Tuckey post-hoc analysis was carried out *a posteriori* to identify which depth or time point differed from the others when the ANOVA analysis showed significant difference ($p<0.05$). All statistical analyses were carried out using the R software.

Mean apparent growth rates were calculated for each depth sampled in 2019 following this equation:

$$\text{Apparent growth rate } (cells.day^{-1}) = \frac{\ln\ (Cells\ abundances)_{t1} - \ln\ (Cells\ abundances)_{t0}}{t_1 - t_0}$$

This growth rate is considered as "apparent" since it does not only take in account the growth of *O.* cf. *ovata* cells but both the gains of cells by cell division and losses of cells by resuspension, predation or death.

3. Results

3.1. Abundance variations at different depths

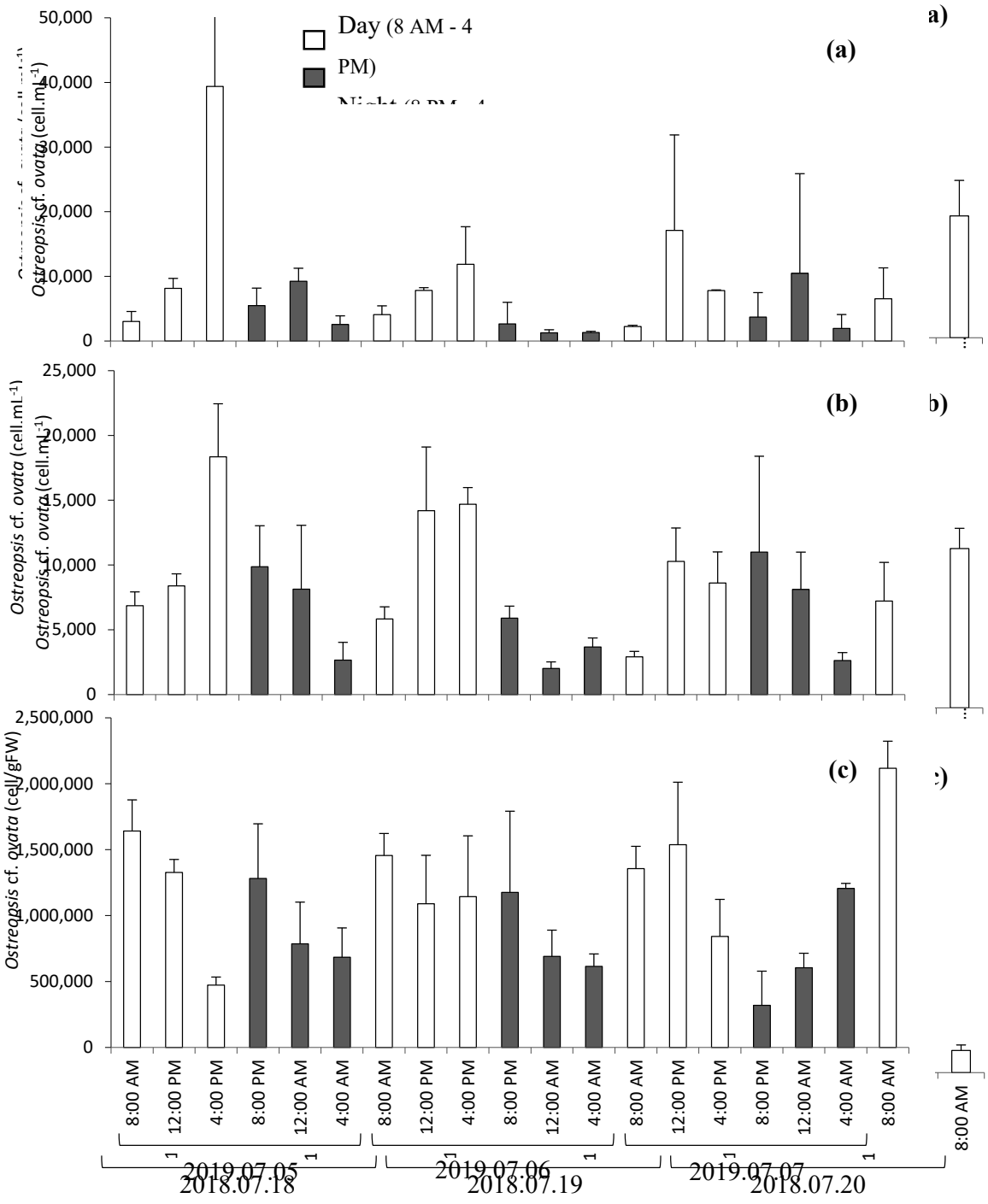

Figure 3 : Sea-surface (a), planktonic (b) and epibenthic (c) *Ostreopsis* cf. *ovata* abundances (Mean ± SE) measured over three days in 2019 (n=3).

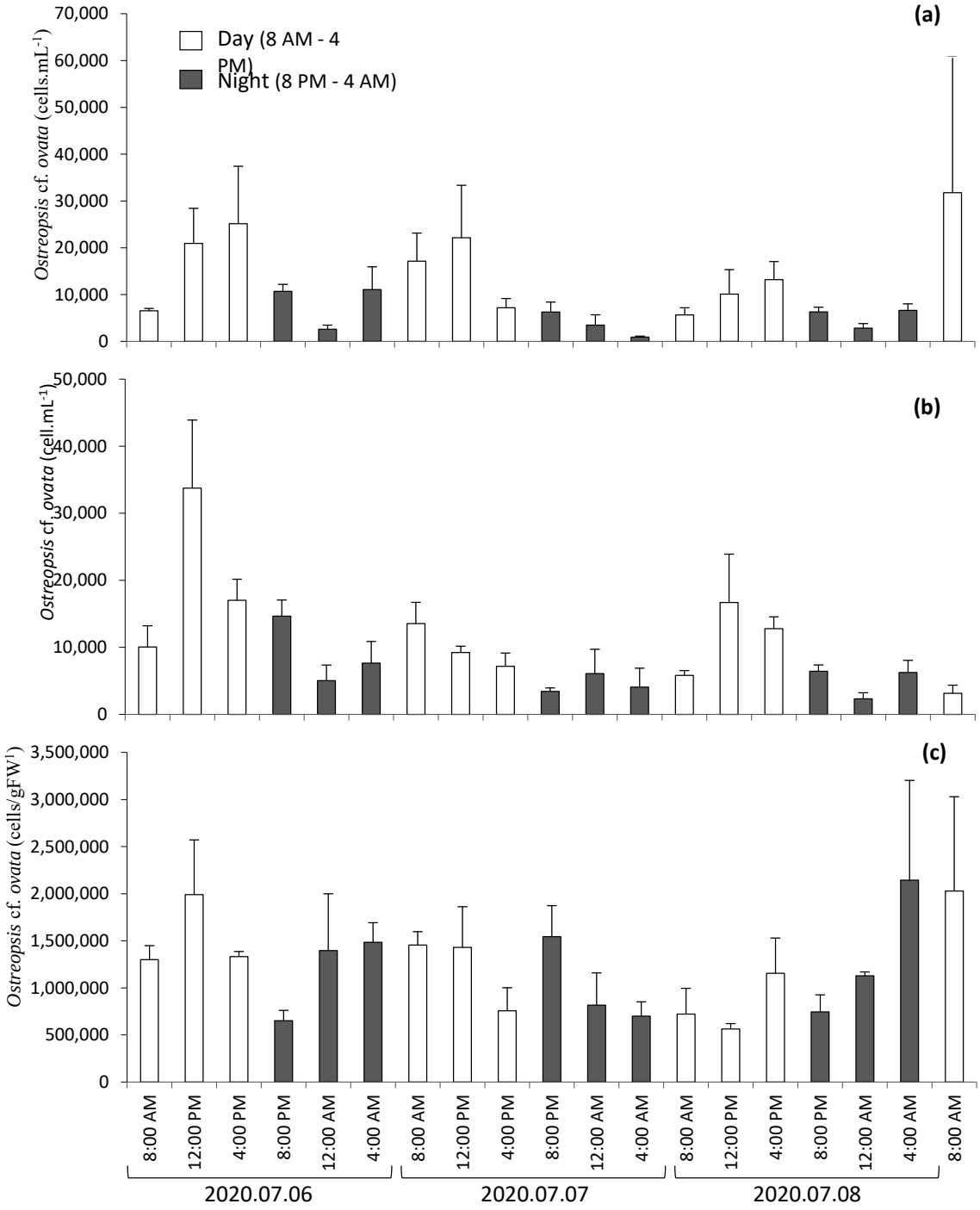

Figure 5: Sea-surface (a), planktonic (b) and epibenthic (c) *Ostreopsis* cf. *ovata* abundances (Mean ± SE) measured over three days in 2020 (n=3).

During the high frequency sampling, *Ostreopsis* cf. *ovata* cells were more abundant in samples from 2020 and 2019 than 2018, at all analysed depths. Abundances of epibenthic cells reached $2.1*10^6$ cells.gFW^{-1} and $1.4*10^5$ cells.gFW^{-1} in 2019 and 2018 respectively (Figure 3, 4). This 20 fold difference between 2019 and 2018 abundances is probably linked to the phase of the bloom when sampling was carried out (exponential vs decline phase – Figure 2).

Daily variations in *Ostreopsis* cf. *ovata* abundances were observed at all analysed locations (epibenthic, planktonic and-surface), both in 2018, 2019 and in 2020 (Figure 3, 4 and 5). Interestingly, abundances were higher during the day and decreased at night. The 6th of july 2018, epibenthic abundances reached $1.3*10^5$ cells.gFW^{-1} at noon and decreased during the day to reach the lowest concentration of $1.6*10^3$ cells.gFW^{-1} at 8:00 PM (100 fold difference). Surface and planktonic abundances followed the same trend and reached their maximum peaks (respectively $7.3*10^3$ and $4.3*10^3$ cells.mL^{-1}) the 19th of July at 04:00 PM and then fell to 180 and 246 cells.mL^{-1} respectively the same day, at 04:00 AM. Benthic abundances in 2020 did not follow this trend since no difference could be observed during the night and the day. Indeed, epibenthic abundances reached $1.40*10^6$ cells.gFW^{-1} and $1.43*10^6$ the 5th of July 2020 at 12:00 AM and 12:00 PM respectively.

Table 1 : Sea water surface, planktonic and benthic mean apparent growth rate in 2018, 2019 and 2020.

Mean apparent growth rate (cells.day^{-1})		**Sea water surface**	**Water column**	**Macroalgae**
2018	Day	-0.34	-0.14	-3.91
	Night	1.19	1.1	2.95
2019	Day	0.43	1.13	-1.27
	Night	0.073	-1.1	1.44
2020	Day	-0.27	-0.59	-0.4
	Night	1.33	-0.18	0.7

Mean growth rate completely changed from day to night and from the phase of the bloom (Table 1).

In 2018, apparent growth rates were mostly null for surface and planktonic samples and negative for benthic samples (-3.91 cells.day^{-1}) at day, suggesting loses of cells from macroalgae during the day. At night, whatever the considered sample, apparent growth rates increased and reached -3,91 cells. day^{-1}for benthic samples suggesting an increase of the number of cells on macroalgae.

In 2019, at the sea surface, growth rate reached 0.43 cells.day^{-1} at day and were almost null at night (0.073 cells.day^{-1}) suggesting an increase of the number of cells during the day and a balance between gains and losses of cells at night. In the water column, mean apparent growth rates reached 1.13 cells.day^{-1} during the day and became negative at night (-1.10 cells.day^{-1}). At least, apparent growth rate for epibenthic cells was completely different since it was negative during the day (suggesting a losses of cells) and positive at night (gains of cells).

In 2020, apparent growth rates were almost null during the day (-0.27 cells. day^{-1} and -0.4 cells. day^{-1} for surface and benthic samples respectively). At night, it increased and respectively reached 1.33 cells. day^{-1} and 0.7 cells. day^{-1} for surface and benthic samples although it was almost null for water column samples (-0.18 cells. day^{-1}).

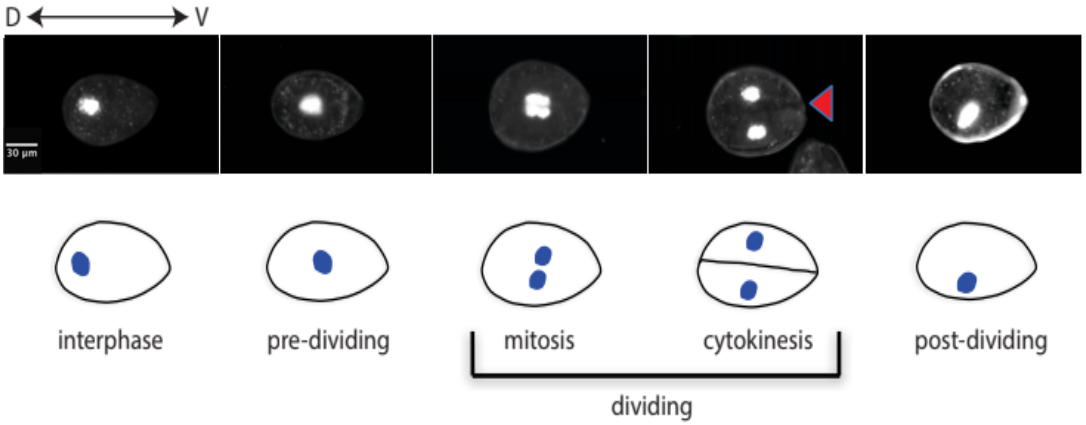

3.2. Abundance variations during the day

Figure 5: Sea-water surface (dotted lines), planktonic (dashed lines) and benthic (full lines) proportion of abundances during the day in 2018-bloom decline (a), 2019-bloom peak (b) and 2020-bloom exponential.

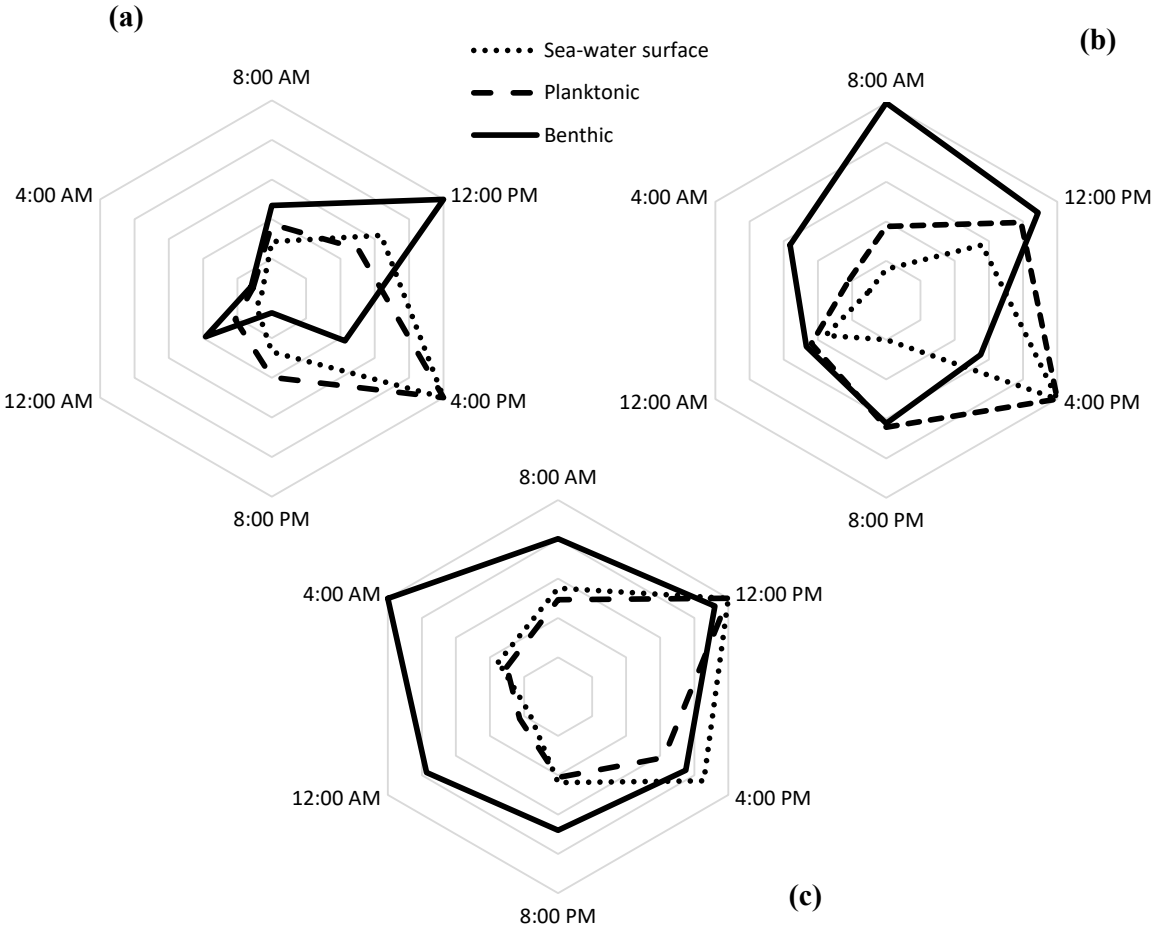

A radar chart was used to compare mean abundances throughout the day (Figure 5). As previously shown, *Ostreopsis* cf. *ovata* abundances varied over the day. Interestingly we observed that the maximal abundances were reached at different time of the day depending on the depth. In 2018, the abundance of epibenthic cells was higher at 12:00 PM whereas for surface and planktonic samples, the highest peak of abundance was reached at 04:00 PM (Figure 5 a). This difference was also observed in 2019 when the abundance of epibenthic cells reached the maximum peak at 08:00 AM whereas surface and planktonic abundances reached their peak at 04:00 PM. As previously shown, no abundances peaks were observed for benthic samples in 2020. However, the highest peak of abundance was reached at 12:00 PM or surface and planktonic samples.

3.3. Cell division occurs during the night

Figure 7: Representative images of *O.* cf *ovata* cells taken at different cell cycle stages (a) non-dividing interphase cells with nucleus in dorsal position; (b) pre-dividing cells with nucleus in central position ; (c) bi-nucleated cells in mitosis; (d) bi-nucleated cell undergoing cytokinesis. Red arrow points to site of cytokinesis; (e) post-dividing cells with nucleus in lateral position. Scale bar is µm.

Cell division was monitored during 3 days (from the 5th of July 08:00 AM until the 8th of July 08:00 AM) and five cell cycle stages were distinguished, as previously described by Bravo et al. (2012): (i) non-dividing cell (or interphase cells) characterized by a single nucleus in dorsal position (Figure 7a); (ii) pre-dividing cells with a single nucleus in central position (Figure 7b); (iii) mitotic bi-nucleated cells (Figure 7c); (iv) bi-nucleated cells undergoing cytokinesis cells (Figure 7d); and (v) post-dividing cells with a single nucleus in lateral position (Figure 7e). Non-dividing cells were the most abundant, ranging from 58% to 96% of total cells, depending on sample, in 2019 (Figure 8b) and were present both during the day and during the night (data not shown). For simplicity non-dividing cells are not reported in Figure 8 and we combined mitotic and cytokinetic cells together, as dividing cells (Figure 8). Dividing cells never exceeded 20% either in 2018 or in 2019.

As shown in Figure 8, the abundances of pre-dividing, dividing and post-dividing cells changed during the day, increasing at night and decreasing during the day. The 5th of July 2019 at 12:00 PM, only 2.5% of cells were identified as post-dividing cells (Figure 8 b) but, at 04:00 AM, they represented 20.9 % of total cells. Post-dividing cells then decreased again to 3.5% by 04:00 PM.

As expected, the number of pre-dividing cells reached its peak first, followed by dividing cells and finally by post-dividing cells. Pre-dividing cells increased in the evening between 08:00 PM and 12:00 AM, with peaks ranging between 8% and 20%. *Ostreopsis* cf. *ovata* cells then divided during the dark period with peaks between 12:00 AM (mainly cells in mitosis) and 04:00 AM (mostly cytokinetic cells – data not shown). Peaks of dividing cells ranged between 8 and 14% in 2018 and 4 and 12% in 2019. Post-dividing cells (8-14% in 2018 and 15-20% in 2019) were observed mainly early in the morning (08:00 AM) with some cells still in late cytokinesis.

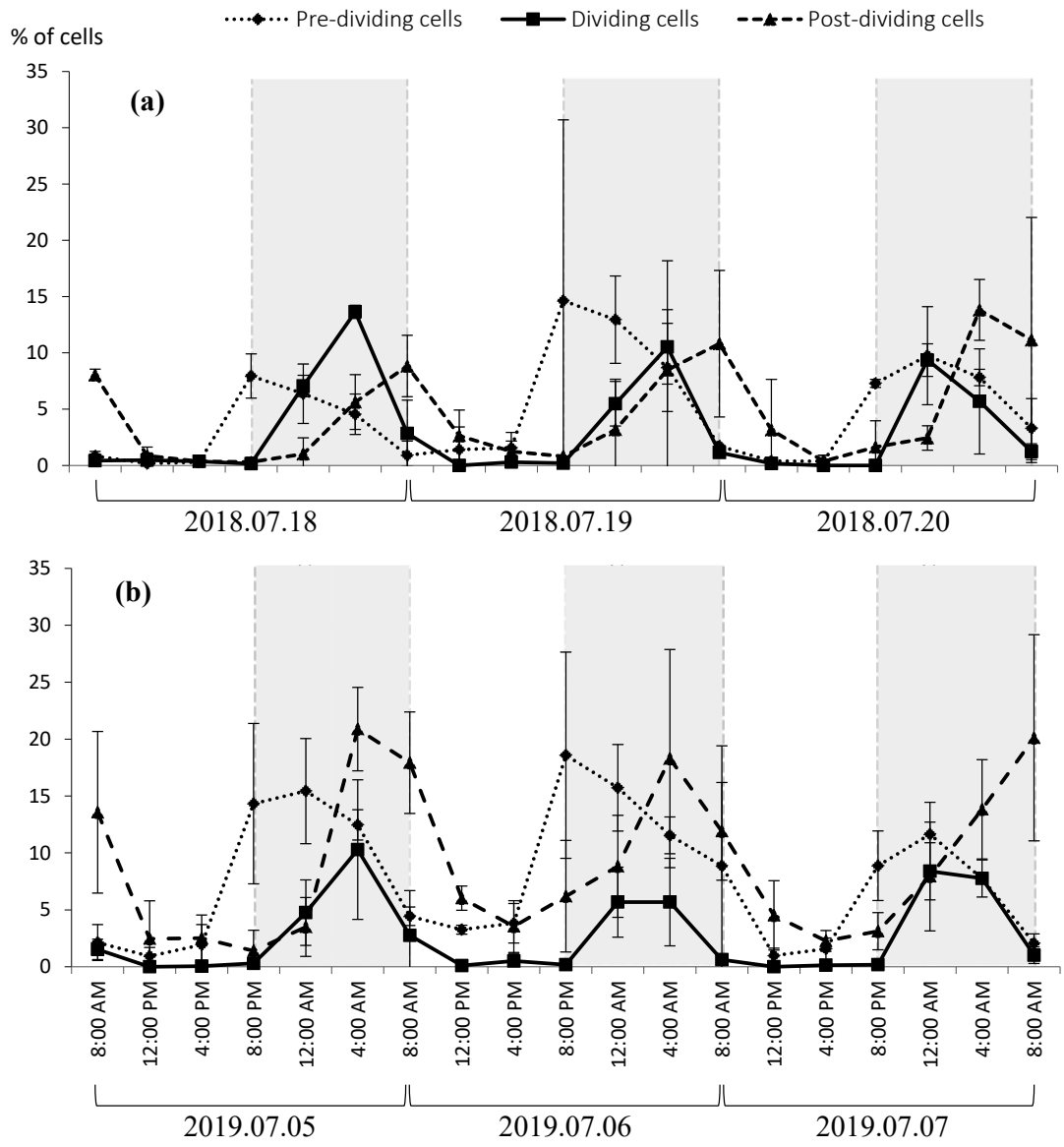

Figure 8: Percentage of pre-dividing (dashed lines), dividing (full lines) and post-dividing (dotted lines) *Ostreopsis* cf. *ovata* cells in 2018 (a) and 2019 (b) blooms. Grey bars

4. Discussion

4.1. Variation of abundances according to the day and to the depth

The high temporal frequency monitoring of *Ostreopsis* cf. *ovata* revealed that cell number were higher during the day and were significantly reduced at night. Such variations were observed in 2018, 2019 and 2020 although the analysis was made at a different phase of the bloom (i.e. decline phase in 2018, peak of the bloom in 2019 and exponential phase in 2020), excepted for 2020-benthic samples which abundances were maximal all over the day, probably linked to high division rates occurring during the exponential phase of the bloom. It is important to note that a time lag was observed between the peaks of abundances of

epibenthic and planktonic cells with epibenthic cells reaching their maximum abundance earlier than planktonic and sea surface cells. This lag suggests a potential active migration of cells from the benthic environment to planktonic and sea-water surface environments during the day, independently of the period of the bloom. Consistently apparent growth rates followed the same trend. During the day, the 2019- and 2018-growth rate was negative for epibenthic cells, suggesting that losses (by migration, death and predation) outweighed gains. On the contrary growth rates were positive for planktonic and sea water surface cells in 2019, suggesting an input of cells by migration through the water column. We do not favour a contribution by cell division since this took place at night. However, these growth rates were negative or almost null in 2018, certainly linked to the decline phase of the bloom. At night, instead, the apparent growth rate was positive for epibenthic cells, probably due to active cell division, and negative and almost absent for planktonic and sea water surface cells respectively. In 2020, trends were completely different linked to the exponential phase of the bloom and high division rates associated to this phase of the bloom.

Even if our results suggest an active vertical migration of *O*. cf. *ovata* cells, more studies are needed to confirm the nature of this migration. Active vertical migration has already been described for other planktonic toxic dinoflagellate, such as *Karenia brevis* (Schofield et al., 2006) and *Gymnodinium catenatum* (Doblin et al., 2006) to facilitate N uptake at depth. This active migration in dinoflagellates was suggested as an ecological strategy which provides dinoflagellates with an advantage over other phytoplanktonic species (Ault, 2000; Doblin et al., 2006; Jephson and Carlsson, 2009; Olsson and Granéli, 1991). However, active migration has not yet been described for any benthic dinoflagellates. Inactive migration of cells should also be considered as thermal wind, very active at night, could lead to a vertical or even horizontal resuspension. Other mechanisms at finer physical scales could also influence this resuspension. Oxygen bubbles could be trapped in the mucilaginous matrix produced by *O*. cf. *ovata* leading to a vertical migration of cells. Moreover, no study has examined on the effect of this mucilaginous matrix on the physical environment of *O*. cf. *ovata* cells which could affect the viscosity of sea water.

4.2. *Ostreopsis* cf. *ovata* life cycle

The asexual life cycle of *Ostreopsis* cf. *ovata* was described by Bravo et al. (2012). The authors observed that each cell cycle stage is associated with a specific organisation of the cell nuclear material. Using these morphological descriptions, we distinguished 3 main cell cycle stages: pre-dividing, dividing and post-dividing cells. As previously described by Bravo et al. (2012), we confirmed that *Ostreopsis* cf. *ovata* cells divide during the night, as only post-dividing cells were observed after 08:00 AM. Interestingly, the percentage of dividing cells was very similar in 2018 and 2019 although sampling was carried out at completely different phases of the bloom (Figure 2). In 2019, at the peak of the bloom, the percentage of dividing cells did not exceed 20%, which seems extremely low considering the explosive increase in cell abundance occurring during this phase of *O*. cf. *ovata* bloom. However, as we sampled every 4 hours and Bravo et al. (2012) observed that *O*. cf. *ovata* divides in approximately 1 hour, this limited percentage of dividing cells may indicate that either we missed the main peak of division or that cells are not completely synchronized and divide throughout the night.

4.3. Implications of daily variations of *Ostreopsis* cf. *ovata* abundances for health monitoring

Variations in epibenthic, planktonic and sea-water surface abundances have to be considered when setting up monitoring strategies. Despite harmonization efforts made to improve the monitoring of *Ostreopsis* cf. *ovata* around the world, there are numerous sources of variation in the estimation of *O*. cf. *ovata* abundances. Classical microscopy-based

identification of cells remains complex due to the strong intraspecific variability in cell morphology and the co-occurrence of different species. It requires extensive taxonomic expertise (Battocchi et al., 2010) even if new quantification methods relying on molecular biology approaches are implemented (Battocchi et al., 2010; Casabianca et al., 2013). Long term spatial variability leading to earlier blooms in the Ligurian Sea than along the Catalan coast (Mangialajo et al., 2011; Vila et al., 2016, 2012) and short term variability due to substrate composition and distribution in both time and space also constitute a wide source of variability in abundance estimation. Finally, the variety of methods employed for sampling (vacuum apparatus (Parsons et al., 2010), syringes (Abbate et al., 2012), artificial substrates (Faust, 2009; Jauzein et al., 2016; Tester et al., 2014) or macrophytes also introduces a source of variability, as well as the diversity of units (per weight or surface – Jauzein et al., 2016). Daily variations in *O.* cf. *ovata* abundances further complicate harmonization efforts since according to the sampling time, conclusions are different. Italian and French alert thresholds (Tichadou et al., 2010) are based on planktonic abundances although this has been criticized due to their strong variability observed in time and space (Lemée et al., 2012). Coupling of benthic and planktonic samples was strongly indicated as an alternative method to produce a more reliable picture of the presence and abundance of *O.* cf. *ovata* (Lemée et al., 2012; Vila et al., 2012). The observations reported here that planktonic abundances vary depending on depth and along the day adds another layer of complexity which will need to be considered when designing new monitoring strategies.

Acknowledgements

This work was supported by the French ANR project (OCEAN 15: *Ostreopsis* Chemical Ecology and Allelopathy Network; project ANR-15-CE35-0002) and the project COCLIME (which is part of ERA4CS, an ERA-NET initiated by JPI Climate, and funded by EPA (IE), ANR (FR), BMBF (DE), UEFISCDI (RO), RCN (NO) and FORMAS (SE), with co-funding by the European, Union; Grant 6904462).

Supplementary Data – Article

Table 1. Cell classification during the senescence of 2018 bloom.

Time	Non-dividing	Pre-karyokinetic cells	Karyokinetic cells	Cytokinesis	Post-dividing cells	Total of cells
08:00	487	5	2	1	44	539
12:00	601	1	1	2	5	610
16:00	1225	5	0	5	5	1240
20:00	412	39	1	0	2	454
00:00	2130	148	85	86	20	2469
04:00	201	12	10	26	15	264
08:00	665	4	6	9	60	744
12:00	516	4	0	0	10	530
16:00	812	8	1	3	7	831
20:00	299	69	1	0	3	372
00:00	445	94	36	5	36	616
04:00	314	31	21	36	63	465
08:00	866	18	3	9	144	1040
12:00	1661	7	2	3	19	1692
16:00	454	3	0	0	3	460
20:00	240	19	0	0	7	266
00:00	440	72	42	18	18	590
04:00	186	20	8	10	38	262
08:00	161	5	1	1	28	196
						13640

Table 2: Cell classification during the peak of 2019 bloom

Time	Non-dividing	Pre- dividing cells	Mitotic cells	Cytokinetic cells	Post-dividing cells	Total
08:00	1705	47	3	26	294	2075
12:00	1273	9	0	0	17	1299
16:00	1072	14	0	1	19	1106
20:00	638	104	2	1	12	757
00:00	1724	322	111	18	57	2232
04:00	522	112	48	39	193	914
08:00	625	37	11	10	152	835
12:00	503	19	0	1	31	554
16:00	738	35	3	0	34	810
20:00	455	132	2	0	24	613
00:00	779	170	53	9	85	1096
04:00	816	151	52	30	224	1273
08:00	1584	101	4	10	263	1962
12:00	643	6	0	0	38	687
16:00	1221	21	2	0	27	1271
20:00	300	28	1	0	12	341
00:00	991	167	76	39	87	1360
04:00	341	40	19	19	73	492
08:00	837	18	0	6	149	1010
						20687

Table 3A. Cell classification during the proliferative phase of 2020 bloom

Time	Non-dividing	Pre-dividing cells	Mitotic cells	Cytokinesis	Post-dividing cells	Total of cells
18:00	1705	47	3	26	294	2075
20:00	1273	9	0	0	17	1299
22:00	1072	14	0	1	19	1106
00:00	638	104	2	1	12	757
02:00	1724	322	111	18	57	2232
04:00	522	112	48	39	193	914
06:00	625	37	11	10	152	835
Total						**15576**

Table 3B. Cell classification during the peak of 2020 bloom

Time	Non-dividing	Pre-dividing cells	Mitotic cells	Cytokinesis	Post-dividing cells	Total of cells
18:00	3587	467	5	0	102	4161
20:00	3482	466	17	0	84	4049
22:00	2857	646	24	3	82	3612
00:00	3363	693	78	25	340	4499
02:00	3246	822	120	55	599	4842
04:00	3119	387	48	63	772	4389
06:00	2931	275	29	40	645	3920
Total						**29472**

Abbate, M., Bordone, A., Cerrati, G., Di Festa, T., Melchiorre, N., Pastorelli, A.M., Peirano, A., Petruzzelli, M.R., Ungaro, N., 2012. A New Method for Sampling Potentially Toxic Benthic Dinoflagellates. Cryptogamie, Algologie 33, 165–170. https://doi.org/10.7872/crya.v33.iss2.2011.165

Accoroni, S., Colombo, F., Pichierri, S., Romagnoli, T., Marini, M., Battocchi, C., Penna, A., Totti, C., 2012. Ecology of *Ostreopsis* cf. *ovata* Blooms in the Northwestern Adriatic Sea. Cryptogamie, Algologie 33, 191–198. https://doi.org/10.7872/crya.v33.iss2.2011.191

Accoroni, S., Totti, C., Romagnoli, T., Giulietti, S., Glibert, P.M., 2020. Distribution and potential toxicity of benthic harmful dinoflagellates in waters of Florida Bay and the Florida Keys. Marine Environmental Research 155, 104891. https://doi.org/10.1016/j.marenvres.2020.104891

Ault, T.R., 2000. Vertical migration by the marine dinoflagellate *Prorocentrum triestinum* maximises photosynthetic yield. Oecologia 125, 466–475. https://doi.org/10.1007/s004420000472

Battocchi, C., Totti, C., Vila, M., Masó, M., Capellacci, S., Accoroni, S., Reñé, A., Scardi, M., Penna, A., 2010. Monitoring toxic microalgae *Ostreopsis* (dinoflagellate) species in coastal waters of the Mediterranean Sea using molecular PCR-based assay combined with light microscopy. Marine Pollution Bulletin 60, 1074–1084. https://doi.org/10.1016/j.marpolbul.2010.01.017

Bravo, I., Vila, M., Casabianca, S., Rodriguez, F., Rial, P., Riobó, P., Penna, A., 2012. Life cycle stages of the benthic palytoxin-producing dinoflagellate *Ostreopsis* cf. *ovata* (Dinophyceae). Harmful Algae 18, 24–34. https://doi.org/10.1016/j.hal.2012.04.001

Brescianini, C., Grillo, C., Melchiorre, N., Bertolotto, R., Ferrari, A., Vivaldi, B., Icardi, G., Gramaccioni, L., Funari, E., Scardala, S., 2006. *Ostreopsis ovata* algal blooms affecting human health in Genova, Italy, 2005 and 2006. Weekly releases (1997–2007) 11, 3040. https://doi.org/10.2807/esw.11.36.03040-en

Casabianca, S., Casabianca, A., Riobó, P., Franco, J.M., Vila, M., Penna, A., 2013. Quantification of the toxic dinoflagellate *Ostreopsis* spp. by qpcr assay in marine aerosol. Environmental Science & Technology 47, 3788–3795. https://doi.org/10.1021/es305018s

Casabianca, S., Perini, F., Casabianca, A., Battocchi, C., Giussani, V., Chiantore, M., Penna, A., 2014. Monitoring toxic *Ostreopsis* cf. *ovata* in recreational waters using a qPCR based assay. Marine Pollution Bulletin 88, 102–109. https://doi.org/10.1016/j.marpolbul.2014.09.018

Ciminiello, P., Dell'Aversano, C., Iacovo, E.D., Fattorusso, E., Forino, M., Tartaglione, L., Benedettini, G., Onorari, M., Serena, F., Battocchi, C., Casabianca, S., Penna, A., 2014. First Finding of *Ostreopsis* cf. *ovata* Toxins in Marine Aerosols. Environmental Science & Technology 48, 3532–3540. https://doi.org/10.1021/es405617d

Cohu, S., Mangialajo, L., Thibaut, T., Blanfuné, A., Marro, S., Lemée, R., 2013. Proliferation of the toxic dinoflagellate *Ostreopsis* cf. *ovata* in relation to depth, biotic substrate and environmental factors in the North West Mediterranean Sea. Harmful Algae 24, 32–44. https://doi.org/10.1016/j.hal.2013.01.002

Cohu, S., Thibaut, T., Mangialajo, L., Labat, J.-P., Passafiume, O., Blanfuné, A., Simon, N., Cottalorda, J.-M., Lemée, R., 2011. Occurrence of the toxic dinoflagellate *Ostreopsis* cf. *ovata* in relation with environmental factors in Monaco (NW Mediterranean). Marine Pollution Bulletin 62, 2681–2691. https://doi.org/10.1016/j.marpolbul.2011.09.022

Cullen, J.J., 1985. Diel vertical migration by dinoflagellates: roles of carbohydrate metabolism and behavioral flexibility. Contrib Mar Sci 27, 135–152.

David, H., Laza-Martínez, A., Miguel, I., Orive, E., 2013. *Ostreopsis* cf. *siamensis* and *Ostreopsis* cf. *ovata* from the Atlantic Iberian Peninsula: Morphological and phylogenetic characterization. Harmful Algae 30, 44–55. https://doi.org/10.1016/j.hal.2013.08.006

Del Favero, G., Sosa, S., Pelin, M., D'Orlando, E., Florio, C., Lorenzon, P., Poli, M., Tubaro, A., 2012. Sanitary problems related to the presence of *Ostreopsis* spp. in the Mediterranean Sea: a multidisciplinary scientific approach. Annali dell'Istituto Superiore di Sanità 48, 407–414. https://doi.org/10.4415/ANN_12_04_08

Doblin, M.A., Thompson, P.A., Revill, A.T., Butler, E.C.V., Blackburn, S.I., Hallegraeff, G.M., 2006. Vertical migration of the toxic dinoflagellate *Gymnodinium catenatum* under different concentrations of nutrients and humic substances in culture. Harmful Algae 5, 665–677. https://doi.org/10.1016/j.hal.2006.02.002

Durando, P., Ansaldi, F., Oreste, P., Moscatelli, P., Marensi, L., Grillo, C., Gasparini, R., Icardi, G., Surveillance, C.G. for the L.S.A., 2007. *Ostreopsis ovata* and human health: epidemiological and clinical features of respiratory syndrome outbreaks from a two-year syndromic surveillance, 2005-06, in north-west Italy. Weekly releases (1997–2007) 12, 3212. https://doi.org/10.2807/esw.12.23.03212-en

Eppley, R.W., Holm-Harisen, O., Strickland, J.D.H., 1968. SOME OBSERVATIONS ON THE VERTICAL MIGRATION OFDINOFLAGELLATES 1 2. Journal of Phycology 4, 333–340.

Escalera, L., Benvenuto, G., Scalco, E., Zingone, A., Montresor, M., 2014. Ultrastructural Features of the Benthic Dinoflagellate *Ostreopsis* cf. *ovata* (Dinophyceae). Protist 165, 260–274. https://doi.org/10.1016/j.protis.2014.03.001

Fauchot, J., Levasseur, M., Roy, S., 2005. Daytime and nighttime vertical migrations of Alexandrium tamarense in the St. Lawrence estuary (Canada). Marine Ecology Progress Series 296, 241–250. https://doi.org/10.3354/meps296241

Faust, M.A., 2009. Ciguatera-Causing Dinoflagellates in a Coral-reef Mangrove Ecosystem, Belize. Atoll Research Bulletin 1–32. https://doi.org/10.5479/si.00775630.569.1

Gallitelli, M., Ungaro, N., Addante, L.M., Procacci, V., Silver, N.G., Sabbà, C., 2005. Respiratory illness as a reaction to tropical algal blooms occurring in a temperate climate. JAMA 293, 2595–2600. https://doi.org/10.1001/jama.293.21.2599-c

Gémin, M.-P., Réveillon, D., Hervé, F., Pavaux, A.-S., Tharaud, M., Séchet, V., Bertrand, S., Lemée, R., Amzil, Z., 2020. Toxin content of Ostreopsis cf. ovata depends on bloom phases, depth and macroalgal substrate in the NW Mediterranean Sea. Harmful Algae 101727. https://doi.org/10.1016/j.hal.2019.101727

Happey-Wood, C.M., 1976. Vertical migration patterns in phytoplankton of mixed species composition. British Phycological Journal 11, 355–369. https://doi.org/10.1080/00071617600650411
Hasle, G.R., 1950. Phototactic Vertical Migration in Marine Dinoflagellates. Oikos 2, 162–175. https://doi.org/10.2307/3564790
Honsell, G., Bonifacio, A., De Bortoli, M., Penna, A., Battocchi, C., Ciminiello, P., Dell'Aversano, C., Fattorusso, E., Sosa, S., Yasumoto, T., Tubaro, A., 2013. New Insights on Cytological and Metabolic Features of *Ostreopsis* cf. *ovata* Fukuyo (Dinophyceae): A Multidisciplinary Approach. PLoS ONE 8, e57291. https://doi.org/10.1371/journal.pone.0057291
Illoul, H., Hernández, F.R., Vila, M., Adjas, N., Younes, A.A., Bournissa, M., Koroghli, A., Marouf, N., Rabia, S., Ameur, F.L.K., 2012. The genus *Ostreopsis* along the Algerian coastal waters (SW Mediterranean Sea) associated with a human respiratory intoxication episode. Cryptogamie, Algologie 33, 209–216. https://doi.org/10.7872/crya.v33.iss2.2011.209
Jauzein, C., Açaf, L., Accoroni, S., Asnaghi, V., Fricke, A., Hachani, M.A., Chiantore, M., Mangialajo, L., Totti, C., Zaghmouri, I., 2018. Optimization of sampling, cell collection and counting for the monitoring of benthic harmful algal blooms: application to Ostreopsis spp. blooms in the Mediterranean Sea. Ecological Indicators 91, 116–127.
Jauzein, C., Couet, D., Blasco, T., Lemée, R., 2017. Uptake of dissolved inorganic and organic nitrogen by the benthic toxic dinoflagellate *Ostreopsis* cf. *ovata*. Harmful Algae 65, 9–18. https://doi.org/10.1016/j.hal.2017.04.005
Jauzein, C., Fricke, A., Mangialajo, L., Lemée, R., 2016. Sampling of *Ostreopsis* cf. *ovata* using artificial substrates: Optimization of methods for the monitoring of benthic harmful algal blooms. Marine Pollution Bulletin 107, 300–304. https://doi.org/10.1016/j.marpolbul.2016.03.047
Jephson, T., Carlsson, P., 2009. Species- and stratification-dependent diel vertical migration behaviour of three dinoflagellate species in a laboratory study. J Plankton Res 31, 1353–1362. https://doi.org/10.1093/plankt/fbp078
Kermarec, F., Dor, F., Armengaud, A., Charlet, F., Kantin, R., Sauzade, D., Haro, L. de, 2008. Les risques sanitaires liés à la présence d'*Ostreopsis ovata* dans les eaux de baignade ou d'activités nautiques. Environnement, Risques & Santé 7, 357–363. https://doi.org/10.1684/ers.2008.0167
Lemée, R., Mangialajo, L., Cohu, S., Amzil, Z., Blanfune, A., Chomerat, N., Ganzin, N., Gasparini, S., Grossel, H., Guidi-Guivard, L., Hoareau, L., Duff, F. le, Marro, S., Simon, N., Nezan, E., Pedrotti, M.-L., Sechet, V., Soliveres, O., Thibaut, T., 2012. Interactions between Scientists, Managers and Policy Makers in the Framework of the French MediOs Project on *Ostreopsis* (2008–2010). Cryptogamie, Algologie 33, 137–142. https://doi.org/10.7872/crya.v33.iss2.2011.137
Mangialajo, L., Ganzin, N., Accoroni, S., Asnaghi, V., Blanfuné, A., Cabrini, M., Cattaneo-Vietti, R., Chavanon, F., Chiantore, M., Cohu, S., Costa, E., Fornasaro, D., Grossel, H., Marco-Miralles, F., Masó, M., Reñé, A., Rossi, A.M., Sala, M.M., Thibaut, T., Totti, C., Vila, M., Lemée, R., 2011. Trends in *Ostreopsis* proliferation along the Northern Mediterranean coasts. Toxicon 57, 408–420. https://doi.org/10.1016/j.toxicon.2010.11.019
Monti, M., Minocci, M., Beran, A., Iveša, L., 2007. First record of Ostreopsis cfr. ovata on macroalgae in the Northern Adriatic Sea. Marine Pollution Bulletin 54, 598–601. https://doi.org/10.1016/j.marpolbul.2007.01.013
Nascimento, S.M., Corrêa, E.V., Menezes, M., Varela, D., Paredes, J., Morris, S., 2012a. Growth and toxin profile of *Ostreopsis* cf. *ovata* (Dinophyta) from Rio de Janeiro, Brazil. Harmful Algae 13, 1–9. https://doi.org/10.1016/j.hal.2011.09.008
Nascimento, S.M., França, J.V., Gonçalves, J.E.A., Ferreira, C.E.L., 2012b. *Ostreopsis* cf. *ovata* (Dinophyta) bloom in an equatorial island of the Atlantic Ocean. Marine Pollution Bulletin 64, 1074–1078. https://doi.org/10.1016/j.marpolbul.2012.03.015
Nascimento, S.M., Neves, R.A.F., De'Carli, G.A.L., Borsato, G.T., da Silva, R.A.F., Melo, G.A., de Morais, A.M., Cockell, T.C., Fraga, S., Menezes-Salgueiro, A.D., Mafra, L.L., Hess, P., Salgueiro, F., 2020. *Ostreopsis* cf. *ovata* (dinophyceae) molecular phylogeny, morphology,

and detection of ovatoxins in strains and field samples from Brazil. Toxins 12, 70. https://doi.org/10.3390/toxins12020070
Olsson, P., Granéli, E., 1991. Observations on diurnal vertical migration and phased cell division for three coexisting marine dinoflagellates. J Plankton Res 13, 1313–1324. https://doi.org/10.1093/plankt/13.6.1313
Parsons, M.L., Settlemier, C.J., Bienfang, P.K., 2010. A simple model capable of simulating the population dynamics of *Gambierdiscus*, the benthic dinoflagellate responsible for ciguatera fish poisoning. Harmful Algae 10, 71–80. https://doi.org/10.1016/j.hal.2010.07.002
Pavaux, A.-S., Berdalet, E., Lemée, R., 2020. Chemical Ecology of the Benthic Dinoflagellate Genus Ostreopsis: Review of Progress and Future Directions. Frontiers in Marine Science 7, 498.
Penna, A., Galluzzi, L., 2013. The quantitative real-time PCR applications in the monitoring of marine harmful algal bloom (HAB) species. Environ Sci Pollut Res 20, 6851–6862. https://doi.org/10.1007/s11356-012-1377-z
Penna, A., Vila, M., Fraga, S., Giacobbe, M.G., Andreoni, F., Riobó, P., Vernesi, C., 2005. Characterization of ostreopsis and coolia (dinophyceae) isolates in the western mediterranean sea based on morphology, toxicity and internal transcribed spacer 5.8s rdna sequences1. Journal of Phycology 41, 212–225. https://doi.org/10.1111/j.1529-8817.2005.04011.x
Perini, F., Casabianca, A., Battocchi, C., Accoroni, S., Totti, C., Penna, A., 2011. New approach using the real-time PCR method for estimation of the toxic marine dinoflagellate *Ostreopsis* cf. *ovata* in marine environment. PLoS One 6. https://doi.org/10.1371/journal.pone.0017699
Pfannkuchen, M., Godrijan, J., Marić Pfannkuchen, D., Iveša, L., Kružić, P., Ciminiello, P., Dell'Aversano, C., Dello Iacovo, E., Fattorusso, E., Forino, M., Tartaglione, L., Godrijan, M., 2012. Toxin-producing *Ostreopsis* cf. *ovata* are likely to bloom undetected along coastal areas. Environ. Sci. Technol. 46, 5574–5582. https://doi.org/10.1021/es300189h
Ralston, D.K., McGillicuddy, D.J., Townsend, D.W., 2007. Asynchronous vertical migration and bimodal distribution of motile phytoplankton. J Plankton Res 29, 803–821. https://doi.org/10.1093/plankt/fbm061
Sansoni, G., Borghini, B., Camici, G., Casotti, M., Righini, P., Rustighi, C., 2003. Fioriture algali di *Ostreopsis ovata* (Gonyaulacales: Dinophyceae): un problema emergente. Biologia Ambientale 17, 17–23.
Schofield, O., Kerfoot, J., Mahoney, K., Moline, M., Oliver, M., Lohrenz, S., Kirkpatrick, G., 2006. Vertical migration of the toxic dinoflagellate *Karenia brevis* and the impact on ocean optical properties. Journal of Geophysical Research: Oceans 111, 1–11. https://doi.org/10.1029/2005JC003115
Smayda, T.J., 1997. Harmful algal blooms: Their ecophysiology and general relevance to phytoplankton blooms in the sea. Limnology and Oceanography 42, 1137–1153. https://doi.org/10.4319/lo.1997.42.5_part_2.1137
Staker, R.D., Bruno, S.F., 1980. Diurnal Vertical Migration in Marine Phytoplankton. Botanica Marina 23, 167–172. https://doi.org/10.1515/botm.1980.23.3.167
Sullivan, J.M., Swift, E., Donaghay, P.L., Rines, J.E.B., 2003. Small-scale turbulence affects the division rate and morphology of two red-tide dinoflagellates. Harmful Algae 2, 183–199.
Tester, P.A., Kibler, S.R., Holland, W.C., Usup, G., Vandersea, M.W., Leaw, C.P., Teen, L.P., Larsen, J., Mohammad-Noor, N., Faust, M.A., Litaker, R.W., 2014. Sampling harmful benthic dinoflagellates: Comparison of artificial and natural substrate methods. Harmful Algae 39, 8–25. https://doi.org/10.1016/j.hal.2014.06.009
Tibiriçá, C.E.J.A., Leite, I.P., Batista, T.V.V., Fernandes, L.F., Chomérat, N., Herve, F., Hess, P., Mafra, L.L., 2019. *Ostreopsis* cf. *ovata* bloom in currais, brazil: phylogeny, toxin profile and contamination of mussels and marine plastic litter. Toxins 11, 446. https://doi.org/10.3390/toxins11080446
Tichadou, L., Glaizal, M., Armengaud, A., Grossel, H., Lemée, R., Kantin, R., Lasalle, J.-L., Drouet, G., Rambaud, L., Malfait, P., de Haro, L., 2010. Health impact of unicellular algae of the *Ostreopsis* genus blooms in the Mediterranean Sea: experience of the French Mediterranean coast surveillance network from 2006 to 2009. Clinical Toxicology 48, 839–844. https://doi.org/10.3109/15563650.2010.513687

Vila, M., Abós-Herràndiz, R., Isern-Fontanet, J., Àlvarez, J., Berdalet, E., 2016. Establishing the link between *Ostreopsis* cf. *ovata* blooms and human health impacts using ecology and epidemiology. Scientia Marina 80, 107–115. https://doi.org/10.3989/scimar.04395.08A

Vila, M., Arin, L., Battocchi, C., Bravo, I., Fraga, S., Penna, A., Reñé, A., Riobó, P., Rodriguez, F., Sala, M.M., Camp, J., de Torres, M., Franco, J.M., 2012. Management of *Ostreopsis* Blooms in Recreational waters along the Catalan Coast (NW Mediterranean Sea): Cooperation between a Research Project and a Monitoring Program. Cryptogamie, Algologie 33, 143–152. https://doi.org/10.7872/crya.v33.iss2.2011.143

Vila, M., Garcés, E., Masó, M., 2001. Potentially toxic epiphytic dinoflagellate assemblages on macroalgae in the NW Mediterranean. Aquatic Microbial Ecology 26, 51–60. https://doi.org/10.3354/ame026051

Annex 2. Colchicine and agitation affect mitosis and cytokinesis in *Ostreopsis* cf. *ovata*.

Quantification of the different morphotypes in bloom samples. Data associated with Figure 39.

External control								
Time	Interphase	Pre-dividing	Normal mitosis	Normal cytokinesis	Post-dividing	Affected mitosis	Affected cytokinesis	Total of cells
0:00	1228	218	27	6	132	0	0	1611
2:00	1326	374	46	21	230	0	0	1997
4:00	954	83	18	22	185	0	0	1262
6:00	735	103	15	13	178	0	0	1044
Internal Control								
Time	Interphase	Pre-dividing	Normal mitosis	Normal cytokinesis	Post-dividing	Affected mitosis	Affected cytokinesis	Total of cells
0:00	501	158	48	12	42	1	0	762
2:00	215	46	3	4	41	0	1	310
4:00	263	40	8	10	26	1	2	350
6:00	677	61	12	18	35	2	4	809
Colchicine								
Time	Interphase	Pre-dividing	Normal mitosis	Normal cytokinesis	Post-dividing	Affected mitosis	Affected cytokinesis	Total of cells
0:00	474	131	38	14	60	0	0	717
2:00	378	32	13	16	49	29	16	533
4:00	512	51	7	17	56	24	11	678
6:00	882	32	3	28	65	31	14	1055
Agitation								
Time	Interphase	Pre-dividing	Normal mitosis	Normal cytokinesis	Post-dividing	Affected mitosis	Affected cytokinesis	Total of cells
0:00	326	55	18	8	40	1	0	448
2:00	467	22	1	16	60	14	11	591
4:00	212	27	1	4	25	5	4	278
6:00	527	40	3	8	39	5	14	636

Annex 3 – Transcriptomic data

Table 1. List of homologous proteins between *O.* cf. *ovata* and *Saccharomyces cerevisiae*. The first column contains the protein names assigned by uniport database; the second column shows the homologous proteins found in *O.* cf. *ovata* and the assigned transcript ID. The third column indicates the function of the budding yeast protein. The functions were assigned to cytokinesis, cyclins and mitosis which includes spindle, kinetochore and APC/C.

Protein name	ID_Ostreops	Function associated
Anaphase-promoting complex subunit 1	TRINITY_DN49105_c0_g2_i1.p1	Mitosis-APC/C
Anaphase-promoting complex subunit DOC1	TRINITY_DN96864_c0_g1_i1.p2	Mitosis-APC/C
Anaphase-promoting complex subunit 11	TRINITY_DN6695_c0_g1_i1.p4	Mitosis-APC/C
Anaphase-promoting complex subunit 2	TRINITY_DN15922_c0_g1_i1.p1	Mitosis-APC/C
Anaphase-promoting complex subunit CDC16	TRINITY_DN15730_c0_g1_i1.p1	Mitosis-APC/C
Anaphase-promoting complex subunit CDC23	TRINITY_DN117627_c0_g1_i1.p1	Mitosis-APC/C
Anaphase-promoting complex subunit CDC27 (Anaphase-promoting complex subunit 3)	TRINITY_DN23979_c0_g1_i1.p1	Mitosis-APC/C
APC/C activator protein CDH1 (CDC20 homolog 1)	TRINITY_DN98275_c0_g1_i1.p1	Mitosis-APC/C
Serine/threonine-protein kinase MPS1 (Monopolar spindle protein 1)	TRINITY_DN20727_c0_g2_i1.p1	Mitosis-Kinetochore
Kinetochore protein NDC80 (80 kDa spindle component protein) (Nuclear division cycle protein 80)	TRINITY_DN4604_c0_g1_i3.p1	Mitosis-Kinetochore
Phosphatidylinositol 4-kinase PIK1 (PI4-kinase)	TRINITY_DN18913_c0_g2_i1.p1	Mitosis-Kinetochore
Protein SGT1 (Suppressor of G2 allele of SKP1)	TRINITY_DN19239_c0_g1_i1.p1	Mitosis-Kinetochore
Suppressor of kinetochore protein 1 (Centromere DNA-binding protein complex CBF3 subunit D)	TRINITY_DN7822_c0_g3_i1.p2	Mitosis-Kinetochore
YAP1-binding protein 2 (YBP1 homolog protein 1)	TRINITY_DN45996_c0_g1_i1.p1	Mitosis-Kinetochore
Protein BIM1	TRINITY_DN1814_c0_g1_i1.p1	Mitosis-Spindle
Protein BMH2	TRINITY_DN3798_c0_g1_i8.p2	Mitosis-Spindle
Protein BNI1	TRINITY_DN11334_c0_g2_i1.p1	Mitosis-Spindle
Serine/threonine-protein kinase CBK1 (Cell wall biosynthesis kinase)	TRINITY_DN3145_c0_g1_i3.p1	Mitosis-Spindle
Spindle assembly checkpoint kinase	TRINITY_DN97004_c0_g1_i1.p1	Mitosis-Spindle
Nucleosome assembly protein	TRINITY_DN1504_c0_g3_i3.p1	Mitosis-Spindle
Nucleoporin NUP170	TRINITY_DN30525_c0_g2_i1.p1	Mitosis-Spindle
Protein STU2	TRINITY_DN13432_c0_g2_i1.p1	Mitosis-

		Spindle
Serine/threonine-protein phosphatase PP1-2	TRINITY_DN10959_c0_g1_i1.p1	Mitosis
Structural maintenance of chromosomes	TRINITY_DN38588_c0_g1_i1.p1	Mitosis
Mitosis inhibitor protein kinase SWE1 (EC 2.7.11.1) (Wee1 homolog)	TRINITY_DN5846_c0_g1_i1.p1	Mitosis
Exportin-1 (Chromosome region maintenance protein 1)	TRINITY_DN24525_c0_g2_i1.p1	Mitosis
Cell division control protein 31 (Nuclear pore protein CDC31) (Nucleoporin CDC31)	TRINITY_DN3040_c0_g1_i13.p1	Mitosis
Cell cycle serine/threonine-protein kinase CDC5/MSD2	TRINITY_DN124690_c0_g1_i1.p1	Mitosis
Histone H4	TRINITY_DN255_c0_g2_i1.p1	Mitosis
Protein arginine N-methyltransferase HSL7 (Histone synthetic lethal protein 7)	TRINITY_DN1778_c0_g1_i2.p1	Mitosis
Kelch repeat-containing protein 2	TRINITY_DN95742_c0_g1_i1.p1	Mitosis
F-box protein MET30 (E3 ubiquitin ligase complex SCF(Met30) subunit MET30)	TRINITY_DN126225_c0_g1_i1.p1	Mitosis
Protein phosphatase PP2A regulatory subunit B	TRINITY_DN3182_c0_g6_i1.p1	Mitosis
Sister chromatid cohesion protein PDS5	TRINITY_DN6329_c1_g3_i2.p1	Mitosis
Condensin complex subunit 1	TRINITY_DN6926_c0_g1_i1.p1	Mitosis
Condensin complex subunit 2	TRINITY_DN77149_c0_g1_i1.p1	Mitosis
Kinesin-like protein KAR3	TRINITY_DN999_c0_g3_i2.p1	Mitosis
DBF2 kinase activator protein MOB1 (MPS1 binder 1)	TRINITY_DN106482_c0_g1_i1.p1	Mitosis
Tyrosine-protein phosphatase CDC14	TRINITY_DN9399_c0_g1_i3.p1	Mitosis and Cytokinesis
CBK1 kinase activator protein MOB2 (MPS1 binder 2)	TRINITY_DN3145_c0_g1_i3.p1	Mitosis and Cytokinesis
Cyclin-dependent kinase 1	TRINITY_DN2511_c0_g3_i2.p2	Cyclin
G2/mitotic-specific cyclin-1	TRINITY_DN108329_c0_g1_i1.p1	Cyclin
G2/mitotic-specific cyclin-3	TRINITY_DN78099_c0_g1_i1.p1	Cyclin
G2/mitotic-specific cyclin-4	TRINITY_DN7490_c0_g1_i2.p1	Cyclin
S-phase entry cyclin-6	TRINITY_DN12532_c0_g1_i1.p1	Cyclin
PHO85 cyclin-7 (PHO85-associated protein 1)	TRINITY_DN116097_c0_g1_i1.p1	Cyclin
G1-specific transcriptional repressor WHI5	TRINITY_DN17261_c1_g1_i1.p1	Cyclin
Actin	TRINITY_DN1689_c0_g1_i1.p1	Cytokinesis
Actin-interacting protein 1	TRINITY_DN22811_c0_g1_i1.p1	Cytokinesis
Actin-related protein 2/3 complex subunit 1	TRINITY_DN42384_c0_g1_i1.p2	Cytokinesis
Actin-related protein 2/3 complex subunit 2	TRINITY_DN35177_c0_g1_i1.p1	Cytokinesis
Actin-related protein 2/3 complex subunit 3	TRINITY_DN118357_c0_g1_i1.p2	Cytokinesis
Cell division control protein 10	TRINITY_DN47140_c0_g1_i1.p1	Cytokinesis
Cofilin	TRINITY_DN122525_c0_g1_i1.p2	Cytokinesis
DOA4-independent degradation protein 4 - ESCRT3	TRINITY_DN5417_c0_g1_i2.p1	Cytokinesis
EH domain-containing and endocytosis protein 1 (Bud site selection protein 15)	TRINITY_DN42096_c0_g1_i1.p1	Cytokinesis
Kinesin-like protein KIP3	TRINITY_DN44795_c0_g1_i1.p2	Cytokinesis

Rho-GTPase-activating protein LRG1 (LIM-RhoGAP protein 1)	TRINITY_DN48867_c0_g1_i2.p1	Cytokinesis
Myosin light chain 1 (Calmodulin-like myosin light chain MLC1) (Myosin-2 light chain)	TRINITY_DN4758_c0_g5_i1.p1	Cytokinesis
Protein MLP1 (Myosin-like protein 1)	TRINITY_DN24869_c0_g4_i1.p1	Cytokinesis
Mannose-1-phosphate guanyltransferase	TRINITY_DN58489_c0_g1_i1.p1	Cytokinesis
Myosin-1 (Type II myosin)	TRINITY_DN4758_c0_g5_i1.p1	Cytokinesis
Ribosome biogenesis protein 15 (Nucleolar protein 15)	TRINITY_DN31813_c1_g1_i1.p1	Cytokinesis
Reduced viability upon starvation protein 167	TRINITY_DN18708_c0_g1_i1.p1	Cytokinesis
Tubulin alpha-1 chain	TRINITY_DN2223_c0_g1_i8.p2	Cytokinesis
Tubulin beta chain (Beta-tubulin)	TRINITY_DN5283_c0_g1_i9.p1	Cytokinesis
Vacuolar protein sorting-associated protein 20 - ESCRT3	TRINITY_DN3167_c0_g7_i1.p2	Cytokinesis
Vacuolar protein-sorting-associated protein 24 - - ESCRT3	TRINITY_DN15459_c0_g1_i1.p1	Cytokinesis
VPS4	TRINITY_DN105171_c0_g1_i1.p1	Cytokinesis

Table 2. List of homologous proteins between *O.* cf. *ovata* and *Chlamydomonas reinhardtii*. The first column contains the protein names assigned by uniport, Phycocosm and PlantGDB databases; the second column shows the homologous proteins found in *O.* cf. *ovata* and the assigned transcript ID. The third column indicates the function of the budding yeast protein. The functions were assigned to cytokinesis, cyclins, basal body and mitosis which includes spindle, kinetochore and APC/C.

Protein name	Gene	Function associated
WD_REPEATS_REGION domain-containing protein	TRINITY_DN31085_c0_g1_i1.p2	Mitosis-Spindle
Caltractin (20 kDa calcium-binding protein) (Centrin)	TRINITY_DN3040_c0_g1_i13.p1	Mitosis-Spindle
Spindle pole body protein- Cre09.g404500.t1.1	TRINITY_DN5676_c0_g5_i1.p1	Mitosis-Spindle
abnormal spindle-like microcephaly-associated protein (ASPM, ASP)	TRINITY_DN125387_c0_g1_i1.p2	Mitosis-Spindle
Centriole proteome protein	TRINITY_DN10248_c0_g1_i1.p1	Mitosis-Spindle
PTHR22545:SF0 - CENTROSOMAL PROTEIN OF 95 KDA	TRINITY_DN88232_c0_g1_i1.p1	Mitosis-Spindle
A8J9P1_CHLRE - Predicted protein	TRINITY_DN23274_c0_g1_i1.p1	Mitosis-Spindle
APC1_C domain-containing protein - A0A2K3D074_CHLRE	TRINITY_DN49105_c0_g2_i1.p1	Mitosis-APC/C
APC2 - A8I146_CHLRE	TRINITY_DN15922_c0_g2_i1.p1	Mitosis-APC/C
APC10, CHLREDRAFT_134900 - A0A2K3E6Z1_CHLRE	TRINITY_DN36763_c0_g1_i1.p1	Mitosis-APC/C
APC10, CHLREDRAFT_134900 A8HSJ9_CHLRE	TRINITY_DN96864_c0_g1_i1.p2	Mitosis-APC/C
APC11, CHLRE_13g590900v5, CHLREDRAFT_117084	TRINITY_DN6695_c0_g1_i1.p4	Mitosis-APC/C
APC13, CHLRE_03g186900v5, CHLREDRAFT_170601	TRINITY_DN2695_c0_g1_i2.p1	Mitosis-APC/C
CDH1, CHLREDRAFT_35396	TRINITY_DN98275_c0_g1_i1.p1	Mitosis-APC/C
Flagellar associated protein Fap18 - A8JFR3_CHLRE	TRINITY_DN9568_c0_g1_i2.p1	Mitosis-APC/C

Protein kinase domain-containing protein A0A2K3DKN0_CHLRE	TRINITY_DN20727_c0_g2_i1.p1	Mitosis- Kinet
DHR10 domain-containing protein - A0A2K3E580_CHLRE	TRINITY_DN5539_c0_g1_i2.p1	Mitosis- Kinet
WD_REPEATS_REGION domain-containing protein \	TRINITY_DN31085_c0_g1_i1.p2	Mitosis- Kinet
CENPE- centromeric protein E Cre17.g741350.t1.2	TRINITY_DN3213_c0_g1_i3.p1	Mitosis- Kinet
ARL3_CHLRE - GEF protein	TRINITY_DN1616_c0_g1_i3.p2	Cytokinesis
CDKA1 CHLRE_A8I1P3_CHLRE	TRINITY_DN2511_c0_g3_i2.p2	Cytokinesis
Protofilament ribbon of flagellar microtubules (RIB72 protein) (p72)	TRINITY_DN18766_c0_g1_i2.p1	Cytokinesis
Dynamin-type G domain-containing protein	TRINITY_DN76381_c0_g1_i1.p1	Cytokinesis
Aurora-like kinase Alk-2	TRINITY_DN97004_c0_g1_i1.p1	Cytokinesis
Cpl1 Cyclopropyl isomerase-like protein	TRINITY_DN116403_c0_g1_i1.p1	Cytokinesis
Mob1 Cytokinesis-related protein	TRINITY_DN106482_c0_g1_i1.p1	Cytokinesis
Drp1 Dynamin-related GTPase	TRINITY_DN105479_c0_g1_i1.p1	Cytokinesis
Vfl1 Variable flagella protein 1 (cyt1 variable) Q9SWH3_CHLRE	TRINITY_DN1345_c0_g2_i1.p1	Cytokinesis
Actin act1 A0A0F7RLL1_CHLMO	TRINITY_DN1689_c0_g1_i1.p1	Cytokinesis
Kcbp Kinesin like calmodulin binding pro… Q19QU5_CHLRE	TRINITY_DN11460_c0_g1_i1.p1	Cytokinesis
Intraflagellar transport protein 27 IFT27_CHLRE	TRINITY_DN87366_c0_g1_i1.p1	Cytokinesis
Aurora-like kinase A8ISU1_CHLRE	TRINITY_DN97004_c0_g1_i1.p1	Cytokinesis
CFAP20 BUG22 FAP20 CHLREDRAFT_189631 CFA20_CHLRE	TRINITY_DN87679_c0_g1_i2.p1	Basal body
IFT46_CHLRE	TRINITY_DN343_c0_g1_i1.p1	Basal body
IFT25_CHLRE	TRINITY_DN109614_c0_g1_i1.p3	Basal body
Cytoplasmic dynein 2 heavy chain 1 DYHC2_CHLRE	TRINITY_DN4379_c0_g6_i2.p1	Basal body
Dynein regulatory complex subunit 4 DRC4_CHLRE	TRINITY_DN76913_c0_g1_i1.p1	Basal body
DRC2_CHLRE	TRINITY_DN115952_c0_g1_i1.p1	Basal body
IFT27_CHLRE	TRINITY_DN89557_c0_g1_i1.p2	Basal body
Dynein 1b light intermediate chain DC2L1_CHLRE	TRINITY_DN26196_c0_g1_i1.p1	Basal body
Cfap 300 Cilia- and flagella-associated protein 300 CF300_CHLRE	TRINITY_DN37126_c0_g1_i1.p2	Basal body
IF172_CHLRE	TRINITY_DN905_c0_g1_i1.p1	Basal body
Caltractin (20 kDa calcium-binding protein) (Centrin)	TRINITY_DN3040_c0_g1_i13.p1	Basal body
DAW1_CHLRE	TRINITY_DN116748_c0_g1_i1.p2	Basal body
IFT57_CHLRE	TRINITY_DN29070_c0_g1_i1.p2	Basal body
FAP116 A8JBY2_CHLRE	TRINITY_DN21028_c0_g1_i1.p2	Basal body
FAP133 CHLREDRAFT_111920 A8I3B3_CHLRE	TRINITY_DN25351_c0_g1_i2.p1	Basal body
Cilia- and flagella-associated protein 52 CFA52_CHLRE	TRINITY_DN24510_c0_g1_i1.p1	Basal body
Tubulin alpha chain Q540H1_CHLRE	TRINITY_DN2223_c0_g1_i8.p2	Basal body
Bug25 - A8JD01_CHLRE	TRINITY_DN46644_c0_g1_i1.p1	Basal body

Flagellar basal body protein FBB18 A8JBA8_CHLRE	TRINITY_DN126799_c0_g1_i1.p2	Basal body
IFT88 CHLRE_07g335750v5 A8JCJ2_CHLRE	TRINITY_DN125713_c0_g1_i1.p1	Basal body
FAP178 CHLREDRAFT_53378 A8ID60_CHLRE	TRINITY_DN27800_c0_g1_i1.p1	Basal body
BBS1 domain-containing protein CRT2_CHLRE	TRINITY_DN126405_c0_g1_i1.p1	Basal body
FBB7 CHLREDRAFT_149939 A8J390_CHLRE	TRINITY_DN28049_c0_g1_i1.p1	Basal body
FBB11 CHLREDRAFT_160148 A8JGF9_CHLRE	TRINITY_DN19513_c0_g1_i1.p1	Basal body
FBB19 CHLREDRAFT_150998 A8J8E1_CHLRE	TRINITY_DN35644_c0_g1_i1.p1	Basal body
FAP259 CHLRE_07g342200v5 A8ITN7_CHLRE	TRINITY_DN18093_c0_g1_i1.p2	Basal body
FBB13 CHLREDRAFT_145923 A8ITI8_CHLRE	TRINITY_DN13203_c0_g1_i2.p2	Basal body
TPR_REGION A0A2K3CTW3_CHLRE	TRINITY_DN44552_c0_g1_i1.p1	Basal body
Bug23 A8I180_CHLRE	TRINITY_DN35893_c0_g2_i1.p1	Basal body
FBB17 A8HSR5_CHLRE	TRINITY_DN38776_c0_g1_i1.p1	Basal body
FBB9 A8J795_CHLRE	TRINITY_DN9540_c0_g1_i2.p2	Basal body
FBB10 A8I6L8_CHLRE	TRINITY_DN41322_c0_g1_i1.p1	Basal body
Flagellar/basal body protein, PACRG-like protein A8I2Z6_CHLRE	TRINITY_DN4462_c0_g3_i1.p1	Basal body
IFT52 Q944U2_CHLRE	TRINITY_DN126608_c0_g1_i1.p2	Basal body
BBS5 Q6PSU7_CHLRE	TRINITY_DN11726_c0_g1_i1.p1	Basal body
DIP13_CHLRE	TRINITY_DN10376_c0_g1_i2.p1	Basal body
RIB72 Q8LKK4_CHLRE	TRINITY_DN18766_c0_g1_i2.p1	Basal body
HSP90A A8J1U1_CHLRE	TRINITY_DN366_c0_g1_i3.p1	Basal body
CCT3_A8II42_CHLRE	TRINITY_DN105898_c0_g1_i1.p2	Basal body
SAS-6 A9CQL4_CHLRE	TRINITY_DN4439_c2_g2_i1.p1	Basal body
NIMA-related kinase 2 CNK2 Q6UPR4_CHLRE	TRINITY_DN1726_c0_g4_i1.p1	Basal body
POC7, A8JFW5_CHLRE	TRINITY_DN5177_c0_g1_i1.p1	Basal body
POC1, A8I2S8_CHLRE	TRINITY_DN76837_c0_g2_i1.p2	Basal body
RIB43a, Q9M6B0_CHLRE	TRINITY_DN6640_c0_g1_i1.p1	Basal body
KCBP Kinesin binding protein Q19QU5_CHLRE	TRINITY_DN11460_c0_g1_i1.p1	Basal body
Tubulin beta chain A8IXZ0_CHLRE	TRINITY_DN5283_c0_g1_i9.p1	Basal body
Vps4 A8IAJ1_CHLRE	TRINITY_DN105171_c0_g1_i1.p1	Basal body
Vps 23 A8IU80_CHLRE	TRINITY_DN21080_c0_g2_i3.p1	Basal body
Vps 28 A8J3R6_CHLRE	TRINITY_DN88990_c0_g1_i1.p1	Basal body
Vps60 A8HTH0_CHLRE	TRINITY_DN3591_c0_g1_i1.p1	Basal body
Cyclin N-terminal domain-containing protein A0A2K3DQ78_CHLRE	TRINITY_DN24140_c0_g1_i1.p1	Cyclins
A-type cyclin A8IX31_CHLRE	TRINITY_DN78099_c0_g1_i1.p1	Cyclins
B type cyclin A8JER8_CHLRE	TRINITY_DN7490_c0_g1_i2.p1	Cyclins
Cyclin-dependent kinases regulatory… A8IDD8_CHLRE	TRINITY_DN6251_c0_g1_i1.p1	Cyclins

Table 3. List of homologous proteins between *O.* cf. *ovata* and *Plasmodium falciparum*. The first column contains the protein names assigned by plasmoDB and uniprot database; the second column shows the homologous proteins found in *O.* cf. *ovata* and the assigned transcript ID. The third column indicates the function of the proteins in budding yeast. The functions were assigned to cytokinesis, cyclins, basal body and mitosis which includes spindle, kinetochore and APC/C.

Protein_name	I.D. *O. cf. ovata*	Function
Anaphase promoting complex subunit 11	TRINITY_DN6695_c0_g1_i1.p4	Mitosis-APC/C
Anaphase promoting complex subunit 3	TRINITY_DN3070_c0_g2_i1.p2	Mitosis-APC/C
Anaphase promoting complex subunit 10	TRINITY_DN96864_c0_g1_i1.p2	Mitosis-APC/C
Cell division cycle protein 20 homolog	TRINITY_DN98275_c0_g1_i1.p1	Mitosis-APC/C
SNF2 helicase	TRINITY_DN9334_c1_g1_i1.p1	Mitosis-Kinet
WD repeat-containing protein 82	TRINITY_DN11527_c0_g1_i1.p1	Mitosis-Kinet
RuvB-like helicase 3 (EC 3.6.4.12)	TRINITY_DN124986_c0_g1_i1.p1	Mitosis-Kinet
Cytoskeleton associated protein	TRINITY_DN29752_c0_g1_i1.p1	Mitosis-Kinet
Snf2-related CBP activator	TRINITY_DN30793_c0_g1_i2.p1	Mitosis-Kinet
Alpha-tubulin Nacetyltransferase	TRINITY_DN29976_c1_g1_i1.p1	Mitosis-Kinet
condensin complex subunit 2	TRINITY_DN77149_c0_g1_i1.p1	Mitosis-Kinet
Histone H3 variant	TRINITY_DN106572_c0_g1_i1.p2	Mitosis-Kinet
Microtubule-associated protein RP/EB family	TRINITY_DN106062_c0_g1_i1.p1	Mitosis-Kinet
Histone H2A.2	TRINITY_DN9097_c0_g1_i1.p1	Mitosis-Kinet
Centrin-1 CEN1	TRINITY_DN3040_c0_g1_i13.p1	Mitosis-Kinet
Gamma-tubulin complex component	TRINITY_DN105741_c0_g1_i1.p1	Mitosis-Kinet
Thioredoxin-like protein 1	TRINITY_DN4688_c0_g1_i3.p1	Mitosis-Kinet
transcription elongation factor 1	TRINITY_DN99985_c0_g1_i1.p1	Mitosis-Kinet
XAP-5 DNA binding protein	TRINITY_DN1051_c12_g1_i1.p1	Mitosis-Kinet
kinesin-13	TRINITY_DN5424_c0_g1_i1.p1	Mitosis-Kinet
GAS8-like protein	TRINITY_DN16607_c0_g1_i1.p1	Mitosis-Kinet
p25-alpha family protein	TRINITY_DN6051_c0_g1_i4.p1	Mitosis-Kinet
Histone chaperone ASF1	TRINITY_DN117866_c0_g1_i1.p1	Mitosis-Kinet
Prefoldin subunit 3	TRINITY_DN124766_c0_g1_i1.p1	Mitosis-Kinet
Histone H2B.Z	TRINITY_DN4135_c0_g2_i1.p1	Mitosis-Kinet
Dynamin-Like protein 1	TRINITY_DN7120_c0_g1_i1.p1	Mitosis-Kinet
condensin-2 complex subunit D3	TRINITY_DN96082_c0_g1_i1.p1	Mitosis-Kinet
RuvB-like helicase 2 (EC 3.6.4.12)	TRINITY_DN22412_c0_g1_i1.p1	Mitosis-Kinet
Histone H4	TRINITY_DN255_c0_g2_i1.p1	Mitosis-Kinet
Chromatin remodeling protein	TRINITY_DN12152_c0_g3_i1.p2	Mitosis-Kinet
Dynamin-Like protein 2	TRINITY_DN25400_c0_g1_i1.p1	Mitosis-Kinet
Transcription elo,ngation factor SPT4	TRINITY_DN86371_c0_g1_i1.p1	Mitosis-Kinet
Centrin-3 CEN3	TRINITY_DN3040_c1_g1_i2.p1	Mitosis-Kinet
Dynein beta chain	TRINITY_DN16278_c4_g1_i6.p1	Mitosis-Kinet
Chromatin assembly factor 1 P55 subunit	TRINITY_DN116485_c0_g1_i1.p1	Mitosis-Kinet

Proliferating cell nuclear antigen 2	TRINITY_DN5283_c0_g1_i9.p1	Mitosis-Kinet-BB
Centrin-2 CEN2	TRINITY_DN13860_c0_g1_i1.p2	Mitosis-Kinet-BB
Double-strand break repair protein MRE11	TRINITY_DN39325_c0_g1_i1.p1	Mitosis
Fructose-bisphosphate aldolase	TRINITY_DN76348_c0_g1_i1.p1	Mitosis
Protein kinase 7 (EC 2.7.11.1)	TRINITY_DN116956_c0_g1_i1.p1	Mitosis
CDC2-related protein kinase 1 CRK-1	TRINITY_DN38588_c0_g1_i1.p1	Mitosis
Structural maintenance of chromosomes protein 4	TRINITY_DN705_c0_g1_i1.p1	Mitosis
Mitosis protein Dim1 (EC 2.1.1.183)	TRINITY_DN95736_c0_g1_i1.p1	Mitosis
DEAD box helicase	TRINITY_DN107869_c0_g1_i1.p1	Mitosis
Structural maintenance of chromosomes protein 2	TRINITY_DN24797_c0_g1_i1.p1	Mitosis
Structural maintenance of chromosomes protein 1	TRINITY_DN51674_c0_g1_i1.p1	Mitosis
Topoisomerase 2	TRINITY_DN10223_c0_g5_i4.p1	Mitosis
SAS-6 like protein	TRINITY_DN98423_c0_g1_i1.p1	Basal body
WD repeat-contains protein 16WDR16	TRINITY_DN24510_c0_g1_i1.p1	Basal body
Calcyclin-binding protein	TRINITY_DN19239_c0_g1_i1.p1	Basal body
DIP13 homolog	TRINITY_DN10376_c0_g1_i2.p1	Basal body
Centrosomal protein CEP76	TRINITY_DN95976_c0_g1_i1.p1	Basal body
NAD-dependent protein deacylase Sir2A	TRINITY_DN32997_c0_g1_i1.p1	Basal body
NIMA related kinase 4 Nek-4	TRINITY_DN20689_c0_g1_i1.p1	cyclin
cyclin dependent kinase binding protein	TRINITY_DN116123_c0_g1_i1.p1	cyclin
Cyclin 4	TRINITY_DN19917_c0_g1_i1.p1	cyclin
Cell cycle regulator protein	TRINITY_DN125209_c0_g1_i1.p1	cyclin
CDC73 domain-containing protein	TRINITY_DN116960_c0_g1_i1.p1	cyclin
CDK-activating kinase assembly factor MAT1	TRINITY_DN97789_c0_g1_i1.p1	cyclin
Suppresor of kinetochore protein 1 ; SKP 1	TRINITY_DN1832_c0_g1_i4.p2	cyclin
Casein kinase 1 CK1	TRINITY_DN6518_c0_g1_i5.p1	cyclin
Casein kinase 2, alpha subunit	TRINITY_DN5165_c0_g1_i1.p1	cyclin
Pescadillo homolog	TRINITY_DN126740_c0_g1_i1.p2	cyclin
Enhancer of rudimentary homolog	TRINITY_DN129342_c0_g1_i1.p1	cyclin
MO15-related protein kinase	TRINITY_DN20311_c0_g1_i1.p1	cyclin
Cyclin 1	TRINITY_DN25337_c0_g1_i1.p1	cyclin
Proliferation-associated protein 2g4	TRINITY_DN404_c0_g1_i1.p2	cyclin
Actin-like protein ALP1	TRINITY_DN6600_c0_g1_i4.p1	Cytokinesis
regulator of chromosome condensation	TRINITY_DN97470_c0_g1_i1.p1	Cytokinesis
kinesin-like protein	TRINITY_DN15774_c0_g1_i1.p1	Cytokinesis
Cell division cycle protein 48 homologue	TRINITY_DN168_c0_g1_i2.p1	Cytokinesis
Aurora related kinase 2	TRINITY_DN7961_c0_g1_i1.p1	Cytokinesis
Tubulin beta chain	TRINITY_DN811_c0_g1_i11.p1	Cytokinesis
Cyclase-associated protein CAP	TRINITY_DN3565_c2_g1_i1.p1	Cytokinesis
Actin-related protein ARP1	TRINITY_DN125293_c0_g1_i1.p1	Cytokinesis

Profilin	TRINITY_DN1529_c0_g3_i1.p2	Cytokinesis
Formin 1	TRINITY_DN24251_c0_g2_i1.p1	Cytokinesis
F-actin-capping protein subunit alpha	TRINITY_DN29300_c5_g4_i1.p1	Cytokinesis
F-actin-capping protein subunit beta	TRINITY_DN44145_c0_g1_i1.p1	Cytokinesis
Coronin	TRINITY_DN449_c0_g1_i1.p1	Cytokinesis
Vacuolar protein sorting-associated protein 16	TRINITY_DN20074_c0_g1_i1.p1	Cytokinesis
Formin 2	TRINITY_DN6074_c0_g3_i1.p1	Cytokinesis
Cofilin/ Actin-depolymerizing factor homolog 2	TRINITY_DN3066_c0_g1_i4.p1	Cytokinesis
Aurora related kinase 3	TRINITY_DN8055_c0_g1_i2.p1	Cytokinesis
Myosin A	TRINITY_DN19372_c0_g1_i1.p1	Cytokinesis
Myosin F	TRINITY_DN11_c0_g1_i3.p1	Cytokinesis
Actin-related protein 2/3 complex subunit 1	TRINITY_DN42384_c0_g1_i1.p2	Cytokinesis
Sortilin	TRINITY_DN1919_c0_g1_i2.p1	Cytokinesis
Serine/threonine protein phosphatase 2A activator	TRINITY_DN125096_c0_g1_i1.p1	Cytokinesis
LCCL Lectin domain Adhesive-like Protein LAP	TRINITY_DN6034_c0_g1_i9.p1	Cytokinesis
Tubulin gamma chain	TRINITY_DN4423_c0_g2_i1.p1	Cytokinesis/BB
DNA repair protein RAD2	TRINITY_DN53333_c0_g1_i1.p1	Cytokinesis/BB

Table 4. Complete list of cell cycle components identified in *O.* cf. *ovata*

Protein name	ID_Ostreops	Category	Organism
Rib72	TRINITY_DN18766_c0_g1_i2.p1	Basal body	*C.r*
Vps 23	TRINITY_DN21080_c0_g2_i3.p1	Basal body	*C.r*
CFA52	TRINITY_DN24510_c0_g1_i1.p1	Basal body	*C.r; P.f*
Bbs1	TRINITY_DN126405_c0_g1_i1.p1	Basal body	*C.r*
Bbs5	TRINITY_DN11726_c0_g1_i1.p1	Basal body	*C.r*
Bug23	TRINITY_DN35893_c0_g2_i1.p1	Basal body	*C.r*
Bug25	TRINITY_DN46644_c0_g1_i1.p1	Basal body	*C.r*
Cct3	TRINITY_DN105898_c0_g1_i1.p2	Basal body	*C.r*
Cfa20	TRINITY_DN87679_c0_g1_i2.p1	Basal body	*C.r*
Cfap 300	TRINITY_DN37126_c0_g1_i1.p2	Basal body	*C.r*
Cnk2	TRINITY_DN1726_c0_g4_i1.p1	Basal body	*C.r*
DAW1	TRINITY_DN116748_c0_g1_i1.p2	Basal body	*C.r*
DRC2	TRINITY_DN115952_c0_g1_i1.p1	Basal body	*C.r*
DRC4	TRINITY_DN76913_c0_g1_i1.p1	Basal body	*C.r*
Dynein 1b light intermediate chain	TRINITY_DN26196_c0_g1_i1.p1	Basal body	*C.r*
Dynein 2 heavy chain 1	TRINITY_DN4379_c0_g6_i2.p1	Basal body	*C.r*
FAP116	TRINITY_DN21028_c0_g1_i1.p2	Basal body	*C.r*
FAP133	TRINITY_DN25351_c0_g1_i2.p1	Basal body	*C.r*
Fap178	TRINITY_DN27800_c0_g1_i1.p1	Basal body	*C.r*

Fap259	TRINITY_DN18093_c0_g1_i1.p2	Basal body	*C.r*
Fbb, PACRG-like	TRINITY_DN4462_c0_g3_i1.p1	Basal body	*C.r*
Fbb10	TRINITY_DN41322_c0_g1_i1.p1	Basal body	*C.r*
Fbb11	TRINITY_DN19513_c0_g1_i1.p1	Basal body	*C.r*
Fbb13	TRINITY_DN13203_c0_g1_i2.p2	Basal body	*C.r*
Fbb17	TRINITY_DN38776_c0_g1_i1.p1	Basal body	*C.r*
FBB18	TRINITY_DN126799_c0_g1_i1.p2	Basal body	*C.r*
Fbb19	TRINITY_DN35644_c0_g1_i1.p1	Basal body	*C.r*
Fbb7	TRINITY_DN28049_c0_g1_i1.p1	Basal body	*C.r*
Fbb9	TRINITY_DN9540_c0_g1_i2.p2	Basal body	*C.r*
Hsp90	TRINITY_DN366_c0_g1_i3.p1	Basal body	*C.r*
Ift172	TRINITY_DN905_c0_g1_i1.p1	Basal body	*C.r*
Ift25	TRINITY_DN109614_c0_g1_i1.p3	Basal body	*C.r*
Ift46	TRINITY_DN343_c0_g1_i1.p1	Basal body	*C.r*
Ift52	TRINITY_DN126608_c0_g1_i1.p2	Basal body	*C.r*
Ift57	TRINITY_DN29070_c0_g1_i1.p2	Basal body	*C.r*
Ift88	TRINITY_DN125713_c0_g1_i1.p1	Basal body	*C.r*
Poc1	TRINITY_DN76837_c0_g2_i1.p2	Basal body	*C.r*
Poc7	TRINITY_DN5177_c0_g1_i1.p1	Basal body	*C.r*
Rib43A	TRINITY_DN6640_c0_g1_i1.p1	Basal body	*C.r*
TPR_REGION	TRINITY_DN44552_c0_g1_i1.p1	Basal body	*C.r*
Vps 28	TRINITY_DN88990_c0_g1_i1.p1	Basal body	*C.r*
Vps60	TRINITY_DN3591_c0_g1_i1.p1	Basal body	*C.r*
Dip13	TRINITY_DN10376_c0_g1_i2.p1	Basal body	*P.f; C.r*
Cep76	TRINITY_DN95976_c0_g1_i1.p1	Basal body	*P.f*
Sir2A	TRINITY_DN32997_c0_g1_i1.p1	Basal body	*P.f*
Sas-6	TRINITY_DN4439_c2_g2_i1.p1	Basal body	*C.r*
Centrin (caltractin)	TRINITY_DN3040_c0_g1_i13.p1	Basal body	*S.c; C.r; P.f*
CENTROSOMAL PROTEIN OF 95 KDA	TRINITY_DN88232_c0_g1_i1.p1	Basal body	*C.r*
Centrin-2 CEN2	TRINITY_DN13860_c0_g1_i1.p2	BB-Mit-Ctkn	*P.f*
Cyclin 4	TRINITY_DN19917_c0_g1_i1.p1	Cyclin	*P.f*
Mat1	TRINITY_DN97789_c0_g1_i1.p1	Cyclin	*P.f*
MO15-related protein kinase	TRINITY_DN20311_c0_g1_i1.p1	Cyclin	*P.f*
Cyclin 6/ ClB6	TRINITY_DN12532_c0_g1_i1.p1	Cyclin	*S.c*
Pcl7	TRINITY_DN116097_c0_g1_i1.p1	Cyclin	*S.c*
Whi5	TRINITY_DN17261_c1_g1_i1.p1	Cyclin	*S.c*
Cyclin 1	TRINITY_DN25337_c0_g1_i1.p1	Cyclin	*P.f*
Cdk1	TRINITY_DN2511_c0_g3_i2.p2	Cyclin	*S.c; C.r*
Cyclin 1/ClB1	TRINITY_DN108329_c0_g1_i1.p1	Cyclin	*S.c*
Cyclin 3/ ClB3	TRINITY_DN78099_c0_g1_i1.p1	Cyclin	*S.c*
Cyclin 4/ ClB4	TRINITY_DN7490_c0_g1_i2.p1	Cyclin	*S.c*

Ck1	TRINITY_DN6518_c0_g1_i5.p1	Cyclin	*P.f*
Enhancer of rudimentary homolog Pf3d7	TRINITY_DN129342_c0_g1_i1.p1	Cyclin	*P.f*
Pf11	TRINITY_DN126740_c0_g1_i1.p2	Cyclin	*P.f*
Pf3d7	TRINITY_DN5165_c0_g1_i1.p1	Cyclin	*P.f*
Proliferation-associated protein 2g4	TRINITY_DN404_c0_g1_i1.p2	Cyclin	*P.f*
Skp1	TRINITY_DN1832_c0_g1_i4.p2	Cyclin	*P.f*
Cdk binding protein	TRINITY_DN116123_c0_g1_i1.p1	Cyclin	*P.f*
Nek-4	TRINITY_DN20689_c0_g1_i1.p1	Cyclin	*P.f*
Cdc73	TRINITY_DN116960_c0_g1_i1.p1	Cyclin	*P.f*
Cks1	TRINITY_DN6251_c0_g1_i1.p1	Cyclin	*C.r*
Cyclin A	TRINITY_DN78099_c0_g1_i1.p1	Cyclin	*C.r*
Cyclin B	TRINITY_DN7490_c0_g1_i2.p1	Cyclin	*C.r*
Cyclin N-terminal domain-containing protein	TRINITY_DN24140_c0_g1_i1.p1	Cyclin	*C.r*
Profilin	TRINITY_DN1529_c0_g3_i1.p2	Cytokinesis	*P.f*
Formin 1	TRINITY_DN24251_c0_g2_i1.p1	Cytokinesis	*P.f*
Dynamin-type G domain-containing protein	TRINITY_DN76381_c0_g1_i1.p1	Cytokinesis	*C.r*
Ift27	TRINITY_DN87366_c0_g1_i1.p1	Cytokinesis	*C.r*
Kcbp	TRINITY_DN11460_c0_g1_i1.p1	Cytokinesis	*C.r*
Drp1 Dynamin-related GTPase	TRINITY_DN105479_c0_g1_i1.p1	Cytokinesis	*C.r*
Cdc10	TRINITY_DN47140_c0_g1_i1.p1	Cytokinesis	*S.c*
Alk2	TRINITY_DN97004_c0_g1_i1.p1	Cytokinesis	*C.r*
Arl3	TRINITY_DN1616_c0_g1_i3.p2	Cytokinesis	*C.r*
CPI1	TRINITY_DN116403_c0_g1_i1.p1	Cytokinesis	*C.r*
Actin-related protein ARP1	TRINITY_DN125293_c0_g1_i1.p1	Cytokinesis	*P.f*
Ark2	TRINITY_DN7961_c0_g1_i1.p1	Cytokinesis	*P.f*
Cdc48	TRINITY_DN168_c0_g1_i2.p1	Cytokinesis	*P.f*
Coronin	TRINITY_DN449_c0_g1_i1.p1	Cytokinesis	*P.f*
Cyclase-associated protein CAP	TRINITY_DN3565_c2_g1_i1.p1	Cytokinesis	*P.f*
F-actin-capping protein subunit alpha	TRINITY_DN29300_c5_g4_i1.p1	Cytokinesis	*P.f*
F-actin-capping protein subunit beta	TRINITY_DN44145_c0_g1_i1.p1	Cytokinesis	*P.f*
Formin 2	TRINITY_DN6074_c0_g3_i1.p1	Cytokinesis	*P.f*
kinesin-like protein	TRINITY_DN15774_c0_g1_i1.p1	Cytokinesis	*P.f*
Lccl -LAP	TRINITY_DN6034_c0_g1_i9.p1	Cytokinesis	*P.f*
Myosin A	TRINITY_DN19372_c0_g1_i1.p1	Cytokinesis	*P.f*
Myosin F	TRINITY_DN11_c0_g1_i3.p1	Cytokinesis	*P.f*
regulator of chromosome condensation	TRINITY_DN97470_c0_g1_i1.p1	Cytokinesis	*P.f*
Ser/thre phosphatase 2A activator	TRINITY_DN125096_c0_g1_i1.p1	Cytokinesis	*P.f*

Tubulin-alpha	TRINITY_DN2223_c0_g1_i8.p2	Cytokinesis	*S.c; C.r*
Actin	TRINITY_DN1689_c0_g1_i1.p1	Cytokinesis	*S.c; C.r; P.f*
tubulin-beta	TRINITY_DN5283_c0_g1_i9.p1	Cytokinesis	*S.c; C.r; P.f*
Mlp1	TRINITY_DN24869_c0_g4_i1.p1	Cytokinesis	*S.c*
Mpg1	TRINITY_DN58489_c0_g1_i1.p1	Cytokinesis	*S.c*
Myosin 1	TRINITY_DN4758_c0_g5_i1.p1	Cytokinesis	*S.c*
Nop15	TRINITY_DN31813_c1_g1_i1.p1	Cytokinesis	*S.c*
Lrg1	TRINITY_DN48867_c0_g1_i2.p1	Cytokinesis	*S.c*
Kip3	TRINITY_DN44795_c0_g1_i1.p2	Cytokinesis	*S.c*
Arpc1	TRINITY_DN42384_c0_g1_i1.p2	Cytokinesis	*S.c; P.f*
Aip1	TRINITY_DN22811_c0_g1_i1.p1	Cytokinesis	*S.c*
Arpc2	TRINITY_DN35177_c0_g1_i1.p1	Cytokinesis	*S.c*
Arpc3	TRINITY_DN118357_c0_g1_i1.p2	Cytokinesis	*S.c*
Cofilin	TRINITY_DN122525_c0_g1_i1.p2	Cytokinesis	*S.c*
Rv167	TRINITY_DN18708_c0_g1_i1.p1	Cytokinesis	*S.c*
Alp1	TRINITY_DN6600_c0_g1_i4.p1	Cytokinesis	*P.f*
Ark3	TRINITY_DN8055_c0_g1_i2.p1	Cytokinesis	*P.f*
Ede1	TRINITY_DN42096_c0_g1_i1.p1	Cytokinesis	*S.c*
Vfl1	TRINITY_DN1345_c0_g2_i1.p1	Cytokinesis	*C.r*
Sortilin	TRINITY_DN1919_c0_g1_i2.p1	Cytokinesis	*P.f*
Vps16	TRINITY_DN20074_c0_g1_i1.p1	Cytokinesis	*P.f*
Vps4	TRINITY_DN105171_c0_g1_i1.p1	Cytokinesis	*S.c; C.r*
Escrt-3	TRINITY_DN5417_c0_g1_i2.p1	Cytokinesis	*S.c*
Vps20	TRINITY_DN3167_c0_g7_i1.p2	Cytokinesis	*S.c*
Vps25	TRINITY_DN15459_c0_g1_i1.p1	Cytokinesis	*S.c*
RAD2	TRINITY_DN53333_c0_g1_i1.p1	Cytokinesis/Basal Body	*P.f*
Cdc14	TRINITY_DN9399_c0_g1_i3.p1	Mitosis and Cytokinesis	*S.c*
Mob2	TRINITY_DN3145_c0_g1_i3.p1	Mitosis and Cytokinesis	*S.c*
Fbpa	TRINITY_DN76348_c0_g1_i1.p1	Mitosis	*P.f*
Dead2 (helicase)	TRINITY_DN107869_c0_g1_i1.p1	Mitosis	*P.f*
Mre11	TRINITY_DN39325_c0_g1_i1.p1	Mitosis	*P.f*
Top2	TRINITY_DN10223_c0_g5_i4.p1	Mitosis	*P.f*
Pp12	TRINITY_DN10959_c0_g1_i1.p1	Mitosis	*S.c*
Smc1	TRINITY_DN51674_c0_g1_i1.p1	Mitosis	*P.f*
Smc2	TRINITY_DN24797_c0_g1_i1.p1	Mitosis	*P.f*
Smc4	TRINITY_DN705_c0_g1_i1.p1	Mitosis	*P.f*
Histone H4	TRINITY_DN255_c0_g2_i1.p1	Mitosis	*S.c; P.f*
Smc3	TRINITY_DN38588_c0_g1_i1.p1	Mitosis	*S.c*
Pds5	TRINITY_DN6329_c1_g3_i2.p1	Mitosis	*S.c*
Cnd2	TRINITY_DN77149_c0_g1_i1.p1	Mitosis	*S.c; P.f*
Cnd1	TRINITY_DN6926_c0_g1_i1.p1	Mitosis	*S.c*

Kar3	TRINITY_DN999_c0_g3_i2.p1	Mitosis	*S.c*
Hsl7	TRINITY_DN1778_c0_g1_i2.p1	Mitosis	*S.c*
KEL2	TRINITY_DN95742_c0_g1_i1.p1	Mitosis	*S.c*
Met30	TRINITY_DN126225_c0_g1_i1.p1	Mitosis	*S.c*
Swe1	TRINITY_DN5846_c0_g1_i1.p1	Mitosis	*S.c*
Xpo1	TRINITY_DN24525_c0_g2_i1.p1	Mitosis	*S.c*
Mob1	TRINITY_DN106482_c0_g1_i1.p1	Mitosis	*S.c; C.r*
Cdc5	TRINITY_DN124690_c0_g1_i1.p1	Mitosis	*S.c*
Crk1	TRINITY_DN38588_c0_g1_i1.p1	Mitosis	*P.f*
Pk7	TRINITY_DN116956_c0_g1_i1.p1	Mitosis	*P.f*
Pp2A	TRINITY_DN3182_c0_g6_i1.p1	Mitosis	*S.c*
Dim1	TRINITY_DN95736_c0_g1_i1.p1	Mitosis	*P.f*
Apc1	TRINITY_DN49105_c0_g2_i1.p1	Mitosis	*S.c; C.r*
Apc2	TRINITY_DN15922_c0_g1_i1.p1	Mitosis	*S.c; C.r*
Apc11	TRINITY_DN6695_c0_g1_i1.p4	Mitosis	*S.c; C.r; P.f*
Cdc20-Cdh1	TRINITY_DN98275_c0_g1_i1.p1	Mitosis	*S.c; C.r; P.f*
Cdc16	TRINITY_DN15730_c0_g1_i1.p1	Mitosis	*S.c*
Cdc23	TRINITY_DN117627_c0_g1_i1.p1	Mitosis	*S.c*
Cdc27	TRINITY_DN23979_c0_g1_i1.p1	Mitosis	*S.c*
Cenp-E	TRINITY_DN3213_c0_g1_i3.p1	Mitosis	*C.r*
DHR10 domain-containing protein	TRINITY_DN5539_c0_g1_i2.p1	Mitosis	*C.r*
Sgt1	TRINITY_DN19239_c0_g1_i1.p1	Mitosis	*S.c; P.f*
Cbf3	TRINITY_DN7822_c0_g3_i1.p2	Mitosis	*S.c*
Ndc80	TRINITY_DN4604_c0_g1_i3.p1	Mitosis	*S.c*
PIK1	TRINITY_DN18913_c0_g2_i1.p1	Mitosis	*S.c*
Ybp1	TRINITY_DN45996_c0_g1_i1.p1	Mitosis	*S.c*
Mps1	TRINITY_DN20727_c0_g2_i1.p1	Mitosis	*S.c; C.r*
Apc13	TRINITY_DN2695_c0_g1_i2.p1	Mitosis	*C.r*
Fap18	TRINITY_DN9568_c0_g1_i2.p1	Mitosis	*C.r*
Apc3	TRINITY_DN3070_c0_g2_i1.p2	Mitosis	*P.f*
condensin-2 complex subunit D3	TRINITY_DN96082_c0_g1_i1.p1	Mitosis	*P.f*
Histone H2B.Z	TRINITY_DN4135_c0_g2_i1.p1	Mitosis	*P.f*
Chromatin assembly factor 1 P55 subunit	TRINITY_DN116485_c0_g1_i1.p1	Mitosis	*P.f*
Xap5	TRINITY_DN1051_c12_g1_i1.p1	Mitosis	*P.f*
RuvB	TRINITY_DN22412_c0_g1_i1.p1	Mitosis	*P.f*
Snf2	TRINITY_DN30793_c0_g1_i2.p1	Mitosis	*P.f*
Snf2L	TRINITY_DN9334_c1_g1_i1.p1	Mitosis	*P.f*
Spt4	TRINITY_DN86371_c0_g1_i1.p1	Mitosis	*P.f*
Asf1	TRINITY_DN117866_c0_g1_i1.p1	Mitosis	*P.f*
Wdr82	TRINITY_DN11527_c0_g1_i1.p1	Mitosis	*P.f*
Histone H2A.2	TRINITY_DN9097_c0_g1_i1.p1	Mitosis	*P.f*

Histone H3	TRINITY_DN106572_c0_g1_i1.p2	Mitosis	*P.f*
Dynein beta chain	TRINITY_DN16278_c4_g1_i6.p1	Mitosis	*P.f*
Cytoskeleton associated protein	TRINITY_DN29752_c0_g1_i1.p1	Mitosis	*P.f*
Tubulin-gamma	TRINITY_DN105741_c0_g1_i1.p1	Mitosis	*P.f*
Gas8	TRINITY_DN16607_c0_g1_i1.p1	Mitosis	*P.f*
Klp8	TRINITY_DN5424_c0_g1_i1.p1	Mitosis	*P.f*
p25-alpha	TRINITY_DN6051_c0_g1_i4.p1	Mitosis	*P.f*
Prefoldin subunit 3	TRINITY_DN124766_c0_g1_i1.p1	Mitosis	*P.f*
Trx1	TRINITY_DN4688_c0_g1_i3.p1	Mitosis	*P.f*
Alpha-tubulin Nacetyltransferase	TRINITY_DN29976_c1_g1_i1.p1	Mitosis	*P.f*
Dynamin-Like protein 1	TRINITY_DN7120_c0_g1_i1.p1	Mitosis	*P.f*
Dynamin-Like protein 2	TRINITY_DN25400_c0_g1_i1.p1	Mitosis	*P.f*
Eb1-Mtb plus ending	TRINITY_DN106062_c0_g1_i1.p1	Mitosis	*P.f*
Elf1	TRINITY_DN99985_c0_g1_i1.p1	Mitosis	*P.f*
Bim1	TRINITY_DN1814_c0_g1_i1.p1	Mitosis	*S.c*
Bmh2	TRINITY_DN3798_c0_g1_i8.p2	Mitosis	*S.c*
Bni1	TRINITY_DN11334_c0_g2_i1.p1	Mitosis	*S.c*
Cbk1	TRINITY_DN3145_c0_g1_i3.p1	Mitosis	*S.c*
Nap1	TRINITY_DN1504_c0_g3_i3.p1	Mitosis	*S.c*
Nup170	TRINITY_DN30525_c0_g2_i1.p1	Mitosis	*S.c*
Stu2	TRINITY_DN13432_c0_g2_i1.p1	Mitosis	*S.c*
Ipl1	TRINITY_DN97004_c0_g1_i1.p1	Mitosis	*S.c*
WD_REPEATS_REGION domain-containing protein	TRINITY_DN31085_c0_g1_i1.p2	Mitosis	*C.r*
Centriole proteome protein	TRINITY_DN10248_c0_g1_i1.p1	Mitosis	*C.r*
Aspm	TRINITY_DN125387_c0_g1_i1.p2	Mitosis	*C.r*
Spindle pole body - Cre09.g404500.t1.1	TRINITY_DN5676_c0_g5_i1.p1	Mitosis	*C.r*
Apc10	TRINITY_DN96864_c0_g1_i1.p2	Mitosis	*S.c; C.r; P.f*
A8J9P1_CHLRE - Predicted protein	TRINITY_DN23274_c0_g1_i1.p1	Mitosis	*C.r*

Table 5. Basal body components of *O.* cf. *ovata*

Protein name	ID_Ostreops	Function associated	Organism
Cfa52	TRINITY_DN24510_c0_g1_i1.p1	Basal body structure	C.r; P.f
Bbs1	TRINITY_DN126405_c0_g1_i1.p1	Basal body structure	C.r
Bbs5	TRINITY_DN11726_c0_g1_i1.p1	Basal body structure	C.r
Bug23	TRINITY_DN35893_c0_g2_i1.p1	Basal body structure	C.r
Bug25	TRINITY_DN46644_c0_g1_i1.p1	Basal body structure	C.r
Cct3	TRINITY_DN105898_c0_g1_i1.p2	Basal body structure	C.r
Cfap 20	TRINITY_DN87679_c0_g1_i2.p1	Basal body structure	C.r

Cfap 300	TRINITY_DN37126_c0_g1_i1.p2	Basal body structure	C.r
Cnk2	TRINITY_DN1726_c0_g4_i1.p1	Basal body structure	C.r
Daw1	TRINITY_DN116748_c0_g1_i1.p2	Basal body structure	C.r
DRC2	TRINITY_DN115952_c0_g1_i1.p1	Basal body structure	C.r
DRC4	TRINITY_DN76913_c0_g1_i1.p1	Basal body structure	C.r
Dynein 1b light intermediate chain	TRINITY_DN26196_c0_g1_i1.p1	Basal body structure	C.r
Dynein 2 heavy chain 1	TRINITY_DN4379_c0_g6_i2.p1	Basal body structure	C.r
FAP116	TRINITY_DN21028_c0_g1_i1.p2	Basal body structure	C.r
FAP133	TRINITY_DN25351_c0_g1_i2.p1	Basal body structure	C.r
Fap178	TRINITY_DN27800_c0_g1_i1.p1	Basal body structure	C.r
Fap259	TRINITY_DN18093_c0_g1_i1.p2	Basal body structure	C.r
Fbb, PACRG-like	TRINITY_DN4462_c0_g3_i1.p1	Basal body structure	C.r
Fbb10	TRINITY_DN41322_c0_g1_i1.p1	Basal body structure	C.r
Fbb11	TRINITY_DN19513_c0_g1_i1.p1	Basal body structure	C.r
Fbb13	TRINITY_DN13203_c0_g1_i2.p2	Basal body structure	C.r
Fbb17	TRINITY_DN38776_c0_g1_i1.p1	Basal body structure	C.r
FBB18	TRINITY_DN126799_c0_g1_i1.p2	Basal body structure	C.r
Fbb19	TRINITY_DN35644_c0_g1_i1.p1	Basal body structure	C.r
Fbb7	TRINITY_DN28049_c0_g1_i1.p1	Basal body structure	C.r
Fbb9	TRINITY_DN9540_c0_g1_i2.p2	Basal body structure	C.r
Hsp90	TRINITY_DN366_c0_g1_i3.p1	Basal body structure	C.r
Ift172	TRINITY_DN905_c0_g1_i1.p1	Basal body structure	C.r
Ift25	TRINITY_DN109614_c0_g1_i1.p3	Basal body structure	C.r
Ift46	TRINITY_DN343_c0_g1_i1.p1	Basal body structure	C.r
Ift52	TRINITY_DN126608_c0_g1_i1.p2	Basal body structure	C.r
Ift57	TRINITY_DN29070_c0_g1_i1.p2	Basal body structure	C.r
Ift88	TRINITY_DN125713_c0_g1_i1.p1	Basal body structure	C.r
Poc1	TRINITY_DN76837_c0_g2_i1.p2	Basal body structure	C.r
Poc7	TRINITY_DN5177_c0_g1_i1.p1	Basal body structure	C.r
Rib43A	TRINITY_DN6640_c0_g1_i1.p1	Basal body structure	C.r
Tpr	TRINITY_DN44552_c0_g1_i1.p1	Basal body structure	C.r
Vps 28	TRINITY_DN88990_c0_g1_i1.p1	Basal body structure	C.r
Vps60	TRINITY_DN3591_c0_g1_i1.p1	Basal body structure	C.r
Dip13	TRINITY_DN10376_c0_g1_i2.p1	Basal body structure	P.f; C.r
Cep76	TRINITY_DN95976_c0_g1_i1.p1	Basal body structure	P.f
Sir2A	TRINITY_DN32997_c0_g1_i1.p1	Basal body structure	P.f
Dynamin-type G domain-containing	TRINITY_DN76381_c0_g1_i1.p1	Basal body associated to cytokinesis	C.r
Ift27	TRINITY_DN87366_c0_g1_i1.p1	Basal body associated to cytokinesis	C.r
Kcbp	TRINITY_DN11460_c0_g1_i1.p1	Basal body associated to cytokinesis	C.r
Rib72	TRINITY_DN18766_c0_g1_i2.p1	Basal body associated to cytokinesis	C.r

Vps 23	TRINITY_DN21080_c0_g2_i3.p1	Basal body associated to cytokinesis	C.r
Centriole proteome protein	TRINITY_DN10248_c0_g1_i1.p1	MTOC, mitosis, cytokinesis	C.r
Sas-6	TRINITY_DN4439_c2_g2_i1.p1	MTOC, mitosis, cytokinesis	C.r
Centrin-2 CEN2	TRINITY_DN13860_c0_g1_i1.p2	MTOC, mitosis, cytokinesis	P.f
Centrin (caltractin)	TRINITY_DN3040_c0_g1_i13.p1	MTOC, mitosis, cytokinesis	S.c; C.r; P.f
Tubulin-gamma	TRINITY_DN105741_c0_g1_i1.p1	MTOC, mitosis, cytokinesis	P.f
Centrosomal protein of 95 Kda	TRINITY_DN88232_c0_g1_i1.p1	MTOC, mitosis, cytokinesis	C.r

Table 6. Mitotic components of *O.* cf. *ovata*. The table shows the protein name assigned by the database where each homologous was found, the transcript ID in the reference transcriptome, the associated function and the organism where it was identified. In addition to the three reference organisms, *Homo sapiens (H.s)*, and the dinoflagellate *Symbiodinium kawagutii (S.k)* were also included. Kinetochore components are shown in red.

Protein name	ID_Ostreops	Function associated	Organism
Apc1	TRINITY_DN49105_c0_g2_i1.p1	APC/C	*S.c; C.r*
Apc2	TRINITY_DN15922_c0_g1_i1.p1	APC/C	*S.c; C.r*
Apc3	TRINITY_DN3070_c0_g2_i1.p2	APC/C	*P.f*
Apc4	TRINITY_DN36763_c0_g1_i1.p1	APC/C	*H.s*
Apc5	TRINITY_DN116163_c0_g2_i1.p1	APC/C	*H.s*
Apc10	TRINITY_DN96864_c0_g1_i1.p2	APC/C	*H.s;S.c; C.r;P.f*
Apc11	TRINITY_DN6695_c0_g1_i1.p4	APC/C	*H.s;S.c; C.r;P.f*
Apc13	TRINITY_DN2695_c0_g1_i2.p1	APC/C	*C.r*
Apc15	TRINITY_DN9869_c0_g1_i2.p1	APC/C	*S.k*
Apc6, Cdc16	TRINITY_DN15730_c0_g1_i1.p1	APC/C	*S.c*
Apc8, Cdc23	TRINITY_DN117627_c0_g1_i1.p1	APC/C	*S.c*
Cdc27	TRINITY_DN23979_c0_g1_i1.p1	APC/C	*S.c*
Fap18	TRINITY_DN9568_c0_g1_i2.p1	APC/C	*S.c*
condensin-2 complex subunit D3	TRINITY_DN96082_c0_g1_i1.p1	chromatid cohesion	*C.r*
Dead2 (helicase)	TRINITY_DN107869_c0_g1_i1.p1	chromatid cohesion	*P.f*
Histone H2B.Z	TRINITY_DN4135_c0_g2_i1.p1	chromatid cohesion	*P.f*
Spt4	TRINITY_DN86371_c0_g1_i1.p1	chromatid segregation	*P.f*
Top2	TRINITY_DN10223_c0_g5_i4.p1	chromatid segregation	*P.f*
Pp12	TRINITY_DN10959_c0_g1_i1.p1	chromatid segregation	*P.f*
Pds5	TRINITY_DN6329_c1_g3_i2.p1	chromatid segregation	*S.c*
Cnd2	TRINITY_DN77149_c0_g1_i1.p1	chromatid segregation	*S.c*
Cnd1	TRINITY_DN6926_c0_g1_i1.p1	chromatid segregation	*S.c; P.f*
Chromatin assembly factor 1 P55 subunit	TRINITY_DN116485_c0_g1_i1.p1	Chromosome organization	*S.c*
Mre11	TRINITY_DN39325_c0_g1_i1.p1	Chromosome organization	*P.f*
Xap5	TRINITY_DN1051_c12_g1_i1.p1	Chromosome organization	*P.f*
RuvB	TRINITY_DN22412_c0_g1_i1.p1	Chromosome organization	*P.f*
Snf2	TRINITY_DN30793_c0_g1_i2.p1	Chromosome organization	*P.f*
Snf2L	TRINITY_DN9334_c1_g1_i1.p1	Chromosome organization	*P.f*
Asf1	TRINITY_DN117866_c0_g1_i1.p1	Chromosome organization	*P.f*
Wdr82	TRINITY_DN11527_c0_g1_i1.p1	Chromosome organization	*P.f*

Histone H2A.2	TRINITY_DN9097_c0_g1_i1.p1	Chromosome organization	*P.f*
Smc1	TRINITY_DN51674_c0_g1_i1.p1	Chromosome organization	*P.f*
Smc2	TRINITY_DN24797_c0_g1_i1.p1	Chromosome organization	*P.f*
Smc4	TRINITY_DN705_c0_g1_i1.p1	Chromosome organization	*P.f*
Histone H4	TRINITY_DN255_c0_g2_i1.p1	Chromosome organization	*P.f*
Smc3	TRINITY_DN38588_c0_g1_i1.p1	Chromosome organization	*S.c; P.f*
Histone H3	TRINITY_DN106572_c0_g1_i1.p2	Chromosome organization	*P.f*
Nup107	TRINITY_DN16807_c0_g1_i1.p1	Nuclear pore complex	*H.s*
Nup85	TRINITY_DN22349_c0_g1_i1.p1	Nuclear pore complex	*H.s*
Tpr	TRINITY_DN24869_c0_g4_i1.p1	Nuclear pore complex	*H.s*
Nup170	TRINITY_DN30525_c0_g2_i1.p1	Nuclear pore complex	*S.c*
Cdc20-Cdh1	TRINITY_DN98275_c0_g1_i1.p1	Outer kinetochore - SAC	*S.c; C.r; P.f*
Mad1	TRINITY_DN45521_c0_g3_i1.p1	Outer kinetochore - SAC	*S.k*
Mad2	TRINITY_DN69405_c0_g1_i1.p1	Outer kinetochore - SAC	*H.s*
Mps1	TRINITY_DN20727_c0_g2_i1.p1	Outer kinetochore - SAC	*H.s; S.c; C.r*
Bub3	TRINITY_DN31085_c0_g1_i1.p2	Outer kinetochore - SAC	*H.s*
CenpE	TRINITY_DN6369_c0_g1_i2.p1	Outer kinetochore	*H.s; C.r*
CenpF	TRINITY_DN16119_c0_g2_i1.p1	Outer kinetochore	*H.s*
Cep57	TRINITY_DN4604_c0_g1_i3.p1	Outer kinetochore	*H.s*
Ndc80	TRINITY_DN4604_c0_g1_i3.p1	Outer kinetochore	*H.s; S.c*
Nuf2	TRINITY_DN5539_c0_g4_i1.p2	Outer kinetochore	*S.k*
Pch2	TRINITY_DN105171_c0_g1_i1.p1	Outer kinetochore	*H.s*
Plk1	TRINITY_DN124690_c0_g1_i1.p1	Outer kinetochore	*H.s*
Red	TRINITY_DN96171_c0_g1_i1.p1	Outer kinetochore	*H.s*
Spc25	TRINITY_DN26159_c0_g1_i1.p1	Outer kinetochore	*H.s*
Aurora	TRINITY_DN97004_c0_g1_i1.p1	Inner kinetochore	*H.s*
Borealin	TRINITY_DN106572_c0_g1_i1.p2	Inner kinetochore	*H.s*
Cbf3c	TRINITY_DN7822_c0_g3_i1.p2	Inner kinetochore	*S.c*
CenpA	TRINITY_DN106572_c0_g1_i1.p2	Inner kinetochore	*P.f*
CenpC	TRINITY_DN1454_c0_g3_i1.p1	Inner kinetochore	*S.k*
Incenp	TRINITY_DN1853_c0_g1_i2.p1	Inner kinetochore	*S.k*
Skp1	TRINITY_DN7822_c0_g3_i1.p2	Inner kinetochore	*H.s; S.c; P.f*
Znf207	TRINITY_DN96496_c0_g1_i1.p1	Inner kinetochore	*H.s*
Zwint	TRINITY_DN20211_c0_g1_i1.p1	Inner kinetochore	*H.s*
DHR10 domain-containing protein	TRINITY_DN5539_c0_g1_i2.p1	Kinetochore	*C.r*

Sgt1	TRINITY_DN19239_c0_g1_i1.p1	Kinetochore	*S.c; P.f*
Ybp1	TRINITY_DN45996_c0_g1_i1.p1	Kinetochore	*S.c*
Gas8	TRINITY_DN16607_c0_g1_i1.p1	Kinetochore	*P.f*
Klp8	TRINITY_DN5424_c0_g1_i1.p1	Kinetochore	*P.f*
p25-alpha	TRINITY_DN6051_c0_g1_i4.p1	Kinetochore	*P.f*
Prefoldin subunit 3	TRINITY_DN124766_c0_g1_i1.p1	Kinetochore	*P.f*
Trx1	TRINITY_DN4688_c0_g1_i3.p1	Kinetochore	*P.f*
A8J9P1_CHLRE - Predicted protein	TRINITY_DN23274_c0_g1_i1.p1	Kinetochore	*C.r*
Alpha-tubulin Nacetyltransferase	TRINITY_DN29976_c1_g1_i1.p1	Kinetochore	*P.f*
Eb1-Mtb plus ending	TRINITY_DN106062_c0_g1_i1.p1	Kinetochore	*P.f*
Elf1	TRINITY_DN99985_c0_g1_i1.p1	Kinetochore	*P.f*
Dynein beta chain	TRINITY_DN16278_c4_g1_i6.p1	Microtubules movement	*S.c; C.r*
Kar3	TRINITY_DN999_c0_g3_i2.p1	Microtubules movement	*S.c*
Dynamin-Like protein 1	TRINITY_DN7120_c0_g1_i1.p1	Microtubules movement	*P.f*
Dynamin-Like protein 2	TRINITY_DN25400_c0_g1_i1.p1	Microtubules movement	*P.f*
Mob1	TRINITY_DN106482_c0_g1_i1.p1	MEN	*S.c; C.r*
Pp2A	TRINITY_DN3182_c0_g6_i1.p1	MEN	*S.c*
Cdc5	TRINITY_DN124690_c0_g1_i1.p1	MEN	*S.c*
Hsl7	TRINITY_DN1778_c0_g1_i2.p1	Mitosis progression	*S.c*
KEL2	TRINITY_DN95742_c0_g1_i1.p1	Mitosis progression	*S.c*
Met30	TRINITY_DN126225_c0_g1_i1.p1	Mitosis progression	*S.c*
Swe1	TRINITY_DN5846_c0_g1_i1.p1	Mitosis progression	*S.c*
Xpo1	TRINITY_DN24525_c0_g2_i1.p1	Mitosis progression	*S.c*
Dim1	TRINITY_DN95736_c0_g1_i1.p1	Mitosis progression	*P.f*
Cdc14	TRINITY_DN9399_c0_g1_i3.p1	Mitosis/cytokinesis progression	*S.c*
Mob2	TRINITY_DN3145_c0_g1_i3.p1	Mitosis/cytokinesis progression	*S.c*
Crk1	TRINITY_DN38588_c0_g1_i1.p1	Mitotic checkpoint	*P.f*
Pk7	TRINITY_DN116956_c0_g1_i1.p1	Mitotic checkpoint	*P.f*
Centriole proteome protein	TRINITY_DN10248_c0_g1_i1.p1	MTOC	*C.r*
Sas-6	TRINITY_DN4439_c2_g2_i1.p1	MTOC	*C.r*
Centrin-2 CEN2	TRINITY_DN13860_c0_g1_i1.p2	MTOC	*P.f*
Tubulin-gamma	TRINITY_DN105741_c0_g1_i1.p1	MTOC	*P.f*
CENTROSOMAL PROTEIN OF 95 KDA	TRINITY_DN88232_c0_g1_i1.p1	MTOC	*C.r*
Centrin (caltractin)	TRINITY_DN3040_c0_g1_i13.p1	MTOC	*S.c; C.r; P.f*
Ipl1	TRINITY_DN97004_c0_g1_i1.p1	Spindle	*S.c*
Cytoskeleton associated protein	TRINITY_DN29752_c0_g1_i1.p1	Spindle	*P.f*
Bim1	TRINITY_DN1814_c0_g1_i1.p1	Spindle	*S.c*
Bmh2	TRINITY_DN3798_c0_g1_i8.p2	Spindle	*S.c*

Bni1	TRINITY_DN11334_c0_g2_i1.p1	Spindle	*S.c*
Cbk1	TRINITY_DN3145_c0_g1_i3.p1	Spindle	*S.c*
Nap1	TRINITY_DN1504_c0_g3_i3.p1	Spindle	*S.c*
Stu2	TRINITY_DN13432_c0_g2_i1.p1	Spindle	*S.c*
WD_REPEATS_REGION domain-containing protein	TRINITY_DN31085_c0_g1_i1.p2	Spindle	*C.r*
Aspm	TRINITY_DN125387_c0_g1_i1.p2	Spindle	*C.r*
Spindle pole body - Cre09.g404500.t1.1	TRINITY_DN5676_c0_g5_i1.p1	Spindle	*C.r*

Table 7. Cytokinetic components of *O.* cf. *ovata*. The table shows the protein name assigned by the database where each homolog was found, the transcript ID in the reference transcriptome, the associated function during cytokinesis and the organism where it was identified.

Protein name	ID_Ostreops	Function associated	Organism
Ark3	TRINITY_DN8055_c0_g1_i2.p1	Mitosis/cytokinesis progresion	P.f
Cdc14	TRINITY_DN9399_c0_g1_i3.p1	Mitosis/cytokinesis progression	S.c
Mob2	TRINITY_DN3145_c0_g1_i3.p1	Mitosis/cytokinesis progression	S.c
Alp1	TRINITY_DN6600_c0_g1_i4.p1	Mitosis/cytokinesis orientation	P.f
Cdc10	TRINITY_DN47140_c0_g1_i1.p1	Cytokinesis orientation	S.c
Centriole proteome protein	TRINITY_DN10248_c0_g1_i1.p1	MTOC	C.r
Sas-6	TRINITY_DN4439_c2_g2_i1.p1	MTOC	C.r
Centrin-2 CEN2	TRINITY_DN13860_c0_g1_i1.p2	MTOC	P.f
Tubulin-gamma	TRINITY_DN105741_c0_g1_i1.p1	MTOC	P.f
Centrosomal protein of 92 Kda	TRINITY_DN88232_c0_g1_i1.p1	MTOC	C.r
Centrin (caltractin)	TRINITY_DN3040_c0_g1_i13.p1	MTOC	S.c; C.r; P.f
Ede1	TRINITY_DN42096_c0_g1_i1.p1	MTOC	S.c
Rib72	TRINITY_DN18766_c0_g1_i2.p1	MTOC	C.r
Dynamin-type G domain-containing protein	TRINITY_DN76381_c0_g1_i1.p1	Basal body associated to cytokinesis	C.r
Ift27	TRINITY_DN87366_c0_g1_i1.p1	Basal body associated to cytokinesis	C.r
Kcbp	TRINITY_DN11460_c0_g1_i1.p1	Basal body associated to cytokinesis	C.r
Vps 23	TRINITY_DN21080_c0_g2_i3.p1	Basal body associated to cytokinesis	C.r
Dynein beta chain	TRINITY_DN16278_c4_g1_i6.p1	Microtubules movement	P.f
Drp1 Dynamin-related GTPase	TRINITY_DN105479_c0_g1_i1.p1	Microtubules movement	C.r
kinesin-like protein	TRINITY_DN15774_c0_g1_i1.p1	Microtubules movement	P.f
Kar3	TRINITY_DN999_c0_g3_i2.p1	Microtubules movement	S.c
Kip3	TRINITY_DN44795_c0_g1_i1.p2	Microtubules movement	S.c
Vfl1	TRINITY_DN1345_c0_g2_i1.p1	Vessicle traffick, progression	C.r
Sortilin	TRINITY_DN1919_c0_g1_i2.p1	Vessicle traffick,	C.r

		progression	
Vps16	TRINITY_DN20074_c0_g1_i1.p1	Vessicle traffick, progression	P.f
Vps4	TRINITY_DN105171_c0_g1_i1.p1	Vessicle traffick, progression	P.f
Escrt-3	TRINITY_DN5417_c0_g1_i2.p1	Vessicle traffick, progression	S.c; C.r
Vps20	TRINITY_DN3167_c0_g7_i1.p2	Vessicle traffick, progression	S.c
Vps25	TRINITY_DN15459_c0_g1_i1.p1	Vessicle traffick, progression	S.c
Lrg1	TRINITY_DN48867_c0_g1_i2.p1	Cytokinesis progression/ cell wall	S.c
Mpg1	TRINITY_DN58489_c0_g1_i1.p1	Cytokinesis progression/ cell wall	S.c
Alk2	TRINITY_DN97004_c0_g1_i1.p1	Cytokinesis progression	C.r
Arl3	TRINITY_DN1616_c0_g1_i3.p2	Cytokinesis progression	C.r
Cpi1	TRINITY_DN116403_c0_g1_i1.p1	Cytokinesis progression	C.r
Ark2	TRINITY_DN7961_c0_g1_i1.p1	Cytokinesis progression	P.f
Cdc48	TRINITY_DN168_c0_g1_i2.p1	Cytokinesis progression	P.f
Coronin	TRINITY_DN449_c0_g1_i1.p1	Cytokinesis progression	P.f
Cyclase-associated protein CAP	TRINITY_DN3565_c2_g1_i1.p1	Cytokinesis progression	P.f
Arp1	TRINITY_DN125293_c0_g1_i1.p1	Cytokinesis progression	P.f
Mlp1	TRINITY_DN24869_c0_g4_i1.p1	Cytokinesis progression	S.c
Nop15	TRINITY_DN31813_c1_g1_i1.p1	Cytokinesis progression	S.c
Rad2	TRINITY_DN53333_c0_g1_i1.p1	Cytokinesis progression	P.f
regulator of chromosome condensation	TRINITY_DN97470_c0_g1_i1.p1	Cytokinesis progression	P.f
Ser/thre phosphatase 2A activator	TRINITY_DN125096_c0_g1_i1.p1	Cytokinesis progression	P.f
Formin 2	TRINITY_DN6074_c0_g3_i1.p1	Cytokinesis progression	P.f
Lccl -LAP	TRINITY_DN6034_c0_g1_i9.p1	Cytokinesis progression	P.f
Tubulin-beta	TRINITY_DN5283_c0_g1_i9.p1	Cytokinesis progression	S.c; C.r; P.f
Tubulin-alpha	TRINITY_DN2223_c0_g1_i8.p2	Cytokinesis progression	S.c; C.r
F-actin-capping protein subunit alpha	TRINITY_DN29300_c5_g4_i1.p1	Cytokinesis progression	P.f
F-actin-capping protein subunit beta	TRINITY_DN44145_c0_g1_i1.p1	Cytokinesis progression	P.f
Myosin A	TRINITY_DN19372_c0_g1_i1.p1	Cytokinesis progression	P.f
Myosin F	TRINITY_DN11_c0_g1_i3.p1	Cytokinesis progression	P.f
Actin	TRINITY_DN1689_c0_g1_i1.p1	Cytokinesis progression	S.c; C.r; P.f
Myosin 1	TRINITY_DN4758_c0_g5_i1.p1	Cytokinesis progression	S.c
Profilin	TRINITY_DN1529_c0_g3_i1.p2	Cytokinesis progression	P.f
Fbpa	TRINITY_DN76348_c0_g1_i1.p1	Cytokinesis progression	P.f
Formin 1	TRINITY_DN24251_c0_g2_i1.p1	Cytokinesis progression	P.f
Arpc1	TRINITY_DN42384_c0_g1_i1.p2	Cytokinesis progression/ ring	S.c; P.f
Aip1	TRINITY_DN22811_c0_g1_i1.p1	Cytokinesis progression/	S.c

		ring	
Arpc2	TRINITY_DN35177_c0_g1_i1.p1	Cytokinesis progression/ ring	S.c
Arpc3	TRINITY_DN118357_c0_g1_i1.p2	Cytokinesis progression/ ring	S.c
Cofilin	TRINITY_DN122525_c0_g1_i1.p2	Cytokinesis progression/ ring	S.c
Rv167	TRINITY_DN18708_c0_g1_i1.p1	Cytokinesis progression/ ring	S.c

Table 8. Cell cycle regulators of *O.* cf. *ovata.* The table shows the protein name assigned by the database where each homolog was found, the transcript ID in the reference transcriptome, the associated function during the cell cycle and the organism where it was identified.

Protein name	ID_Ostreops	Phase regulated	Organism
Mat1	TRINITY_DN97789_c0_g1_i1.p1	G1/S	*P.f*
Cyclin B6/ ClB6	TRINITY_DN12532_c0_g1_i1.p1	G1/S	*S.c*
Pcl7	TRINITY_DN116097_c0_g1_i1.p1	G1/S	*S.c*
Whi5	TRINITY_DN17261_c1_g1_i1.p1	G1/S	*S.c*
Cks1	TRINITY_DN6251_c0_g1_i1.p1	G1/S and G2/M	*C.r*
Cyclin A	TRINITY_DN78099_c0_g1_i1.p1	G2-M	*C.r*
Cdk1	TRINITY_DN2511_c0_g3_i2.p2	G2/M	*S.c; C.r*
Cyclin B1/ClB1	TRINITY_DN108329_c0_g1_i1.p1	G2/M	*S.c*
Cyclin B3/ ClB3	TRINITY_DN78099_c0_g1_i1.p1	G2/M	*S.c*
Cyclin B4/ ClB4	TRINITY_DN7490_c0_g1_i2.p1	G2/M	*S.c; C.r*
Swe1-Wee1	TRINITY_DN5846_c0_g1_i1.p1	G2/M	S.c
Cyclin 1	TRINITY_DN25337_c0_g1_i1.p1	G2-M	*P.f*
Cdk binding protein, putative	TRINITY_DN116123_c0_g1_i1.p1	Mitotic regulator	*P.f*
Cyclin N-terminal domain-containing protein	TRINITY_DN24140_c0_g1_i1.p1	Unknown	*C.r*
Nek-4	TRINITY_DN20689_c0_g1_i1.p1	Unknown	*P.f*
Casein kinase 1	TRINITY_DN6518_c0_g1_i5.p1	Unknown	*P.f*
Enhancer of rudimentary Pf3d7	TRINITY_DN129342_c0_g1_i1.p1	Unknown	*P.f*
Casein kinase 2, alpha subunit	TRINITY_DN5165_c0_g1_i1.p1	Unknown	*P.f*
Pf11 (pescadillo)	TRINITY_DN126740_c0_g1_i1.p2	Unknown	*P.f*
Proliferation-associated protein 2g4	TRINITY_DN404_c0_g1_i1.p2	Unknown	*P.f*
Cdc73	TRINITY_DN116960_c0_g1_i1.p1	Unknown	*P.f*
Cell cycle regulator protein	TRINITY_DN125209_c0_g1_i1.p1	Unknown	*P.f*
Cyclin 4	TRINITY_DN19917_c0_g1_i1.p1	Unknown	*P.f*
MO15-related protein kinase	TRINITY_DN20311_c0_g1_i1.p1	Unknown	*P.f*

Table 9. Components of *O.* cf. *ovata* cell cycle differentially expressed in the meta-transcriptomic analysis. ND= No differential expressed.

Protein	Day_vs_evening	Day_vs_night
Cyclin B1/ClB1	Downregulated	Downregulated
Cell cycle regulator protein	Downregulated	Downregulated
Enhancer of rudimentary Pf3d7	Downregulated	Downregulated
Bbs5	Downregulated	Downregulated
Cfap 20	Downregulated	Downregulated
Dynein 1b light intermediate chain	Downregulated	ND
Fbb11	Downregulated	Downregulated
Fbb17	Downregulated	ND
FBB18	Downregulated	ND
Fbb9	Downregulated	Downregulated
Ift25	Downregulated	Downregulated
Ift46	Downregulated	Downregulated
Ift88	Downregulated	Downregulated
Poc7	Downregulated	Downregulated
Vps 28	Downregulated	Downregulated
Centrin (caltractin)	Downregulated	Downregulated
Apc13	Downregulated	Downregulated
Apc15	Downregulated	Downregulated
Cdc23	Downregulated	ND
Pp12	Downregulated	ND
Asf1	Downregulated	Downregulated
Histone H2B.Z	Downregulated	Downregulated
Histone H4	Downregulated	Downregulated
Nap1	Downregulated	Downregulated
Aurora	Downregulated	ND
Elf1	Downregulated	Downregulated
p25-alpha	Downregulated	ND
Cdc20-Cdh1	Downregulated	Downregulated
Bmh2	Downregulated	Downregulated
Bni1	Downregulated	ND
Ipl1	Downregulated	ND
Alk2	Downregulated	Downregulated
Aip1	Downregulated	Downregulated
Rv167	Downregulated	Downregulated
Cyc 1	Upregulated	ND
Cyc A	Upregulated	ND
Cyclin B4/ ClB4	Upregulated	Upregulated
Fap178	Upregulated	Upregulated

Ift172	Upregulated	Upregulated
Poc1	Upregulated	Upregulated
Rib72	Upregulated	Downregulated
Sas-6	Upregulated	Upregulated
Tubulin-gamma	Upregulated	Upregulated
Apc5	Upregulated	Upregulated
Smc4	Upregulated	Upregulated
Cbf3c	Upregulated	Upregulated
Skp1	Upregulated	Upregulated
Dynamin-Like protein 1	Upregulated	Upregulated
Xpo1	Upregulated	ND
Poc16	Upregulated	ND
Nup107	Upregulated	Upregulated
Nup170	Upregulated	Upregulated
Nup85	Upregulated	Upregulated
Tpr	Upregulated	Upregulated
Cep57	Upregulated	Upregulated
Ndc80	Upregulated	Upregulated
Nuf2	Upregulated	Upregulated
Spc25	Upregulated	ND
Mad1	Upregulated	Upregulated
Mps1	Upregulated	Upregulated
Ark3	Upregulated	ND
Ark2	Upregulated	ND
Mlp1	Upregulated	Upregulated
Myosin 1	Upregulated	Upregulated
Ede1	Upregulated	Upregulated
Vps16	Upregulated	ND
Pf11 (pescadillo)	ND	Upreg
Bbs1	ND	Downregulated
Dynein 2 heavy chain 1	ND	Upregulated
Cnd1	ND	Upregulated
Cnd2	ND	Upregulated
Pds5	ND	Upregulated
Histone H2A.2	ND	Downregulated
Arl3	ND	Downregulated

Figure1. Cdc20 in *O.* cf. *ovata.* Clustal alignment of Cdc20 from *Symbiodinium minitum* and *O.* cf. *ovata*

Figure 2. Cdk1 in *Ostreopsis* cf *ovata*. Ala14 and Phe15 (highlighted in yellow) replace Tyr15 and Thr14 in Cdk1 of fission yeast, respectively. In red, the PSTAIRE sequence.

>TRINITY_DN2511_c0_g3_i2.p2
ILAQATWLRAHGGAFQAVPMEQYEKLEKVGEGTYGVVYKAQDSQGEIYALKTIRLEAEDEGIPSTAIRE
ISLLKELQHPNIVRLCDVIHTERKLTLVFEYLDQDLKKLLDTCDGGLDAATTKSFLYQLLRGIAYCHQHR
VLHRDLKPQNLLINREGALKLADFGLARAFGIPVRSYTHEVVTLWYRAPDVLMGSRKYSTPVDIWSVG
CIFAEMVNGRPLFPGNTDGDQLQKIFKVLGTPSSESWPTVTELPDWKPDFPSYELQPWAHIVPNLDPTG
VDLLSKMLQYFPDKRVAGKLAMEHEYFRGLSEAIKNMK*.